

Dissertation zur Erlangung des Doktorgrades
der Fakultät für Chemie und Pharmazie
der Ludwig-Maximilians-Universität München

PROTEINS AND AZOBENZENES

Alwin Ralf Reiter

aus

Temeschburg

2013

Erklärung

Diese Dissertation wurde im Sinne von § 7 der Promotionsordnung vom 28. November 2011 von Herrn Prof. Dr. Dirk Trauner betreut.

Eidesstattliche Versicherung

Diese Dissertation wurde eigenständig und ohne unerlaubte Hilfe erarbeitet.

München, 22.03.2013

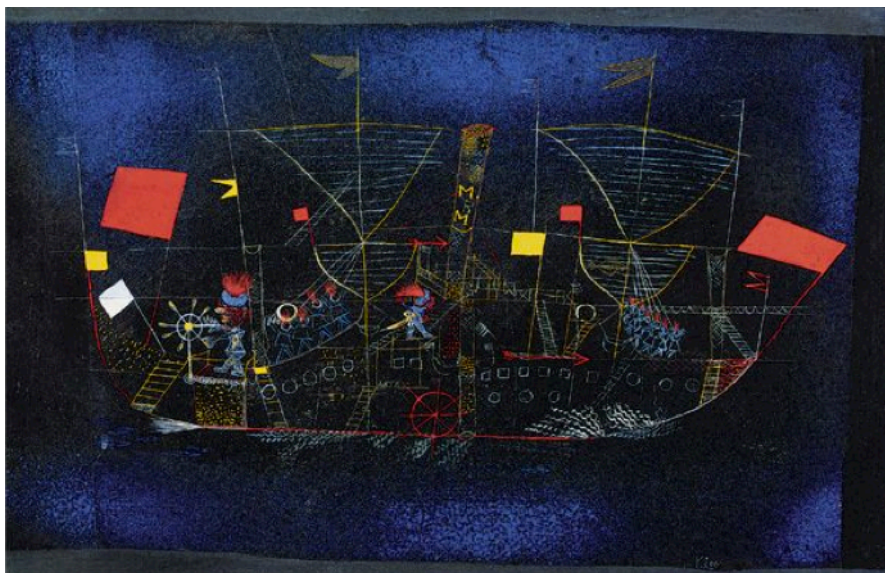
Alwin Reiter

Dissertation eingereicht am: 22.03.2013

1. Gutachter: Prof. Dr. Dirk Trauner

2. Gutachter: Prof. Dr. Thomas Carell

Mündliche Prüfung am: 29.04.2013



Paul Klee: Das Abenteuerschiff, 1927; Pinakothek der Moderne, München

Parts of this work have been published or presented on conferences.

Publications

Reiter, A.; Skerra, A.; Trauner, D.; Schiefner, A.; "**Structural Basis of an Artificial Photoreceptor**" *Angew. Chem. Int. Ed.* (submitted for publication)

Seidel, S. A.; Wienken, C. J.; Geissler, S.; Jerabek-Willemsen, M.; Duhr, S.; Reiter, A.; Trauner, D.; Braun, D.; Baaske, P.; "**Label-Free Microscale Thermophoresis Discriminates Sites and Affinity of Protein–Ligand Binding**" *Angew. Chem. Int. Ed.*, **2012**, *51*, 10656-10659.

Conferences

12.2011: CIPSM Review, Bonn

Poster: **Research Highlights Area F – New Optogenetic Tools – Proteins in Apoptose Signaling – Protein Receptors**

06.2011: LMU-Harvard Young Scientists' Forum, Munich

Presentation: **Crystal Structure of the Ligand-binding Domain of GluK2 with an Optical Switch**

05.2011: FOR1279 Jahrestreffen, Munich

Poster: **Crystal Structure of the Ligand-binding Domain of iGluR6 with an Optical Switch**

06.2009: LMU-Harvard Young Scientists' Forum, Munich

Poster: **Chemical Biology in the Trauner Group**

Acknowledgements

At the beginning of my thesis, I would like to thank all the people who have been with me along the way for so many years. First of all, I would like to express my very grate appreciation to Prof. Dr. Dirk Trauner for giving me the opportunity to work on these highly interesting and challenging projects. It was a pleasure to join the group in its infancy in Munich, to set up the laboratories and to establish new technologies. I am particularly grateful for the maximum freedom in research and for an infinite amount of critical thoughts, patience and encouragement. I really enjoyed working under these excellent conditions.

I am also grateful to Prof. Dr. Arne Skerra and Dr. André Schiefner from the TUM for allowing me free access to the laboratory facilities and for fruitful discussions and mutual teamwork. I would like to extend my thanks to Prof. Dr. Luis Moroder from the MPI and to Dr. Philipp Baaske from NanoTemper for their help with the collection of data and to Dr. Martin Sumser for electrophysiological measurements. I am also thankful to Dr. Mark Mayer for providing the expression vectors. Moreover, I would like to thank Prof. Dr. Thomas Carell for reviewing this thesis and the members of the board of examiners for being available in my thesis defense. Furthermore, I want to thank Prof. Dr. Andreas Plückthun from the UZH, Prof Dr. Eberhard Riedle from the LMU, Prof. Dr. Thorsten Hugel from the TUM and Prof. Dr. Andrew Woolley from the UofT for international and interdisciplinary collaborations that will lead to a better network to carry out research at the interface of biology, chemistry and physics.

I would also like to acknowledge the permanent staff and all current and former members of the Trauner group who contributed to the successful end result. Special thanks go to Laura, Basti, Johannes and David for proofreading of this thesis, to the people of the UV lab and to the Mensa crew, with whom I spent most of my time at the university. Further, I would like to thank the employees of the different divisions of the faculty of chemistry and pharmacy of the LMU and Simone, Benny, Matthias and Nils, the students I supervised.

In addition I want to thank my friends for spending valuable leisure time with me in order to relax from the hard work in the laboratory and to continue with new enthusiasm and new ideas. And last but most important, I thank my family for their continuous support and encouragement. Especially, I would like to thank my parents!

Table of contents

Part I: ABSTRACT

	1
Chapter 1: English	2
Chapter 2: Deutsch	5

Part II: INTRODUCTION

	8
Chapter 3: Ionotropic glutamate receptors	9
3.1 Appearance	9
3.2 General characteristics and architecture	10
3.3 Quaternary structure	13
3.4 Ligand-binding mode	15
3.5 Mechanisms for activation, gating and desensitization	17
Chapter 4: Azobenzenes	19
4.1 Characteristics	19
4.2 Mechanism of isomerization	21
Chapter 5: Azobenzenes in biology	22
5.1 General background	22
5.2 Photoswitchable ligands	23
Chapter 6: Directed evolution	26
6.1 Ribosome display	26
6.2 DARPins	29
Chapter 7: Bonus	30
7.1 Glutamate receptor antagonists	30
7.2 Molecular motors	31
7.3 Ortho-substituted azobenzenes	32

Part III: OBJECTIVES

33

Chapter 8:	Co-crystallization of an azobenzene modified ligand with iGluR-LBDs	34
Chapter 9:	Synthesis of an azobenzene target for ribosome display	36
Chapter 10:	Structure-based design and synthesis of an AMPA receptor antagonist	41
Chapter 11:	Synthesis of an azobenzene with two attachment sites	43
Chapter 12:	Synthesis of <i>ortho</i> -substituted azobenzenes	44

Part IV: EXPERIMENTS

Chapter 13:	Chemistry	45
13.1	<i>General conditions</i>	46
13.1.1	Solvents	46
13.1.2	Reagents	46
13.1.3	Chromatography	47
13.1.4	Chemical analysis	47
13.2	<i>Preparation of 4-Gluazo</i>	48
13.2.1	L-pyroglutamic acid ethyl ester	48
13.2.2	<i>N</i> -Boc-L-pyroglutamic acid ethyl ester	48
13.2.3	Propargyl pyroglutamate	49
13.2.4	Bromoalkyne	50
13.2.5	Vinyl stannane	51
13.2.6	Iodoazobenzene	52
13.2.7	Azobenzene pyroglutamate	52
13.2.8	<i>N</i> -Boc azobenzene glutamic acid	53
13.2.9	4-Gluazo	54
13.3	<i>Preparation of BAG</i>	55

13.3.1	<i>N</i> -tosyl-2,6-dimethylaniline	55
13.3.2	<i>N</i> -tosyl-2,6-dimethyl-4-nitroaniline	56
13.3.3	2,6-dimethyl-4-nitroaniline	57
13.3.4	Nitroazobenzene	57
13.3.5	Aminoazobenzene	58
13.3.6	L-pyroglutamic acid <i>tert</i> -butyl ester	59
13.3.7	<i>N</i> -Boc-L-pyroglutamic acid <i>tert</i> -butyl ester	59
13.3.8	Allylpyroglutamate	60
13.3.9	Acrylic acid pyroglutamate	61
13.3.10	Carboxylic acid pyroglutamate	62
13.3.11	Aminoazobenzene pyroglutamate	62
13.3.12	<i>N</i> -acyl-aminoazobenzene pyroglutamate	63
13.3.13	Azobenzene glutamic acid ester	64
13.3.14	Azobenzene glutamic acid ester γ -amide	65
13.3.15	Biotin azobenzene glutamic acid ester γ -amide	66
13.3.16	BAG	67
13.3.17	Azobenzene glutamic acid γ -amide	68
13.4	<i>Preparation of 2,2',6,6'-tetramethyl-QAQ</i>	69
13.4.1	Betaine acid chloride	69
13.4.2	2,2',6,6'-tetramethyl-QAQ	70
13.5	<i>Preparation of MOBIPHOS and MOBIPHOSen</i>	70
13.5.1	Bisphosphonate	70
13.5.2	Morpholino bisphosphonate	71
13.5.3	Morpholino dihydrobisphosphonate	72
13.5.4	MOBIPHOS	73
13.5.5	MOBIPHOSen	74
13.6	<i>Preparation of ABA</i>	75
Chapter 14: Biology		76
14.1	<i>Materials</i>	76
14.1.1	Chemicals and reagents	76

14.1.2	Buffers, solutions and media	76
14.1.3	Additives	77
14.1.4	Enzymes	78
14.1.5	Bacterial strains	78
14.1.6	Plasmids	78
14.1.7	Equipment	78
14.2	Methods	79
14.2.1	Methods in Molecular Biology	79
14.2.2	Methods in Microbiology	80
14.2.3	Protein qualification and quantification	81
14.2.4	Protein purification	83
14.2.5	Protein digest	85
14.2.6	Isothermal titration calorimetry	85
14.2.7	Microscale thermophoresis	86
14.2.8	Protein–ligand co-crystallization	87
14.2.9	Data collection and structure determination	88
14.2.10	Structural comparison and analyses	88

Part V: RESULTS AND DISCUSSION

Chapter 15:	Protein–4-Gluazo co-crystallization	91
15.1	<i>Synthesis of 4-Gluazo</i>	91
15.2	<i>Verification of plasmid DNA</i>	92
15.3	<i>Protein preparation</i>	92
15.4	<i>Isothermal titration calorimetry</i>	95
15.5	<i>Microscale thermophoresis</i>	97
15.6	<i>Crystallization</i>	98
15.7	<i>GluK2-LBD and GluA2-LBD structures</i>	99
15.7.1	GluK2-LBD dimer	99
15.7.2	GluA2-LBD dimer of dimers	104
Chapter 16:	Synthesis of BAG	111

Chapter 17: Synthesis, electrophysiological characterization and proposed binding mode of MOBIPHOS	111
Chapter 18: Synthesis of ABA	113
Chapter 19: Synthesis of <i>ortho</i> -substituted azobenzenes	113

Part VI: CONCLUSION

114

Part VII: APPENDIX

118

Chapter 20: Abbreviations	119
Chapter 21: Crystallographic data	122
21.1 <i>GluK2-LBD and GluA2-LBD</i>	122
21.2 <i>Propargyl pyroglutamate and bisphosphonate</i>	123
Chapter 22: NMR spectra	124
22.1 <i>Spectra of 4-Gluazo and intermediates</i>	124
22.1.1 <i>N-Boc-L-pyroglutamic acid ethyl ester</i>	124
22.1.2 <i>Propargyl pyroglutamate</i>	125
22.1.3 <i>Bromoalkyne</i>	126
22.1.4 <i>Vinyl stannane</i>	128
22.1.5 <i>Iodoazobenzene</i>	129
22.1.6 <i>Azobenzene pyroglutamate</i>	130
22.1.7 <i>N-Boc azobenzene glutamic acid</i>	131
22.1.8 <i>4-Gluazo</i>	132
22.2 <i>Spectra of BAG and intermediates</i>	133
22.2.1 <i>N-tosyl-2,6-dimethylaniline</i>	133
22.2.2 <i>N-tosyl-2,6-dimethyl-4-nitroaniline</i>	135
22.2.3 <i>2,6-dimethyl-4-nitroaniline</i>	137
22.2.4 <i>Nitroazobenzene</i>	139
22.2.5 <i>Aminoazobenzene</i>	141

22.2.6	<i>N</i> -Boc-L-pyroglutamic acid <i>tert</i> -butyl ester	143
22.2.7	Allylpyroglutamate	145
22.2.8	<i>Cis</i> -allylpyroglutamate	147
22.2.9	Acrylic acid pyroglutamate	149
22.2.10	Carboxylic acid pyroglutamate	151
22.2.11	Aminoazobenzene pyroglutamate	153
22.2.12	<i>N</i> -acyl-aminoazobenzene pyroglutamate	155
22.2.13	Azobenzene glutamic acid ester	157
22.2.14	Biotin azobenzene glutamic acid ester γ -amide	159
22.2.15	BAG	161
22.2.16	Azobenzene glutamic acid γ -amide	163
22.3	<i>Spectra of 2,2',6,6'-tetramethyl-QAQ</i>	165
22.4	<i>Spectra of MOBIPHOS, MOBIPHOSen and intermediates</i>	167
22.4.1	Bisphosphonate	167
22.4.2	Morpholino bisphosphonate	170
22.4.3	Morpholino dihydrobisphosphonate	173
22.4.4	MOBIPHOS	176
22.4.5	MOBIPHOSen	179
22.5	<i>Spectra of ABA</i>	182
Chapter 23: Protein primary structures		184
23.1	<i>GluK2-LBD amino acid sequence</i>	184
23.2	<i>GluA2-LBD amino acid sequence</i>	185

Part VIII: REFERENCES

186

Part I: ABSTRACT

Chapter 1: English

In 1780 Luigi Galvani touched a frog's leg with metal and discovered by accident bioelectricity. He did not notice the coherence, but his observation has provided the basis for the discovery of electro-chemical cells.

With the evolution and progress of neuroscience, the brain has been explored for over two centuries and in the 1950s, L-glutamate has been shown to increase neuronal firing¹. In the 1980s the excitatory neurotransmitter role of glutamate, previously considered to be solely a metabolic precursor, has been discovered at synapses at squid giant axons²⁻⁴.

Ionotropic glutamate receptors (iGluRs) mediate most excitatory neurotransmission in the central nervous system (CNS). These receptors play an important role for the development and function of the nervous system and are essential in learning and memory. At the beginning of this century iGluRs have been turned photosensitive using structure-guided design. Light-switchable agonists based on glutamate have been created that can exist in two different configurations. Depending on the wavelength of light used for illumination, one configuration of the ligand is favoured and according to the design, only one of the two configurations can activate the receptor and allosterically open the ion channel^{5,6}.

X-ray crystallography can provide three-dimensional (3-D) information on macromolecular structures and can show details of protein–ligand interactions. Numerous crystal structures of iGluRs including different ligands are available. However, not much is known about the molecular details concerning the binding mechanism and the spatial arrangement of photoswitches in iGluRs. As a proof of principle, the crystal structure of the ligand-binding domain (LBD) of GluK2 in complex with a photoswitchable agonist has now been solved. This is the first structure showing a membrane receptor bound to a synthetic photoswitchable ligand. The GluK2-LBD crystallized in a physiological mixed dimer with one closed, ligand-bound protomer and one open, apo-like protomer. Furthermore, the affinity of the ligand towards different glutamate receptor subtypes has been determined with isothermal titration calorimetry (ITC) and with microscale thermophoresis (MST). Thereby, the intrinsic fluorescence of the proteins has been used to quantify the binding affinities with MST, which has been newly developed⁷.

ABSTRACT

The structural and functional data have formed a powerful platform for deeper mechanistic studies and for molecular design investigations concerning different long-term objectives in this area of research. With these azobenzene-modified ligands, microelectrodes and light, the behaviour of single neurons in the brain could be resolved in a precise spatio-temporal manner in the future. Moreover, targeting of glutamate receptors in retinal ganglion cells with photoswitchable ligands could possibly restore vision to blind retinæ⁸.

With protein design by directed evolution polypeptides with new or enhanced activity can be created by mimicking the natural process in a series of diversification and selection cycles. On the one hand proteins can be designed *de novo* by making use of chemical information. On the other hand proteins can be redesigned by using an existing scaffold as starting template⁹.

Ribosome display is a very powerful technique to select proteins binding to a specific target immobilized on a surface. Besides antibodies, designed ankyrin repeat proteins (DARPin) are established as binding proteins¹⁰. The hydrophobic core of DARPin is an ideal scaffold to directly bind to an azobenzene moiety. The target molecule for the evolution of an azobenzene-binding protein (ABP) has been prepared. If the ribosome display experiments are successful, ABPs could be combined with other systems and could for example be applied as light-switchable diagnostics and therapeutic agents.

Apart from the role as neurotransmitter, glutamate can be excitotoxic to neurons if present at higher concentrations at the appropriate glutamate receptor. Hyperactivity at synapses might play a role in schizophrenia and in neurodegenerative disorders such as Huntington's chorea, epilepsy and Alzheimer's disease¹¹. Hence, in recent years the challenge has been to develop iGluR antagonists with an acceptable therapeutic tolerability and a high safety profile.

Trials to co-crystallize the GluA2-LBD with a photoswitchable ligand resulted in a tetrameric structure. But instead of being occupied by the photoswitch, the ligand-binding cavity harbours a buffer molecule and a sulfate ion. A new class of glutamate receptor antagonists has been designed from this structure. The molecule has been prepared and electrophysiological experiments have proven the mode of action

ABSTRACT

expected. The solubility of the antagonist in water is very high and the structure leaves room for additional substituents in order to influence the affinity towards the receptor.

Light-powered molecular machines could play a role in future nanoscale devices¹². For this purpose an azobenzene with two attachment sites has been prepared. The two states of a molecular motor could correlate to the different, possible configurations of the molecule. Overall, the molecular motor would be created by using DNA origami and the azobenzene molecule. Unfortunately, further experiments currently stagnate due to early stage technical limitations.

Ortho-substituted azobenzenes show interesting characteristics concerning the stability and the absorption behaviour. Particular substituents generate molecules with very long half-lives in both configurations¹³. Such a molecule has been prepared and attempts to monitor molecular chirality induced with circularly polarized light could possibly be performed in the near future.

Other substituents lead to red-shifted action spectra¹⁴. This is advantageous for medical or biological applications with the depth of penetration increasing and the phototoxicity decreasing. For example, red-shifted compounds are in demand for experiments concerning the restoration of vision. A building block of a red-shifted iGluR agonist has been prepared and final experiments towards the completion of the ligand are currently under investigation.

Chapter 2: Deutsch

1780 berührte Luigi Galvani einen Froschschenkel mit Metall und entdeckte zufällig die Bioelektrizität. Zwar erkannte er nicht die Zusammenhänge, jedoch legte seine Beobachtung die Grundlage für die Entdeckung elektro-chemischer Zellen.

Durch die Entfaltung und die Fortschritte der Neurowissenschaften wird das Gehirn schon seit über zwei Jahrhunderten erforscht und in den 1950er Jahren wurde gezeigt, dass L-Glutamat neuronale Reize verstärkt¹. In den 1980er Jahren wurde die Rolle von Glutamat, das zuvor lediglich als Stoffwechselforstufe angesehen wurde, als aktivierender Neurotransmitter an Synapsen der Riesenaxone des Tintenfisches entdeckt²⁻⁴.

Ionotrope Glutamatrezeptoren (iGluRs) steuern die meiste anregende Neurotransmission im zentralen Nervensystem (ZNS). Diese Rezeptoren haben eine wichtige Rolle in der Entwicklung und in der Funktion des ZNS und sind essentiell für Lernvorgänge und für das Gedächtnis. Zu Beginn dieses Jahrhunderts wurden lichtempfindliche iGluRs durch strukturbasiertes Design entwickelt. Auf Glutamat aufbauend wurden lichtsichtbare Agonisten erstellt, die in zwei unterschiedlichen Konfigurationen existieren können. Abhängig von der Wellenlänge des Lichtes der gewählten Beleuchtung, ist eine Konfiguration des Liganden bevorzugt, und aufgrund des jeweiligen Designs, kann der Ligand nur in einer der zwei Konfigurationen den Rezeptor aktivieren und somit den Ionenkanal allosterisch öffnen^{5,6}.

Mit Hilfe der Röntgenstrukturanalyse können drei dimensionale (3-D) Informationen makromolekularer Strukturen gewonnen werden, und es können Details der Protein–Ligand Wechselwirkung dargestellt werden. Zahlreiche Kristallstrukturen von iGluRs mit unterschiedlichen Liganden sind inzwischen verfügbar. Jedoch ist noch sehr wenig über den zugrundeliegenden detaillierten Mechanismus der Bindung und der räumlichen Orientierung von Photoschaltern und iGluRs bekannt. Als prinzipieller Beweis wurde nun die Kristallstruktur der ligandenbindenden Domäne (LBD) des GluK2 Rezeptors mit einem gebundenen photoschaltbaren Agonisten gelöst. Dies ist die erste Struktur, die einen Membranrezeptor mit einem gebundenen, synthetischen Photoschalter zeigt. Die GluK2-LBD kristallisierte als ein gemischtes physiologisches Dimer mit einem geschlossenen, Liganden gebundenen und einem offenen, Apo ähnlichen Protomer. Außerdem wurde die Affinität des Liganden für verschiedene Klassen von iGluRs durch isothermale Titrationskalorimetrie (ITC) und durch

ABSTRACT

mikroskalige Thermophorese (MST) bestimmt. Hierbei wurde für die MST die intrinsische Fluoreszenz der Proteine verwendet um die Bindungsaffinitäten zu quantifizieren. Diese Technik wurde neu entwickelt⁷.

Die strukturellen und funktionellen Studien haben eine mächtige Plattform für weiterführende Untersuchungen geschaffen, die den Mechanismus und das molekulare Design betreffen, um langfristige Ziele in diesem Forschungsgebiet zu erreichen. Mit diesen Azobenzol enthaltenden Liganden, mit Mikroelektroden und mit Licht, könnte in Zukunft das Verhalten einzelner Neuronen im Gehirn mit einer hohen zeitlichen und räumlichen Auflösung bestimmt werden. Des Weiteren kann mit lichtschtbaren Liganden für Glutamatrezeptoren der retinalen Ganglienzellen möglicherweise das Sehvermögen in blinden Retinae wiederhergestellt werden⁸.

Durch das Design von Proteinen mit Hilfe der direkten Evolution können Polypeptide durch das Nachahmen des natürlichen Prozesses, in einer Serie von Diversifikations- und Selektions-Zyklen, mit neuer oder erhöhter Aktivität erschaffen werden. Einerseits können Proteine dementsprechend unter Berücksichtigung der chemischen Information *de novo* gestaltet werden. Andererseits können Proteine aber auch umgestaltet werden, indem man zu Beginn des Designs ein existierendes Gerüst als Templat verwendet⁹.

Ribosomales Display ist eine leistungsstarke Technik um Proteine, die an ein bestimmtes immobilisiertes Ziel binden, zu selektieren. Neben Antikörpern wurden auch designte Ankyrin-Repeat Proteine (DARPin) als bindende Proteine etabliert¹⁰. Der hydrophobe Kern der DARPin ist ein ideales Gerüst um direkt an eine Azobenzol Gruppe zu binden. Das Zielmolekül für die Entwicklung eines Azobenzol Bindeproteins (ABP) wurde synthetisiert. Wenn die Experimente des ribosomalen Displays erfolgreich sind, könnten ABPs mit anderen Systemen kombiniert werden und zum Beispiel als lichtschtbare Diagnostika und Therapeutika Anwendung finden.

Abgesehen von der Rolle als Neurotransmitter, kann Glutamat auch exzitotoxisch auf Neuronen wirken, wenn es in hohen Konzentrationen in der Nähe der entsprechenden Glutamatrezeptoren vorliegt. Die Hyperaktivität an Synapsen könnte eine Rolle bei Schizophrenie und bei den neurodegenerativen Erkrankungen wie

ABSTRACT

Chorea Huntington, Epilepsie und Alzheimer spielen¹¹. In den vergangenen Jahren wurde deshalb versucht iGluR Antagonisten mit einer akzeptablen therapeutischen Verträglichkeit und mit einem hohen Sicherheitsprofil zu entwickeln.

Co-Kristallisationsversuche der GluA2-LBD mit einem lichtschtbaren Liganden ergaben eine tetramere Struktur. Die Bindungsstelle des Liganden war jedoch anstatt des Lichtschalters mit einem Puffermolekül und einem Sulfation besetzt. Anhand dieser Struktur wurde eine neue Klasse von Glutamaterezeptor Antagonisten konzipiert. Das Molekül wurde synthetisiert und elektrophysiologische Experimente bestätigten die erwartete Wirkungsweise. Die Wasserlöslichkeit des Antagonisten ist sehr hoch und seine Struktur lässt noch Raum für zusätzliche Substituenten um die Affinität zu beeinflussen.

Mit Licht betriebene molekulare Maschinen könnten in Zukunft bei Geräten auf der Nanometerskala eine Rolle spielen¹². Zu diesem Zweck wurde ein Azobenzol mit zwei Befestigungsstellen synthetisiert. Die zwei Takte eines molekularen Motors könnten den unterschiedlichen möglichen Konfigurationen des Moleküls entsprechen. Allgemein würde der molekulare Motor aus DNA Origami und dem Azobenzol Molekül bestehen. Jedoch befinden sich die Experimente gegenwärtig in einer frühen Phase und stagnieren aufgrund technischer Limitierungen.

Ortho-substituierte Azobenzole besitzen interessante Eigenschaften in Bezug auf die Stabilität und das Absorptionsverhalten. Durch bestimmte Substituenten können Moleküle erzeugt werden, die sehr lange Halbwertszeiten in beiden Konfigurationen aufweisen¹³. Solch ein Molekül wurde synthetisiert und Versuche der Kontrolle der molekularen Chiralität mit zirkular polarisiertem Licht können möglicherweise in naher Zukunft durchgeführt werden.

Andere Substituenten führen zu rot verschobenen Wirkungsspektren¹⁴. Dies ist aufgrund einer höheren Eindringtiefe und einer geringeren Phototoxizität von Vorteil für medizinische und biologische Anwendungen. Rot verschobene Verbindungen werden zum Beispiel für Experimente zur Wiederherstellung des Sehvermögens benötigt. Ein Baustein eines rot verschobenen iGluR Agonisten wurde hergestellt und die letzten Experimente zur Synthese des Liganden werden derzeit durchgeführt.

Part II: INTRODUCTION

Chapter 3: Ionotropic glutamate receptors

3.1 Appearance

Chapter 3 about ionotropic glutamate receptors is based on a book and a review published in 2008 and 2011, respectively^{15,16}. The CNS is a never resting conglomeration of cells permanently receiving, analysing and realizing information. To manage all these tasks and to control the entire body directly or in an indirect fashion, the nervous system possesses an immense amount of specific cells. In 1891 Waldeyer formulated his neuron theory, which said that the CNS does not consist of a continuum of cytoplasm but many individual cells – the neurons¹⁷.

Although the brain is a very complex neural network there are many characteristics that simplify the understanding of its *modus operandi*. For example, there are only two types of signals in the nervous system, an electrical and a chemical one. In 1848 Du Bois-Reymond showed that electric current plays a role in neural conduction¹⁸. The electrical signals in all neurons of the body are in principle identical and they are very similar in different animals. Therefore, the neural impulse can be handled as stereotypical unit and universal carrier for transmitting information. In 1952 Huxley and Hodgkin yielded together with Katz the sodium theory of the action potential. These signals propagate along the nerve with a velocity of approximately 80 m/s, are about 0.1 volt in amplitude and last about 1 millisecond.

In synapses, a term introduced by Sherrington in 1897, the electrical signal can be transformed into a chemical one, which passes on the information to the following cell. Chemical synapses can be excitatory or inhibitory. The synaptic cleft between two neurons spans 20 – 40 nm. It consists of a nerve ending on the presynaptic side and the specialized area of a receiving cell on the postsynaptic side. The presynaptic nerve ending contains characteristic vesicles, the synaptic vesicles, in which transmitters are stored¹⁷. These chemical signals are called neurotransmitters. Glutamate is a low molecular weight active substance and the most frequently occurring excitatory neurotransmitter. The major precursor of the neurotransmitter glutamate is glutamine. The conversion of glutamine to glutamate is carried out by the enzyme glutaminase in nerve terminal mitochondria¹⁹.

When an action potential arrives at the synapse, vesicles containing glutamate merge within the neuron's plasma membrane and release their contents outside the cell.

INTRODUCTION

Glutamate diffuses from the presynaptic to the postsynaptic neuron and binds to receptors there, activating the postsynaptic cell. The released glutamate in the cleft is cleared away by glutamate transporters²⁰. In summary, chemical transmitters released from presynaptic terminals diffuse across the synaptic cleft and activate receptors on the postsynaptic cell, with glutamate being the predominant molecule for transmitting the flow of information from one neuron to another in an excitatory fashion^{1,21,22}.

3.2 General characteristics and architecture

Proteins can be divided into different classes. Membrane receptor proteins belong to the class of membrane proteins and initiate the first step in the cellular response to a signal. The subclass of ligand-gated ion channel (LGIC) protein complexes is a group of transmembrane ion channels that open or close in response to specific chemical ligands, such as neurotransmitters. LGICs that participate in fast synaptic transmission comprise the nicotinic acetylcholine, 5-hydroxytryptamine₃, γ -aminobutyric acid_A, glycine, P2X and iGluR families²³. iGluRs are implicated in nearly all aspects of nervous system development and function. Also, they are involved in chronic neurodegenerative conditions, in psychiatric disorders and in acute injury or trauma²⁴⁻²⁷.

In general, iGluRs belong to the glutamate receptor family, which also includes metabotropic glutamate receptors (mGluRs)²⁸⁻³⁰. The iGluR subunits can be subdivided into four main subfamilies, the *N*-methyl-D-aspartate (NMDA) type, the α -amino-3-hydroxy-5-methyl-4-isoxazolepropionic acid (AMPA) type, the kainate type and the orphan receptors. This thesis only focuses on the AMPA and kainate family of non-NMDA ionotropic receptors, which are clearly distinguished from NMDA receptors²⁴. Non-NMDA receptors are the key players for mediating excitatory synaptic transmission in the brain. Moreover, non-NMDA receptors show kinetics on a millisecond timescale in contrast to a timescale of tens of hundreds of milliseconds for NMDA receptors^{31,32}. Furthermore, NMDA receptors require membrane depolarization to release the magnesium block together with binding of glycine and glutamate for activation. In opposition, AMPA and kainate receptors only demand glutamate^{33,34}.

INTRODUCTION

Despite divergent functional properties, the resemblances between different iGluR family members show strong links in the structures. The high homology among all iGluRs suggests a common ancestral gene³⁵. NMDA and non-NMDA receptors are tetrameric and the given combination of subunits is expressed as a tetramer^{36,37}.

The identification of different subtypes of receptors is mainly based on electrophysiological and biochemical studies using selective agonists and antagonists. In 2000, a new terminology for glutamate receptor subunits was proposed by Lodge and Dingledine, which is more in line with IUPHAR guidelines and the previous and present nomenclature is shown below for non-NMDA receptors²³.

New terminology	GluA1	GluA2	GluA3	GluA4	GluK1	GluK2	GluK3	GluK4	GluK5
Previous name	iGluR1	iGluR2	iGluR3	iGluR4	iGluR5	iGluR6	iGluR7	KA1	KA2
	AMPA family				Kainate family				

Table 1: Previous and present iGluR nomenclature.

There are four known subunits of AMPA receptors with two alternative splice variants of each designated as flip and flop, and five high affinity kainate receptor subunits^{38,39}. In 1989, the first functional iGluR has been cloned. Most kainate receptor subunits have been cloned in the early 1990s by the groups of Heinemann and Seeburg. The genes are denoted *GRIK1 – 5* in sequential order of cloning⁴⁰⁻⁴³. Genes encoding the AMPA receptors are named *GRIA1 – 4* and share similar overall structures. The translated protein subunits contain 850 – 900 amino acids^{44,45}. All AMPA and kainate receptor subtype complexes are permeable to Na⁺ and K⁺. Receptors lacking Q/R site-edited GluA2 or GluK5/6 subunits are also permeable to Ca²⁺⁴⁶.

The linear polypeptide chain with the domain organization is shown in **figure 1 A** and the topological overview is illustrated in **figure 1 B**. All AMPA and kainate receptor subunit proteins have an amino- or N-terminal domain (A/NTD) and a LBD, extracellularly. The ATD and the LBD show strong sequence homology to periplasmic bacterial amino acid binding-proteins and fold into clamshell-like structures^{47,48}. In addition there are three transmembrane domains (TMD) M1, M3

INTRODUCTION

and M4, one reentrant loop M2, which enters and exits the membrane on the cytoplasmic side, and an intracellular C-terminal part⁴⁹.

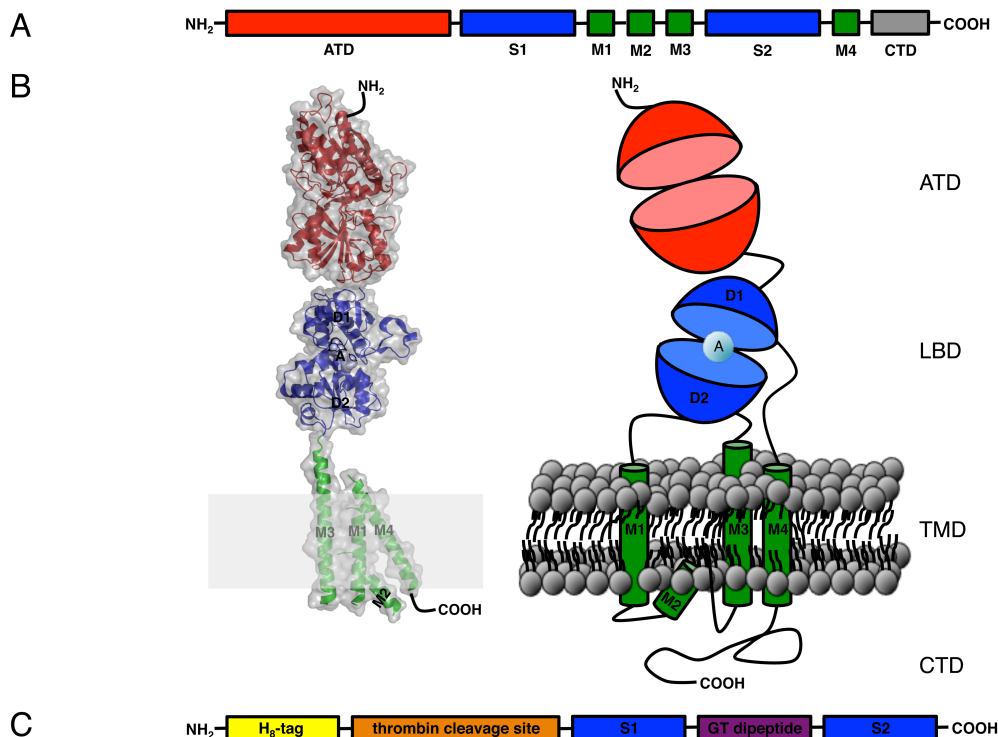


Figure 1: Topology of the iGluR subunit and construct for crystallization. (A and B, PDB entry 3KG2) Linear polypeptide chain and schematic representations of the domain organization with the ATD in red, the LBD consisting of the S1 and S2 segments divided into domain1 (D1) and domain2 (D2) in blue, with a bound agonist or competitive antagonist (A) in light blue, the TMD with helices M1, M2, M3 and M4 in green and the C-terminal domain (CTD). (C) Construct for crystallization of soluble LBDs with an octa histidine tag (yellow), a thrombin cleavage site (orange) and S1 and S2 (blue) connected *via* a GT dipeptide (magenta).

Previous to the ATD there is a short signal peptide that targets the protein to the membrane and which is removed by proteolytic cleavage after membrane insertion²⁴. The ATD does not bind glutamate but is important for subunit-specific assembly and may have roles in desensitization and modulation of other channel kinetics^{50,51}. The bi-lobate LBD-structure is comprised of two separate polypeptide segments named S1 and S2, which are intermitted by the ion channel pore⁵². The notations D1 and D2 represent the overall folds of the two lobes, which are differing slightly from the S1 and S2 sequences. The LBD is essential for agonist/competitive antagonist binding. It is possible to excise the LBD from an iGluR subunit and express this part as a soluble protein suitable for crystallization^{53,54}. Engineering efforts have succeeded in creating a recombinant construct, which is depicted in **figure 1C** and which is

INTRODUCTION

composed of the S1 and S2 sequences connected through a short polypeptide^{53,55}. For purification reasons there is additionally an N-terminal octa histidine tag, which can be removed *via* a thrombin cleavage site. The soluble construct shows ligand-binding affinities comparable to that of full-length subunits and has been crystallized in complex with a number of agonists and antagonists⁵⁶⁻⁶³.

In the full-length receptor the LBD is connected to the membrane-spanning ion channel through three short linker segments. These linker regions are important for gating in response to agonist binding⁶⁴⁻⁶⁶. For example, the S1-M1 linker harbours a short pre-M1 helix acting like a cuff around the top of the ion channel domain⁶⁰.

M1, M3 and M4 are transmembrane spanning α -helices and M2 is a central pore-like helix^{67,68}. M1 and M4 reside on the exterior of the ion channel, with M4 making extensive interactions with adjacent subunits resembling its crucial role in receptor assembly^{60,66}. M2 is found within the pore and M3 lines the inside of the ion channel forming the putative ion permeation pathway^{60,69}. Superimposing the TMD of GluA2 onto the K⁺ channel from *S. lividans* (KcsA) shows an overall similarity of the ion conduction pathway. Moreover, the central cavity in GluA2 is similar to that observed in potassium channels^{60,68}. The region in KcsA that confers ion selectivity, however, is disordered and completely different in amino acid sequence. This is consistent with the fact that K⁺ channels are highly selective in contrast to iGluRs.

The C-terminal intracellular domain, which is involved in receptor localization and regulation, is highly variable in sequence and size among iGluRs and can be alternatively spliced and modulated by specific interactions with phosphatases and protein kinases. This is the main anchoring domain for protein–protein interactions as well^{24,70,71}.

3.3 Quaternary structure

Mature functional iGluRs are tetramers existing as dimer of dimers formed in the endoplasmic reticulum⁴⁹. Although native receptors are thought to exist almost exclusively as heterotetramers⁷²⁻⁷⁴, AMPA and kainate subunits can also form functional homotetramers^{37,75-77}.

Electron microscopy structures supported the tetrameric stoichiometry of recombinant and native AMPA receptors⁷⁸⁻⁸⁰. In 2009, the X-ray structure of an intact full-length homotetrameric eukaryotic GluA2 receptor in complex with a competitive

INTRODUCTION

antagonist has been solved at 3.6 Å resolution by Sobolevsky and presents detailed information about symmetry and mechanisms⁶⁰. This structure is shown in **figure 2**.

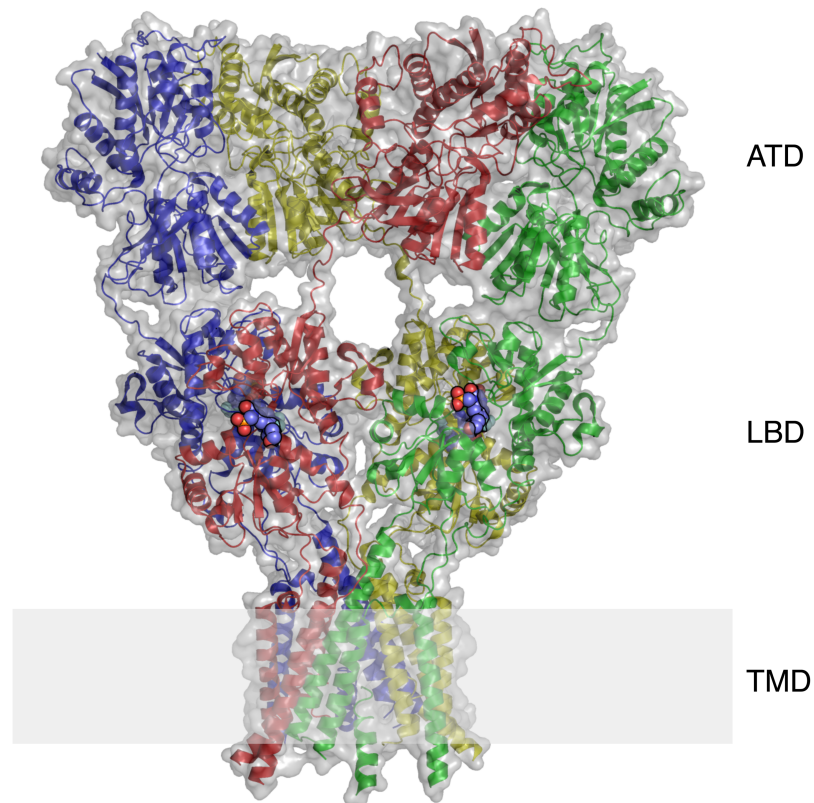


Figure 2: GluA2 quaternary structure. Full-length GluA2 homotetramer (PDB entry 3KG2) shown with a translucent surface bound to ZK200775 highlighted as spheres in blue. The individual subunits are diagrammed as cartoons in green, yellow, red and blue, respectively, and the membrane is displayed as a gray rectangle.

The three main domains are arranged in layers, with the LBD sandwiched in between the TMD and the ATD. The receptor is shaped like the capital letter Y and reflects an overall axis of two-fold symmetry with the extracellular domains organized as pairs of local dimers and the ion channel featuring four-fold symmetry⁶⁰. The overall two-fold axis relates one LBD- and ATD-dimer to the second, respectively, and half of the pore-forming TMD to the other half^{81,82}.

The ATDs and the LBDs form each two different types of subunit–subunit contacts, one within each dimer and one at the dimer–dimer interface, which is located on the overall axis of symmetry. This is in accordance with data observed in crystals of the isolated LBD and ATD^{56,82}. However, the local dimer two-fold axes for the ATDs and LBDs do not align with each other, the relationship between LBD dimers is not perfectly two-fold symmetric and there is a subunit-crossover between the ATD- and the LBD-layer. This means, that subunits switch proximity to the overall two-fold axis

INTRODUCTION

between the ATD and LBD layer, which is mediated by the polypeptides linking the individual domains⁶⁰.

This unorthodox subunit arrangement and molecular symmetry has been confirmed by subunit disulphide crosslinking experiments under native conditions⁶⁰. Due to the observation that GluK2-ATD and -LBD structures show similar dimer-of-dimer arrangements, kainate receptors should exhibit a similar quaternary structure as well^{83,84}.

The four-fold axis of the pore is very well aligned with the overall two-fold axis of symmetry. Transitions in symmetry between the ion channel and the extracellular domains are located on the linker regions between the LBD and TMD. These linker regions are the central elements of the gating machinery transforming ligand-induced changes in the LBD into movement of the TMD⁶⁰.

Altogether, the full-length GluA2 structure proves the mechanisms developed for activation, desensitization and inhibition. The basis for the development of mechanistic models for functional and pharmacological features of iGluRs have been provided by the huge amount of LBD and ATD X-ray structures solved beforehand.

3.4 Ligand-binding mode

The LBD folds into a clamshell-like structure with S1 and S2 individually comprising most of each clamshell (D1 and D2). D1 is predominantly composed of the N-terminal side of M1 in S1 and D2 is in large part formed by the S2 segment between M3 and M4. The binding pocket is located deep within the cleft between the two globular domains, which are held together by a flexible hinge region. The numerous crystal structures existing are the structural basis for evaluating agonist selectivity among different subclasses and molecular determinants of full agonists and partial agonists as well as competitive antagonists^{85,86}. The ligand glutamate interacting with receptor residues of GluA2 and GluK2 is depicted in **figure 3 A** and **B**, respectively.

In GluA2 the α -amino group of glutamate forms a tetrahedral network of interactions with the backbone carbonyl group of a proline (P478), the hydroxyl group on the side chain of a threonine (T480) and the γ -carboxyl group on the side chain of a glutamic acid residue (E705) of the protein. The α -carboxyl group interacts with the guanidinium group on the side chain of an arginine (R485), the backbone NH of a threonine (T480) and the backbone NH of a serine (S654). The γ -carboxyl group

INTRODUCTION

forms a contact to the backbone NH and to the hydroxyl group on the side chain of a threonine (T655) protein residue. The position occupied by the γ -carboxyl group of glutamate shows some variability among different iGluR agonists. For example, the interaction of the isoxazole hydroxyl group of AMPA and the backbone NH of the same threonine (T655) is mediated *via* a water molecule. The side chain of a tyrosine (Y450) forms a lid and narrows the space in the ligand-binding pocket⁵⁶. On the basis of ligand-binding affinities comparable to the full-length subunit, this binding mode observed in the crystallizable LBD construct accurately resembles the binding sites in intact receptors⁶⁰.

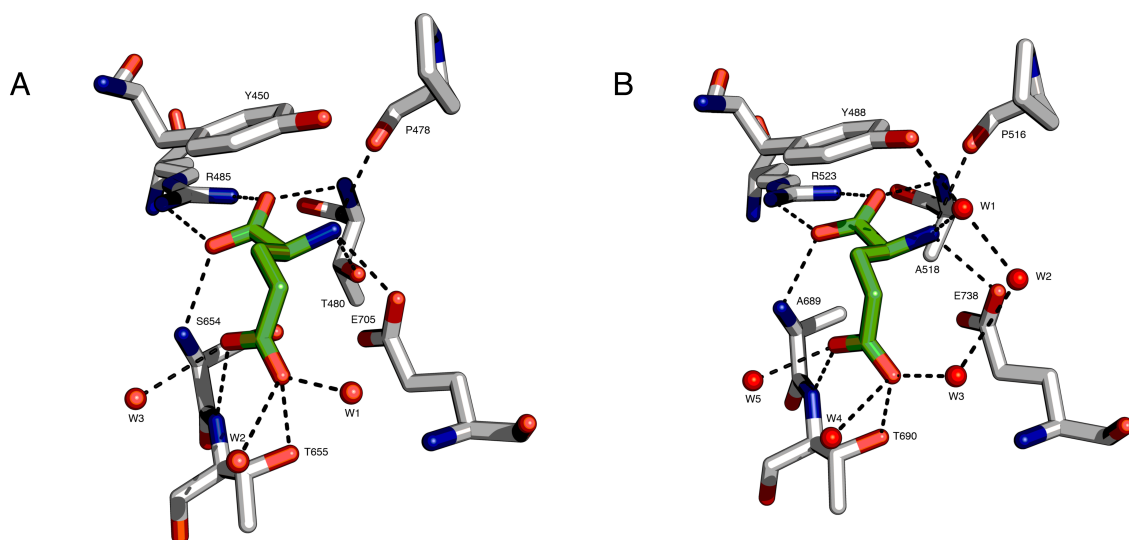


Figure 3: Glutamate–receptor interactions in the binding pocket. (A and B) Overview of the GluA2 (PDB entry 2UXA) and GluK2 (PDB entry 1S7Y) ligand-binding sites (gray sticks), respectively, with bound glutamate (green sticks) and trapped water molecules (red spheres). Black, dashed lines indicate hydrogen bonds and ion pair interactions. Residues are numbered according to the total protein without the signal peptide for GluA2 and with the signal peptide for GluK2.

In contrast to AMPA receptors, kainate receptors have larger binding cavities. GluK1 and GluK2 binding pockets are 40% and 16% larger than the one of GluA2. Therefore, steric occlusion is one important parameter to discriminate between AMPA and kainate receptors as well as between GluK1 and GluK2^{87,88}. According to the available space in the binding pocket, there are different amounts of water molecules involved in the binding of glutamate. Six and five water molecules are present in GluK1 and GluK2, respectively, opposed to four in GluA2. The additional water molecule in GluK1 is responsible for selective ligands over GluK2⁶¹. Thus, the

arrangement of water molecules participating in bridged interactions is the key for subunit selectivity.

Another difference in GluK2 is a missing hydrogen bond present between the α -amino group of glutamate and the side chain hydroxyl group of a threonine in GluA2 (T480) and in GluK1 (T533)⁸⁹. The threonine is replaced by an alanine (A518) at this position and an additional water molecule forms a hydrogen bond to the α -amino group of glutamate⁶¹.

Competitive antagonists in contrast stabilize a conformation similar to the empty apo state with little or no clamshell closure. This is in agreement with the fact that clamshell closure is needed for receptor activation⁶⁰. There are three mechanisms known for competitive antagonism. One is steric hindrance of cleft closure by a bulky γ -substituent (ATPO). Other molecules (DNQX) shield the agonist from binding to its initial contact sites and the third type of molecules (willardiines and ZK200775) have a bulky γ -substituent and stabilize the LBD closer to the resting state^{59,62}.

3.5 Mechanisms for activation, gating and desensitization

The mechanism for activation and gating involves a sequence of discrete conformational changes. While in NMDA receptors all four subunits in the tetramer are required to be activated in order to open the channel, in AMPA receptors each subunit can autonomously activate the ion channel^{37,90}. First, the energy-generating process of agonist binding concomitantly changes the conformation of the LBD from the open apo state to the closed holo state^{56,91-93}. Binding of glutamate proceeds *via* a two step dock-and-lock mechanism. A fast docking of the ligand to the residues on S1 is followed by a slow closure with ligand–S2 and D1–D2 interactions taking place^{94,95}. The clamshell closure is allosterically coupled to the opening of the pore through a rotation-leverarm-combination mechanism.

Dimer structures show the monomers to be arranged as two-fold symmetric pairs with the dimer interface formed between the D1 domains *via* hydrophobic interactions^{56,60,61,96}. Therefore, D1 is relatively fixed, whereas D2 is free to move. M1 and M3 of the TMD are attached to the LBD at a position that corresponds to the dipeptide linking S1 and S2 in the construct used for crystallization. An alignment of an apo and a holo structure shows a striking displacement of this linker region by several angstroms as can be seen in **figure 4**. Upon ligand binding, D2 movement

INTRODUCTION

consequently leads to a displacement of this linker region and therefore exposes M1 and especially M3 to conformational strain, driving the channel to open^{56,61,93,97}. With this mechanism not only agonism, but antagonism and partial agonism can be explained as well. The differences of clamshell closure correspond to a variation in strain pulled on the TMD⁵⁸.

Mutational studies showed that the molecular determinants critical for gating appear to be within M3, which contains the SYTANLAAF motif⁹⁷⁻⁹⁹. This highly conserved motif is in proximity to the crossing of the M3 helices in the closed conformation, occluding the ion channel permeation pathway. Furthermore, the pathway is clogged above this motif by a pair of methionine residues⁶⁰. The extent of conformational movement is greater for the distal subunits when compared to the proximal pairs. Consequently, they might be more important for gating. All in all, the transmembrane helices will be bend and splay away from the central axis of the channel upon ligand-binding, mimicking the iris-like opening of K⁺ channels^{60,100}.

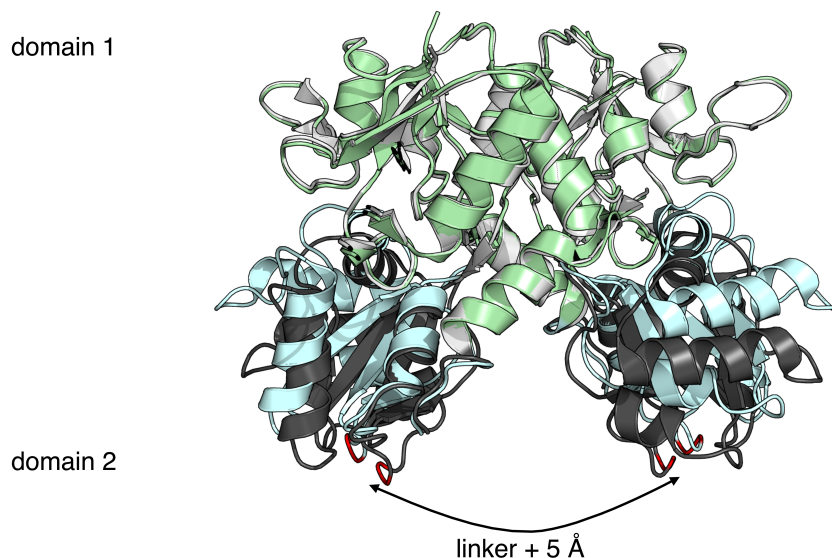


Figure 4: Separation of linker segments upon ligand binding. Closed GluA2-LBD•glutamate (PDB entry 1FTJ; D1 green and D2 blue) and open apo GluA2-LBD (PDB entry 1FTO; D1 light grey and D2 dark gray) structure. The alignment of the glutamate bound GluA2-LBD-D1 with the apo GluA2-LBD-D1 shows a rotation of D2 (19°) upon ligand binding along with a displacement of the linker region (red, 5 Å) that corresponds to the attachment of the transmembrane domains in the full length subunits.

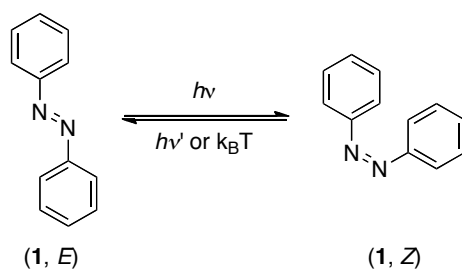
In addition to the agonist-binding site, the LBD is also involved in binding of various allosteric modulators that can influence desensitization and deactivation. Desensitization could modulate the excitatory postsynaptic transmission, but may also provide a protective mechanism against receptor overactivation^{101,102}. AMPA

and kainate receptors exhibit a fast desensitization. Domains involved in desensitization have been determined by mutational studies and the dimer interface of the LBD is important for the transition to this state^{96,103,104}. On a structural basis, the strain generated through closing of the clamshell upon agonist binding can either be released by movement of the gating domain in the ion channel or by reorientation of the dimer interface into a relaxed, desensitized conformation, with a different dimer interface, which is energetically more favorable⁸¹. The rupture of the LBD D1–D1 interface and rigid-body rotation of the individual binding domains allow the receptor to stay in a closed like state, without opening the LBD. This rearrangement should also demand movement of the ATD and ATD-LBD linkers⁶⁰. In contrast, Cyclothiazide, an inhibitor of desensitization and a non-desensitizing mutant, both mediate additional interactions and influence the stability of the dimer interface. By stabilization of the constraint interface cleft opening and agonist release is prevented. Therefore the receptor is trapped in the active state¹⁰⁵.

Chapter 4: Azobenzenes

4.1 Characteristics

Chapter 4 briefly summarizes a book and a review published in 2009 and 2012, respectively^{106,107}. In 1834, azobenzene has been observed for the first time by Mitscherlich¹⁰⁸. In 1856, Noble described azobenzene as yellowish-red crystalline plates¹⁰⁹. The completely reversible photochemical *E,Z*-isomerization of the $-(N=N)-$ bond has been reported by Hartley in 1937¹¹⁰. The isomerization is shown for azobenzene (**1**) in **scheme 1**.



Scheme 1: Azobenzene isomerization. Photoisomerization between the two azobenzene (**1**) states is reversible and the (*E*) configuration (left) is thermodynamically more stable than the (*Z*) configuration (right).

INTRODUCTION

Upon absorption of photons of different wavelengths of light ($h\nu$, $h\nu'$) the steady-state *trans*–*cis* composition in the photostationary state can be shifted. The unique steady-state composition mainly depends on the quantum yields (Φ_{trans} and Φ_{cis}) and the thermal relaxation. In general, the *trans* form, which adopts a planar structure with C_{2h} symmetry is about 50 kJ/mole more stable than the *cis* isomer assuming a non-planar conformation with C_2 symmetry. In the dark > 99.99% are in the *trans* state¹¹¹⁻¹¹⁴. The energy barrier of the photoexcited state is about 200 kJ/mol and the barrier for thermal isomerization is about 90 kJ/mole^{115,116}. Azobenzenes show a high photostability even after prolonged irradiation and due to the thermodynamic stability of the *trans* isomer, the *cis* \rightarrow *trans* isomerization occurs spontaneously in the dark, except for bulky substituted azobenzenes or inverted bridged azobenzenes^{89,117}. *Ortho*-alkylated azobenzenes show twisting of the phenyl rings in the *trans* configuration and slower thermal isomerization rates can be attributed to steric hindrance between the *ortho* alkyl substituent and the orbitals on N-atoms undergoing inversion^{118,119}.

Spectra of *trans*- and *cis*-azobenzenes are distinct but can be overlapping. The *trans*-azobenzene has two well separated absorption bands. A strong, symmetry allowed $\pi \rightarrow \pi^*$ ultraviolet (UV) band, and a weak, symmetry forbidden $n \rightarrow \pi^*$ visible region band. The $n \rightarrow \pi^*$ transition is allowed because of vibrational coupling and a minimal extent of nonplanarity^{120,121}. The *cis*-azobenzene has a weaker $\pi \rightarrow \pi^*$ transition, but the $n \rightarrow \pi^*$ transition absorbs more strongly than the *trans*-azobenzene^{122,123}. The different transitions excite azobenzenes to S1 ($n \rightarrow \pi^*$) and S2 ($\pi \rightarrow \pi^*$) states^{124,125}. The strong absorption of the π system can be affected by different substituents on the phenyl ring and can thereby vary from the UV to visible red regions. *Ortho*- or *para*-substitution with electron donating groups leads to the group of aminoazobenzenes, which have very close, almost overlapping $n \rightarrow \pi^*$ and $\pi \rightarrow \pi^*$ bands. Acceptor- and donor-substitution with a push–pull substitution pattern shifts the $\pi \rightarrow \pi^*$ to the red, but does not change the $n \rightarrow \pi^*$, leading to a reversed ordering of absorption bands observable in this class of pseudo-stilbenes^{114,126}.

This effect can be explained by regarding the excited state with a higher dipole character than the ground state. Donating substituents better stabilize the excited state, which leads to ground state red-shifts with increasing dipole character. The

activation barrier is lower, and therefore thermal relaxation is accelerated as well^{122,127,128}.

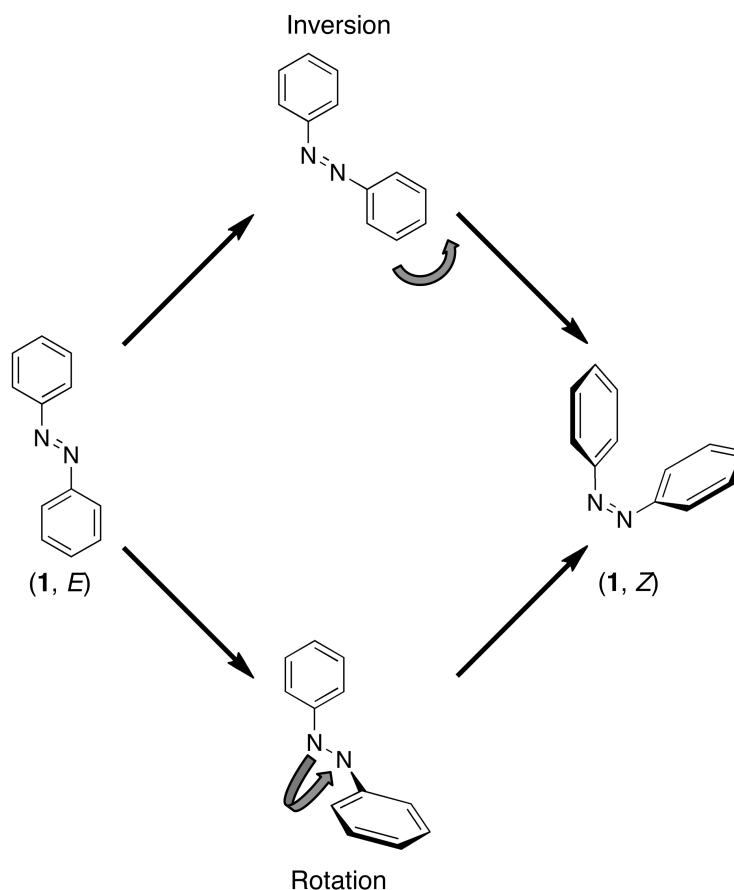
Moreover, the absorption of azobenzenes can also be solvent- and packing-dependent (π -stacking), amino- and pseudo-stilbene-azobenzenes can show fluorescence, but phosphorescence is absent in all azobenzenes. The chemical fine tuning of these compounds was extensively studied in connection with dyes and colorants and approximately 70% of the world's commercial dyes are azobenzene derivatives^{129,130}.

4.2 Mechanism of isomerization

The first *cis*-azobenzene was isolated more than eighty years ago by Hartley¹¹⁰. However, the mechanism of isomerization is still of interest and there is a lot of controversy about it. The rotation about the N–N bond with a rupture of the π bond is one possibility. In the other, the molecule has a semilinear and hybridized transition state with the π bond intact. The two pathways described are depicted in **scheme 2**. Rotation changes the C–N–N–C dihedral angle while the N–N–C angle remains fixed at 120° ¹³¹. In the inversion mechanism, one N=N–C angle increases to 180° while the C–N=N–C dihedral angle remains fixed at 0° with one sp-hybridized azo-nitrogen atom¹³². Also, concerted-inversion and inversion-assisted rotation mechanisms are in discussion¹⁰⁷.

Relaxation to *trans* and *cis* is allowed from all transition states. Thermal relaxation occurs *via* rotation, whereas photochemically both routes seem to be accomplishable¹³³. First, a rotation mechanism with little inversion contribution has been favoured, but more recently inversion is strongly supported^{134,135}. Calculations report both pathways to be energetically accessible^{136,137}. The preferred pathway depends on the substitution pattern and the environment¹³⁸.

Upon isomerization, the characteristics of azobenzenes change. The phenyl rings are twisted about 55° out of plane from the azo group, the distance between the 4 and 4' positions is reduced from 0.99 nm in the *trans* to 0.55 nm in the *cis* state and the dipole moment increases from near zero for *trans* to 3.1 D for *cis*^{110,139-141}.



Scheme 2: Azobenzene isomerization. The isomerization from (*E*)-azobenzene (**1**) (left) to the (*Z*)-isomer (right) can, *inter alia*, proceed *via* inversion (top) or through rotation (bottom).

Chapter 5: Azobenzenes in biology

5.1 General background

Chapter 5 mainly refers to a book and a review published in 2009 and 2011, respectively^{106,142}. The most interesting property of azobenzenes is the conformational change they undergo upon irradiation, and in combination with their geometrically rigid structure the molecules have a great potential for different applications^{5,143-146}. Diverse biological processes such as photosynthesis and vision are triggered by light^{147,148}. Here, proteins have light sensitive properties in regard to the chromophore they harbour. Opsin, for example, is regulated through *cis/trans* isomerization of the reversibly bound cofactor retinal¹⁴⁹.

One of the earliest studies of azobenzenes in biological systems regarded these molecules in model membrane systems, and pioneering work with azobenzenes and acetylcholine receptor channels in the late 1970s showed their potential for future investigations^{150,151}. The important changes of properties such as molecular shape

and dipole moment can be imparted to structures hosting the azobenzene. The volume required for isomerization *via* inversion and rotation is about 0.12 nm³ and 0.38 nm³, respectively, and the force generated is on the nanoscale^{117,152-154}. In molecular dimensions this is a very large volume and therefore it is ideal for affecting host systems like proteins¹⁵⁵. The isomerization of azobenzenes is in the picosecond timescale, thus faster than most biological processes^{156,157}.

Photoregulated polypeptides with reversible α -helix to β -sheet conversions or DNA-binding have been investigated¹⁵⁸⁻¹⁶². Also, light dependent activity control of enzymes such as papain, chymotrypsin, lysozyme, tyrosinase and of restriction enzymes have been in the context of research¹⁶³⁻¹⁶⁶. Other research topics are the incorporation of non-natural chiral azobenzene amino acids into proteins and monitoring of protein folding¹⁶⁷⁻¹⁷⁰. Moreover, light can also be a powerful external stimulus to trigger a change of the properties of effectors such as membrane proton pumps. A bacteriorhodopsin analog hosting an azobenzene rather than retinal was a model for studying rhodopsin and the physicochemical properties of the complex¹⁷¹.

5.2 Photoswitchable ligands

The photocontrol of proteins can be achieved *via* two different approaches. On the one hand, azobenzene photoswitches can be directly used to influence the protein structure and thereby function by crosslinking experiments or incorporation of azobenzenes into proteins^{168,172-176}. On the other hand, protein function can be controlled with photoswitchable ligands. In contrast to the caging approach with irreversible photochemistry the most widely used class of azobenzene photoswitches are reversible ones¹⁷⁷.

Ligands in general control the function of many proteins by means of binding to their active sites, thereby activating or inhibiting their response. Photochromic ligands (PCLs) are ligands, which are conjugated to an azobenzene. With different wavelengths of light, the azobenzene can be reversibly isomerized affecting the ligand structure and activity. Photoswitched tethered ligands (PTLs) act the same way as PCLs, but can be additionally attached to the protein, for example *via* conjugation to a cysteine.

INTRODUCTION

Erlanger and Lester have performed essential work with photoswitchable ligands of the nicotinic acetylcholine receptor and with blockers on chymotrypsin¹⁷⁸⁻¹⁸⁰. In 1991, Gramicidin, a small protein ion channel, has been turned photosensitive¹⁸¹⁻¹⁸³.

Trauner, Isacoff and Kramer applied this concept of photo-controlling ion channels to K⁺ channels and iGluRs^{5,146}. By switching between *cis* and *trans* states of the azobenzene, substituents on the phenyl ring concomittant move and perform a task. Initially, K⁺ ion channels could be gated with light by reversibly blocking or unblocking the pore¹⁸⁴⁻¹⁸⁶. The experiments showed high spatiotemporal precision and the possibility to quickly and cleanly turn a biological process on and off using light in combination with azobenzenes. More recently, iGluRs could be controlled with light by conjugating an azobenzene to the neurotransmitter glutamate. After transferring the PTL approach, also the PCL strategy has been applied to these ligand-gated ion channels^{6,187}.

In **figure 5**, 4-Gluazo (**2**), a PCL reversibly acting on iGluRs, is shown. In the *trans* configuration (500 nm) the ligand binds to the LBD and upon binding the LBD closes like a clamshell. This closure is allosterically coupled to the opening of the pore. In contrast, with the ligand in its *cis* configuration (380 nm), the clamshell cannot close significantly. Therefore, the channel remains in its closed state. However, in order to confirm this mode of action, an image of 4-Gluazo (**2**) bound to its target would be highly informative. X-ray crystallography provides the most direct way of forming images of macromolecules like proteins. With a 3-D image at atomic resolution, detailed information about the binding mode can be obtained.

Biological systems like hippocampal neurons and Purkinje neurons have been photoregulated *in vitro* with this glutamate derivative¹⁸⁸. The PTL strategy with light-gated iGluR (LiGluR) has also been applied *in vivo*, and the behaviour of a zebrafish could be controlled with light¹⁸⁹. Although the PTL approach shows a high degree of specificity, it is often more practical to target wild type systems. For example, the expression of modified genes may have disadvantages under certain environments like the human retina¹⁴².

INTRODUCTION

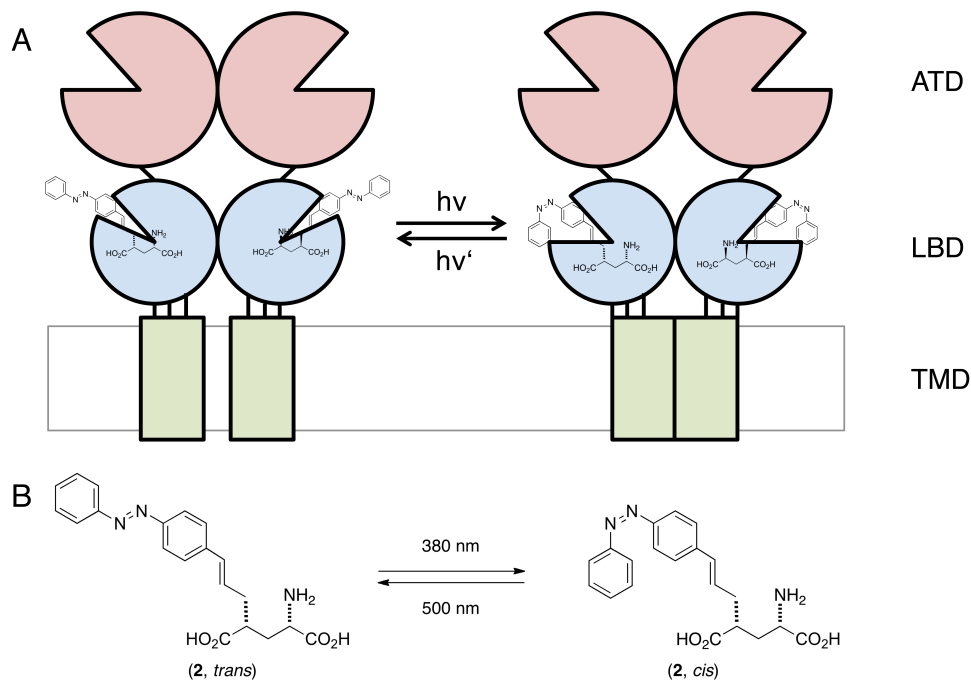


Figure 5: Schematic mode of action and chemical structure of the photoswitch 4-Gluazo (2). (A) Schematic representation of iGluRs with the ATD (red), the LBD (blue) and the TMD (green). The membrane is shown as a gray rectangle. The *trans* configuration of the switch stabilizes the LBD in the closed, active conformation and allosterically opens the pore (left), whereas the *cis* form prevents the LBD from closure upon binding (right). (B) Chemical structure of 4-Gluazo (2) in the *trans* state (500 nm) and in the *cis* state (380 nm).

The photoswitchable ligand approach has also been applied to other and new targets like nicotinic acetyl choline and GABA_A receptors, lately¹⁹⁰⁻¹⁹³. Basically, it is possible to reprogram a wealth of photoinactive biological systems into phototriggerable systems by incorporating azobenzenes, and the studies in this field range from answering fundamental questions to the exploitation of applications.

However, the use inside living organisms is more complicated, since azobenzenes have to fulfill several prerequisites in order to function *in vivo*. Extracellular LBDs of iGluRs have been targeted¹⁹⁴. Though, in order to address targets intracellularly, the photoswitch should be membrane permeable. Also, the wavelength used for isomerization should be compatible with cells and tissues. Moreover, the azobenzene must be stable in the reducing intracellular environment^{195,196}. Some azobenzenes could be reduced by glutathione *in vitro*, while others survived an overnight period, and experiments with azobenzenes have already been successfully conducted inside cells with excellent photoswitching for at least two days¹⁹⁷⁻²⁰⁰.

Chapter 6: Directed evolution

6.1 Ribosome display

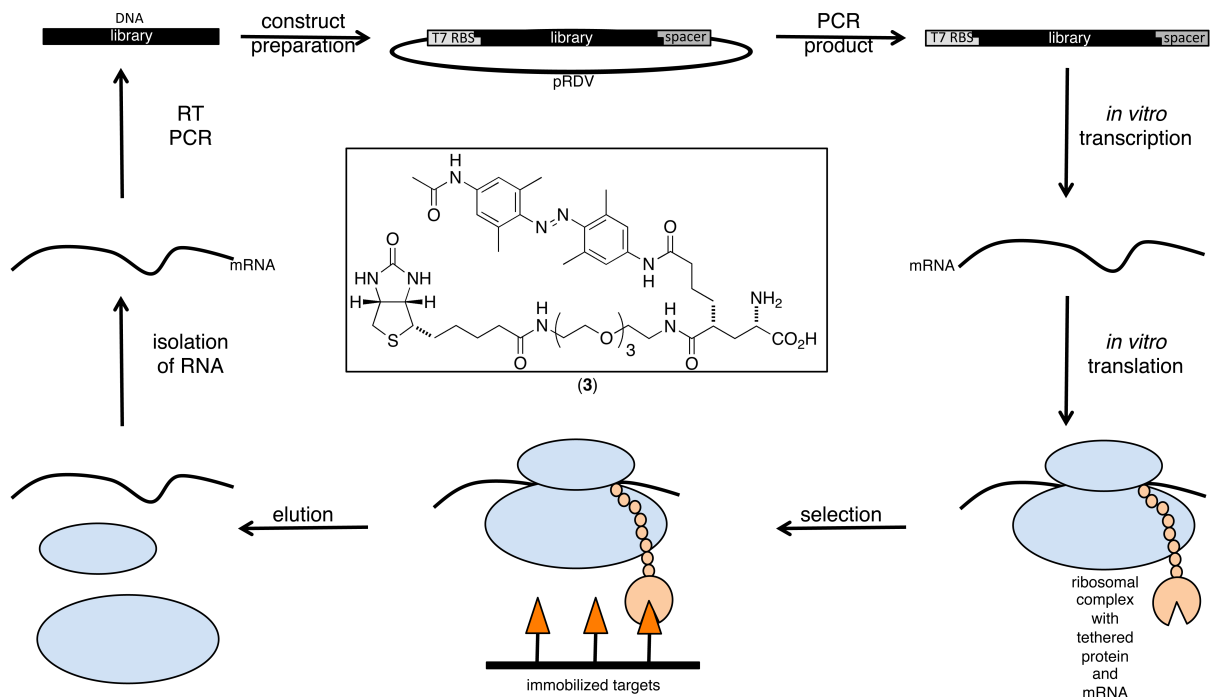
Chapter 6 is based on a review published in 2012²⁰¹. Protein design by evolutionary mimicry can be divided into three parts. First, mutations are introduced to randomize genes. Within the second step, the selection process, interesting molecules are separated. Members with particular properties can be identified either by scrutinizing each member individually or by testing all members simultaneously. Finally, during amplification beneficial mutations accumulate²⁰².

In nature, peptides and proteins have, due to stability reasons, mainly replaced RNA ligands during evolution. With a nucleic acid selection method termed systematic evolution of ligands by exponential enrichment (SELEX) the *in vitro* evolution of functional proteins has been achieved²⁰³. However, the first entirely *in vitro* performed evolution technology for proteins is ribosome display. After key observations, ribosome display has first been described in 1994 and Plückthun reported the first application to whole proteins in 1997²⁰⁴⁻²⁰⁶. The selection method couples phenotype (protein) and genotype (mRNA), and random mutagenesis can be incorporated into the procedure²⁰⁷.

In the first step of ribosome display, which is described in **scheme 3**, DNA with an open reading frame (ORF) of the protein of interest is ligated into the ribosome display vector pRDV, genetically fusing it 3' to a spacer sequence in-frame. The spacers are often derived from the *E. coli* genes *tolA* or *tonB*. At the 5' end, a strong promoter for transcription (T7) and a translation initiation region (a ribosome binding site (RBS) on mRNA level) is provided. In order to prevent the mRNA from degradation through ribonucleases (RNases), the construct should additionally include 5' and 3' stemloops²⁰⁶. The final ribosome display construct is obtained by a polymerase chain reaction (PCR) amplification of both flanking regions and the library insert²⁰⁸. *In vitro* transcription of this PCR product yields mRNA, which does not contain a stop codon. The encoding mRNA is read by the ribosome with the small subunit mediating codon–anti-codon contact to the tRNA and cell-free *in vitro* translation can run to the end of this mRNA.

The protein slides out of the ribosomal tunnel within the large subunit with the peptide chain staying connected to the peptidyl-tRNA through an ester bond within the P-site.

INTRODUCTION



Scheme 3: Overview of the ribosome display selection cycle and target molecule. A DNA library coding for DARPin is ligated into pRDV and amplified by PCR with flanking regions. *In vitro* transcription yields mRNA and after *in vitro* translation, the ternary mRNA-ribosome-protein complex is used for affinity selection of the immobilized target molecule, which is shown in the box in the center. Upon elution and washing, the mRNA is isolated, reverse transcribed and amplified by PCR. This cycle can be repeated iteratively with the selected pools of binders until a binding protein with high affinity has evolved.

Thus, neither protein nor mRNA can leave, generating the ternary complex consisting of displayed proteins and mRNA with the ribosome as the connector. An unstructured region of the protein occupies the ribosomal tunnel and correlates to the spacer on DNA level. Between 20 and 30 C-terminal amino acids are covered by the ribosome and best results have been achieved with a much more longer spacer²⁰⁹⁻²¹¹. The upstream encoded protein is outside the ribosome, can fold correctly and there is sufficient space and flexibility to recognize and interact with ligands. Nascent proteins can fold co-translationally in a cell free system on ribosomes and the crystal structure of the large ribosomal subunit provides the basis for understanding this process^{212,213}. After an optimized period of time with the amount of ternary complex being at the maximum, translation is stopped by fourfold dilution at low temperatures²⁰⁶. These complexes are stable for several days under the appropriate conditions²¹⁴. Next, the ribosomal complexes are exposed to the target of interest in a magnesium containing buffer. One possible target for future experiments is biotin azobenzene glutamate (BAG) (3), which is shown in the center of **scheme 3**. The

INTRODUCTION

target includes a biotin moiety in order to be immobilized to a surface *via* streptavidin, neutravidin or avidin interactions. The overall ligand contains a 30 Å linker towards the biotin moiety, such that the actual ligand part is still accessible to the protein and not hidden in the streptavidin binding pocket. Proteins binding to the target are enriched on the target and competitors are used to wash out binders with low affinity and selectivity. After selection, the small and large ribosomal subunits are eluted and dissociated by the addition of EDTA. The mRNAs are directly isolated, reverse transcribed and PCR amplified for the transcription of the next cycle of ribosome display. Also, random mutagenesis, dNTP analogues or low-fidelity DNA polymerases could be implemented at this stage to diversify the initial library, if evolution is desired²¹⁵⁻²¹⁷. Only proteins that survived the selection will be further used, and during all following selections the mutated proteins have to compete with their progenitors²¹⁴. Thus, this technology allows continuous expanding of new diversity during selection.

In the course of a standard ribosome display reaction $1 - 3 \times 10^{13}$ mRNA molecules are applied and from the amount of *E. coli* extract used, a sufficient excess of about $1 - 4 \times 10^{14}$ assembled ribosomes pass each cycle. With the screening of very large libraries, the possibility to select high affinity binders increases tremendously²¹⁸. Moreover, in contrast to phage technologies, there is no need to introduce the genetic information into cells, which can be quite laborious and library-size limiting²¹⁹⁻²²¹. Furthermore, *in vitro* methods show a higher degree of control²¹⁶. In ribosome display transcription and translation can be carried out either in coupled or in separate reactions, depending on the conditions. T7 RNA polymerase for example requires β -mercaptoethanol, which is reductive, but the generation of disulfide bonds in proteins requires oxidizing conditions^{222,223}. Individual steps can be tailored to the optimal conditions of the protein species assayed.

With the use of a ribosome display system specific binders can be identified from a pool of variants or a given structure can evolve in order to generate new or improved functions^{224,225}. Besides identifying or enhancing binding interactions, factors like enzymatic turnovers, protein stability and biophysical properties in general could be influenced, too²²⁶⁻²²⁸. Ribosome display can be combined with other selection technologies and at the end of the ribosome display procedure individual mutants are expressed in *E. coli* and can be analyzed by different assays^{229,230}.

6.2 DARPins

Proteins comprising an ankyrin repeat motif mediate key protein–protein interactions in nature^{231,232}. These proteins have repeating structural motifs of 20 – 50 amino acids which stack together to form elongated stable structures to allow large surface areas for potential binding²³³.

First, ribosome display evolved and selected specific antibody scFv fragments from immune libraries²²⁵. More recently, DARPins, which are artificial antibody mimetic binding proteins, have been used with ribosome display successfully, too²³⁴.

DARPins contain no cysteine residues, are robust in engineering, show favorable biophysical properties and fold extremely well in an *in vitro* translation system. DARPins consist of a β -turn followed by two antiparallel α -helices and a loop reaching the β -turn of the next repeat^{235,236}. Overall, the repeating units are a 33 amino acid sequence and seven residues can be randomized. The theoretical diversity of this module is 7.2×10^7 . Randomizing these seven residues is enough to screen sufficient sequence space without destroying the structure and function of the protein. Moreover, one domain usually consists of four to six stacking repeats, thereby potentiating the theoretical diversity²³².

DARPins have been generated through consensus and structure based design. The introduction of N- and C-terminal capping repeats is essential for efficient folding and avoids aggregation. While the internal ankyrin repeats have two hydrophobic interfaces, the capping repeats only have one. Instead of the second interface, they have a solvent exposed hydrophilic surface¹⁰. Thus, the hydrophobic core is shielded from the solvent and a concave, groove-like binding surface is generated. The overall structure is stabilized by hydrophobic interactions and hydrogen bonds within and between adjacent repeats.

The domains comprise a variable and modular target-binding surface and typically interact with their partners *via* the protruding β -turns and the following α -helices. There are numerous possibilities for binding a diverse set of ligands in a specific manner, and high affinity binders, some with novel binding specificities, could already be generated down to the picomolar range^{234,237-241}. Moreover, DARPins allow addition, deletion and exchange of individual repeats^{10,240,242,243}. Most of the characteristics mentioned above are in demand for biotechnological applications.

Chapter 7: Bonus

7.1 Glutamate receptor antagonists

The synapse is the site of action of external regulation, *i.e.* the influence of drugs and toxins. Numerous anaesthetics affect synaptic transmission and synapses are the site of a wide range of pathological disorders¹⁷. iGluRs may be important in various pathological conditions and AMPA antagonists may be good candidates for clinical development, as they lack the psychotomimetic action and neurotoxicity observed with NMDA antagonists²⁴⁴.

Neuroprotective effects with the competitive AMPA receptor antagonist NBQX have first been reported in gerbil global ischaemia, but clinical development has been stopped due to the low solubility and the risk of formation of crystals in the tubuli of the kidney^{245,246}. The introduction of a phosphonate group has improved the solubility of quinoxaline diones while maintaining the activity and ZK200775 has had a long therapeutic window. The molecule has made it to the clinic and has progressed to phase IIa, but has then been abandoned²⁴⁷.

Newer molecules appear to show increased solubility, selectivity for various iGluR subunits and seem to produce more robust effects²⁴⁴. The newly developed antagonists morpholino bisphosphonate (MOBIPHOS) (**4**), shown in **figure 6**, is of interest as neuroprotective agent. Moreover, this molecule could possibly be turned into a photoswitchable antagonist.

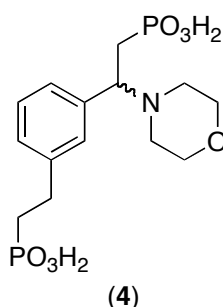


Figure 6: MOBIPHOS (4). An AMPA receptor antagonist.

7.2 Molecular motors

Another application of azobenzenes is the photo-control of DNA. Photoswitchable molecules can interact with oligonucleotides but can also be covalently tethered to oligonucleotides in order to control gene expression with light^{248,249}.

An artificial molecular motor based on azobenzenes has already been demonstrated and recently linear movement of DNA has been achieved^{12,250}. In principle it may be possible to design and build a bio-inspired, light driven artificial molecular motor using DNA-Origami and azobenzenes^{251,252}. The fuel for switching the motor between two states, a contracted and an extended one, like with two-cycle Otto motors, would be light. Myosin switches between two states, too, hydrolysing ATP with the transition being activated by Brownian motion²⁵³.

Azobenzene bis(iodoacetamide) (ABA) (**5**), depicted in **figure 7**, could be used to incorporate an azobenzene into DNA. This type of molecule can be directly attached to a modified DNA backbone *via* its bis(iodoacetamide) moiety through reaction with a phosphorothioate.

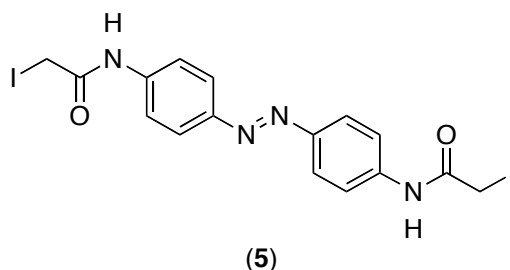


Figure 7: ABA (5). An azobenzene with two attachment sites.

The molecular motor would consist of DNA and would glide on a track consisting of DNA as well. The track would exhibit an affinity gradient repeating itself within each monomer. One could imagine this for example in the context of a charged track. In contrast to the rail, the molecular motor would be asymmetric with a forward negative and a backward positive charge. Moreover, the molecular motor would contain the azobenzene switch. A structural element, for example two rings, would keep the motor on the track. Switching with light between the two different azobenzene configurations would move the motor away from or close to the track. The movement of the motor would be driven by Brownian motion²⁵⁴.

7.3 *Ortho*-substituted azobenzenes

The properties of azobenzenes can be influenced by different substituents. Bulky *ortho* substituted azobenzenes can be stable in both configurations. For example, tetramethyl substituted azobenzenes, like 2,2',6,6'-tetramethyl – quaternary-ammonium – azobenzene – quaternary-ammonium (QAQ) (**6**), pictured in **figure 8**, is a K_v channel blocker and exhibits very long half-lives of the *cis*-isomer^{13,255}. This property is ideal for monitoring the molecular chirality of the azobenzene induced by circularly polarized light. A possible enrichment of one enantiomer upon exposure to right or left circularly polarized light could possibly be interesting for different applications in material science and technology^{256,257}.

Other *ortho*-modified azobenzenes allow photoswitching without UV light. This might be useful for biological applications, because UV light can lead to sideeffects in biological systems, like cellular apoptosis¹⁴. Moreover, red-shifted iGluR ligands, similar to 2,2',6,6'-tetrachloro – maleimide – azobenzene – glutamate (MAG) (**7**), shown in **figure 8**, could possibly be used to treat blindness in humans suffering from macular degeneration and retinitis pigmentosa⁸.

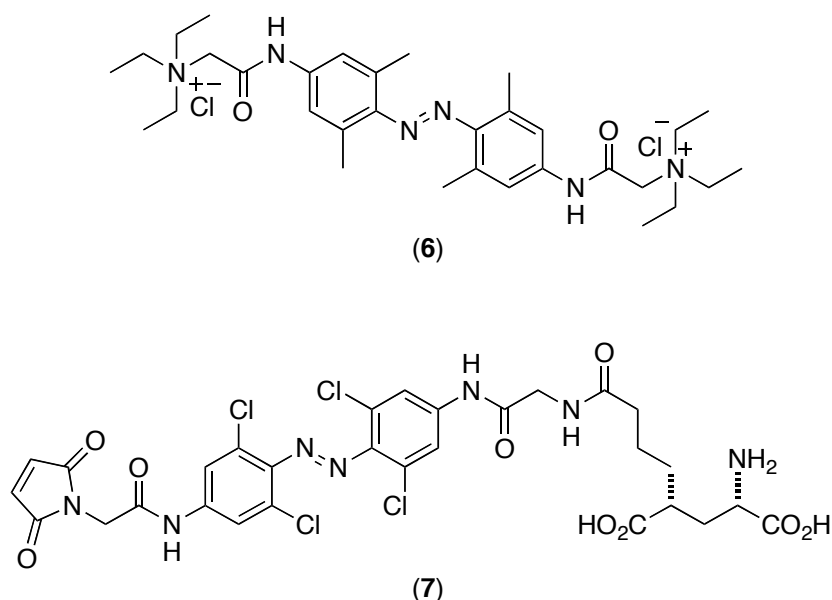
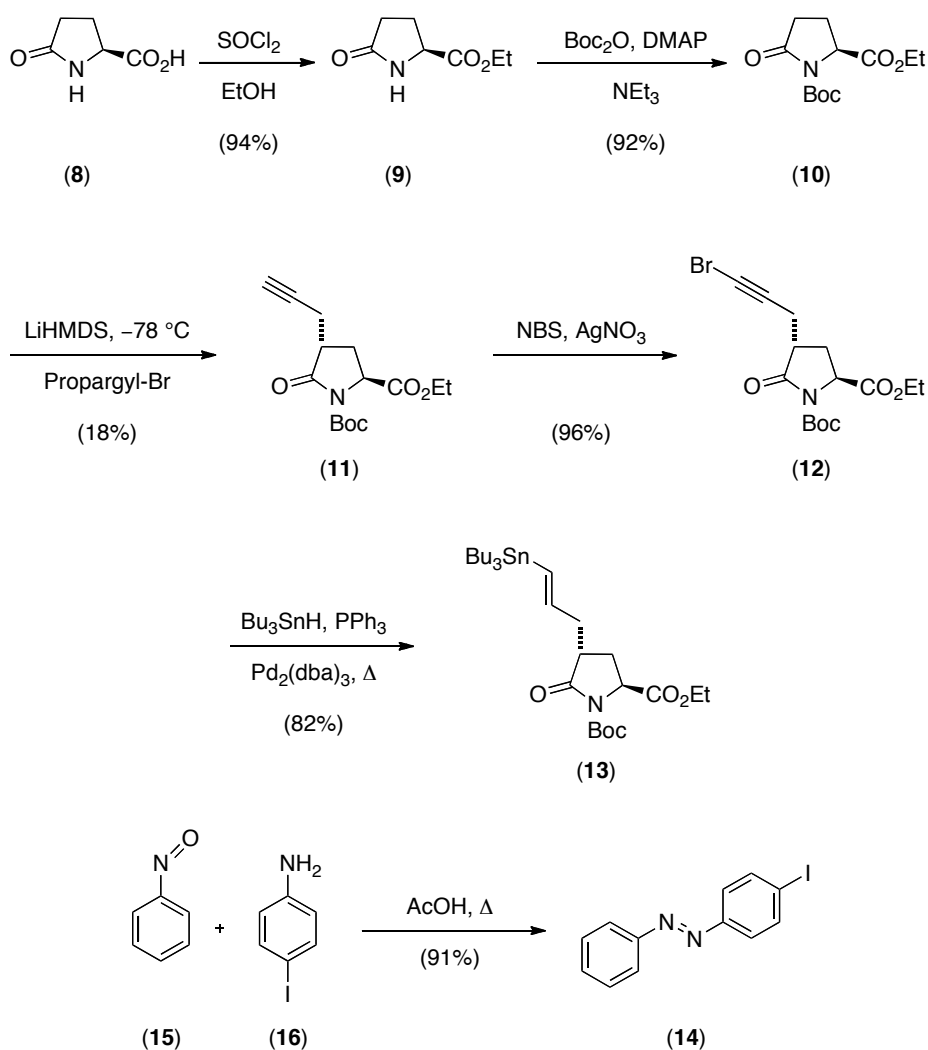


Figure 8: 2,2',6,6'-tetramethyl QAQ (**6**) and 2,2',6,6'-tetrachloro MAG (**7**). *Ortho*-substituted azobenzenes with interesting properties.

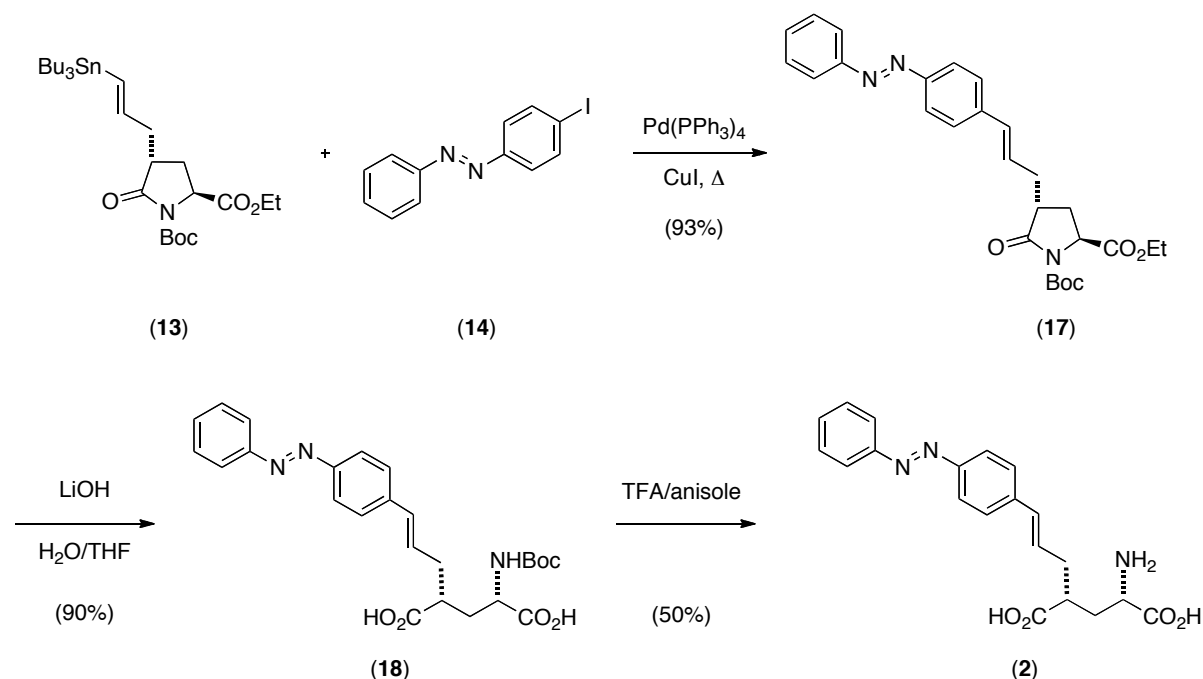
Part III: OBJECTIVES

Chapter 8: Co-crystallization of an azobenzene modified ligand with iGluR-LBDs

In order to study the specific interactions of 4-Gluazo (**2**) with the GluK2- and GluA2-LBDs a co-crystal structure is highly revealing. Therefore, the photoswitch has to be prepared. Moreover, the LBDs of GluK2 and GluA2 have to be expressed and purified. With both, photoswitch and protein in a state of high purity, affinity measurements and co-crystallization experiments have been performed. Finally, diffraction data have been collected from crystals and the structure has been solved, showing the protein–ligand interactions in molecular detail. Results are illustrated in chapter 15. The overview of the synthesis of 4-Gluazo (**2**) is depicted in **scheme 4**.



OBJECTIVES



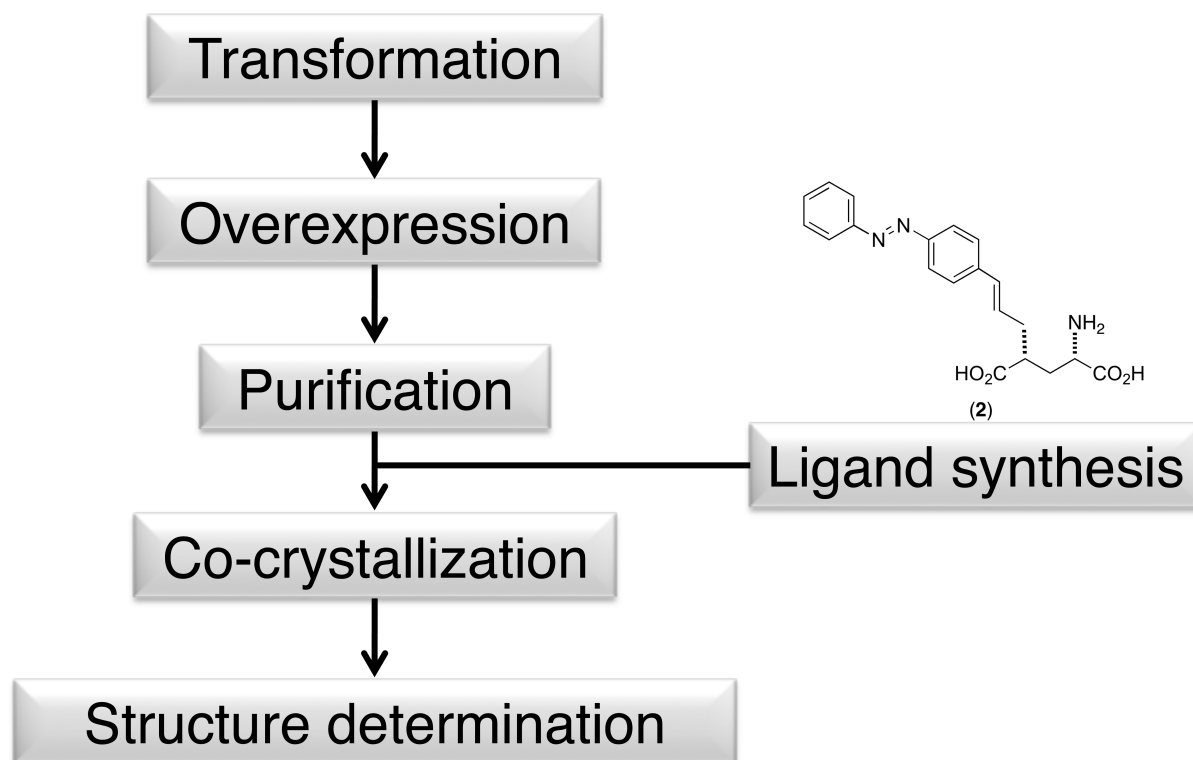
Scheme 4: Synthesis of 4-Gluazo (2).

The preparation is achieved starting from L-pyroglutamic acid (**8**), which is protected as an ester using thionylchloride in ethanol to give L-pyroglutamic acid ethyl ester (**9**), which is further protected under Steglich conditions to give *N*-Boc-L-pyroglutamic acid ethyl ester (**10**). Diastereoselective alkylation of (**10**) is carried out with LiHMDS and propargyl bromide to yield propargyl pyroglutamate (**11**). Bromination with *N*-bromosuccinimide gives bromoalkyne (**12**), which undergoes a palladium catalyzed hydrostannylation, to afford vinyl stannane (**13**). Iodoazobenzene (**14**) is obtained by the condensation of nitrosobenzene (**15**) and 4-iodoaniline (**16**). Stille cross coupling of **13** and **14** gives azobenzene pyroglutamate (**17**). Saponification and pyroglutamate hydrolysis yields *N*-Boc azobenzene glutamic acid (**18**), which is deprotected with TFA to result in 4-Gluazo (**2**) as the monosodium dihydrate salt⁶. Detailed procedures for the individual steps are specified in chapter 13.2.

In **scheme 5** a flow chart is shown, illustrating the different steps towards the co-crystal structure of the protein and 4-Gluazo (**2**). In protein crystallography, the purity of a protein is the most important requisite. In order to achieve highest purity, different methods can be performed. To begin with, a crystallizable construct of the protein of interest is required. In this case S1S2 constructs of the GluK2- and GluA2-LBD (provided by Dr. Mark Mayer) are ligated into the expression vectors pET-22b(+)

OBJECTIVES

and pETGQ (derivative of pET30b), respectively. After isolation, amplification and validation, the plasmids are transformed into *E. coli* and the proteins are overexpressed and purified. In order to purify the proteins, Ni-NTA affinity chromatography, cation exchange chromatography and gel filtration have been performed. After Ni-NTA, a thrombin digest is carried out to remove the N-terminal histidine tag. Prior to protein–ligand co-crystallization and structure determination, affinity measurements are conducted to receive an impression about the strength of ligand binding. The detailed experimental methods used for transformation, overexpression and purification of iGluR-LBDs and experimental details regarding the affinity measurements and the co-crystallization process are described in chapter 14.2.



Scheme 5: Flow chart of the protein–ligand co-crystallization process.

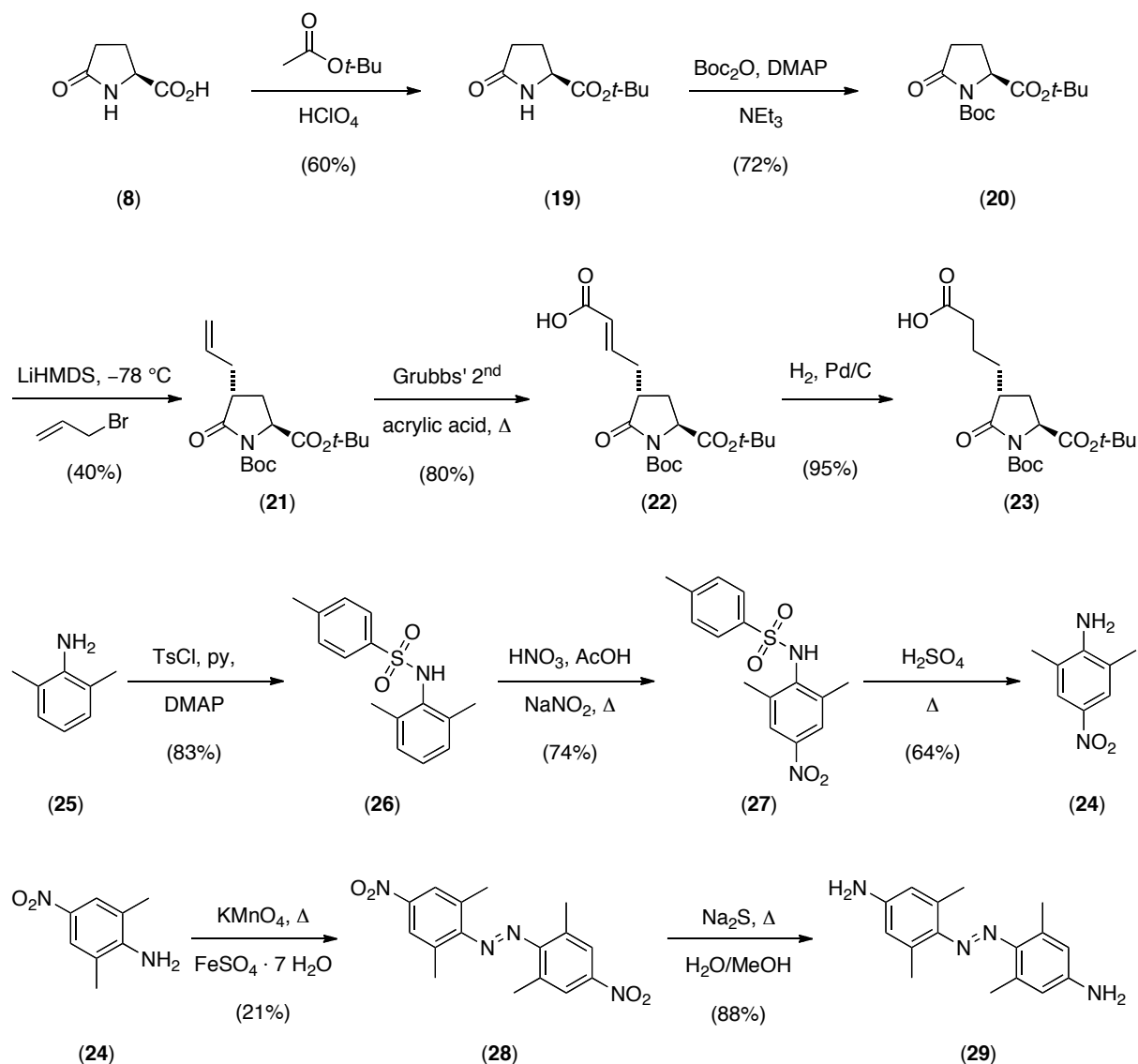
Chapter 9: Synthesis of an azobenzene target for ribosome display

The ultimate goal of this research topic is the creation of a protein scaffold, which binds to the azobenzene moiety with high affinity and specificity. In order to evolve a DARPIn based ABP, the target molecule and competitors, which are used in the selection process of ribosome display, have to be prepared and characterized. The molecules (**scheme 6: 3 and 29; scheme 7: 6 and 35**) have been sent to the group

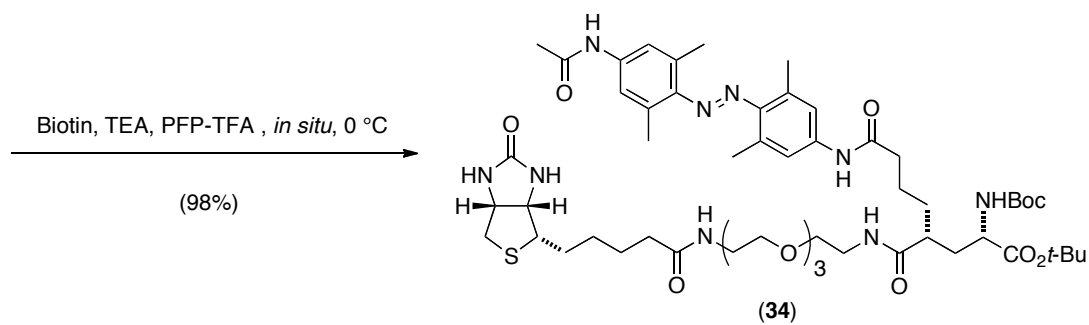
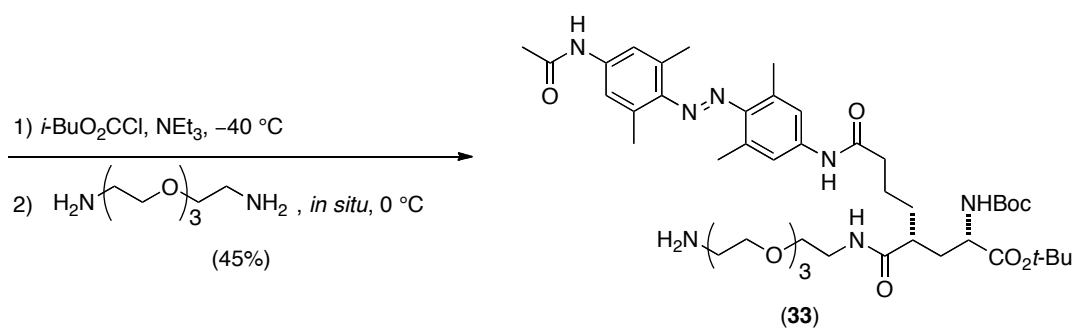
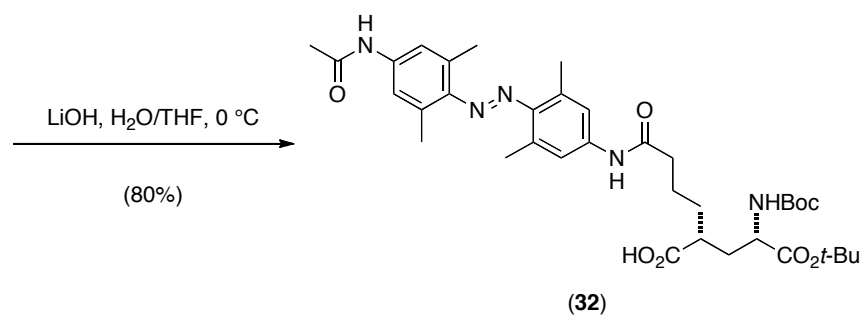
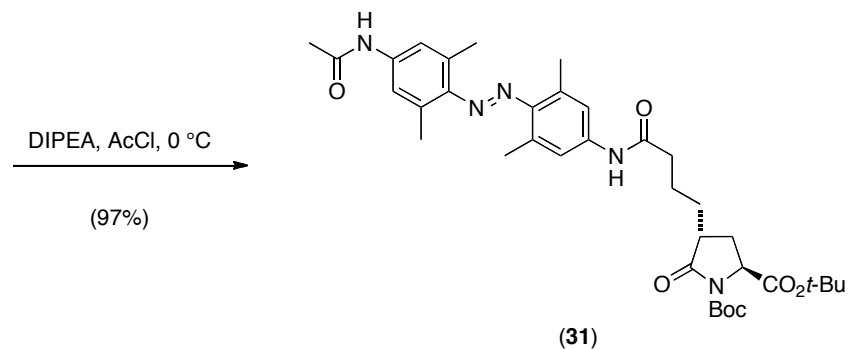
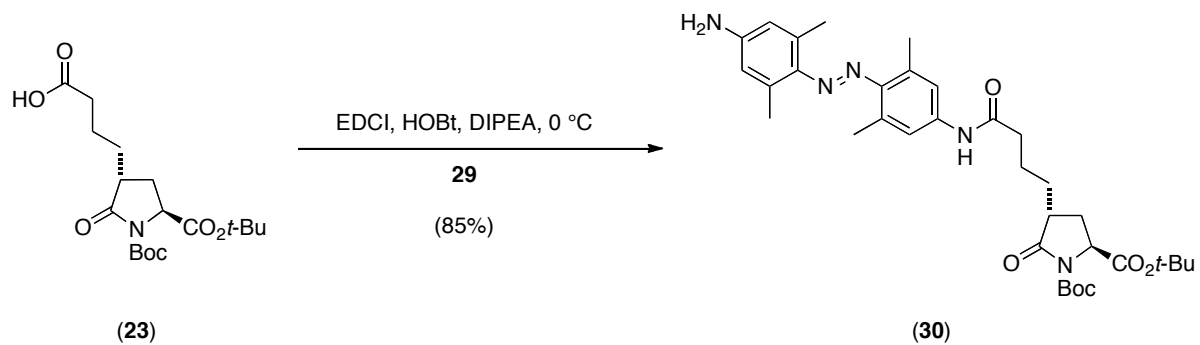
OBJECTIVES

of Prof. A. Plückthun (University of Zürich, Department of Biochemistry, 8057 Zürich, Switzerland; Email: Plueckthun@bioc.uzh.ch). In this group, the ribosome display technique with a library of DARPins is going to be carried out in the near future in order to develop an ABP. The new binding protein could be regulated with light by directly binding to the chromophore and switchable unit. ABPs could affect a wide range of life sciences and could in general be used as a toolbox in research.

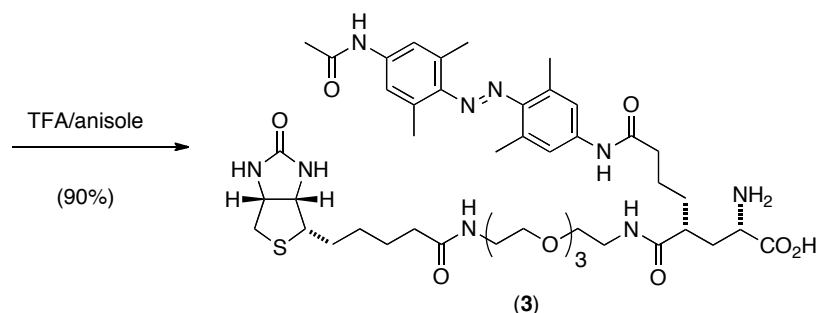
Results are described in chapter 16. The synthetic route leading to the target molecule BAG (**3**) is described in **scheme 6** and experimental procedures are described in chapter 13.3. After protection of (*S*)-2-pyrrolidone-5-carboxylic acid (**8**) as an ester with *tert*-butyl acetate in the presence of perchloric acid yielding *L*-pyroglutamic acid *tert*-butyl ester (**19**), the molecule was further protected to give *N*-Boc-*L*-pyroglutamic acid *tert*-butyl ester (**20**)²⁵⁸.



OBJECTIVES



OBJECTIVES



Scheme 6: Synthesis of BAG (3).

Diastereoselective allylation with LiHMDS and allyl bromide yields allylpyroglutamate (**21**). Grubbs' cross metathesis with acrylic acid gives acrylic acid pyroglutamate (**22**), which undergoes hydrogenation with palladium on carbon to afford carboxylic acid pyroglutamate (**23**). 2,6-dimethyl-4-nitroaniline (**24**) is obtained by starting from 2,6-dimethylaniline (**25**) in a tosylation – nitration – detosylation three step procedure *via* the intermediates *N*-tosyl-2,6-dimethylaniline (**26**) and *N*-tosyl-2,6-dimethyl-4-nitroaniline (**27**)²⁵⁹. Oxidative coupling of two equivalents of 2,6-dimethyl-4-nitroaniline (**24**) with potassium permanganate yields nitroazobenzene (**28**), which is reduced to aminoazobenzene (**29**) with sodium sulfide. Carboxylic acid pyroglutamate (**23**) and aminoazobenzene (**29**) are coupled in the presence of EDCI and HOBT to give aminoazobenzene pyroglutamate (**30**), which is acetylated to yield *N*-acyl-aminoazobenzene pyroglutamate (**31**). Hydrolysis of the γ -lactam with aqueous lithium hydroxide gives azobenzene glutamic acid ester (**32**), which is converted to the mixed anhydride with *iso*-butyl chloroformate and reacted *in situ* with 1,11-diamino-3,6,9-trioxaundecane to give azobenzene glutamic acid ester γ -amide (**33**). An activated biotin derivative is generated by the action of PFP-TFA on biotin and azobenzene glutamic acid ester γ -amide (**33**) is added *in situ* to the crude pentafluorophenyl ester. Thus, biotin azobenzene glutamic acid ester γ -amide (**34**) is realized. Finally, deprotection with TFA yields BAG (**3**).

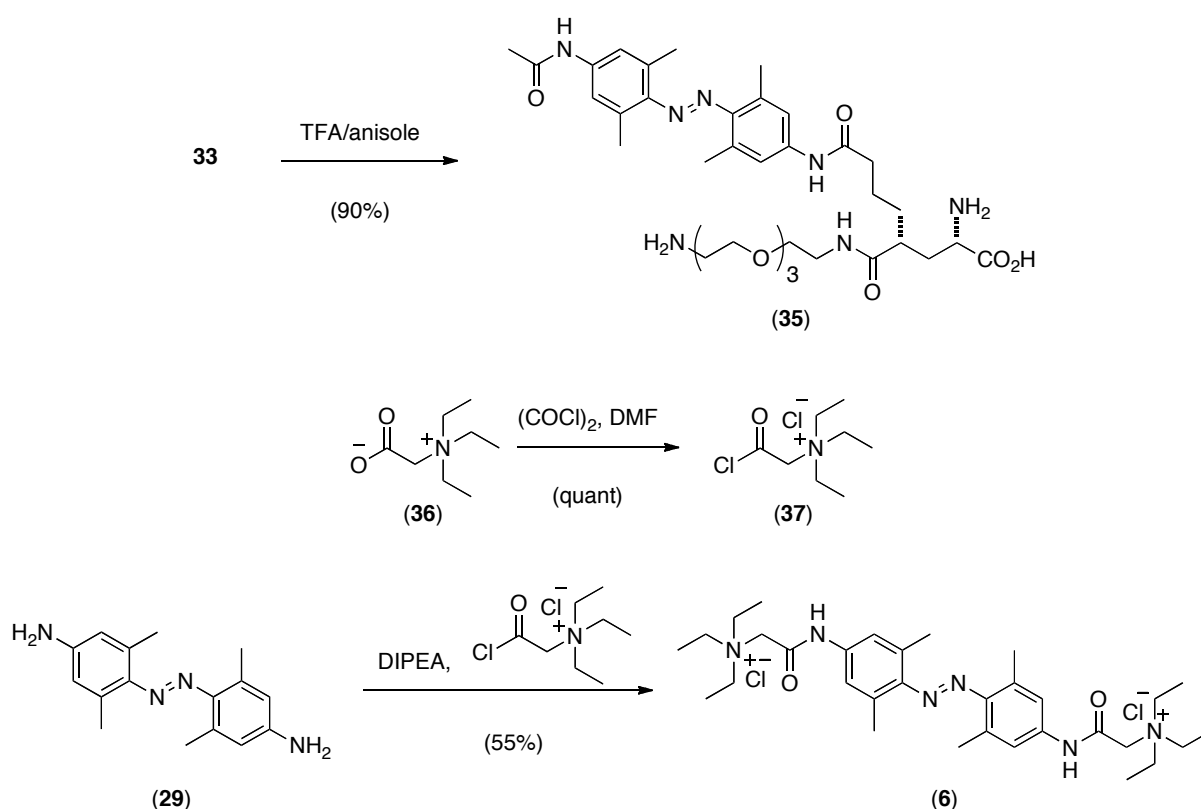
BAG is composed of a biotin, an azobenzene, a glutamate and a linker moiety. For the technique of ribosome display, the biotin functionality is needed in order to immobilize the molecule on the surface. The linker, in combination with the glutamate part, ensures sufficient distance between the biotin and the azobenzene part, which is the target of the DARPin to be evolved.

In order to generate a specific high affinity binder, several competitors are needed during the selection process of ribosome display. Therefore, azobenzene glutamic

OBJECTIVES

acid γ -amide (**35**), aminoazobenzene (**29**) and 2,2',6,6'-tetramethyl-QAQ (**6**) have also been prepared and experiments are described in chapter 13.3 and 13.4.

The preparation of aminoazobenzene (**29**) is described in **scheme 6**. The synthesis of azobenzene glutamic acid γ -amide (**35**) and 2,2',6,6'-tetramethyl-QAQ (**6**) is shown in **scheme 7**. Global deprotection of azobenzene glutamic acid ester γ -amide (**33**) with TFA yields azobenzene glutamic acid γ -amide (**35**). The synthesis of 2,2',6,6'-tetramethyl-QAQ (**6**) starts with the conversion of the betaine analogon (**36**) to the betaine acid chloride (**37**), which is added to aminoazobenzene (**29**) in a double amidation reaction to give 2,2',6,6'-tetramethyl-QAQ (**6**).



Scheme 7: Synthesis of azobenzene glutamic acid γ -amide (35**) and 2,2',6,6'-tetramethyl-QAQ (**6**).**

Azobenzene glutamic acid γ -amide (**35**) resembles the structure of BAG (**3**) without the biotin part. In contrast to BAG (**3**), aminoazobenzene (**29**) and 2,2',6,6'-tetramethyl-QAQ (**6**) are sterically less and more demanding at the 4 and 4' positions of the azobenzene core, respectively. With these three competitors, low affinity binders and unspecific binders can be removed during the selection process of ribosome display. Competitors are added in excess, compete for binding and thus all low affinity binders, which are unspecific and recognize both, the target and a

OBJECTIVES

competitor, are washed away. Accordingly, the background of molecules binding unspecifically is reduced. An additional strategy to develop high affinity binders is to immobilize just a minimal amount of the target. Binders with different affinities will equilibrate and just high affinity binders will occupy all the sites.

Chapter 10: Structure-based design and synthesis of an AMPA receptor antagonist

Co-crystallisation experiments of GluA2-LBD and 4-Gluazo (**2**) resulted in a LBD dimer of dimers structure occupied by 2-(*N*-morpholino)ethanesulfonic acid (MES), sulfate and ethylene glycol, which is described in chapter 15.7. This structure provides molecular insights into key interactions between MES, a sulfate and the receptor and paves the way for molecular modeling studies, which are illustrated in **figure 9**. MES in combination with the sulfate ion have been used as a lead structure for the design of MOBIPHOS (**4**), which is a GluA2 antagonist.

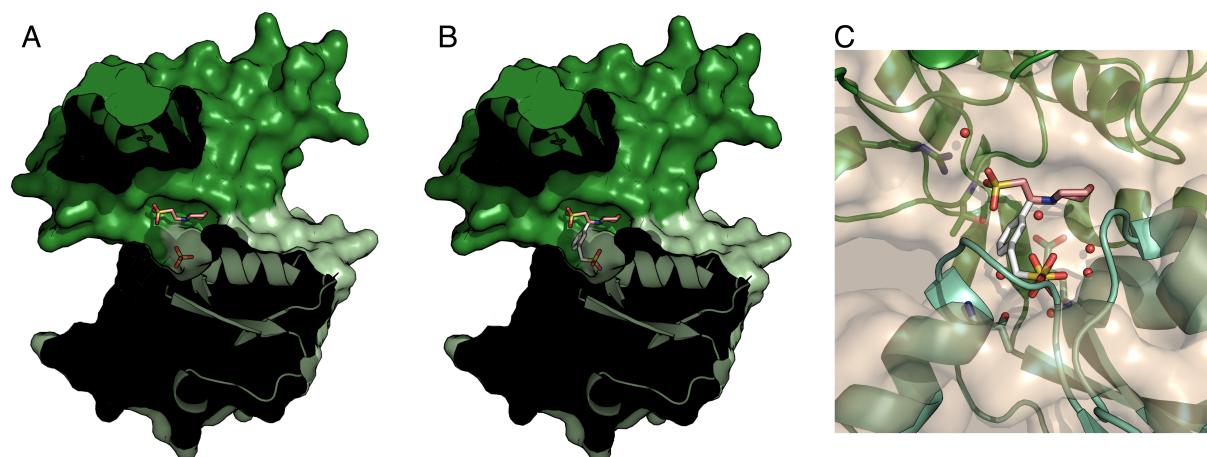


Figure 9: Longitudinal cross section of GluA2-LBD•MES and design of MOBIPHOS (4). (A and B) Surface representation and cross section of the GluA2-LBD with D1 and D2 coloured in shades of green (D1: dark green, D2: light green) with (A) MES and sulfate (sticks) and (B) designed (*S*)-MOBIPHOS (**4**, mixed salmon and gray sticks) which is superimposed onto the MES and sulfate positions. (C) Close-up view with the protein ligand-binding cavity shown as a wheat surface with (*S*)-MOBIPHOS (**4**, mixed salmon and gray sticks), water molecules (red spheres), sulfate (sticks) and parts of D1 (dark green cartoon) and D2 (light green cartoon).

MOBIPHOS (**4**) is preshaped to match the geometry of the binding site of the protein. In order to restrict the conformational flexibility and to gain high hydrophobicity, a phenyl ring is introduced to combine the position of the sulfate ion with MES. A high degree of hydrophobicity and conformationally constrained ligands show higher

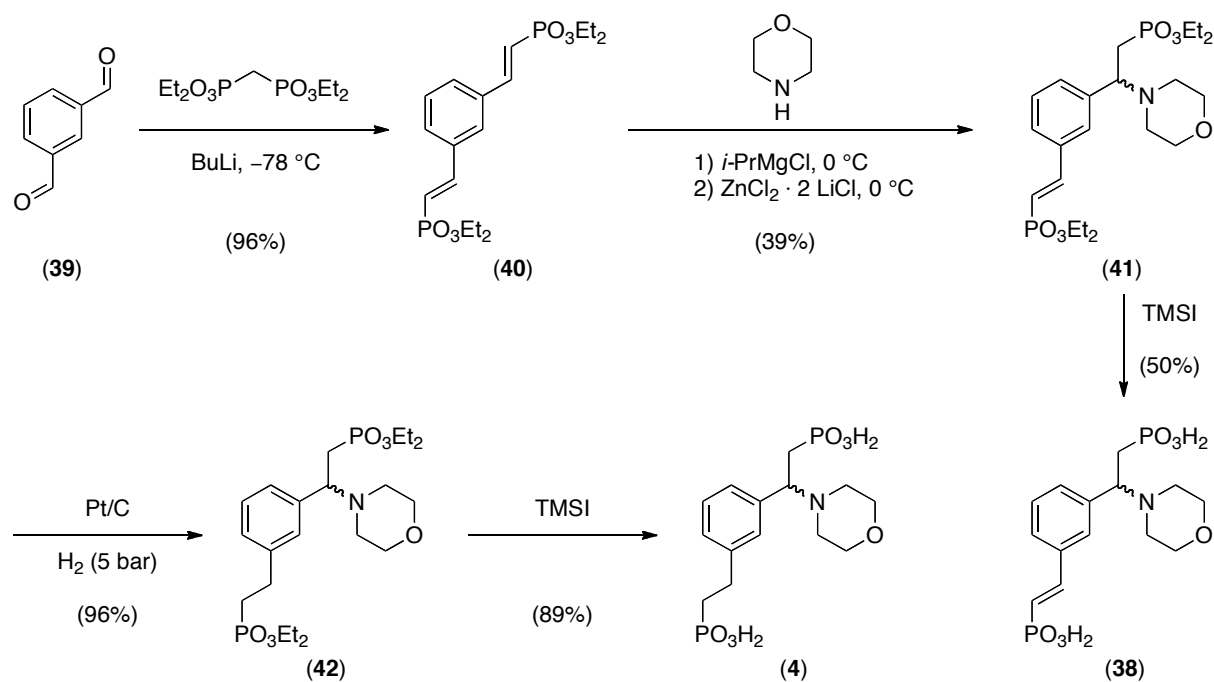
OBJECTIVES

specificity and affinity compared to more hydrophilic and more relaxed counterparts, because of more solvent release and a smaller conformational entropy loss upon binding²⁶⁰. Different substitution patterns of the phenyl ring have been applied and *meta* substitution have resulted in the best alignment. This sort of substitution can best balance the low structural stability of the ligand-binding region of the apo-like protein conformation. Afterwards, different additional substituents can be introduced by molecular engineering. For synthetic reasons, the sulfonate moiety of MES and the sulfate ion are replaced by phosphonate moieties, which mimic these two groups.

Finally, MOBIPHOS (**4**) is modeled into the GluA2-LBD•MES structure (**Fig. 9 A**) in a way, that it perfectly aligns with MES and the sulfate ion (**Fig. 9 B and C**). This does not represent the energetically most favorable conformation of MOBIPHOS (**4**), but with the angle of clamshell closure of the protein being variable, the LBD might adopt a slightly different orientation compared to the GluA2-LBD•MES structure, when it is bound to MOBIPHOS (**4**). In order to eliminate this potential problem the derivative MOBIPHOSen (**38**) has been prepared in addition to MOBIPHOS (**4**). These two molecules exhibit different dihedral angles between the phenyl and the phosphonate group.

The synthesis of MOBIPHOS (**4**) and MOBIPHOSen (**38**) is depicted in **scheme 8** and starts with a Horner-Wadsworth-Emmons (HWE) reaction of isophthalaldehyde (**39**) to give the bisphosphonate (**40**). The morpholine part is introduced *via* a newly developed 1,4-addition method for phosphonates to yield morpholino bisphosphonate (**41**). The remaining double bond is hydrogenated with platinum on carbon to produce morpholino dihydrobisphosphonate (**42**). Finally, the phosphonate moieties are deprotected with TMSI to result in MOBIPHOS (**4**). MOBIPHOSen (**38**) is prepared by deprotection of morpholino bisphosphonate (**41**) with TMSI. The biological activity of the final molecules has been confirmed with electrophysiological experiments and detailed synthetic procedures are given in chapter 13.5. Results are depicted in chapter 17.

OBJECTIVES

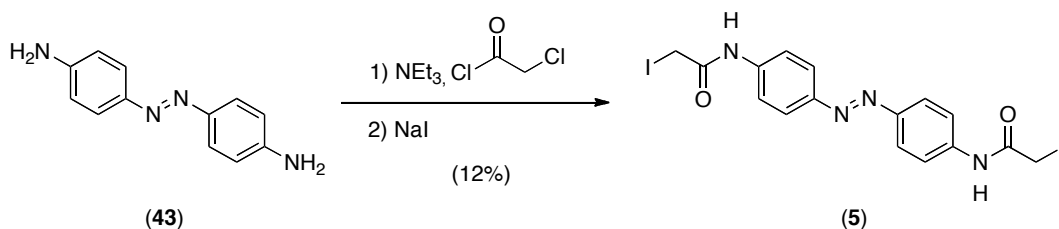


Scheme 8: Synthesis of MOBIPHOS (4) and MOBIPHOSen (38).

Chapter 11: Synthesis of an azobenzene with two attachment sites

The plunger of a light driven molecular motor could be an azobenzene molecule. In order to build this molecular motor, ABA (5) has to be prepared and characterized. After the synthesis, the molecule has been sent to the group of Prof. T. Hugel (TUM, Department of Physics, 85748 Garching, Germany; Email: thorsten.hugel@ph.tum.de) and DNA origami and further experiments leading to a light driven molecular motor will be carried out in this group.

The synthesis is described in **scheme 9** and starts with the commercially available 4,4'-diaminoazobenzene (43). After the reaction with two equivalents of chloroacetyl chloride in the presence of TEA, a Finkelstein reaction with sodium iodide gives ABA (5). Experiments are specified in chapter 13.6 and results are described in chapter 18.



Scheme 9: Synthesis of ABA (5).

Chapter 12: Synthesis of *ortho*-substituted azobenzenes

Ortho-substituted azobenzenes show interesting characteristics. Results of this topic are specified in chapter 19. The synthesis of 2,2',6,6'-tetramethyl-QAQ (**6**), which is stable in both azobenzene configurations, is shown in **scheme 7** and detailed in chapter 13.4. The molecule has been sent to the group of Prof. E. Riedle (LMU, Department of Physics, 80538 Munich, Germany; Email: riedle@physik.uni-muenchen.de), where optical activity studies to examine the possibility of chiral induction of a racemic mixture of the azobenzene by exposure to circular polarized light will be carried out. Irradiation of the racemate with circular polarized light should cause a partial enrichment of one of the enantiomers.

2,2',6,6'-tetrachloro-MAG (**7**) is prepared in collaboration with the group of Prof. A. Woolley (University of Toronto, Department of Chemistry, M5S 3H6 Toronto, Canada; Email: awoolley@chem.utoronto.ca). The synthesis of the building block carboxylic acid pyroglutamate (**23**) is depicted in **scheme 6** and is accurately described in chapter 13.3. The molecule has been prepared and sent to Toronto, where the synthesis towards 2,2',6,6'-tetrachloro-MAG (**7**) will be completed. The molecule will be tested for its switching behaviour and activity on iGluRs with electrophysiological experiments.

Part IV: EXPERIMENTS

Chapter 13: Chemistry

13.1 General conditions

All reactions were carried out with magnetic stirring and, if air or moisture sensitive, in flame-dried glassware under argon or nitrogen. Syringes, which were used to transfer reagents and solvents, were purged with argon or nitrogen prior to use.

13.1.1 Solvents

Solvents were dried according to standard methods by distillation over drying agents as stated below or were purchased and used without further purification. They were stored under argon or nitrogen.

Solvents	Supplier
Acetone	Acros (water < 0.005%)
Acetonitrile	Acros (over molecular sieves, water < 0.005%)
Dichloromethane	Acros (over molecular sieves, water < 50 ppm)
Diisopropylethylamine	Sigma-Aldrich (continuously refluxed over calcium hydride under nitrogen and distilled off)
Dimethylformamide	Acros (over molecular sieves, water < 50 ppm)
Ethyl acetate	Acros (water < 0.005%)
Methanol	Acros (over molecular sieves, water < 0.005%)
Pyridine	Sigma-Aldrich (anhydrous, 99.8%)
Tetrahydrofuran	Acros (continuously refluxed and freshly distilled from sodium benzophenone ketyl under nitrogen)
Triethylamine	Sigma-Aldrich (continuously refluxed over calcium hydride under nitrogen and distilled off)

Table 2: Solvents.

13.1.2 Reagents

Commercially available reagents of > 98% purity were used as obtained. Organolithium solutions were titrated prior to use with diphenylacetic acid and organozinc solutions were titrated at 0 °C with benzoic acid and (phenyl)[4-(phenylazo)phenyl]amine as indicator²⁶¹. Tributyltin hydride (6.8 x 10⁻¹ mbar, 75 °C) and acrylic acid (44 °C, 20 mbar) were freshly distilled prior to use.

EXPERIMENTS

13.1.3 Chromatography

Mixtures were separated and analysed by thin layer chromatography (TLC) using precoated [(normal phase: Merck silica gel 60, F₂₅₄); (reversed phase: Mechery-Nagel, Silica RP-18W/UV₂₅₄)] glass plates. Colourless substances were detected due to fluorescence quenching under UV light and/or by staining with iodine or with one of the solutions below.

Basic KMnO₄:

KMnO₄ (0.3 g), K₂CO₃ (20 g), KOH (0.3 g) in water (300 mL).

CAM:

Ammonium molybdate (25.0 g), Ce(SO₄)₂ (5.0 g), conc. H₂SO₄ (50 mL) in water (450 mL).

Normal phase flash column chromatography was performed using silica gel (60 Å, 40 – 63 μm) from Merck. Reversed phase flash column chromatography was performed using preparative C₁₈ (125 Å, 55 – 105 μm) bulk packing material from waters corporation. The diameters of the columns and the amount of the stationary phase were estimated by experience. The solvents for chromatography were distilled or used as received in p.a. or HPLC quality.

13.1.4 Chemical analysis

Methods	Instruments
HPLC/LCMS (HR-)MS	Varian SD1/Agilent 1260 G1964 Finnigan MAT 95Q (EI) Thermo Finnigan LTQ FT (ESI)
IR spectroscopy	Perkin Elmer Spectrum BX-59343 FT-IR
Melting point	Büchi B-450
NMR spectroscopy	Varian NMR-systems (200, 300, 400, 600 MHz)

Table 3: Analytical methods and instruments.

For nuclear magnetic resonance (NMR) spectra, chemical shifts were reported in parts per million (ppm) and refer to tetramethylsilane (TMS, δ_H: 0.00, δ_C: 0.00) in

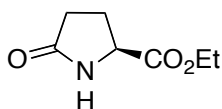
EXPERIMENTS

CDCl_3 as internal standard or were reported relative to the solvent residual signals. Melting points were uncorrected and infrared (IR) spectra were detected with a Smiths Detection DuraSample/IR II Diamond attenuated total reflection (ATR) sensor and were recorded from $4000 - 650 \text{ cm}^{-1}$.

13.2 Preparation of 4-Gluazo⁶

13.2.1 L-pyroglutamic acid ethyl ester

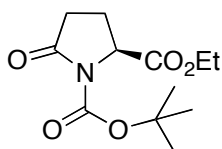
L-pyroglutamic acid (25.0 g, 194 mmol) was dissolved in ethanol (360 mL). It was cooled to $0 \text{ }^\circ\text{C}$ and thionylchloride (16.0 mL, 221 mmol) was slowly added to the suspension. After stirring for 10 min at the stated temperature, it was allowed to warm to room temperature and was stirred for 2 h 30 min. A saturated solution of NaHCO_3 was added and the mixture was extracted with chloroform. The combined organic layers were washed with a saturated solution of NaCl , dried over Na_2SO_4 , filtered and concentrated *in vacuo*. The product was allowed to crystallize at $4 \text{ }^\circ\text{C}$ overnight to yield **9** (28.6 g, 182 mmol, 94%) as a colourless solid. The product was directly used for the next step without further purification.



13.2.2 N-Boc-L-pyroglutamic acid ethyl ester

Triethylamine (72.0 mL, 518 mmol) was added to a solution of L-pyroglutamic acid ethyl ester (**9**) (27.0 g, 172 mmol), di-*tert*-butyl dicarbonate (75.4 g, 345 mmol) and 4-(dimethylamino)-pyridine (3.50 g, 28.6 mmol) in CH_2Cl_2 (440 mL) and the reaction was stirred at room temperature overnight. The mixture was washed with 10% citric acid and with a saturated solution of NaCl , was dried over Na_2SO_4 , filtered and concentrated *in vacuo*. Purification by normal phase chromatography (hexanes : EtOAc = 3 : 2, $R_f = 0.35$) and recrystallization from ethanol yielded **10** (40.7 g, 158 mmol, 92%) as a colourless solid.

EXPERIMENTS



mp.: 60 °C.

IR (ATR): $\tilde{\nu}_{\text{max}}$ (cm⁻¹) = 2978 (m), 1770 (vs), 1734 (vs), 1701 (m), 1459 (w), 1366 (m), 1306 (s), 1273 (s), 1209 (m), 1144 (s), 1046 (s), 1025 (s), 905 (w), 842 (w), 778 (m), 751 (w).

¹H-NMR (300 MHz, CDCl₃, 23 °C): δ (ppm) = 4.60 (dd, *J* = 3 Hz and 12 Hz, 1H), 4.24 (q, *J* = 6 Hz, 2H), 2.59 (m, 1H), 2.49 (m, 1H), 2.31 (m, 1H), 2.01 (m, 1H), 1.48 (s, 9H), 1.28 (t, *J* = 9 Hz, 3H).

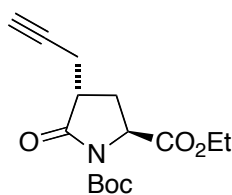
¹³C-NMR (75 MHz, CDCl₃, 23 °C): δ (ppm) = 173.4, 171.3, 149.3, 83.5, 61.7, 59.0, 31.1, 27.9, 21.5, 14.2.

HR-MS (ESI) [M + H]⁺: calc for [C₁₂H₂₀NO₅]⁺: 258.1333; found: 258.1330.

13.2.3 Propargyl pyroglutamate

Freshly prepared lithium bis(trimethylsilyl)amide [*n*-BuLi (23.3 mL, 58.2 mmol, 2.50 M) was added dropwise to a solution of hexamethyldisilazane (12.4 mL, 58.4 mmol) in THF (195 mL) at -78 °C and was stirred for 1 h at the stated temperature] was added dropwise to a solution of *N*-Boc-L-pyroglutamic acid ethyl ester (**10**) (12.0 g, 46.6 mmol) in THF (52.2 mL) at -78 °C. After stirring at -78 °C for 1 h, propargyl bromide (15.0 mL, 80% in toluene, 174 mmol) was added fast and the resulting solution was stirred for additional 2 h at -78 °C. A saturated solution of ammonium chloride was added at -78 °C. After extraction with CH₂Cl₂, the combined organic layers were washed with a saturated solution of NaCl, dried over Na₂SO₄, filtered, and concentrated. Purification by normal phase chromatography (hexanes : Et₂O = 1 : 1, , R_f = 0.45) gave **11** (2.45 g, 8.3 mmol, 18%) as a colourless solid.

EXPERIMENTS



mp.: 78 °C.

IR (ATR): $\tilde{\nu}_{\text{max}}$ (cm⁻¹) = 3373 (br), 3270 (s), 2981 (m), 1735 (vs), 1710 (vs), 1593 (m), 1366 (m), 1318 (s), 1259 (m), 1204 (m), 1148 (s), 1017 (m), 666 (m).

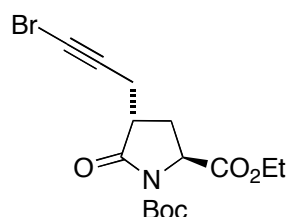
¹H-NMR (200 MHz, CDCl₃, 23 °C): δ (ppm) = 4.61 (dd, *J* = 2 Hz and 8 Hz, 1H), 4.28 (q, *J* = 6 Hz, 2H), 2.87 (m, 1H), 2.68 (m, 1H), 2.49 (m, 1H), 2.30 (m, 2H), 2.0 (t, *J* = 2 Hz, 1H), 1.49 (s, 9H), 1.32 (t, *J* = 9 Hz, 3H).

¹³C-NMR (75 MHz, CDCl₃, 23 °C): δ (ppm) = 173.0, 171.2, 149.3, 83.8, 80.1, 70.7, 61.8, 57.0, 40.7, 27.9, 27.5, 19.4, 14.2.

HR-MS (ESI) [M + H]⁺: calc for [C₁₅H₂₂NO₅]⁺: 296.1490; found 296.1490.

13.2.4 Bromoalkyne

N-bromosuccinimide (1.27 g, 7.14 mmol) and propargyl pyroglutamate (**11**) (1.91 g, 6.47 mmol) were dissolved in acetone (26.0 mL). Silver nitrate (97.0 mg, 0.573 mmol) was added and the mixture was stirred for 2 h at room temperature. Hexanes were added and the mixture was washed with water. After extracting the separated aqueous layer with a mixture of diethylether and hexanes (1:1) the combined organic layers were dried over Na₂SO₄ and filtered through a pad of silica. Evaporation of the solvent gave **12** (2.32 g, 6.22 mmol, 96%) as a colourless oil (hexanes : Et₂O = 1 : 1, *R_f* = 0.45).



EXPERIMENTS

IR (ATR): $\tilde{\nu}_{\max}$ (cm⁻¹) = 2981 (m), 2936 (m), 1789 (s), 1742 (s), 1717 (s), 1311 (s), 1147 (vs).

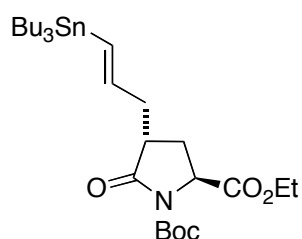
¹H-NMR (200 MHz, CDCl₃, 23 °C): δ (ppm) = 4.61 (dd, J = 2 Hz and 10 Hz, 1H), 4.26 (q, J = 6 Hz, 2H), 2.76 (m, 2H), 2.46 (m, 1H), 2.25 (m, 2H), 1.50 (s, 9H), 1.29 (t, J = 6 Hz, 3H).

¹³C-NMR (75 MHz, CDCl₃, 23 °C): δ (ppm) = 172.9, 171.1, 149.3, 83.8, 76.1, 61.8, 57.0, 40.7, 40.6, 27.9, 27.6, 20.7, 14.2.

HR-MS (EI) [M]⁺: calc for [C₁₅H₂₀BrNO₅]⁺: 373.0525; found: 373.0529.

13.2.5 Vinyl stannane

Triphenylphosphine (34.0 mg, 0.13 mmol), bromoalkyne (**12**) (1.22 g, 3.26 mmol), and tris(dibenzylideneacetone)dipalladium (15.0 mg, 0.0170 mmol) were dissolved in THF (17.0 mL) and tributyltin hydride (1.80 mL, 6.70 mmol) was added dropwise over 30 min at 0 °C. After stirring the mixture at room temperature for 2 h, a saturated aqueous solution of KF was added. The reaction mixture was extracted with hexanes and the separated organic layer was washed with water and a saturated solution of NaCl. After drying over Na₂SO₄, filtration and evaporation of the solvent, the crude product was purified by normal phase chromatography (hexanes : Et₂O = 5 : 1; R_f = 0.20) to yield **13** (1.57 g, 2.67 mmol, 82%) as a colourless oil.



IR (ATR): 2959 (m), 2925 (m), 1793 (s), 1748 (s), 1718 (s), 1458 (w), 1368 (m), 1315 (vs), 1189 (s), 1153 (vs), 1027 (m), 773 (m).

¹H-NMR (300 MHz, CDCl₃, 23 °C): δ (ppm) = 5.97 (m, 1H), 5.87 (m, 1H), 4.56 (dd, J = 3 Hz and 12 Hz, 1H), 4.25 (q, J = 6 Hz, 2H), 2.77 (m, 2H), 2.25 (m, 1H), 2.15 (m, 1H), 2.04 (m, 1H), 1.51 (s, 9H), 1.48 (m, 6H), 1.29 (m, 9H), 0.89 (m, 15H).

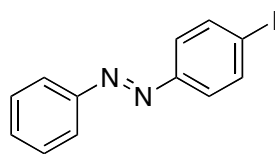
¹³C-NMR (75 MHz, CDCl₃, 23 °C): δ (ppm) = 174.6, 171.4, 149.5, 144.4, 132.0, 83.5, 61.6, 57.2, 41.2, 38.6, 29.1, 27.9, 27.8, 27.2, 14.2, 13.7, 9.4.

EXPERIMENTS

MS (EI): m/z (%) = 530.4 (85) [M – C₄H₉], 514.4 (7).

13.2.6 Iodoazobenzene

Nitrosobenzene (**15**) (2.00 g, 18.6 mmol) was dissolved in glacial acetic acid (130 mL) and 4-iodoaniline (**16**) (3.40 g, 15.5 mmol) was added to the solution. After stirring at 40 °C for 12 h, the mixture was diluted with water and extracted with CH₂Cl₂. The organic layer was washed with a saturated solution of NaCl, dried over Na₂SO₄, filtered, and concentrated *in vacuo*. Purification by normal phase chromatography (100 : 1, hexanes : Et₂O, R_f = 0.29) afforded **14** (4.34 g, 14.1 mmol 91%) as an orange solid.



mp.: 95 °C.

IR (ATR): $\tilde{\nu}_{\max}$ (cm⁻¹) = 3072 (w), 1563 (m), 1474 (s), 1391 (m), 1294 (m), 1049 (m), 998 (s), 838 (s), 768 (s).

¹H-NMR (200 MHz, CDCl₃, 27 °C): δ (ppm) = 7.89 (m, 4H), 7.68 (m, 2H), 7.50 (m, 3H).

¹³C-NMR (75 MHz, CDCl₃, 23 °C): δ (ppm) = 152.4, 151.9, 138.4, 131.4, 129.2, 124.5, 123.0, 97.7.

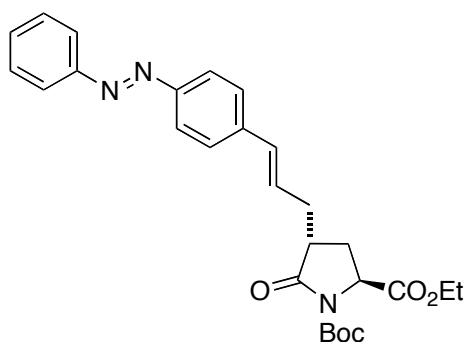
HR-MS (ESI) [M + H]⁺: calc for [C₁₂H₁₀I₁N₂]⁺: 308.9880; found: 308.9876.

13.2.7 Azobenzene pyroglutamate

Vinyl stannane (**13**) (1.27 mg, 2.17 mmol), 4-iodoazobenzene (**14**) (514 mg, 1.67 mmol), tetrakis(triphenylphosphine)palladium (96.0 mg, 0.0830 mmol) and copper iodide (32 mg, 0.168 mmol) were dissolved in DMF (50.0 mL) and stirred at 65 °C overnight. Water (770 mL) was added and the mixture was extracted with EtOAc. The combined organic layers were washed with a saturated solution of NaCl, dried over Na₂SO₄, filtered and concentrated. Purification by normal phase

EXPERIMENTS

chromatography (hexanes : Et₂O = 4 : 1, R_f = 0.23) yielded **17** (741 mg, 1.55 mmol, 93%) as an orange solid.



mp.: 115 °C.

IR (ATR): $\tilde{\nu}_{\text{max}}$ (cm⁻¹) = 2957 (br), 1782 (vs), 1746 (s), 1597 (w), 1463 (w), 1389 (w), 1368 (w), 1314 (m), 1286 (m), 1252 (m), 1195 (m), 1148 (s), 1032 (w), 838 (w), 764 (w), 685 (m).

¹H-NMR (600 MHz, CDCl₃, 23 °C): δ (ppm) = 7.89 (m, 4H), 7.48 (m, 5H), 6.56 (d, *J* = 16 Hz, 1H), 6.30 (m, 1H), 4.60 (dd, *J* = 2 Hz and 10 Hz, 1H), 4.25 (q, *J* = 8 Hz, 2H), 2.79 (m, 2H), 2.43 (m, 1H), 2.23 (m, 1H), 2.11 (m, 1H), 1.51 (s, 9H), 1.29 (t, *J* = 8 Hz, 3H).

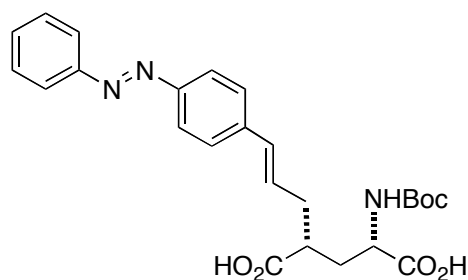
¹³C-NMR (150 MHz, CDCl₃, 23 °C): δ (ppm) = 174.2, 171.2, 152.7, 151.7, 149.4, 139.6, 132.4, 130.9, 129.1, 127.9, 126.8, 123.3, 122.8, 83.6, 61.7, 57.1, 41.6, 33.7, 27.9, 27.8, 14.2.

HR-MS (ESI) [M + H]⁺: calc for [C₂₇H₃₂N₃O₅]⁺: 478.2334; found: 478.2327.

13.2.8 *N*-Boc azobenzene glutamic acid

An aqueous solution of LiOH (60.0 mL, 60 mmol, 1 M) was slowly added to a solution of azobenzene pyroglutamate (**17**) (530 mg, 1.11 mmol) in THF (60.0 mL). After stirring at room temperature for 2 h, the mixture was acidified to pH = 2 with an aqueous solution of HCl (1 M) and extracted with EtOAc. The combined organic layers were dried over Na₂SO₄, filtered, and concentrated. Purification by normal phase chromatography (CH₂Cl₂ : MeOH : AcOH = 94 : 4 : 2, R_f = 0.26) afforded **18** (467 mg, 1.00 mmol, 90%) as an orange solid.

EXPERIMENTS



mp.: 85 °C.

IR (ATR): $\tilde{\nu}_{\text{max}}$ (cm⁻¹) = 2976 (br), 1707 (vs), 1394 (w), 1154 (m).

¹H-NMR (400 MHz, CD₃OD, 27 °C): δ (ppm) = 7.86 (m, 4H), 7.51 (m, 5H), 6.53 (d, J = 16 Hz, 1H), 6.38 (m, 1H), 4.17 (m, 1H), 2.70 (m, 1H), 2.56 (m, 1H), 2.51 (m, 1H), 2.24 (m, 1H), 1.79 (m, 1H), 1.42 (s, 9H).

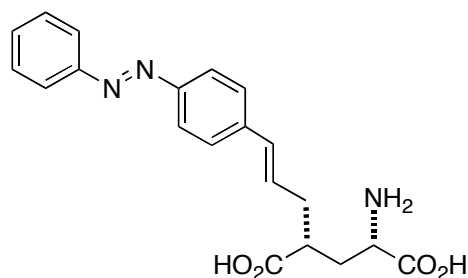
¹³C-NMR (100 MHz, CD₃OD, 27 °C): δ (ppm) = 176.7, 174.6, 156.7, 152.7, 151.5, 140.4, 131.4, 130.7, 128.8, 126.6, 122.7, 122.3, 79.1, 78.0, 52.0, 41.9, 35.9, 33.0, 27.3.

HR-MS (ESI) [M + H]⁺: calc for [C₂₅H₃₀N₃O₆]⁺: 468.2126; found: 468.2132.

13.2.9 4-Gluazo

Anisole (0.940 mL, 8.59 mmol) and *N*-Boc azobenzene glutamic acid (**18**) (136 mg, 0.291 mmol) were dissolved in CH₂Cl₂ (9.40 mL). TFA (5.10 mL, 69.0 mmol) was added dropwise at 0 °C and after stirring the mixture at room temperature for 1 h, Et₂O (85.0 mL) was added. The resulting precipitate was separated from the solution by centrifugation. The remaining solution was concentrated and subsequently redissolved in a minimal amount of methanol and a saturated solution of NaHCO₃. Purification by reversed phase chromatography (H₂O : MeOH = 100:0 → 70:30) gave **2** (61.8 mg, 0.146 mmol, 50%) as an orange solid as the monosodium dihydrate salt.

EXPERIMENTS



mp.: 290 °C (dec.).

IR (ATR): $\tilde{\nu}_{\max}$ (cm⁻¹) = 3030 (br), 1565 (vs), 1401 (s), 1153 (m), 766 (m), 686 (m).

¹H-NMR (400 MHz, D₂O, 27 °C): δ (ppm) = 7.55 (m, 2H), 7.50 (d, J = 8 Hz, 2H), 7.38 (m, 3H), 7.32 (d, J = 8 Hz, 2H), 6.35 (d, J = 16 Hz, 1H), 6.20 (m, 1H), 3.58 (m, 1H), 2.42 (m, 1H), 2.34 (m, 1H), 2.28 (m, 1H), 2.04 (m, 1H), 1.81 (m, 1H).

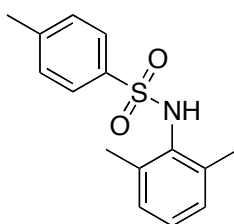
¹³C-NMR (100 MHz, D₂O, 27 °C): δ (ppm) = 182.5, 175.1, 152.0, 150.7, 140.7, 131.5, 130.7, 130.5, 129.4, 126.9, 122.9, 122.3, 53.5, 44.9, 36.2, 33.0.

MS (ESI) [M + H]⁺: calc for [C₂₀H₂₂N₃O₄]⁺: 368.1602; found: 368.1606.

13.3 Preparation of BAG

13.3.1 *N*-tosyl-2,6-dimethylaniline²⁵⁹

Tosyl chloride (63.9 g, 336 mmol) was dissolved in pyridine (75.0 mL). 2,6-dimethylaniline (**25**) (35.0 mL, 281 mmol) and 4-(dimethylamino)-pyridine (500 mg, 4.00 mmol) were added and the mixture was heated to 125 °C for 4 h. The solution was allowed to cool to room temperature and was added to an aqueous solution of HCl (2 M, 250 mL). After extracting with Et₂O, the solvent was removed *in vacuo* and the remaining crude product was recrystallized from ethanol. **26** (64.2 g, 233 mmol, 83%) was isolated as a colourless solid (hexanes : EtOAc = 4 : 1; R_f = 0.44).



EXPERIMENTS

mp.: 134 °C.

IR (ATR): $\tilde{\nu}_{\text{max}}$ (cm⁻¹) = 3267 (w), 1597 (w), 1370 (w), 1325 (m), 1157 (s), 672 (s).

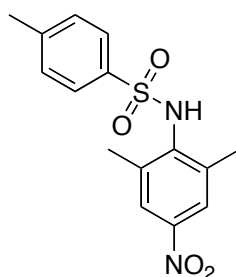
¹H-NMR (400 MHz, CD₃OD, 25 °C): δ (ppm) = 7.58 (d, *J* = 8 Hz, 2H), 7.29 (d, *J* = 8 Hz, 2H), 7.01 (m, 3H), 2.41 (s, 3H), 1.99 (s, 6H).

¹³C-NMR (100 MHz, CD₃OD, 25 °C): δ (ppm) = 143.3, 138.9, 137.9, 133.1, 129.2, 128.1, 127.1, 126.7, 20.0, 17.6.

HR-MS (EI) [M]⁺: calc for [C₁₅H₁₇NO₂S]⁺: 275.0980; found: 275.0975.

13.3.2 *N*-tosyl-2,6-dimethyl-4-nitroaniline²⁵⁹

Water (435 mL), glacial acetic acid (435 mL) and concentrated nitric acid (90.0 mL) were added to *N*-tosyl-2,6-dimethylaniline (**26**) (21.2 g, 76.8 mmol). Sodium nitrite (10.6 g, 154 mmol) was added and the mixture was heated to 140 °C. After 4 h the solution was cooled to room temperature and was kept at -80 °C overnight. The colourless crystalline product (**27**) (17.1 g, 53.4 mmol, 69%), (hexanes : EtOAc = 3 : 1, *R_f* = 0.31) was filtered off, washed with cold water and dried under high vacuum.



mp.: 165 °C.

IR (ATR): $\tilde{\nu}_{\text{max}}$ (cm⁻¹) = 3267 (m), 1596 (w), 1510 (s), 1332 (vs), 1156 (vs), 673 (vs).

¹H-NMR (400 MHz, CD₃OD, 27 °C): δ (ppm) = 7.87 (s, 2H), 7.57 (d, *J* = 8 Hz, 2H), 7.33 (d, *J* = 8 Hz, 2H), 2.41 (s, 2H), 2.10 (s, 2H).

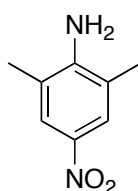
¹³C-NMR (100 MHz, CD₃OD, 27 °C): δ (ppm) = 146.0, 143.9, 139.8, 139.6, 138.6, 129.4, 126.6, 122.6, 20.0, 17.8.

HR-MS (EI) [M]⁺: calc for [C₁₅H₁₇NO₄S]⁺: 320.0831; found: 320.0823.

EXPERIMENTS

13.3.3 2,6-dimethyl-4-nitroaniline²⁵⁹

N-tosyl-2,6-dimethyl-4-nitroaniline (**27**) (8.04 g, 25.1 mmol) was dissolved in a mixture of H₂SO₄ (96% v/v, 41.0 mL) and water (3.00 mL). After stirring the solution in a sealed tube at 40 °C overnight, it was slowly added to an aqueous solution of NaOH (2 M, 80.0 mL) at 0 °C. The resulting suspension was extracted with EtOAc, dried over Na₂SO₄, filtered and concentrated. The remaining crude product was purified by normal phase chromatography (hexanes : CH₂Cl₂ = 1 : 1, R_f = 0.30) to yield **24** (2.67 g, 16.1 mmol, 64%) as a yellow solid.



mp.: 162 °C.

IR (ATR): $\tilde{\nu}_{\max}$ (cm⁻¹) = 3494 (m), 3387 (m), 1624 (s), 1594 (s), 1487 (vs), 1240 (s), 888 (s), 748 (s).

¹H-NMR (300 MHz, CD₃OD, 27 °C): δ (ppm) = 7.84 (s, 2H), 2.22 (s, 6H).

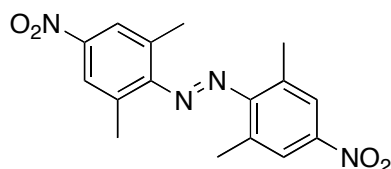
¹³C-NMR (75 MHz, CD₃OD, 27 °C): δ (ppm) = 151.2, 136.6, 124.0, 120.1, 16.3.

HR-MS (ESI) [M – H]⁻: calc for [C₈H₉N₂O₂]⁻: 165.0672; found: 165.0671.

13.3.4 Nitroazobenzene

2,6-dimethyl-4-nitroaniline (**24**) (2.00 g, 12 mmol) was dissolved in CH₂Cl₂ (120 mL) and a homogenous mixture of KMnO₄ (6.00 g, 38.0 mmol) and FeSO₄ · 7 H₂O (6.00 g, 21.6 mmol) was added. After heating the suspension to 50 °C overnight, the mixture was filtered through celite and the residue was washed with CH₂Cl₂ and Et₂O. The organic solvents were removed *in vacuo* and the remaining crude product was purified by normal phase chromatography (hexanes : CH₂Cl₂ = 1 : 1, R_f = 0.51) to give **28** (827 mg, 2.52 mmol, 21%) as purple needles.

EXPERIMENTS



mp.: 244 °C (dec.).

IR (ATR): $\tilde{\nu}_{\max}$ (cm⁻¹) = 3093 (m), 2928 (m), 2359 (w), 1505 (vs), 1350 (vs), 1301 (vs), 1108 (s), 1036 (s), 943 (s), 900 (vs), 810 (s), 722 (vs).

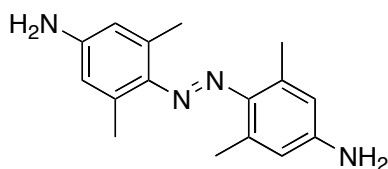
¹H-NMR (200 MHz, CDCl₃, 23 °C): δ (ppm) = 8.06 (s, 4H), 2.47 (s, 12H).

¹³C-NMR (75 MHz, CDCl₃, 23 °C): δ (ppm) = 154.8, 146.9, 132.6, 124.4, 19.6.

MS (ESI) [M - H]⁻: calc for [C₁₆H₁₅N₄O₄]⁻: 327.1102; found: 327.1097.

13.3.5 Aminoazobenzene

Nitroazobenzene (**28**) (50.0 mg, 0.152 mmol) was dissolved in a mixture of methanol and water (3 : 1, 1.70 mL) and heated to 70 °C. Na₂S (420 mg, 5.38 mmol) was slowly added at this temperature. Additional methanol and water (3 : 1, 1.70 ml) was added, in order to rinse the flask, and the mixture was heated to 90 °C for 45 min. After acidifying to pH = 7 with an aqueous solution of HCl (1 M), the mixture was cooled to room temperature, diluted with a saturated solution of NaHCO₃ and was extracted with EtOAc. The organic layer was washed with water, a saturated solution of NaHCO₃, a saturated solution of NaCl, and was dried over Na₂SO₄ and filtered. The organic solvent was removed *in vacuo* and purification by normal phase chromatography (CH₂Cl₂ : methanol = 98 : 2, R_f = 0.44) gave **29** (36 mg, 0.134 mmol, 88%) as a red solid.



mp.: 196 °C (dec.).

IR (ATR): $\tilde{\nu}_{\max}$ (cm⁻¹) = 3418 (w), 3327 (w), 3202 (w), 2909 (w), 1593 (vs), 1463 (m), 1372 (m), 1317 (s), 1164 (s), 1035 (m), 851 (vs).

EXPERIMENTS

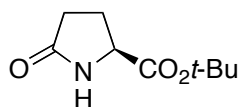
¹H-NMR (400 MHz, CD₃OD, 27 °C): δ (ppm) = 6.43 (s, 4H), 2.37 (s, 12H).

¹³C-NMR (100 MHz, CD₃OD, 27 °C): δ (ppm) = 147.7, 143.1, 133.8, 115.2, 20.1.

HR-MS (ESI) [M + H]⁺: calc for [C₁₆H₂₁N₄]⁺: 269.1758; found: 269.1757.

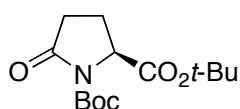
13.3.6 L-pyroglutamic acid *tert*-butyl ester²⁵⁸

(S)-2-pyrrolidine-5-carboxylic acid (**8**) (40.0 g, 310 mmol) was suspended in *tert*-butyl acetate (200 mL) and perchloric acid (10.0 mL, 70% v/v) was slowly added. After stirring for 24 h at room temperature, the mixture was cooled to 0 °C and a saturated solution of NaHCO₃ (500 mL) was added. Furthermore, solid NaHCO₃ was added in order to neutralize the solution. The mixture was extracted with EtOAc and the organic layer was washed with a saturated solution of NaCl, dried over Na₂SO₄ and filtered. The solvent was removed *in vacuo* and the product (**19**) (34.4 g, 186 mmol, 60%) was isolated as a colourless solid, which was directly taken for the next step without further purification.



13.3.7 N-Boc-L-pyroglutamic acid *tert*-butyl ester²⁵⁸

Triethylamine (37.0 mL, 266 mmol) was added to a solution of L-pyroglutamic acid *tert*-butyl ester (**19**) (16.3 g, 87.9 mmol), di-*tert*-butyl dicarbonate (38.5 g, 176 mmol) and 4-(dimethylamino)-pyridine (1.80 g, 14.7 mmol) in CH₂Cl₂ (225 mL). After stirring the reaction at room temperature overnight, the mixture was washed with 10% citric acid (2x, 500 mL), with a saturated solution of NaCl and was dried over Na₂SO₄. After filtration, the mixture was concentrated *in vacuo*. Purification by normal phase chromatography (hexanes : EtOAc = 3 : 2, R_f = 0.43) and recrystallization from ethanol yielded **20** (18.1 g, 63.5 mmol, 72%) as a colourless solid.



EXPERIMENTS

$[\alpha]^{25}_{\text{D}}$ (c 1.0, in CHCl_3): -39.8 .

mp.: $57\text{ }^\circ\text{C}$.

IR (ATR): $\tilde{\nu}_{\text{max}}$ (cm^{-1}) = 2975 (m), 1774 (s), 1720 (s), 1363 (m), 1288 (s), 1142 (vs), 1023 (m), 842 (m).

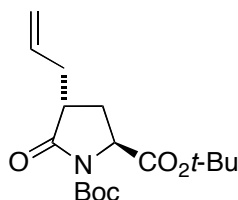
$^1\text{H-NMR}$ (300 MHz, CDCl_3 , $23\text{ }^\circ\text{C}$): δ (ppm) = 4.47 (dd, $J = 3\text{ Hz}$ and 12 Hz , 1H), 2.55 (m, 1H), 2.45 (m, 1H), 2.26 (m, 1H), 1.96 (m, 1H), 1.48 (s, 9H), 1.46 (s, 9H).

$^{13}\text{C-NMR}$ (75 MHz, CDCl_3 , $23\text{ }^\circ\text{C}$): δ (ppm) = 173.5, 170.3, 149.3, 83.3, 82.2, 59.6, 31.1, 27.9, 27.9, 21.6, 15.5.

HR-MS (ESI) $[\text{M} + \text{Na}]^+$: calc for $[\text{C}_{14}\text{H}_{23}\text{NNaO}_5]^+$: 308.1466; found: 308.1466.

13.3.8 Allylpyroglutamate

N-Boc-L-pyroglutamic acid *tert*-butylester (**20**) (6.00 g, 21.0 mmol) was dissolved in THF (86.0 mL) and cooled to $-78\text{ }^\circ\text{C}$. Fresh LiHMDS solution (36.0 mL, 0.670 M) [prepared by the dropwise addition of *n*-BuLi (10.5 mL, 26.3 mmol, 2.50 M) to a solution of HMDS (5.60 mL, 26.3 mmol) in THF (20.0 mL) at $0\text{ }^\circ\text{C}$ and stirring for 1 h at $-78\text{ }^\circ\text{C}$] was added dropwise at $-78\text{ }^\circ\text{C}$ and the mixture was stirred for 1 h at the stated temperature. A solution of allyl bromide (7.30 mL, 85.0 mmol) in THF (73.0 mL), cooled to $-78\text{ }^\circ\text{C}$, was added fast and the reaction mixture was stirred for 2 h 30 min at $-78\text{ }^\circ\text{C}$. A saturated solution of NH_4Cl was added at $-78\text{ }^\circ\text{C}$ and the reaction mixture was extracted with CH_2Cl_2 . The organic fractions were combined, washed with a saturated solution of NaCl, dried over Na_2SO_4 , filtered and concentrated. Purification by normal phase chromatography (hexanes : $\text{Et}_2\text{O} = 3 : 2$, $R_f = 0.43$) gave **21** (2.73 g, 8.40 mmol, 40%) as a colourless solid.



$[\alpha]^{25}_{\text{D}}$ (c 5.0, in CHCl_3): -28.52 .

mp.: $47\text{ }^\circ\text{C}$.

EXPERIMENTS

IR (ATR): $\tilde{\nu}_{\max}$ (cm⁻¹) = 3355 (s), 2972 (s), 2291 (w), 1695 (vs), 1519 (s), 1366 (s), 1250 (s), 1152 (vs), 1026 (m), 852 (w).

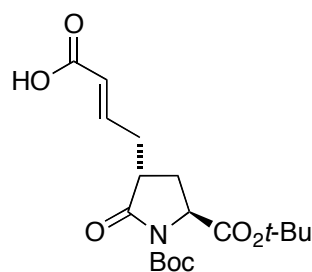
¹H-NMR (300 MHz, CDCl₃, 27 °C): δ (ppm) = 5.77 (m, 1H), 5.11 (m, 2H), 4.45 (dd, J = 3 Hz and 12 Hz, 1H), 2.69 (m, 2H), 2.18 (m, 2H), 2.00 (m, 1H), 1.52 (s, 9H), 1.49 (s, 9H).

¹³C-NMR (75 MHz, CDCl₃, 27 °C): δ (ppm) = 174.5, 170.3, 149.4, 134.5, 117.6, 83.3, 82.3, 57.8, 41.1, 34.5, 27.9, 27.9.

HR-MS (ESI) [2M + Na]⁺: calc for [C₃₄H₅₄N₂NaO₁₀]⁺: 673.3668; found: 673.3667.

13.3.9 Acrylic acid pyroglutamate

Allylpyroglutamate (**21**) (1.50 g, 4.62 mmol) was dissolved in CH₂Cl₂ (22.0 mL) and freshly distilled acrylic acid (0.950 mL, 13.8 mmol) was added at room temperature. After adding the mixture to Grubbs' 2nd generation catalyst (197 mg, 0.232 mmol, 5 mol%), the mixture was stirred at 40 °C overnight. The solvent was removed *in vacuo* and purification by normal phase chromatography (CH₂Cl₂ : EtOAc = 8.5 : 1.5 with 1% AcOH, R_f = 0.25) afforded **22** (1.36 g, 3.68 mmol, 80%) as a colourless solid.



[α]²⁵_D (c 1.2, in CHCl₃): -24.1.

mp.: 160 °C.

IR (ATR): $\tilde{\nu}_{\max}$ (cm⁻¹) = 2979 (w), 1778 (s), 1732 (m), 1683 (m), 1650 (m), 1370 (m), 1290 (s), 1250 (s), 1147 (vs), 991 (m), 959 (m), 842 (m), 776 (s), 687 (m).

¹H-NMR (600 MHz, CDCl₃, 27 °C): δ (ppm) = 6.98 (m, 1H), 5.90 (d, J = 18 Hz, 1H), 4.44 (dd, J = 6 Hz and 12 Hz, 1H), 2.80 (m, 2H), 2.32 (m, 1H), 2.18 (m, 1H), 1.91 (m, 1H), 1.49 (s, 9H), 1.46 (s, 9H).

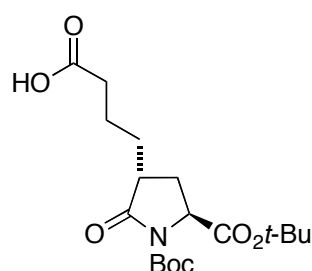
¹³C-NMR (150 MHz, CDCl₃, 27 °C): δ (ppm) = 173.6, 170.7, 170.0, 149.2, 147.3, 123.2, 83.6, 82.6, 57.6, 40.5, 33.0, 28.1, 27.9, 27.9.

EXPERIMENTS

HR-MS (ESI) [2M + Na]⁺: calc for [C₃₆H₅₄N₂NaO₁₄]⁺: 761.3466; found: 761.3465.

13.3.10 Carboxylic acid pyroglutamate

Acrylic acid pyroglutamate (**22**) (1.33 g, 3.60 mmol) was dissolved in methanol (240 mL) and Pd/C (600 mg, 0.560 mmol) was added. The solution was stirred under an atmosphere of hydrogen overnight and was filtered through celite. The solvent was removed *in vacuo* and the product (**23**) (1.27 g, 3.42 mmol, 95%) was isolated as a colourless solid (CH₂Cl₂ : EtOAc = 8.5 : 1.5 with 1% AcOH, R_f = 0.25).



[α]²⁵_D (c 1.0, in CHCl₃): -25.0.

mp.: 82 °C.

IR (ATR): $\tilde{\nu}_{\max}$ (cm⁻¹) = 2978 (w), 2361 (w), 1779 (s), 1732 (s), 1704 (s), 1368 (m), 1320 (s), 1249 (s), 1150 (vs), 1010 (m), 942 (m), 844 (m), 777 (m), 732 (m).

¹H-NMR (600 MHz, CDCl₃, 27 °C): δ (ppm) = 4.41 (dd, *J* = 6 Hz and 12 Hz, 1H), 2.56 (m, 1H), 2.33 (m, 2H), 2.17 (m, 1H), 1.92 (m, 2H), 1.65 (m, 2H), 1.47 (m, 9H), 1.45 (m, 9H), 1.38 (m, 1H).

¹³C-NMR (150 MHz, CDCl₃, 27 °C): δ (ppm) = 178.5, 175.3, 170.3, 149.4, 83.4, 82.3, 57.8, 41.4, 34.1, 29.7, 28.4, 27.9, 27.9, 22.1.

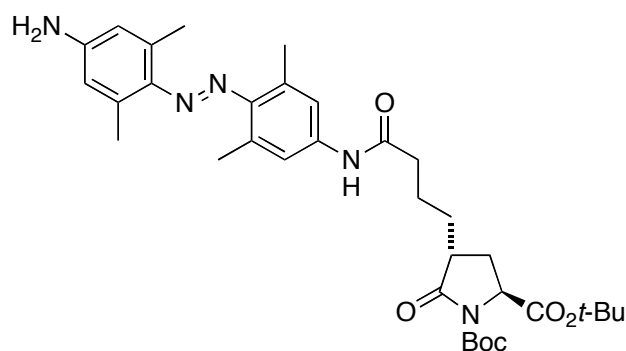
HR-MS (ESI) [M + Na]⁺: calc for [C₁₈H₂₉NNaO₇]: 394.1834; found: 394.1832.

13.3.11 Aminoazobenzene pyroglutamate

Aminoazobenzene (**29**) (360 mg, 1.34 mmol), HOBt (137 mg, 1.01 mmol; + 12% H₂O → 153 mg) and EDCI (168 mg, 0.880 mmol) were dissolved in acetonitrile (27.0 mL). DIPEA (0.588 mL, 3.38 mmol) was added slowly and a solution of carboxylic acid pyroglutamate (**23**) (250 mg, 0.673 mmol) in acetonitrile (4.00 mL) was added dropwise at 0 °C. After stirring at room temperature overnight, CH₂Cl₂ (100 mL) was

EXPERIMENTS

added and the mixture was washed with a saturated solution of NaHCO_3 and with a saturated solution of NaCl . The organic fraction was dried over Na_2SO_4 , filtered and the solvent was removed *in vacuo*. Purification by normal phase chromatography (CH_2Cl_2 : MeOH = 98 : 3, R_f = 0.33) gave **30** (355 mg, 0.571 mmol, 85%) as an orange solid.



$[\alpha]_D^{25}$ (c 0.5, in CHCl_3): 65.2.

mp.: 98 °C.

IR (ATR): $\tilde{\nu}_{\text{max}}$ (cm^{-1}) = 3360 (w), 2976 (w), 2361 (w), 1782 (s), 1734 (m), 1672 (m), 1597 (s), 1536 (m), 1456 (m), 1368 (m), 1311 (s), 1249 (w), 1147 (vs), 845 (m), 728 (s).

$^1\text{H-NMR}$ (400 MHz, CD_3OD , 27 °C): δ (ppm) = 7.31 (s, 2H), 6.43 (s, 2 H), 4.48 (dd, J = 4 Hz and 8 Hz, 1H), 2.61 (m, 1H), 2.42 (s, 6H), 2.39 (m, 2H), 2.34 (s, 6H), 2.23 (m, 1H), 2.05 (m, 1H), 1.90 (m, 1H), 1.75 (m, 3H), 1.47 (s, 18H).

$^{13}\text{C-NMR}$ (100 MHz, CD_3OD , 27 °C): δ (ppm) = 176.4, 172.5, 170.7, 149.5, 149.4, 148.3, 141.9, 137.1, 135.5, 131.4, 120.1, 114.8, 83.2, 82.2, 58.0, 41.2, 36.2, 29.7, 27.8, 26.8, 26.7, 22.4, 20.4, 19.1.

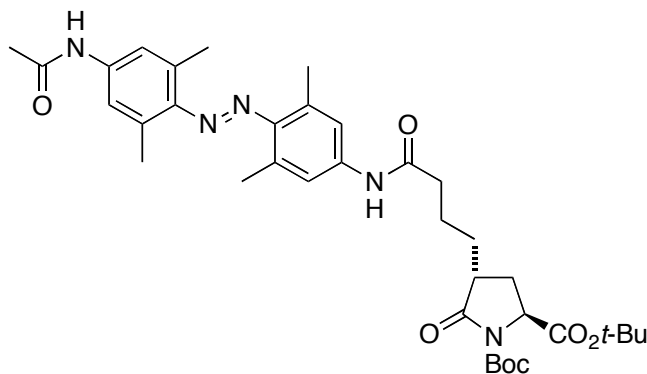
HR-MS (ESI) $[\text{M} + \text{H}]^+$: calc for $[\text{C}_{34}\text{H}_{48}\text{N}_5\text{O}_6]^+$: 622.3596; found: 622.3596.

13.3.12 *N*-acyl-aminoazobenzene pyroglutamate

Aminoazobenzene pyroglutamate (**30**) (350 mg, 0.563 mmol) was dissolved in THF (31.0 mL). DIPEA (192 μL , 1.13 mmol) was added and acetyl chloride (61.0 μL , 0.845 mmol) in THF (12.0 mL) was added at 0 °C over 45 min. After stirring for 15 min at this temperature, the reaction mixture was allowed to warm to room temperature and was stirred for 1 h. The solvent was removed *in vacuo* and the

EXPERIMENTS

remaining crude product was purified by normal phase chromatography (CH₂Cl₂ : MeOH = 95 : 5, R_f = 0.33) to provide **31** (362 mg, 0.546 mmol, 97%) as an orange solid.



$[\alpha]_D^{25}$ (c 0.5, in CHCl₃): 76.8.

mp.: 126 °C.

IR (ATR): $\tilde{\nu}_{\text{max}}$ (cm⁻¹) = 3333 (w), 2977 (w), 2361 (w), 1782 (s), 1737 (m), 1673 (m), 1594 (s), 1533 (s), 1473 (m), 1368 (s), 1315 (s), 1249 (s), 1150 (vs), 1037 (w), 868 (m), 727 (vs).

¹H-NMR (600 MHz, CDCl₃, 27 °C): δ (ppm) = 7.65 (s, 1H), 7.34 (s, 2H), 7.29 (s, 2H), 4.44 (dd, *J* = 6 Hz and 12 Hz, 1H), 2.63 (m, 1H), 2.45 (m, 1H), 2.42 (s, 12H), 2.22 (m, 1H), 2.18 (s, 3H), 1.99 (m, 3H), 1.81 (m, 2H), 1.63 (m, 1H), 1.49 (s, 9H), 1.47 (s, 9H).

¹³C-NMR (150 MHz, CDCl₃, 27 °C): δ (ppm) = 175.5, 170.9, 170.2, 168.3, 149.3, 147.5, 147.3, 137.8, 137.6, 133.4, 133.4, 130.3, 120.2, 120.1, 83.4, 82.4, 57.8, 41.5, 37.2, 29.6, 28.5, 27.9, 27.9, 24.7, 22.7, 20.6, 20.6, 19.8.

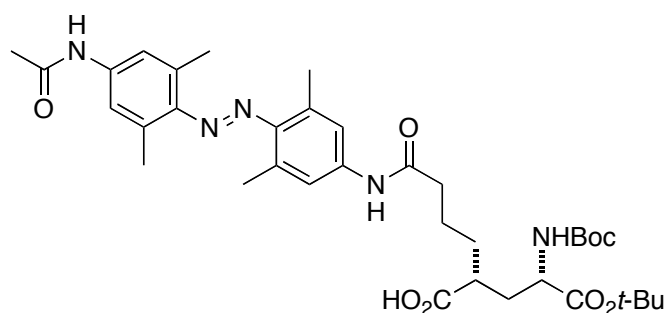
HR-MS (ESI) [M + H]⁺: calc for [C₃₆H₅₀N₅O₇]⁺: 664.3702; found: 664.3704.

13.3.13 Azobenzene glutamic acid ester

N-acyl-aminoazobenzene pyroglutamate (**31**) (351 mg, 0.529 mmol) was dissolved in THF (70.0 mL). An aqueous solution of LiOH (1.00 M, 16.5 ml, 16.5 mmol) was added dropwise at 0 °C. After stirring for 1 h, EtOAc (46.0 mL) and a saturated solution of NaHCO₃ (46.0 mL) were added and the mixture was stirred for 1 h at 0 °C. Water (70.0 ml) was added and the mixture was acidified to pH = 2 with an aqueous solution of HCl (1 M) at 0 °C. The reaction mixture was extracted with EtOAc and the

EXPERIMENTS

combined organic layers were washed with water and a saturated solution of NaCl, dried over Na₂SO₄ and the solvent was removed *in vacuo* after filtration. Purification by normal phase chromatography (CH₂Cl₂ : MeOH : AcOH = 94 : 4 : 2, R_f = 0.21) yielded **32** (288 mg, 0.423 mmol, 80%) as an orange solid.



$[\alpha]_D^{25}$ (c 0.25, in MeOH): 3.2.

mp.: 136 °C.

IR (ATR): $\tilde{\nu}_{\max}$ (cm⁻¹) = 3311 (w), 2976 (w), 2361 (m), 1671 (s), 1594 (s), 1540 (s), 1366 (s), 1319 (s), 1256 (s), 1152 (vs), 1033 (m), 865 (m), 747 (m), 668 (m).

¹H-NMR (400 MHz, CD₃OD, 27 °C): δ (ppm) = 7.87 (s, NH, exch.), 7.38 (s, 2H-*trans*), 7.37 (s, 2H-*trans*), 7.20 (s, 2H-*cis*), 7.19 (s, 2H-*cis*), 4.00 (dd, *J* = 4 Hz and 12 Hz, 1H), 2.52 (m, 2H), 2.41 (s, 12H-*trans*), 2.13 (m, 1H), 2.12 (s, 3H-*trans+cis*), 1.87 (s, 12H-*cis*), 1.70 (m, 4H), 1.59 (m, 2H), 1.44 (s, 9H), 1.42 (s, 9H).

¹³C-NMR (100 MHz, CD₃OD, 27 °C): δ (ppm) = 177.7, 172.8, 172.1, 170.3, 156.7, 147.1, 147.1, 138.5, 132.7, 132.7, 128.6, 120.1, 112.0, 81.2, 79.0, 53.1, 42.0, 36.3, 33.4, 32.0, 27.3, 26.8, 23.1, 22.5, 19.4, 19.4, 17.8.

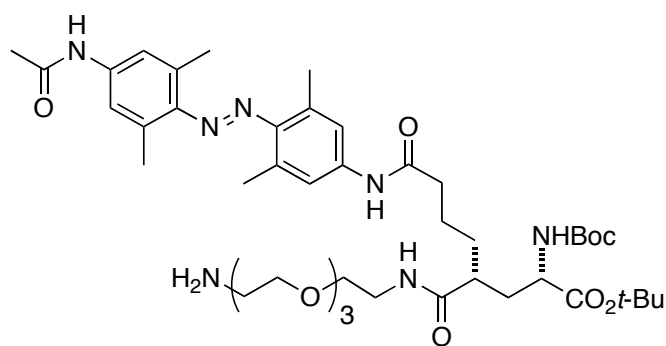
HR-MS (ESI) [M + H]⁺: calc for [C₃₆H₅₂N₅O₈]⁺: 682.3808; found 682.3806.

13.3.14 Azobenzene glutamic acid ester γ -amide

Azobenzene glutamic acid ester (**32**) (262 mg, 0.384 mmol) was dissolved in THF (66.0 mL) and triethylamine (69.5 μ L, 0.497 mmol) was added. *iso*-butyl chloroformate (59.6 μ L, 0.461 mmol) was added at -40 °C and the mixture was stirred at this temperature for 1 h. The mixed anhydride was added dropwise to 1,11-diamino-3,6,9-trioxaundecane (146 μ L, 0.770 mmol) in THF (224 mL) at 0 °C and the mixture was stirred for 1 h at 0 °C followed by 1 h at room temperature. After adding

EXPERIMENTS

a saturated solution of NaCl (280 mL) at 0 °C, the mixture was allowed to warm to room temperature and was extracted with EtOAc. The organic layers were washed with water and the aqueous layer was reextracted with EtOAc. The combined organic fractions were washed with a saturated solution of NaCl, dried over Na₂SO₄ and concentrated. The solvent was removed *in vacuo* and the crude mixture was purified by column chromatography (amine functionalized silica, EtOAc : CH₂Cl₂ : MeOH = 100 : 0 : 0 → 0 : 100 : 0 → 0 : 99 : 1) to give **33** (148 mg, 0.173 mmol, 45%) as a red solid (CH₂Cl₂ : MeOH : TEA = 93 : 5 : 2, R_f = 0.19). The product was characterized by mass spectrometry and was directly taken for the next step.

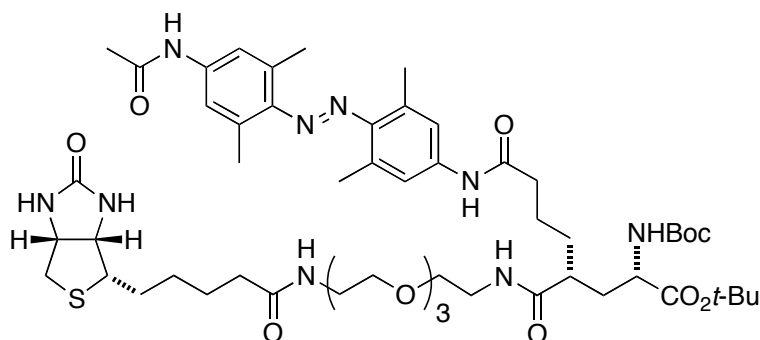


HR-MS (ESI) [M + H]⁺: calc for [C₄₄H₇₀N₇O₁₀]⁺: 856.5176; found: 856.5176.

13.3.15 Biotin azobenzene glutamic acid ester γ -amide

D-biotin (20.3 mg, 0.0829 mmol) was dissolved in DMF (5.00 mL) and TEA (35.0 μ L, 0.2487 mmol) was added at 0 °C. After stirring for 10 min, pentafluorophenyl trifluoroacetate (17.2 μ L, 0.0995 mmol) was added and the reaction mixture was allowed to warm to room temperature and was stirred for 4 h. Azobenzene glutamic acid ester γ -amide (**33**) (71.0 mg, 0.0829 mmol) was dissolved in DMF (2.50 mL) and was added dropwise to the biotin pentafluorophenyl ester. The reaction was stirred overnight at room temperature and the crude mixture was purified by normal phase chromatography (CHCl₃ : MeOH = 9 : 1, R_f = 0.38) to yield **34** (88.0 mg, 0.0814 mmol, 98%) as a red solid.

EXPERIMENTS



$[\alpha]_D^{25}$ (c 0.5, in MeOH): 13.8.

mp.: 250 °C.

IR (ATR): $\tilde{\nu}_{\max}$ (cm⁻¹) = 3305 (m), 1691 (vs), 1597 (vs), 1539 (s), 1155 (s).

¹H-NMR (400 MHz, CD₃OD, 27 °C): δ (ppm) = 7.39 (s, 2H-*trans*), 7.37 (s, 2H-*trans*), 7.21 (s, 2H-*cis*), 7.20 (s, 2H-*cis*), 4.43 (m, 1H), 4.25 (m, 1H), 3.87 (dd, J = 8 Hz and 12 Hz, 1H), 3.53 (m, 14H), 3.32 (t, J = 6 Hz, 2H), 3.14 (m, 1H), 2.86 (m, 1H), 2.68 (d, J = 12 Hz, 1H), 2.41 (s, 12H-*trans*), 2.37 (m, 2H), 2.17 (m, 3H), 2.12 (s, 3H-*trans+cis*), 1.87 (12H-*cis*), 1.62 (m, 9H), 1.43 (s, 9H), 1.43 (s, 9H), 1.39 (m, 2H).

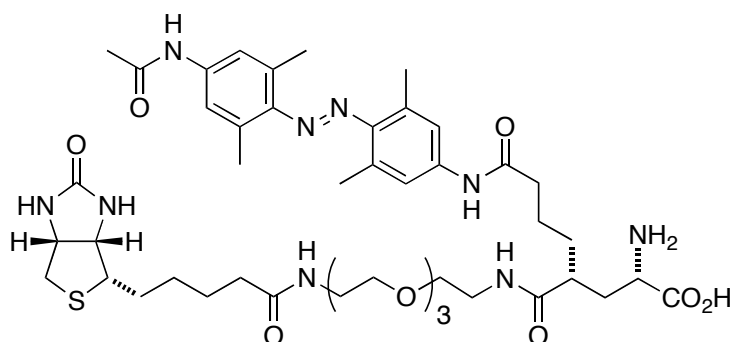
¹³C-NMR (100 MHz, CD₃OD, 27 °C): δ (ppm) = 175.6, 174.6, 172.8, 172.0, 170.3, 164.6, 156.7, 149.2, 147.1, 138.6, 138.3, 132.7, 128.6, 120.0, 120.0, 119.7, 119.6, 81.2, 79.0, 70.2, 70.1, 69.8, 69.2, 61.9, 60.2, 55.5, 52.9, 43.2, 39.6, 38.9, 36.5, 35.3, 33.7, 32.5, 28.3, 28.1, 27.4, 26.8, 25.4, 23.4, 22.6, 19.5, 17.9, 17.8.

HR-MS (ESI) [M + H]⁺: calc for [C₅₄H₈₄N₉O₁₂S]⁺: 1082.5952; found: 1082.5952.

13.3.16 BAG

Biotin azobenzene glutamic acid ester γ -amide (**34**) (2.60 mg, 0.00240 mmol) was dissolved in CH₂Cl₂ (2.60 mL) and anisole (15.7 μ L, 0.140 mmol) was added. After adding TFA (0.162 mL, 2.20 mmol) dropwise at 0 °C, the mixture was stirred at room temperature for 1 h. The addition of TFA and stirring for 1 h was sequentially repeated six times. The reaction mixture was stirred overnight, diluted with Et₂O (26.0 mL), and the resulting precipitate was collected by centrifugation to yield **3** (2.00 mg, 0.00216 mmol, 90%) as an orange solid as the free base. In order to prepare the HCl salt, the solid was dissolved in MeOH (2.00 mL) and HCl in MeOH (0.500 M) was added dropwise until the colour changed to red.

EXPERIMENTS



$^1\text{H-NMR}$ (600 MHz, CD_3OD , 27 °C): δ (ppm) = 7.40 (s, 2H-*trans*), 7.37 (s, 2H-*trans*), 7.22 (s, 2H-*cis*), 7.20 (s, 2H-*cis*), 4.45 (m, 1H), 4.26 (m, 1H), 3.59 (m, 15H), 3.34 (t, J = 6 Hz, 2H), 3.15 (m, 1H), 2.88 (m, 1H), 2.68 (d, J = 12 Hz), 2.52 (m, 2H), 2.41 (s, 12H-*trans*), 2.20 (m, 3H), 2.13 (s, 3H-*trans+cis*), 1.87 (s, 12H-*cis*), 1.64 (m, 9H), 1.41 (t, J = 6 Hz, 2H).

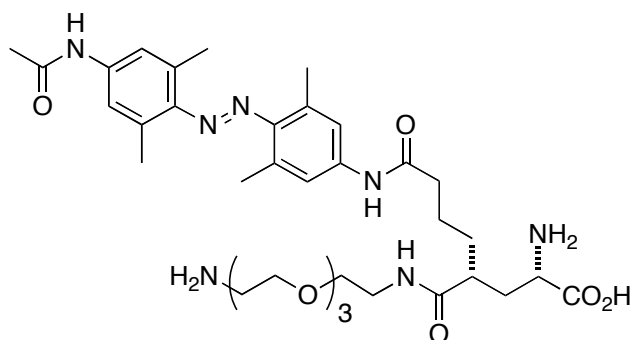
$^{13}\text{C-NMR}$ (150 MHz, CD_3OD , 27 °C): δ (ppm) = 176.3, 174.8, 172.7, 170.3, 164.6, 147.1, 138.6, 132.7, 128.6, 120.0, 120.0, 119.7, 119.6, 113.7, 70.1, 70.0, 69.8, 69.7, 69.3, 69.2, 61.9, 60.2, 55.6, 39.6, 38.9, 38.8, 36.4, 35.3, 28.3, 28.1, 25.5, 23.2, 22.5, 19.5, 17.8.

HR-MS (ESI) $[\text{M} + \text{H}]^+$: calc for $[\text{C}_{45}\text{H}_{68}\text{N}_9\text{O}_{10}\text{S}]^+$: 926.4802; found: 926.4814.

13.3.17 Azobenzene glutamic acid γ -amide

Azobenzene glutamic acid ester γ -amide (**33**) (2.70 mg, 0.00317 mmol) was dissolved in CH_2Cl_2 (3.40 mL) and anisole (20.7 μL , 0.190 mmol) was added. After adding TFA (0.214 mL, 2.90 mmol) dropwise at 0 °C, the mixture was stirred at room temperature for 1 h. The addition of TFA and stirring for 1 h was sequentially repeated four times. The reaction mixture was stirred overnight, diluted with hexanes (34.0 mL) and the resulting precipitate was collected by centrifugation to yield **35** (2.00 mg, 0.00286 mmol, 90%) as an orange solid as the free base. In order to prepare the HCl salt, the solid was dissolved in MeOH (2.00 mL) and HCl in MeOH (0.500 M) was added dropwise until the colour changed to red.

EXPERIMENTS



$^1\text{H-NMR}$ (400 MHz, CD_3OD , 25 °C): δ (ppm) = 7.41 (s, 2H-*trans*), 7.39 (s, 2H-*trans*), 7.23 (s, 2H-*cis*), 7.21 (s, 2H-*cis*), 3.62 (m, 13H), 3.42 (t, $J = 4\text{Hz}$, 2H), 3.13 (t, $J = 4\text{Hz}$, 2H), 2.58 (m, 2H), 2.43 (s, 12H-*trans*), 2.19 (m, 1H), 2.14 (s, 3H-*trans+cis*), 1.88 (s, 12H-*cis*), 1.69 (m, 6H).

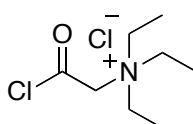
$^{13}\text{C-NMR}$ (100 MHz, CD_3OD , 25 °C): δ (ppm) = 175.9, 172.7, 170.3, 147.1, 147.1, 138.7, 138.6, 132.7, 132.7, 120.0, 119.7, 70.0, 70.0, 69.6, 69.6, 69.2, 66.4, 52.1, 42.9, 39.1, 38.9, 36.2, 33.0, 31.3, 23.0, 22.5, 19.4, 17.8.

MS (ESI) $[\text{M} + \text{H}]^+$: calc for $[\text{C}_{35}\text{H}_{54}\text{N}_7\text{O}_8]^+$: 700.4026; found: 700.4030.

13.4 Preparation of 2,2',6,6'-tetramethyl-QAQ

13.4.1 Betaine acid chloride

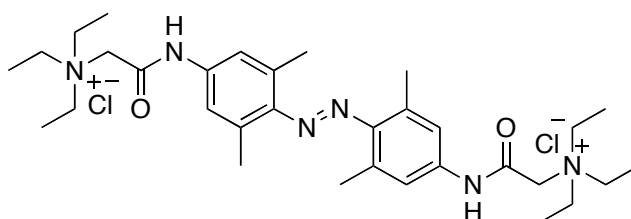
Triethylammonium acetate (**36**) (100 mg, 0.628 mmol) was dissolved in MeCN (0.60 mL) and a solution of oxalyl chloride in CH_2Cl_2 (0.314 mL, 0.628 mmol, 2.00 M) was added. After adding two drops of DMF, the solution was stirred at room temperature for 15 min. The solvent was removed *in vacuo* and the product (**37**) (134 mg, 0.628 mmol, quant.) was isolated as a light yellow solid and was used without further purification.



EXPERIMENTS

13.4.2 2,2',6,6'-tetramethyl-QAQ

Aminoazobenzene (**29**) (48.0 mg, 0.179 mmol) was dissolved in MeCN : DMF = 1 : 1 (10.0 mL) and DIPEA (106 μ L, 0.628 mmol) was added. Betaine acid chloride (**37**) (134 mg, 0.628 mmol) in MeCN : DMF = 1 : 1 (20.0 mL) was added at 0 °C over 1 h. The reaction was stirred for 15 min, warmed to room temperature and was stirred overnight. The precipitate was collected by centrifugation. Purification by reversed phase chromatography (H₂O : MeOH = 100 : 0 \rightarrow 80 : 20, 0.1% formic acid) gave **6** (57.0 mg, 0.089 mmol, 50%) as an orange solid.



mp.: 276 °C.

IR (ATR): $\tilde{\nu}_{\text{max}}$ (cm⁻¹) = 3377 (w), 2980 (w), 1683 (m), 1593 (vs), 1472 (s), 1364 (s), 1318 (s), 1159 (m), 1007 (m), 880 (m), 765 (m).

¹H-NMR (400 MHz, CD₃OD, 25 °C): δ (ppm) = 7.46 (s, 2H-*trans*), 7.29 (s, 2H-*cis*), 4.20 (s, 4H), 3.67 (q, J = 16 Hz, 12H), 2.44 (s, 12H-*trans*), 1.91 (s, 12H-*cis*), 1.40 (t, J = 8Hz, 16H).

¹³C-NMR (100 MHz, CD₃OD, 25 °C): δ (ppm) = 161.7, 147.7, 137.4, 132.9, 120.3, 56.2, 54.4, 19.3, 17.8, 6.6.

HR-MS (ESI) [M – H]⁺: calc for [C₃₂H₅₁N₆O₂]⁺: 551.4071; found 551.4077.

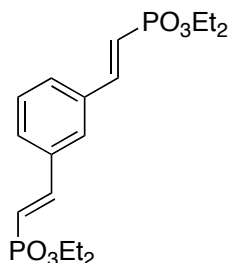
13.5 Preparation of MOBIPHOS and MOBIPHOSen

13.5.1 Bisphosphonate

Tetraethyl methylenebisphosphonate (3.00 mL, 12.1 mmol) was dissolved in THF (28.0 mL) and *n*-BuLi (4.40 mL, 11.0 mmol, 2.50 M) was added dropwise at –78 °C. After stirring at this temperature for 15 min, a solution of isophthalaldehyde (**39**) (736 mg, 5.49 mmol) in THF (14.0 mL) was cooled to 0 °C and added fast at –78 °C. The mixture was allowed to warm to room temperature and was stirred overnight. The

EXPERIMENTS

crude mixture was concentrated and purified by normal phase chromatography (Et₂O : hexanes : MeOH = 5 : 4 : 1, R_f = 0.26) to yield **40** (2.12 g, 5.27 mmol, 96%) as a colourless solid.



mp.: 102 °C.

IR (ATR): $\tilde{\nu}_{\text{max}}$ (cm⁻¹) = 2978 (w), 1616 (m), 1429 (w), 1234 (s), 1165 (m), 1019 (s), 1108 (s), 940 (vs), 848 (s), 787 (s).

¹H-NMR (300 MHz, CDCl₃, 27 °C): δ (ppm) = 7.47 (m, 6H), 6.27 (m, 2H), 4.12 (m, 8H), 1.33 (t, *J* = 9 Hz, 12H).

¹³C-NMR (75 MHz, CDCl₃, 27 °C): δ (ppm) = 147.7, 147.6, 135.7, 135.7, 135.4, 135.4, 129.4, 129.1, 126.7, 116.6, 114.1, 61.9, 61.9, 16.4, 16.3.

³¹P-NMR (80 MHz, CDCl₃, 23 °C): δ (ppm) = 19.9.

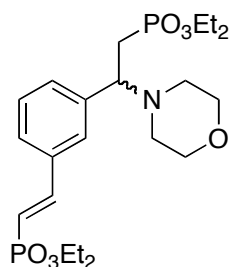
HR-MS (EI) [M]⁺: calc for [C₁₈H₂₈O₆P₂]⁺: 402.1361; found: 402.1358.

13.5.2 Morpholino bisphosphonate

ZnCl₂ (3.14 g, 23.0 mmol) and LiCl (1.94 g, 46.0 mmol) were heated to 150 °C under high vacuum for 6 h. After cooling to room temperature, THF (20.0 mL) was added and the suspension was stirred at 60 °C overnight. Isopropylmagnesium chloride (0.750 mL, 1.50 mmol, 2.00 M) was added dropwise to a solution of morpholine (132 μ L, 1.50 mmol) in THF (15.0 mL) at 0 °C. After stirring for 30 min, ZnCl₂ · 2 LiCl (ZnCl₂: 1.15 M, LiCl: 2.30 M) in THF (0.660 mL) was added dropwise and the solution was stirred at 0 °C for 30 min. The freshly prepared (morpholine)₂Zn · 2 MgCl₂ · 2 LiCl solution was titrated prior to use and the concentration was determined to be 52.0 mM. The *in situ* prepared morpholine compound (11.7 mL, 608 μ mol) was added dropwise to the bisphosphonate (**40**) (82.0 mg, 203 μ mol) in THF (6.00 mL) at 0 °C. The solution was allowed to warm to

EXPERIMENTS

room temperature and was slowly heated to 40 °C for 4 hours. After stirring overnight at room temperature, a saturated solution of NH₄Cl was added and the mixture was extracted with CH₂Cl₂. The organic layer was washed with water and a saturated solution of NaCl, dried over Na₂SO₄, filtered and concentrated. Purification by normal phase chromatography (Et₂O : hexanes : MeOH = 10 : 7 : 3, R_f = 0.25) yielded **41** (39.0 mg, 80.0 μmol, 39%) as a colourless oil.



IR (ATR): $\tilde{\nu}_{\max}$ (cm⁻¹) = 3447 (w), 2981 (w), 2361 (w), 1619 (w), 1447 (w), 1393 (w), 1229 (s), 1115 (m), 1020 (vs), 958 (vs), 849 (s), 804 (s).

¹H-NMR (400 MHz, CD₃CN, 27 °C): δ (ppm) = 7.55 (m, 1H), 7.42 (m, 4H), 6.45 (m, 1H), 4.08 (m, 4H), 3.96 (m, 2H), 3.86 (m, 2H), 3.81 (m, 1H), 3.60 (m, 4H), 2.49 (m, 2H), 2.38 (m, 4H), 1.32 (t, *J* = 4 Hz, 6H), 1.20 (t, *J* = 4 Hz, 3H), 1.11 (t, *J* = 4 Hz, 3H).

¹³C-NMR (100 MHz, CD₃CN, 27 °C): δ (ppm) = 147.8, 147.8, 134.9, 134.6, 130.9, 128.4, 128.1, 127.0, 115.9, 114.1, 69.8, 66.6, 64.1, 61.6, 61.6, 61.2, 61.1, 49.6, 28.9, 27.5, 15.8, 15.7, 15.7, 15.6, 15.6, 15.6.

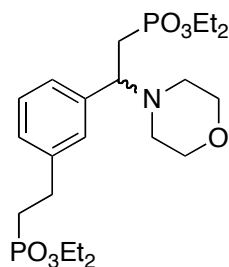
³¹P-NMR (80 MHz, CD₃CN, 23 °C): δ (ppm) = 19.7, 29.9.

HR-MS (ESI) [M + H]⁺: calc for [C₂₂H₃₈NO₇P₂]⁺: 490.2115; found: 490.2111.

13.5.3 Morpholino dihydrobisphosphonate

Morpholino bisphosphonate (**41**) (39.0 mg, 0.0800 mmol) was dissolved in EtOAc (3.90 mL) and 5% Pt/C (25 wt%, 9.70 mg) was added. After stirring under an atmosphere of H₂ at 5 bar for five hours, the mixture was filtered through celite. Removal of the solvent gave **42** (38.0 mg, 0.0770 mmol, 96%) as a colourless oil. The product (Et₂O : hexanes : MeOH = 10 : 7 : 3, R_f = 0.25) did not need further purification.

EXPERIMENTS



IR (ATR): $\tilde{\nu}_{\max}$ (cm⁻¹) = 3464 (w), 2980 (w), 2361 (w), 1449 (w), 1239 (s), 1116 (m), 1022 (vs), 955 (vs), 803 (s), 707 (m).

¹H-NMR (600 MHz, CD₃CN, 27 °C): δ (ppm) = 7.21 (m, 4H), 4.06 (m, 4H), 3.97 (m, 2H), 3.89 (m, 2H), 3.81 (m, 1H), 3.59 (m, 4H), 2.87 (m, 2H), 2.50 (m, 1H), 2.38 (m, 4H), 2.27 (m, 1H), 2.06 (m, 2H), 1.29 (t, J = 6 Hz, 6H), 1.21 (t, J = 6 Hz, 3H), 1.13 (t, J = 6 Hz, 3H).

¹³C-NMR (150 MHz, CD₃CN, 27 °C): δ (ppm) = 141.0, 140.9, 137.6, 137.5, 128.7, 128.0, 127.3, 126.9, 66.6, 64.2, 61.5, 61.4, 61.4, 61.3, 61.3, 61.2, 49.6, 28.9, 28.3, 28.2, 27.9, 27.2, 26.3, 15.8, 15.8, 15.7, 15.7, 15.7, 15.6.

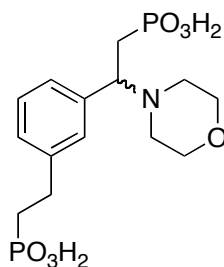
³¹P-NMR (80 MHz, CD₃CN, 23 °C): δ (ppm) = 31.3, 30.3.

HR-MS (ESI) [M + H]⁺: calc for [C₂₂H₄₀NO₇P₂]⁺: 492.2272; found: 492.2269.

13.5.4 MOBIPHOS

The crude hydrogenation product (**42**) (32.0 mg, 0.0650 mmol) was dissolved in MeCN (7.00 mL) and the solution was cooled to 0 °C. After adding trimethylsilyl iodide (39.0 μ L, 0.260 mmol) in MeCN (97.0 μ L) dropwise at 0 °C and stirring for 1 h at this temperature, the solution was warmed to room temperature and was additionally stirred for 1 h. The reaction mixture was concentrated *in vacuo* and MeCN : water : AcOH (8 : 1 : 1, 5.00 mL) was added to the crude mixture. The mixture was stirred for 20 min and was concentrated. Again MeCN : water : AcOH (8 : 1 : 1, 5.00 mL) was added and evaporated immediately. After co-evaporation with toluene (2x), the solid was taken up in water (5.00 mL) and concentrated two times. Purification by reverse phase HPLC (5% MeCN in H₂O, 0.1% TFA, Microsorb 60 C18, L x ID (mm) = 250 x 4.6, retention time of the peak of interest: 9 min) gave **4** (29.0 mg, 0.0580 mmol, 89%) as the TFA salt as a colourless oil.

EXPERIMENTS



IR (ATR): $\tilde{\nu}_{\max}$ (cm⁻¹) = 2606 (w), 2331 (w), 1785 (m), 1667 (m), 1449 (m), 1123 (s), 903 (vs), 775 (s), 704 (s).

¹H-NMR (400 MHz, D₂O, 27 °C): δ (ppm) = 7.30 (m, 4H), 4.44 (m, 1H), 3.89 (m, 2H), 3.56 (m, 3H), 3.09 (m, 1H), 2.95 (m, 1H), 2.82 (m, 3H), 2.53 (m, 2H), 1.98 (m, 2H).

¹³C-NMR (100 MHz, D₂O, 27 °C): δ (ppm) = 142.3, 142.2, 130.4, 130.3, 130.3, 129.7, 129.4, 127.9, 67.3, 67.3, 63.8, 63.8, 50.5, 48.0, 28.5, 28.0, 28.0, 27.2.

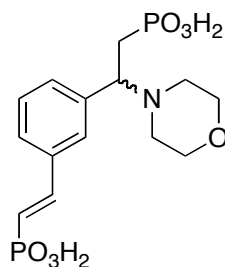
³¹P-NMR (80 MHz, D₂O, 23 °C): δ (ppm) = 20.3, 31.0.

HR-MS (ESI) [M + H]⁺: calc for [C₁₄H₂₄NO₇P₂]⁺: 380.1020; found: 380.1020.

13.5.5 MOBIPHOSen

Morpholino bisphosphonate (**41**) (20.0 mg, 0.0410 mmol) was dissolved in MeCN (4.50 mL) and the solution was cooled to 0 °C. After adding trimethylsilyl iodide (25.0 μ L, 0.160 mmol) in MeCN (65.0 μ l) dropwise at 0 °C and stirring for 1 h at this temperature, the solution was warmed to room temperature and was additionally stirred for 1 h. The reaction mixture was concentrated *in vacuo* and MeCN : water : AcOH (8 : 1 : 1, 5.00 mL) was added to the crude mixture. After stirring for 20 min, the mixture was concentrated. Again MeCN : water : AcOH (8 : 1 : 1, 5.00 mL) was added and evaporated immediately. After co-evaporation with toluene (2x), the solid was taken up in water (5.00 mL) and concentrated two times. Purification by reverse phase HPLC (5% MeCN in H₂O, 0.1% TFA, Microsorb 60 C18, L x ID (mm) = 250 x 4.6, retention time of the peak of interest: 7 min) gave **38** (10.0 mg, 0.0200 mmol, 50%) as the TFA salt as a colourless oil.

EXPERIMENTS



IR (ATR): $\tilde{\nu}_{\max}$ (cm⁻¹) = 2301 (br), 1668 (m), 1439 (m), 1126 (s), 931 (vs), 791 (s), 702 (s).

¹H-NMR (400 MHz, D₂O, 27 °C): δ (ppm) = 7.62 (m, 1H), 7.40 (m, 4H), 6.44 (m, 1H), 4.50 (m, 1H), 3.93 (m, 2H), 3.60 (m, 3H), 3.14 (m, 1H), 2.99 (m, 1H), 2.84 (m, 1H), 2.49 (m, 2H).

¹³C-NMR (100 MHz, D₂O, 27 °C): δ (ppm) = 144.2, 144.2, 136.3, 136.0, 131.2, 131.1, 131.0, 129.7, 129.4, 129.1, 119.7, 117.9, 117.7, 114.8, 67.4, 63.9, 50.6, 47.8, 28.6, 27.3.

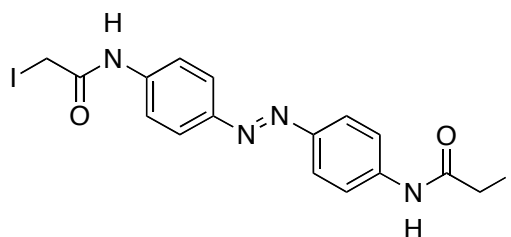
³¹P-NMR (80 MHz, D₂O, 23 °C): δ (ppm) = 17.1, 18.9.

MS (ESI) [M – H]⁻: calc for [C₁₄H₂₀NO₇P₂]⁻: 376.0723; found: 376.0720 (100).

13.6 Preparation of ABA

4,4'-diaminoazobenzene (**43**) (127 mg, 0.600 mmol) was dissolved in THF (25.0 mL). TEA (0.240 mL, 1.75 mmol) was added and the mixture was stirred for 5 min. After adding chloroacetylchloride (0.140 mL, 1.75 mmol) dropwise at 0 °C, the mixture was stirred for 30 min at this temperature, was allowed to warm to room temperature and was stirred for 4 h. The mixture was filtered and the solvent was removed *in vacuo*. Sodium iodide (10.0 g, 66.0 mmol) was dissolved in acetone (40.7 mL) and THF (12.5 mL), was cannulated to the crude mixture and the solution was stirred overnight protected from light. The reaction mixture was filtered and the solvent was evaporated. The solid was dissolved in THF (5.00 mL) and after filtra, icecold water (7.00 mL) was added. The precipitate (**5**) (39.0 mg, 0.0720 mmol, 12%) was collected by centrifugation.

EXPERIMENTS



mp.: 252 °C (dec.).

IR (ATR): $\tilde{\nu}_{\max}$ (cm⁻¹) = 3474 (br), 3297 (m), 3264 (m), 3143 (w), 1656 (s), 1610 (m), 1544 (s), 1411 (m), 1332 (m), 1081 (w), 844 (m).

¹H-NMR (200 MHz, DMSO, 23 °C): δ (ppm) = 10.63 (s, 2H), 7.88 (d, J = 10 Hz, 4H), 7.78 (d, J = 10 Hz, 4H), 3.85 (s, 4H).

¹³C-NMR (100 MHz, DMSO, 27 °C): δ (ppm) = 167.5, 148.3, 143.0, 123.9, 119.8, 1.8.

HR-MS (ESI) [M + H]⁺: calc for [C₁₆H₁₅I₂N₄O₂]: 548.9276; found: 548.9282.

Chapter 14: Biology

14.1 Materials

14.1.1 Chemicals and reagents

Commercially available reagents of > 98% purity were used as obtained.

14.1.2 Buffers, solutions and media

Buffers, solutions and media	Components
Cation exchange buffer (GluK2)	A = 20 mM NaOAc pH = 5.0, 1 mM EDTA, 1 mM monosodium glutamate, 5 mM methionine
	B = 20 mM NaOAc pH = 5.0, 1 M NaCl, 1 mM EDTA, 1 mM monosodium glutamate, 5 mM methionine
Cation exchange buffer (GluA2)	A = 20 mM NaOAc pH = 6.0, 1 mM EDTA, 1 mM monosodium glutamate, 5 mM methionine
	B = 20 mM NaOAc pH = 6.0, 0.5 M NaCl, 1 mM EDTA, 1 mM monosodium glutamate, 5 mM methionine

EXPERIMENTS

Cell lysis buffer	50 mM Tris pH = 8.0, 200 mM NaCl, 5 mM MgCl ₂
Coomassie staining solution	41.5% MeOH, 8.3% HOAc, 50% H ₂ O, 0.2% (w/v) Coomassie Brilliant Blue R 250
Crystallization buffer	10 mM HEPES pH = 8.0, 150 mM NaCl, 1 mM EDTA
Destaining solution	10% HOAc, 20% EtOH, 70% H ₂ O
DNase solution	4000 units/mL in 10 mM HEPES pH = 7.0, 150 mM NaCl, 10% (w/v) glycerol
ITC buffer	10 mM HEPES pH = 8.0, 100 mM NaCl, 1 mM EDTA, 5 mM methionine
LB agar	LB medium with 15 g/l agar-agar
LB medium	10 g tryptone (peptone from casein), 10 g NaCl, 5 g yeast extract, per litre, pH = 7.5
Lysozyme solution	4 mg/mL in 10 mM HEPES pH = 7.0, 150 mM NaCl, 5% (w/v) glycerol
Ni-NTA buffer (GluK2 and GluA2)	A = 50 mM Tris pH = 8.0, 200 mM NaCl, 2 mM monosodium glutamate B = 50 mM Tris pH = 8.0, 200 mM NaCl, 2 mM monosodium glutamate, 500 mM imidazole
Post Ni-NTA buffer	10 mM HEPES pH = 7.4, 100 mM NaCl, 1 mM EDTA, 1 mM monosodium glutamate, 5 mM methionine
Seperating gel buffer	1.5 M Tris pH = 8.8
Stacking gel buffer	1 M Tris pH = 6.8
TE buffer	10 mM Tris pH = 8.0, 1 mM EDTA
Thrombin solution	100 units/mL in 10 mM HEPES pH = 6.5, 0.1% (w/v) BSA
10x SDS running buffer	0.25 M Tris, 1.92 M glycine, 1% SDS
5x SDS sample buffer	0.2 M Tris pH = 6.8, 10% (w/v) SDS, 20% (v/v) glycerol, 10 mM DTT or β-mercapto-ethanol, 0.05% (w/v) bromphenolblue

Table 4: Buffers, solutions and media.

14.1.3 Additives

	Additive	Final concentration
Ampicilline		100 µg/mL
Complete, EDTA free, protease inhibitor cocktail tablets; Roche		1 tablet per 50 mL
IPTG		100 µM
Kanamycine		15 µg/mL
PEFA		1 mM
Protein Marker, BioLabs, Broad Range, 2 – 212 kDa #P7702S; Fermentas #sm1891		10 µL/pocket
SOC medium (Novagen)		as obtained

EXPERIMENTS

Tetracycline	12.5 µg/mL
--------------	------------

Table 5: Additives.

14.1.4 Enzymes

Enzyme	Supplier
DNase I	Roche
Lysozyme	Sigma-Aldrich
Thrombin	Sigma-Aldrich

Table 6: Enzymes.

14.1.5 Bacterial strains

Strain	Resistances	Supplier
NEB 10-beta	Streptomycin	BioLabs
Origami B (DE3)	Kanamycin, Tetracyclin	Novagen

Table 7: Bacterial strains.

14.1.6 Plasmids

Plasmid	Resistance	Supplier
pET-22b(+)	Ampicillin	Dr. Mark Mayer
pETGQ (derivative of pET30b)	Ampicillin	Dr. Mark Mayer

Table 8: Plasmids.

14.1.7 Equipment

Equipment	Supplier
-80 °C freezer	GFL
37 °C incubator	Memmert
0.45 µM Spin-X filter unit	Corning Life Sciences
AEKTA purifier	GE Healthcare
Autoclave	Systec
Bio Photometer	Eppendorf
Centrifuge 5810R	Eppendorf
Centrifuge rotor A-4-62	Eppendorf

EXPERIMENTS

Centrifuge rotor F-34-6-38	Eppendorf
Centrifuge rotor F45-30-11	Eppendorf
Centrifuge rotor SLA-3000	Thermo
Centrifuge rotor SS-34	Thermo
Centrifuge Sorval Evolution _{RC}	Thermo
Concentrators (15 mL, 10 kDa MWCO)	Millipore
Concentrators (0.5 mL, NMWL membrane, -10 K)	Millipore
Crystallization plates VDX 24 well	Hampton Research
CrystalQuick 96 well sitting drop plate (Greiner)	Hampton Research
Crystallization robot	Tecan
Dialysis tubing, 10K MWCO	Roth
French pressure cell press	Thermo
Gel shaker	neoLab
HiLoad 16/60 Superdex 75 prep grade (gelfiltration)	GE Healthcare
HiPrep 26/10 (desalting)	GE Healthcare
HisTrap TM HP (Ni-NTA, 5 mL (GluK2), 1 mL (GluA2))	GE Healthcare
HiTrap TM SP HP (cation exchange, 1 mL)	GE Healthcare
ITC-200 calorimeter	MicroCal
MASTERBLOCK 96 deep well plate (Greiner)	Hampton Research
Microscale thermophoresis instrument	NanoTemper
Microscope	Leica
NanoDrop UV Spectrometer ND-1000	PeqLab
pH electrode	Mettler Toledo
pH meter SevenEasy pH S20	Mettler Toledo
Pipettes	Eppendorf
Power supply PowerPac	BioRad
Mini-PROTEAN Tetra Cell protein gel chamber	BioRad
Seeding tool	Hampton Research
Shaker incubator 44R	New Brunswick Scientific
Siliconized glass cover slides	Hampton Research
Thermomixer comfort	Eppendorf
TrayCell 105.800	Hellma
Ultrapure water	TKA MicroPure
UV-Vis spectrometer	Varian
Vortex mixer	VWR

Table 9: Equipment.

EXPERIMENTS

14.2 Methods

14.2.1 Methods in Molecular Biology²⁶²

Plasmid recovery from filter paper:

Indicated circles were cut out from filter paper (Whatmann 3MM) and incubated in 50 μ L TE buffer (containing nuclease inhibitor) for 10 min. The solution was separated from the filter paper and chemically competent bacteria were transformed (see 14.2.2) in order to amplify the plasmids provided by Dr. Mark Mayer.

Isolation and purification of plasmid DNA from bacteria:

Small-scale DNA preparations from 4 mL overnight culture were performed with the HiYield Plasmid Mini Kit provided by SLG. The kit was used according to the manufacturer's recommendations.

Assessment of DNA concentration:

The DNA concentration was determined by an absorption measurement at 260 nm. The purity of the DNA sample was assessed by considering the ratio of A_{260}/A_{280} . A ratio of 1.8 and higher indicates the absence of protein contaminants and therefore good quality of DNA.

Sequencing of the purified plasmid DNA:

In order to validate the sequence of the purified plasmid DNA it was sent to GATC-Biotech and the .fas, .seq and .ab1 files were evaluated with the software 4Peaks and SerialCloner.

14.2.2 Methods in Microbiology

Transformation of chemically competent bacteria:

E. coli can be rendered competent for DNA uptake by exposure to a heat shock²⁶³. 50 μ L of chemically competent cells (DNA amplification: *E. coli*, NEB 10-beta; protein expression: *E. coli*, Origami B (DE3)) were thawed on ice and 40 ng of purified plasmid DNA was added. The suspension was mixed by gently tapping the tube and

EXPERIMENTS

was incubated on ice for 30 min. Cells were transformed by exposing them to a heat-shock for 30 sec at 42 °C and cooled down on ice for 5 min. 250 µL SOC medium without antibiotics was added and the bacteria culture was incubated at 37 °C on a thermomixer at 50 rpm for 1h. After the bacteria were given time to express the resistancy genes, 5 µL and 295 µL of the mixture were plated on separate agar plates containing the appropriate antibiotic. Plates were incubated at 37 °C overnight.

Protein expression in bacteria by induction with IPTG:

The pET series of vectors allow regulated expression of foreign genes²⁶⁴. For large-scale protein expression, 5 L of LB medium containing the appropriate antibiotics were inoculated to an OD₆₀₀ of 0.05 using an overnight culture (100 mL), which was inoculated with 500 µL from a -80 °C glycerol stock of transformed bacteria. The bacteria were grown at 37 °C while shaking. The OD₆₀₀ was monitored over time against an aliquot of LB medium used for expression. When the OD₆₀₀ reached a value of 0.9, the temperature was immediately changed to 20 °C. IPTG was added at this temperature to a final concentration of 100 µM. After induction of expression, cells were incubated shaking at 20 °C overnight.

Preparation of a cleared bacterial cell lysate:

For the recovery of proteins cells can be disrupted²⁶⁵. Induced bacteria were harvested by centrifugation at 8000 rpm for 8 min at 4 °C. The supernatant was discarded and the pellet was stored at -80 °C if desired. On the day of purification, pellets from 5 L of culture were thawed and resuspended in 50 mL of icecold lysis buffer containing one tablet of complete EDTA free protease inhibitor, 500 µL/L DNase solution and 500 µL/L lysozyme solution. The suspension was passed through a pre-cooled French press 5 to 6 times at 4 °C. The insoluble fraction was removed by centrifugation at 18000 rpm for 30 min at 4 °C. The resulting supernatant was used for protein purification (see 14.2.4).

14.2.3 Protein qualification and quantification

Protein qualification:

Proteins were separated according to their molecular weight by discontinuous SDS-

EXPERIMENTS

PAGE²⁶⁶. The solutions of the separating and stacking gel were prepared according to the following pipetting scheme (volumes are given for one gel):

	Stacking gel (5%)	Separating gel (10%)
30% acrylamide (mL)	0.42	1.68
10% APS (μ L)	25	50
10% SDS (μ L)	25	50
Separating gel buffer (mL)	-	1.25
Stacking gel buffer (mL)	0.32	-
TEMED (μ L)	2.5	5
Water (mL)	1.7	1.98

Table 10: SDS-PAGE.

Both mixtures were prepared without APS and TEMED. To start polymerization, APS and TEMED were added to the separating gel. The gels were cast into the gel cassettes and overlaid with isopropanol. After polymerization, the isopropanol was decanted and APS and TEMED were added to the stacking gel mixture. The stacking gels were poured, combs were inserted and the gels were incubated to polymerize. For immediate use, gels were assembled into an electrophoresis cell, running buffer was added and the combs were removed. Otherwise, the gels were wrapped in aluminium foil for storage at 4 °C.

Protein samples were appropriately diluted and 5x SDS sample buffer was added. After 5 min of incubation at 95 °C, samples were centrifuged at 4000 rpm for 1 min and pipetted into the pockets of the gel. Electrophoresis was carried out with SDS running buffer at 120 mV constant voltage for 1 h at room temperature. Finally, the cell was disassembled and gels were fixed and stained by incubation in Coomassie staining solution modified from Neuhoff at room temperature for 1 h on a shaker²⁶⁷. Wash out was carried out by heating the gels in destaining solution in a microwave and incubating for 1 h on a shaker. Gels were inspected and scanned.

The purity of the protein sample was also controlled by considering the ratio of absorption at 260 nm and 280 nm, respectively. A ratio of A_{260}/A_{280} of about 0.6 is characteristic of pure protein with almost no DNA contamination.

EXPERIMENTS

Protein quantification:

For protein quantification, the BioRad Protein Bradford Assay was used. It was carried out according to the manufacturer's recommendations.

Purified protein was also quantified by comparison of the intensity of gel bands and for a more precise determination of the concentration the absorbance at 280 nm was measured using a NanoDrop ND1000 or a TrayCell in a photometer with a molar extinction coefficient of $40005 \text{ M}^{-1} \text{ cm}^{-1}$ for GluK2 (M = 29336 Da) and $41620 \text{ M}^{-1} \text{ cm}^{-1}$ for GluA2 (M = 30276 Da), respectively.

14.2.4 Protein purification

All protein purification methods were performed on an AEKTA purifier at 4 °C. All buffers were cooled to 4 °C prior to use and in order to minimize losses, sample size never exceeded 80% of the loading loop volume.

Ni-NTA affinity chromatography:

Histidine-tags are used for affinity purification of proteins²⁶⁸. After preparation of a cleared bacterial cell lysate the Ni-NTA column was equilibrated. During equilibration of the 5 mL (GluK2) or 1 mL (GluA2) Ni-NTA column with 3 column volumes (CV) of Ni-NTA buffer A, samples were spun for 2 min at 18000 rpm at 4 °C. After equilibrating the column, the sample was loaded from a 50 mL superloop with a flow rate of 2 mL/min (GluK2) or 1 mL/min (GluA2), followed by washing away unbound material with 10 CV of 5% Ni-NTA buffer B (GluK2 and GluA2). Competitive elution was performed using a stepwise gradient starting with 10% B over a length of 6 CV followed by 20% B over 6 CV collecting 5 mL fractions (GluK2) or with 10% B over 6 CV followed by 20% B over 10 CV collecting 2 mL fractions (GluA2). It was continued with 40% B over 6 CV collecting 3 mL fractions (GluK2) or with 40% B over 10 CV collecting 1 mL fractions (GluA2). At the end, the program was terminated with a linear gradient with a target concentration of 66% B over 5 CV while collecting 5 mL (GluK2) or 2 mL fractions (GluA2). Finally, the columns were cleaned with 5 CV 100% B, followed by 5 CV 0% B and for storage the solution was changed to 20% ethanol after rinsing with water.

GluK2 and GluA2 both eluted at 40% B. Peak fractions were pooled on the basis of the absorption at 280 nm and the buffer was changed to Post Ni-NTA buffer by

EXPERIMENTS

dialysis (3×10^2 fold dilution) overnight at 4 °C. The concentration was determined by the methods described and the protein purity was evaluated by SDS-PAGE. Purified protein was snap frozen in liquid nitrogen and stored at -80 °C until further use in order to perform a thrombin cleavage (see 14.2.5). For crystallization experiments it was continued on the next day without freezing the protein in between.

Desalting:

Desalting can replace the sample buffer with a new buffer²⁶⁹. After thrombin cleavage (see 14.2.5) the sample was concentrated to 5 – 10 mg/mL using a 15 mL concentrator (10 kDa MWCO) and was loaded from a 2 mL sample loop with a flow rate of 10 mL/min on the pre-equilibrated (cation exchange buffer A, 2 CV) desalting column in order to change to cation exchange buffer A. 3 mL fractions were collected while eluting isocratically over 1.5 CV. The column was cleaned with 0.2 M NaOH followed by water and was stored in 20% ethanol. After pooling peak fractions on the basis of the absorption at 280 nm it was continued with cation exchange chromatography.

Cation exchange chromatography:

Ion exchange chromatography separates proteins based on their molecular charge²⁷⁰. After desalting, the sample was loaded from a 2 mL loop on the pre-equilibrated (cation exchange buffer A, 5 CV) cation exchange column at a flow rate of 1 mL/min. After applying the sample, unbound material was washed away with 10 CV of 0% cation exchange buffer B (GluA2) or with 7 CV of 0% cation exchange buffer B (GluK2). Elution was performed using a stepwise gradient starting with 5% B over 10 CV followed by 10% B over 10 CV (GluA2) or with 5.5% B over 5 CV followed by 8% B over 8 CV (GluK2), while collecting 1 mL (GluA2) or 0.8 mL (GluK2) fractions. It was continued with a linear gradient with a target concentration of 40% B over 20 CV while collecting 2 mL fractions (GluA2 and GluK2). Finally, the column was cleaned with 5 CV 100% B, was re-equilibrated with 5 CV 0% B and for storage of the column, the buffer was changed to 20% ethanol, 0.2 M sodium acetate pH = 4.8, after rinsing with water.

Usually GluA2 and GluK2 eluted at 10% and 8% B, respectively. Peak fractions were pooled, the concentration was determined and the protein purity was evaluated by

EXPERIMENTS

SDS-PAGE. It was continued either with affinity measurements (see 14.2.6 and 14.2.7) or with gel filtration.

Gel filtration:

Gel filtration separates molecules on the basis of their molecular size²⁶⁹. After cation exchange, the buffer was changed to crystallization buffer by dialysis at 4 °C. The sample was concentrated to 10 mg/mL using a 15 mL concentrator (10 kDa MWCO) and was loaded from a 2 mL sample loop with a flow rate of 1 mL/min on the pre-equilibrated (2 CV, crystallization buffer) gel filtration column. 2.5 mL fractions were collected while eluting isocratically over 1.5 CV. After rinsing with water, the column was flushed with 20% ethanol for storage.

The GluK2- and GuA2-LBD eluted after 55 – 60 min. Peak fractions were pooled on the basis of the absorption at 280 nm, the concentration of the protein was determined and the purity was evaluated by SDS-PAGE. It was continued with co-crystallization experiments (see 14.2.8).

14.2.5 Protein digest

Thrombin is commonly used for enzymatic cleavage²⁷¹. The recognition site (LVPRG) is next to the N-terminal histidine tag, which needs to be removed.

After Ni-NTA chromatography, the digest was performed for 1 h at room temperature or overnight at 4 °C with 10 mM CaCl₂ using high activity thrombin at a molar ratio of substrate to protease of 600 : 1. Once the reaction was set up, aliquots were taken after different time intervals and were analysed by SDS-PAGE to confirm the success of the cleavage. The digest was stopped with PEFA (final concentration: 1 mM) and after five minutes EDTA (pH = 7.0, final concentration: 25 mM) was added. The sample was placed on ice and for further use the buffer was changed to cation exchange buffer A using a desalting column (see 14.2.4).

14.2.6 Isothermal titration calorimetry

Binding affinities can be determined with ITC^{260,272}. In order to remove glutamate from the buffer after cation exchange, the protein was successively dialysed (10²⁰ fold dilution) against ITC buffer at 4 °C. The titration calorimetry experiments were carried out in an ITC-200 calorimeter at 10 °C. Samples were vacuum-degassed

EXPERIMENTS

while stirring at 10 °C for 20 minutes. The final protein concentration was 91.2 μM for the GluK2-LBD and 196 μM for the GluA2-LBD. The protein was placed in the sample cell and the ligand was added (16 injections at 2 μL per injection with a duration of 4 sec and a filter period of 5 sec; injections were spaced by 180 sec) from a stock solution (975 μM for glutamate binding to the GluK2-LBD, 1200 μM for 4-Gluazo (**2**) binding to the GluK2-LBD, 1200 μM for glutamate binding to the GluA2-LBD and 1580 μM for 4-Gluazo (**2**) binding to the GluA2-LBD) while stirring at 800 rpm. For each titration, the heat effects of buffer dilution were measured in a control experiment in which the ITC buffer was titrated into the protein solution following the same injection schedule as the sample titration. After subtracting the control data, the sample titration was fit to a single-binding-site model. Data were analyzed using MicroCal Origin and parameters were determined using the following equations.

$$\Delta G = -RT \ln K \quad (1)$$

$$\Delta G = \Delta H - T\Delta S \quad (2)$$

14.2.7 Microscale thermophoresis

MST is a new and very powerful technology to measure affinities with high precision and low sample consumption^{7,273}. Thermophoresis is the directed movement of particles in a temperature gradient. A temperature difference leads to a depletion of solvated biomolecules in the region of elevated temperature. The thermophoretic depletion depends on the interface between the molecules and the solvent, *i. e.* the size, charge and solvation entropy of the molecule²⁷⁴.

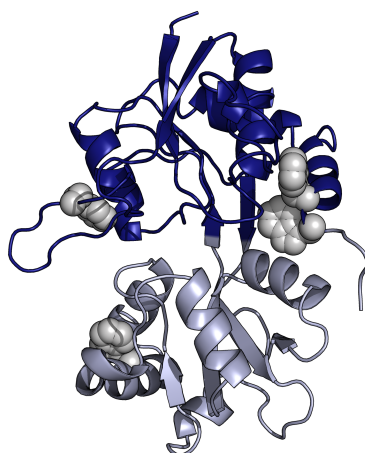


Figure 10: Tryptophane residues of the GluK2-LBD, which are important for label-free microscale thermophoresis. Cartoon representation of the GluK2-LBD (D1: dark blue, D2: light blue) with tryptophane residues (gray spheres).

EXPERIMENTS

Until now, the thermophoretic movement has been detected using a fluorescent tag attached to one of the binding partners²⁷⁵. Recently, a label-free variant of MST has been developed using the intrinsic protein fluorescence⁷. The dominant intrinsic fluorophore is tryptophane and the four Trp residues of the GluK2-LBD are shown in **figure 10**.

After cation exchange, glutamate was removed from the protein solution by exchanging into crystallization buffer by dialysis (10^{20} fold dilution) at 4 °C. For both LBDs a concentration of 2 μ M gave a satisfactory UV-fluorescence intensity without significant bleaching. Protein solutions with constant concentrations were pre-mixed with the respective ligand. The ligands were titrated (from 7.6 nM to 125 μ M for 4-Gluazo (**2**) binding to the GluK2-LBD, from 7.6 nM to 250 μ M for glutamate binding to the GluK2-LBD, from 30.5 nM to 250 μ M for glutamate binding to the GluA2-LBD and from 122.1 nM to 500 μ M for 4-Gluazo (**2**) binding to the GluA2-LBD) and the mixed solutions were incubated on ice for 1 h. After filling the capillaries, they were sealed with wax from both sides and the measurement was started. All measurements were performed at a capillary basis temperature of 20 °C.

Using the law of mass action and solving its quadratic equation for the fraction of bound protein gives the following equation:

$$\frac{[AB]}{[A^0]} = \frac{([A^0] + [B^0] + K_D) \pm \sqrt{([A^0] + [B^0] + K_D)^2 - 4[A^0][B^0]}}{2[A^0]} \quad (3)$$

The fraction of bound protein was fitted to the quadratic solution of the binding reaction equilibrium with K_D being the single free parameter. Thus, the K_D values of the different ligands binding to the LBDs can be obtained from the titration series²⁷⁵⁻²⁷⁷.

14.2.8 Protein–ligand co-crystallization

After size-exclusion chromatography, the purified LBDs (12.4 μ M GluK2-LBD, 14.8 μ M GluA2-LBD) were extensively dialyzed (10^{20} fold dilution) against crystallization buffer over a period of 36 h at 4 °C. After further dialysis in the dark (10^6 fold dilution, 12 h, 4 °C; crystallization buffer + 125 μ M 4-Gluazo (**2**) for the GluK2-LBD; crystallization buffer + 460 μ M 4-Gluazo (**2**) for the GluA2-LBD) to exchange remaining receptor bound glutamate for 4-Gluazo (**2**), the protein concentration was determined at this stage due to strong absorption of 4-Gluazo (**2**) at 280 nm at higher

EXPERIMENTS

concentrations of the ligand. 4-Gluazo (**2**) was added in the same buffer to give a final concentration of 1.3 mM and the protein concentration was adjusted to approximately 6 mg/mL for the GluK2-LBD and 6.4 mg/mL for the GluA2-LBD, estimated from the concentration measured in the presence of a minimal amount of 4-Gluazo (**2**). Prior to crystallization, the protein solutions were passed through a filter.

All crystallization experiments were set up under dimmed light and during crystallization the 96/24-well-plates were kept in the dark. Crystals were observed and manipulated under dimmed light using a Heliopan red filter (cutoff < 600 nm) in combination with the microscope. After a high throughput screening at 4 °C and 20 °C (Hampton screenings) using the crystallization robot, all conditions were examined and a fine screening with macro- and micro-seeding was performed around the most promising conditions. Crystals were grown by the hanging drop vapor diffusion technique by gently mixing 1 μ L reservoir solution with 1 μ L protein solution^{278,279}.

GluK2-LBD crystals grew in the presence of 50 mM MES pH = 6.5, 2.05 M Li₂SO₄, 10 mM MgCl₂ and were transferred into reservoir solution supplemented with 0.75 M LiCl in order to cryo-protect them before freezing in liquid nitrogen. GluA2-LBD crystals grew in the presence of 50 mM MES pH = 5.6 – 6.5, 23 – 27% (w/v) PEG3350, 0.2 M Li₂SO₄ and were transferred into reservoir solution saturated with 4-Gluazo (**2**) and containing 20% (v/v) ethylene glycol prior to cryo-cooling.

14.2.9 Data collection and structure determination

Data collection and structure determination were performed by Dr. André Schiefner. Diffraction data were collected at BESSY and were processed with the XDS Package²⁸⁰. Structures were solved by molecular replacement with PHASER using PDB entries 3G3F and 3BFU as starting models²⁸¹⁻²⁸⁴. Model building and refinement was performed with COOT and REFMAC^{285,286}. Ligand geometry restraints for 4-Gluazo (**2**) were parameterized with PRODRG²⁸⁷. Planarity restraints for the azobenzene moiety were defined manually.

14.2.10 Structural comparison and analyses

Both LBD structures were validated with COOT and MolProbity²⁸⁸. Molecular interfaces and contacts were analyzed with PISA and CONTACT^{289,290}. Structural

EXPERIMENTS

superpositions were performed with SUPERPOSE and molecular graphics were prepared with PyMOL^{291,292}.

The following domain definitions were used for structural comparisons: GluK2-LBD D1: residues 5 – 108 and 216 – 252, D2: residues 109 – 215 and 253 – 260; GluA2-LBD D1: residues 4 – 108 and 219 – 255, D2: residues 109 – 218 and 256 – 264. As reference structures for comparison the wild-type GluK2-LBD in complex with glutamate (PDB entry 3G3F chain B) and the GluA2-LBD in complex with CNQX (PDB entry 3T9V chain A) were used^{282,293}.

Part V: RESULTS AND DISCUSSION

Chapter 15: Protein–4-Gluazo co-crystallization

15.1 Synthesis of 4-Gluazo

The overview of the synthesis of 4-Gluazo (**2**) is described in chapter 8 and experimental details are given in chapter 13.2. According to literature, the preparation has been achieved in good yields and spectra are shown in chapter 22.1⁶.

To gain higher yields, the synthetic route has been optimized. By introducing a bromine at the terminal alkyne position of propargyl pyroglutamate (**11**), the following hydrostannylation has been performed with a higher regioselectivity and yield²⁹⁴. In contrast, direct stannylation of the alkyne without prior bromination results in a low yield with a 1:1 ratio of Markovnikov : anti-Markovnikov product.

The Stille cross coupling reaction has also been changed slightly. It is well known, that a fluoride ion can increase the rate of the coupling reaction and moreover, electronically disfavoured coupling reactions can be performed. Also, the insoluble Bu_3SnF byproduct is formed, which can be easily removed from the reaction mixture by filtration²⁹⁵. However, fluoride ions tend to isomerize substituents at the α -carbonyl position²⁹⁶. Therefore, in this particular case, the yield to give enantiomerically pure azobenzene pyroglutamate (**17**) *via* Stille cross coupling could have been increased by performing the reaction without CsF.

In addition, a crystal structure of propargyl pyroglutamate (**11**) has been obtained, which is depicted in **figure 11**. The corresponding crystallographic data are tabulated in chapter 21.2.

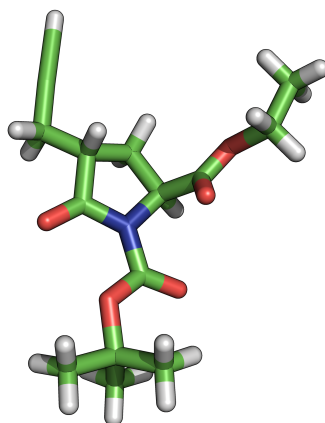


Figure 11: Crystal structure of propargyl pyroglutamate (**11**).

15.2 Verification of plasmid DNA

Crystallizable constructs of the GluK2- and GluA2-LBD, which are schematically shown in the introductory part (Fig. 1 C), have been available in pET22b(+) and pETGQ expression vectors, respectively. The plasmids have been sequenced and the results are shown in chapter 23.1 for GluK2-LBD and in chapter 23.2 for GluA2-LBD with the individual elements boxed and colour coded. Translated protein primary structures are in accordance to the published ones^{54,61}.

GluK2-LBD S1 starts with S³⁹⁸NRS and ends with LYRK⁵¹³. GluK2-LBD S2 starts with P⁶³⁶IDS and ends with GCPE⁷⁷⁵. After thrombin cleavage, a glycine is N-terminal of S1.

GluA2-LBD S1 starts with S³⁸³GND and ends with MIKK⁵⁰⁶. GluA2-LBD S2 starts with P⁶³²IES and ends with ECGS⁷⁷⁵. The sequence GSAMG is N-terminal of S1 after the thrombin cleavage. The sequences are numbered with respect to the first amino acid in the full-length mature protein without the signal peptide for both, GluK2- and GluA2-LBD.

15.3 Protein preparation

After transformation and overexpression in *E. coli*, soluble proteins have been purified with Ni-NTA affinity chromatography, cation exchange chromatography and gel filtration. After Ni-NTA affinity chromatography a thrombin digest has been performed. Methods and conditions are described in chapter 14.2. During protein preparation aliquotes have been taken and have been analysed by SDS-PAGE. Gels are shown in **figure 12** and **13** for the GluK2- and GluA2-LBD, respectively.

In the gel concerning the GluK2-LBD, the individual bands of the marker (Fermentas #sm1891) in lane one did apparently not run accordingly to their molecular weight. The histidine-tagged GluK2-LBD recombinant protein should have a molecular weight of 31.2 kDa. Therefore, the prominent band in lane two, which represents the recombinant GluK2-LBD after Ni-NTA affinity chromatography, should be slightly shifted to the top. After this step of purification, the protein sample is already highly pure with a minimal contamination at the lower part of the lane, observable through a tender band. Thus, almost all endogenous proteins have been removed with the first step of purification.

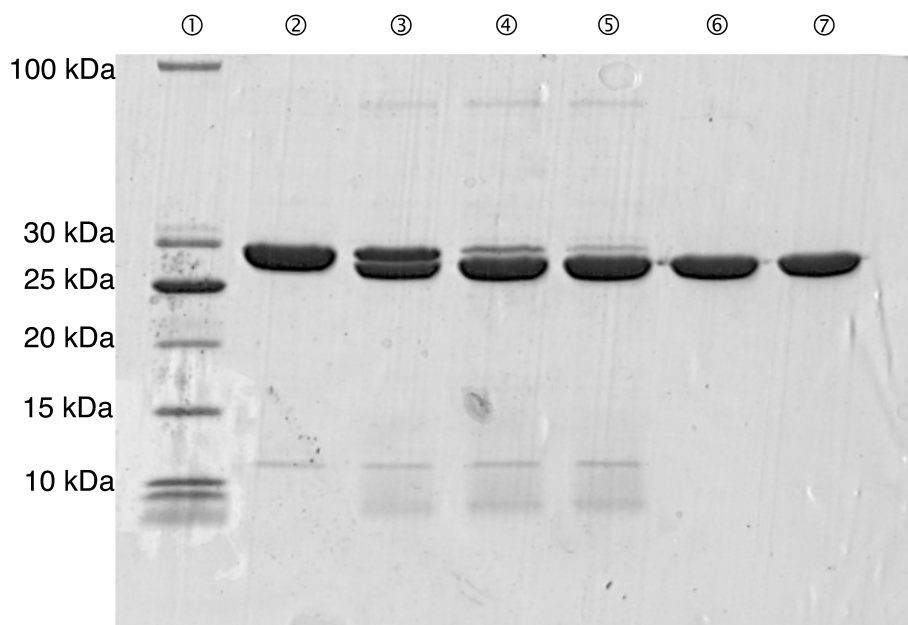


Figure 12: SDS-PAGE analysis of the GluK2-LBD purification and thrombin digest. ① MW marker, ② after Ni-NTA, ③ after 10 sec thrombin digest, ④ after 30 min thrombin digest, ⑤ after 1 h thrombin digest, ⑥ after cation exchange, ⑦ after gel filtration.

A histidine tag can influence the activity of proteins, which can lead to a different affinity in ligand binding assays. Moreover, the tag should be removed in order to perform structural studies, because it might induce different crystal packing. Lanes three to five illustrate the process of the thrombin digest. The gentle prothrombin band is at the very top of these lanes. The band of the his-tagged protein is getting less intense and the band of the digested protein intensifies over time. The cleaved-off histidine tag appears as a diagnostic, blurred band at the very bottom of the gel. The molecular weight of the protein without tag is 29.3 kDa and the difference of 2 kDa between cleaved and uncleaved protein is in accordance with the gel.

With cation exchange, which is the second step of purification, all remaining impurities have been removed, as can be seen in lane six. In addition, gel filtration has been performed to further purify the protein. Results are shown in lane seven and there is only one heavy band pointing out the high purity of the protein sample used for crystallization experiments.

RESULTS AND DISCUSSION

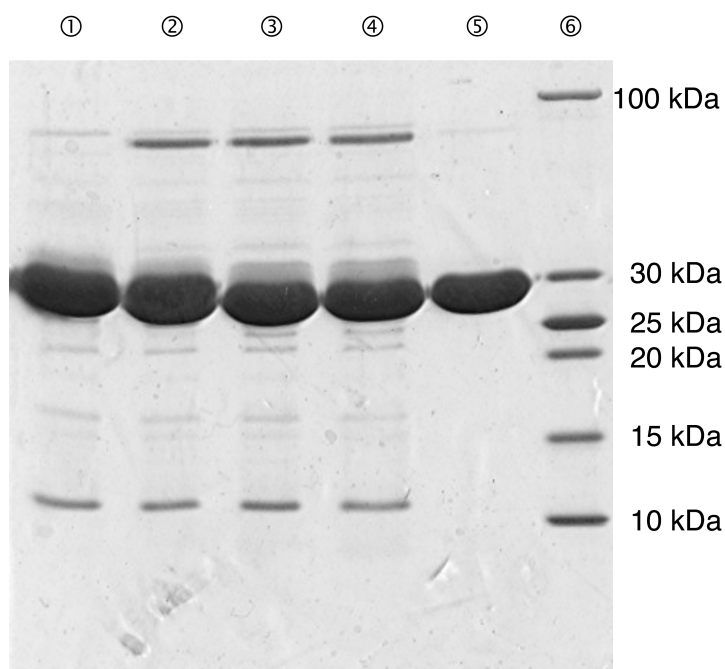


Figure 13: SDS-PAGE analysis of GluA2-LBD purification and thrombin digest. ① after Ni-NTA, ② after 10 sec thrombin digest, ③ after 30 min thrombin digest, ④ after 1 h thrombin digest, ⑤ after cation exchange, ⑥ MW marker.

For GluA2-LBD individual bands of a fresh sample of the marker (Fermentas #sm1891), which was applied to lane six, did run accordingly to their molecular weight. In general, for the GluA2-LBD preparation the same results have been achieved. The protein sample is already very pure after Ni-NTA chromatography (lane one) and the octa histidine tag has been completely removed by the thrombin digest (lanes two to four). The molecular weight of the recombinant protein is 32.2 kDa with his-tag and 30.3 kDa without tag. This shift can be observed in the gel as well. With cation exchange (lane five), remaining thrombin and other minor impurities have been completely separated from the GluA2-LBD, represented by a single heavy band in the gel. Prior to crystallization experiments, a gel filtration has been performed (not shown) to further increase the purity and to exchange into crystallization buffer.

15.4 Isothermal titration calorimetry

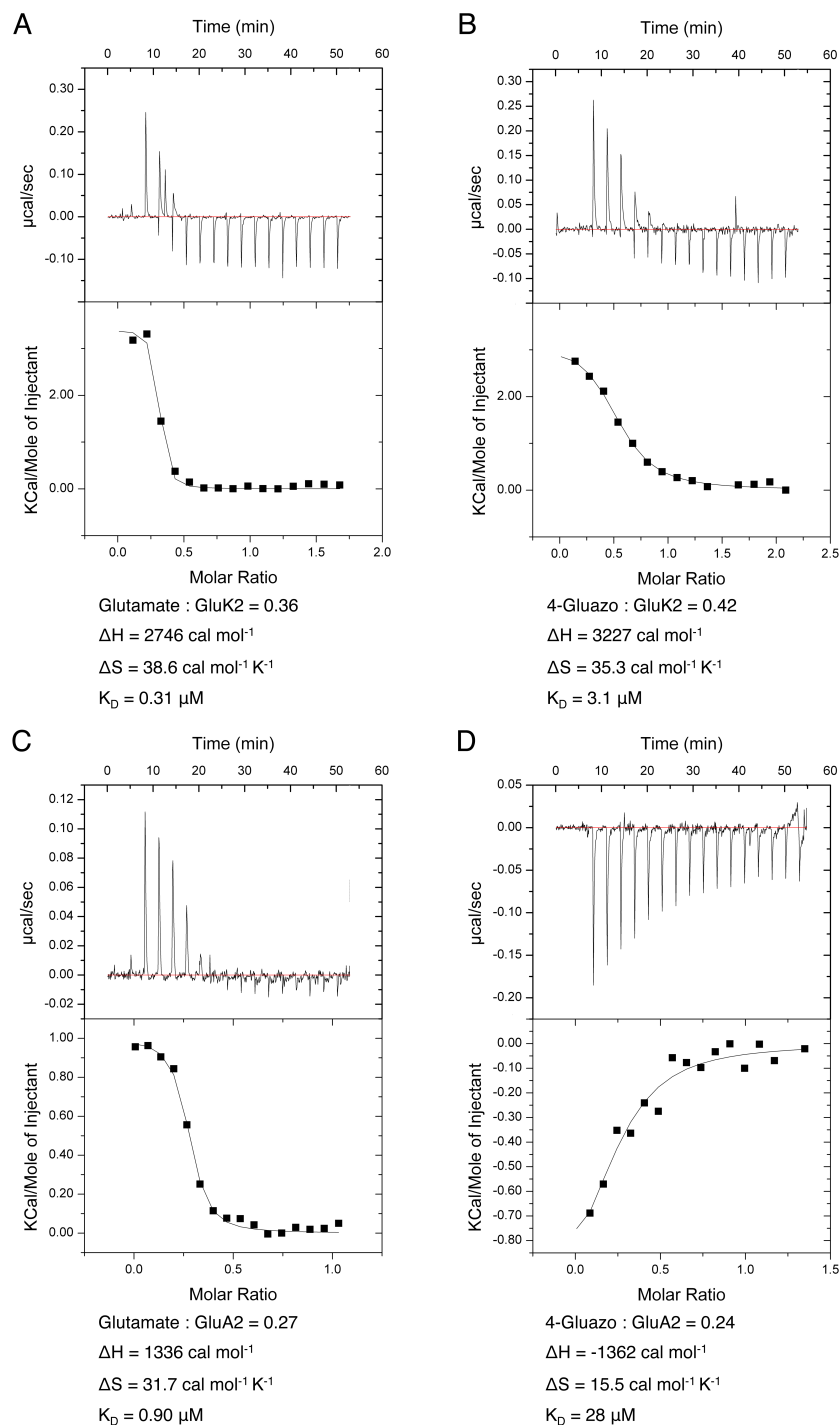


Figure 14: Isothermal titration calorimetry. (A – D) Thermodynamics of the interactions between (A) GluK2-LBD and glutamate, (B) GluK2-LBD and 4-Gluazo (2), (C) GluA2-LBD and glutamate and (D) GluA2-LBD and 4-Gluazo (2). Each panel presents raw data (top) and heat data after peak integration and subtraction of control titrations (bottom). Heat changes are plotted as a function of the molar ratio of protein to ligand for each injection. Curves represent the best nonlinear least-squares fitting of the data to a one-site binding model. The ΔH , ΔS , stoichiometry and K_D values of each reaction correspond to mean values of two experiments.

ITC directly measures the energy associated with a chemical reaction and the binding of glutamate and 4-Gluazo (**2**) to the GluK2- and GluA2-LBD has been investigated by combining protein and ligand for each case. Results are shown in **figure 14**.

The interaction of the GluK2-LBD with glutamate ($K_D = 0.31 \mu\text{M}$) is stronger when compared to the affinity towards 4-Gluazo (**2**, $K_D = 3.1 \mu\text{M}$). Same results have been observed for the GluA2-LBD with the interaction between 4-Gluazo (**2**, $K_D = 28 \mu\text{M}$) and the protein being weaker than the interaction of glutamate ($K_D = 0.90 \mu\text{M}$) and the GluA2-LBD. Overall the GluK2-LBD has a higher affinity towards both ligands. However, the difference in affinity towards glutamate and 4-Gluazo (**2**) is much higher for GluA2-LBD.

The different affinities can mainly be attributed to the different entropy changes (ΔS). For the GluK2-LBD, the entropy change is more favorable in the case of the binding of glutamate, which may be explained by a greater solvent release upon burial of more surface during binding and clam shell closure. Therefore, the clamshell is expected to close more tightly around glutamate than 4-Gluazo (**2**).

Binding is in both cases an endothermic reaction. Simply put, this means that during the binding reaction more hydrogen bonds are broken than newly formed. The change in enthalpy (ΔH) is greater for the binding of 4-Gluazo (**2**). Because of the shape of 4-Gluazo (**2**), more hydrophobic interactions, which are the determining factors for heat capacity change, can take place between the ligand and the protein upon clamshell closure. Therefore, numerous hydrogen bonds between water molecules, or between the protein surface and water molecules, are additionally broken.

Concerning the GluA2-LBD, the difference between the change in entropy is more dramatic between glutamate and 4-Gluazo (**2**) binding. This mainly explains the greater dissimilarity in affinity. Regarding the change of the enthalpy, the binding of glutamate is endothermic, whereas the binding of 4-Gluazo (**2**) is exothermic. In the case of glutamate binding, more hydrogen bonds are broken than newly formed. Thus, the mechanism of binding is similar to that of the binding of glutamate and 4-Gluazo (**2**) to the GluK2-LBD. However, according to the ITC measurement, the binding mode of 4-Gluazo (**2**) binding to the GluA2-LBD, is different. During the binding mechanism, there are more hydrogen bonds formed than broken. It has

already been shown before that 4-Gluazo (**2**) functions as a weak photochromic antagonist of the GluA2-LBD in the presence of glutamate²⁹⁷. Upon binding of 4-Gluazo (**2**) new hydrogen bonds are formed between the protein and the ligand. But the antagonistic action prevents clamshell closure and the concomitant break of hydrogen bonds between the protein and surface bound water molecules. This could explain the exothermic change in enthalpy. The proposed, different mechanism of 4-Gluazo (**2**) binding to the GluA2- and GluK2-LBD, respectively, has been confirmed by this measurement.

For each measurement the binding stoichiometry for ligand–LBD binding is much lower than one, which would be expected for a single binding mode. Either only a fraction of the protein has been properly folded, or the binding kinetics involve a very fast off-rate. As a consequence, the protein is not bound to the ligand all the time during the measurement.

15.5 MST

iGluR-LBDs undergo conformational changes when a ligand binds. This change of shape and solvation entropy of the molecule leads to a significant change in the thermophoretic behaviour, which is the movement of molecules in a thermal gradient. Therefore, the ligand–protein interactions can be measured by MST. The dissociation constants of glutamate and 4-Gluazo (**2**) towards the GluA2- and GluK2-LBD have been inferred. Results are depicted in **figure 15**.

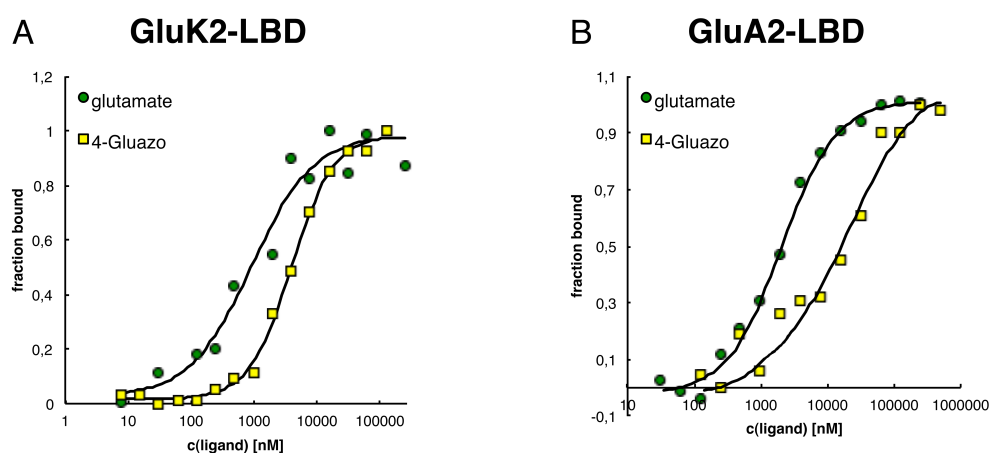


Figure 15: MST binding curves. (A and B) Graphs are derived from specific changes in the thermophoretic mobility upon ligand titration of glutamate (green) and 4-Gluazo (**2**, yellow) to the GluK2- (A) and GluA2-LBD (B). K_D values are given in the text.

The number of independent measurements has been two for the GluK2-LBD and one for the GluA2-LBD. For the GluK2-LBD, the K_D -values are almost perfect in agreement with the values determined by ITC. The K_D has been determined with an upper limit of 0.36 μM for glutamate, and 4-Gluazo (**2**) bound to the GluK2-LBD with a clearly defined K_D of 3.2 μM . For the GluA2-LBD, the K_D of glutamate has been obtained to be 0.84 μM , which is consistent with results from ITC. The MST K_D value of 4-Gluazo (**2**) binding to the GluA2-LBD is 19 μM and does not deviate significantly from the value determined by ITC. These results show that the affinities have been determined sufficiently precise with two different methods leading to the same results. Data measured by MST have been published⁷.

15.6 Crystallization

The GluK2-LBD•4-Gluazo protomer crystallized together with the GluK2-LBD•MES protomer as an overall dimer in the asymmetric unit and the structure has been solved at 2.0 Å resolution. Electron density has been observed for residues 3 – 258 for both protomers as well as for both ligands, a chloride ion and a sulfate ion. Two GluK2-LBD crystals can be seen in **figure 16**. They show a hexagonal bipyramidal morphology and belong to space group $P6_122$.

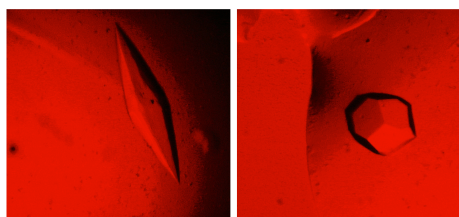


Figure 16: $(\text{GluK2-LBD})_2 \bullet 4\text{-Gluazo} \bullet \text{MES}$ crystals. Two different crystals under the microscope.

GluA2-LBD crystals grew in different lattices exhibiting a similar plate like morphology (not shown) and best crystals diffracted to 1.8 Å resolution and have been obtained in space group $P2_12_12_1$ with four GluA2-LBD molecules per asymmetric unit. Reasonable density has been observed for residues 4 – 264, 4 – 262, 4 – 264, and 4 – 261 of protomers A, B, C and D, respectively. Moreover, two MES molecules, twelve sulfate ions and five ethylene glycol molecules have been clearly observed. A table summarizing all crystallographic data and refinement statistics is depicted in chapter 21.1.

15.7 *GluK2-LBD and GluA2-LBD structures*

15.7.1 *GluK2-LBD dimer*

The *GluK2-LBD* crystallized as physiological dimer with two different LBD conformations. The mixed dimer is illustrated in **figure 17** as cartoon with surface representation (**Fig. 17 A**). Additionally, the structure is depicted from different perspectives (**Fig. 17 B**). Similar mixed dimers have already been reported for the *GluA2-LBD*, but not for the *GluK2-LBD*^{60,298}.

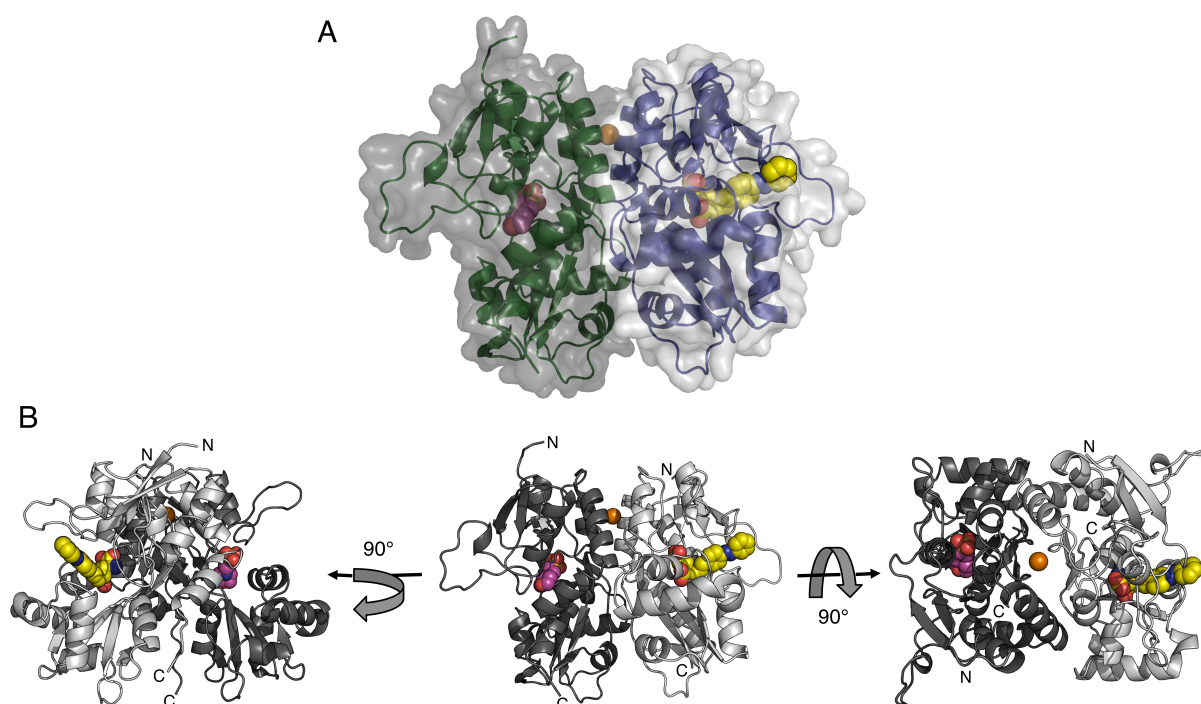


Figure 17: Mixed *GluK2-LBD* dimer. (A) Translucent surface and cartoon representation of *GluK2* with the closed, 4-Gluazo (**2**, yellow spheres) bound LBD (blue cartoon) and the open, MES (magenta spheres) occupied LBD (green cartoon). The central chloride ion is featured as an orange sphere. (B) The *GluK2-LBD* dimer consisting of individual protomers [(*GluK2-LBD*•4-Gluazo: light gray cartoon•yellow spheres), (*GluK2-LBD*•MES: dark gray cartoon•magenta spheres)] is shown in three different orientations (left and middle perpendicular to and right along its dyad axis) with the chloride ion (orange sphere) occupying the dimer interface.

One 4-Gluazo (**2**) bound protomer is closed, while the other one is open and accommodates a MES molecule, which has been present in the reservoir solution. Additionally, a chloride ion bound in a cavity formed at the interface between the subunits of this dimer pair. Chloride ions are essential structural components of kainate receptors and monovalent ions like sodium and chloride play a role in

allosteric modulation. Their absence in the extracellular solution leaves the receptor in a high-affinity closed state²⁹⁹⁻³⁰¹.

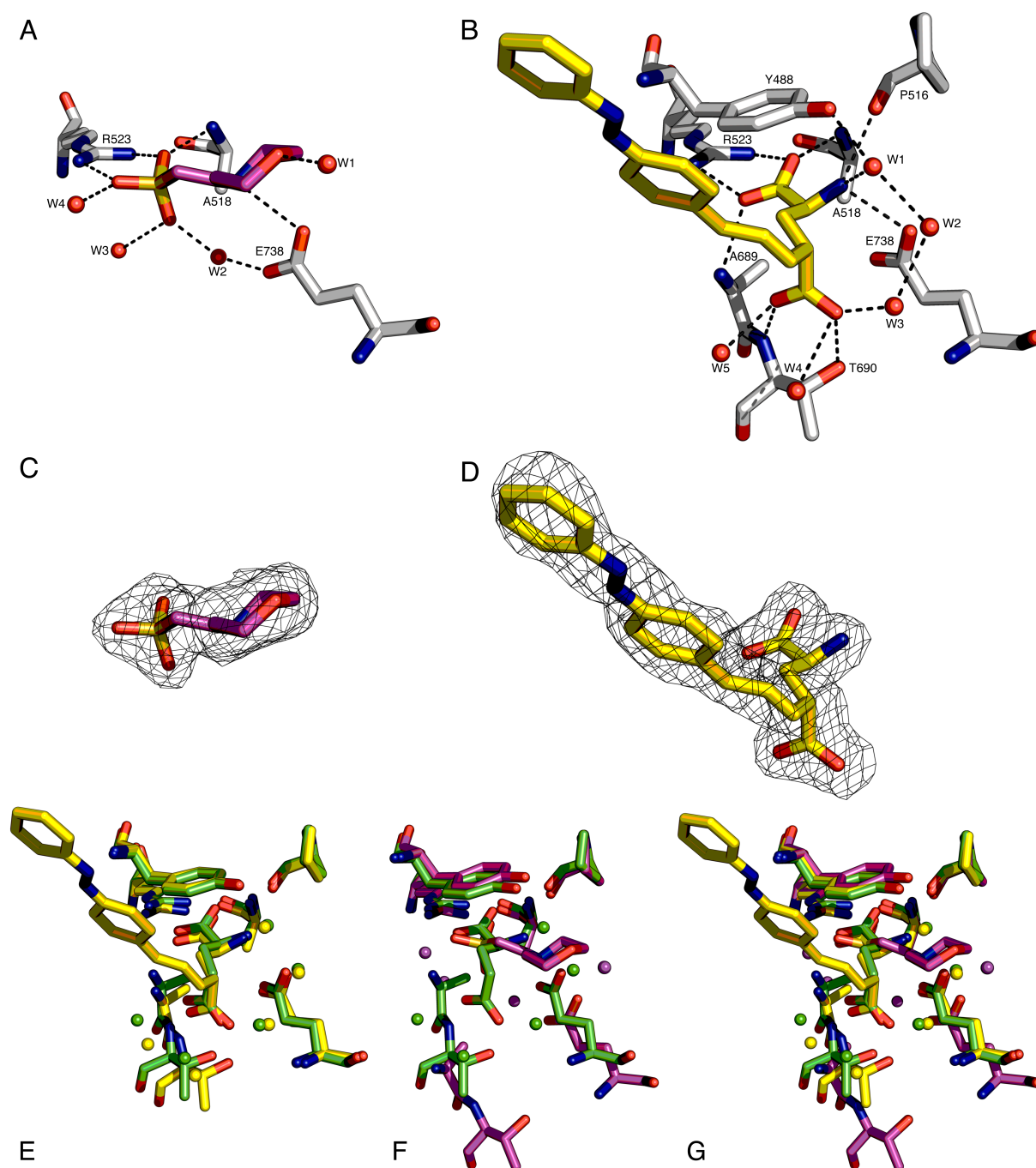
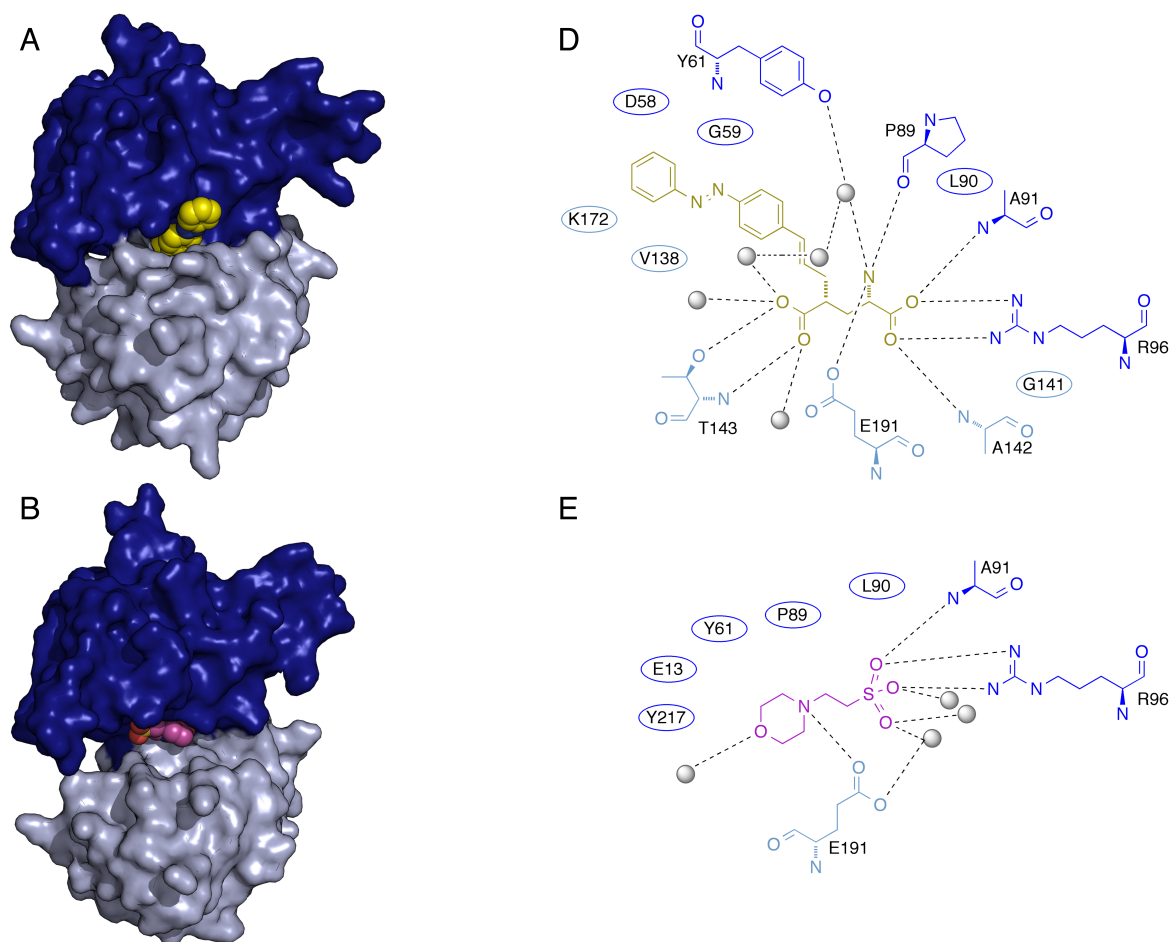


Figure 18: Overview of the GluK2 ligand-binding sites. (A and B) Important ligand (MES: magenta sticks, 4-Gluazo (2): yellow sticks) receptor (gray sticks) interactions with trapped water molecules (red spheres). Hydrogen bonds and ion pair interactions are indicated by black dashed lines. GluK2 residues are numbered according to the mature protein including the signal peptide. (C and D) Omit $2F_o - F_c$ electron density maps are contoured at 0.4σ and are shown as a gray mesh around the two ligands. (E – G) Superpositions of GluK2-LBD•4-Gluazo and GluK2-LBD•MES (yellow and magenta sticks, respectively) with GluK2-LBD•glutamate (green sticks, PDB entry 1S7Y). Superpositions have been performed with D1 aligned and D2 free to move and water molecules are shown as spheres and are coloured according to the structure they belong to.

RESULTS AND DISCUSSION

The interactions of 4-Gluazo (**2**) and MES with receptor residues and surrounding water molecules with the given orientation in space are shown in **figure 18 A** and **B**, respectively. Electron densities for the two ligands are depicted in **figure 18 C** and **D**, and omit maps show unambiguous and contiguous density for both, MES and 4-Gluazo (**2**). The electron density is not so well defined for the azobenzene part of 4-Gluazo (**2**), indicating some flexibility of this part. This is reflected by the B-value, which is twice as high for the azobenzene group when compared to the glutamate moiety of the molecule. Additionally, the binding modes of 4-Gluazo (**2**) and MES are compared with one another and with the natural agonist glutamate in **figure 18 E, F** and **G**.

Moreover, the premium positioning of 4-Gluazo (**2**), MES and glutamate within the LBD is illustrated in **figure 19 A, B** and **C**, respectively, with the protein shown as surface representation. **Figure 19 D, E** and **F** shows simplified, clearly arranged interaction networks between the protein and the different partners.



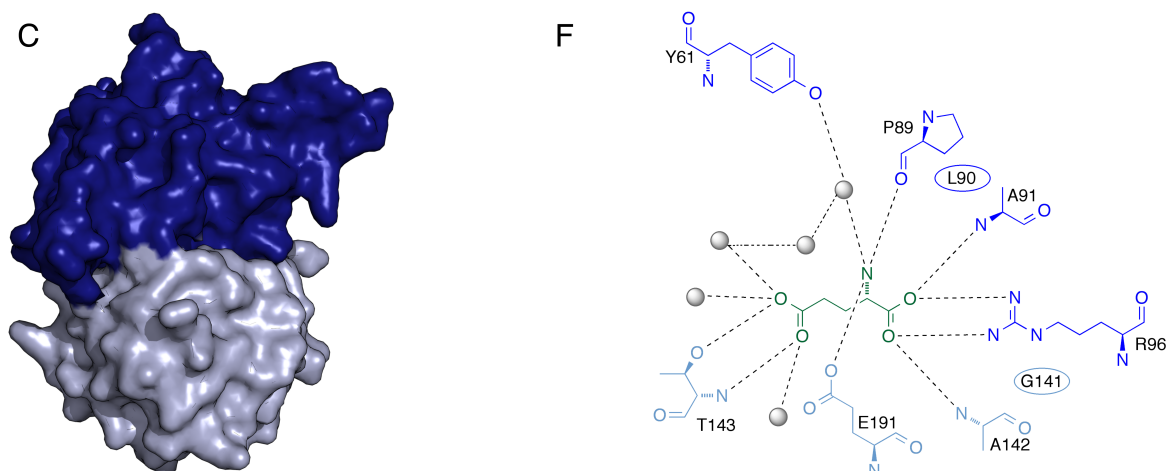


Figure 19: Premium positioning of 4-Gluazo (2) and MES in the GluK2-LBD and comparison with glutamate. (A – C) Surface representation of the GluK2-LBD (D1: dark blue, D2: light blue) with bound (A) 4-Gluazo (2, yellow spheres), (B) MES (magenta spheres) and (C) glutamate (green spheres; PDB entry 1S7Y). (D – F) Overview of the molecular details. Receptor residues interacting with (D) 4-Gluazo (2, yellow sticks), (E) MES (magenta sticks) and (F) glutamate (green sticks) via hydrogen bonds or salt bridges (black, dashed lines) are shown as sticks, whereas residues mediating van der Waals contacts are depicted as ellipses. In general, protein residues are numbered according to the PDB file and are shown in shades of blue according to their location on D1 or D2. Water molecules are shown as gray spheres. For simplicity, all residues have been flattened onto the plane of the page.

As expected, the glutamate part of 4-Gluazo (2) directly interacts with the same key residues of the receptor when compared to a glutamate bound structure⁶¹. Moreover, the amount of conserved water molecules contributing to the overall ligand–receptor interactions is the same with their positions deviating minimally for three out of five water molecules.

Glutamate binds to a cavity, which is almost completely hidden from the external solution and which is formed at the interface between D1 and D2⁶¹. In contrast, the azobenzene part of 4-Gluazo (2) protrudes from this cavity and interacts with the protein through van der Waals forces. This prevents the clamshell from a full closure and the angle of rotation of the rigid body movement of D2 to convert the two structures into each other is eight degree as shown in **figure 20 A**.

The open, MES bound protomer shows the first GluK2-LBD in its apo-like form. The MES molecule is located in the glutamate binding cavity and all the protein residues that interact with MES are part of the binding pocket of the receptor. The oxygen atom of the morpholine ring of MES forms a hydrogen bond to a water molecule and the protonated nitrogen of the six membered ring interacts with the same glutamate residue of the receptor, which normally interacts with the α -amino group of the ligand

RESULTS AND DISCUSSION

glutamate. This protein glutamate residue (E191) indirectly also interacts with the sulfonate moiety of MES, bridged *via* a water molecule. The sulfonate group additionally binds two more water molecules, forms a salt bridge with a highly conserved arginine (R523) and is stabilized by the backbone NH of an alanine (A518). The overall open conformation of the LBD is illustrated by comparing the surface representation of the protein or by considering the huge shift of important ligand binding cavity residues on D2. D2 is clearly separated from D1 and the angle of clamshell closure of the GluK2-LBD•MES structure to match the glutamate bound conformation is 25 degree, which is pointed out in **figure 20 A** as well.

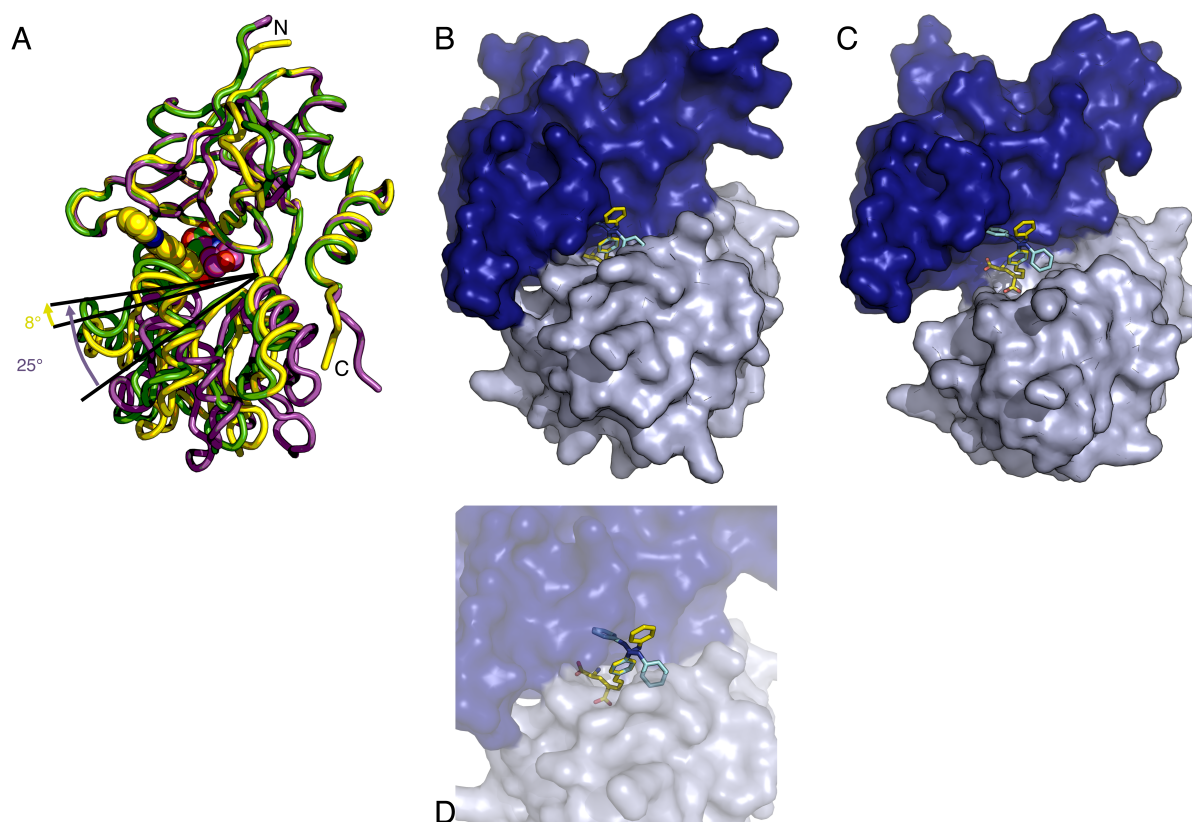


Figure 20: Different conformations and configurations. (A) Superpositions of GluK2-LBD•4-Gluazo (yellow tube•spheres), GluK2-LBD•MES (magenta tube•spheres) and GluK2-LBD•glutamate (green tube, PDB entry 1S7Y) with D1 aligned and D2 free to move. The yellow and magenta arrows indicate the clamshell closure *via* rotation of D2 to match the glutamate bound conformation. Degree values are given and angles are exemplified by black lines. (B – D) *Trans* (yellow sticks) and *cis* (cyan sticks) 4-Gluazo (**2**) in the (B) closed and (C) open conformation of the GluK2-LBD with a (D) close-up view of the closed conformation. D1 (dark blue) and D2 (light blue) are shown as opaque (B and C) or transparent (D) surface representation.

In **figure 20 B, C** and **D** the mechanism for activation and inactivation of the glutamate receptor by photoswitching between the different azobenzene

configurations of 4-Gluazo (**2**) with different wavelenghts of light, is depicted. For this purpose, the coordinates of a *cis* azobenzene have been downloaded from the cambridge crystallographic data centre (CCDC) and the two possible *cis* configurations have been docked onto the *trans* azobenzene part of 4-Gluazo (**2**) in the closed GluK2-LBD•4-Gluazo structure (**Fig. 20 B**)¹⁴⁰. Moreover, all possible configurations of 4-Gluazo (**2**) have been inserted into the open, apo-like GluK2-LBD•MES structure with the ligand occupying the same position relative to D1 of the closed protein conformation (**Fig. 20 C**). The open conformation of the LBD has enough room to host both *cis* configurations of the azobenzene unit of 4-Gluazo (**2**). On the other hand, in the case of the closed GluK2-LBD conformation, the distal phenyl ring of the azobenzene part of 4-Gluazo (**2**) penetrates into the surface of the protein in both *cis* configurations. This is exemplified in an enlarged section with the protein shown with a transparent surface (**Fig. 20 D**). The phenyl ring of one *cis* configuration of 4-Gluazo (**2**) is fully buried in the protein and the ring of the second configuration to two third. Accordingly, the action of 4-Gluazo (**2**) on the glutamate receptor is in agreement with the proposed activation mechanism discussed in the introduction. In the *cis* configuration, 4-Gluazo (**2**) can bind to the open conformation of the protein, but the clamshell can barely close. Contrary, the degree of clamshell closure after binding of the ligand in the *trans* configuration is high enough to allosterically allow the pore to open.

However, the question of inactivation of the receptor with 4-Gluazo (**2**) bound in *trans* and isomerized to *cis* remains unclear. One possibility would be a fast off-rate of bound *trans* 4-Gluazo (**2**) and the subsequent hindrance of clamshell closure upon isomerization to *cis*. With respect to the fast off-rate discussed in the context of the binding stoichiometry within the results of the ITC measurement, this mechanism is possible. The other option would be an active opening of the clamshell by 4-Gluazo (**2**), when isomerized from *trans* to *cis*.

15.7.2 GluA2-LBD dimer of dimers

Unfortunately, the solved structure of the GluA2-LBD does not show 4-Gluazo (**2**) bound to the protein. This can be explained by the low affinity and solubility of the ligand. On the basis of electrophysiological experiments and affinity measurements described above, 4-Gluazo (**2**) would have been expected to stabilize the open

RESULTS AND DISCUSSION

conformation of the GluA2-LBD. The cavity of the GluA2-LBD is smaller than that of the GluK2-LBD⁶¹. A substantially less pronounced closure of the clamshell after binding of 4-Gluazo (**2**) could explain the antagonistic effect on GluA2. This closure would be insufficient to activate the channel.

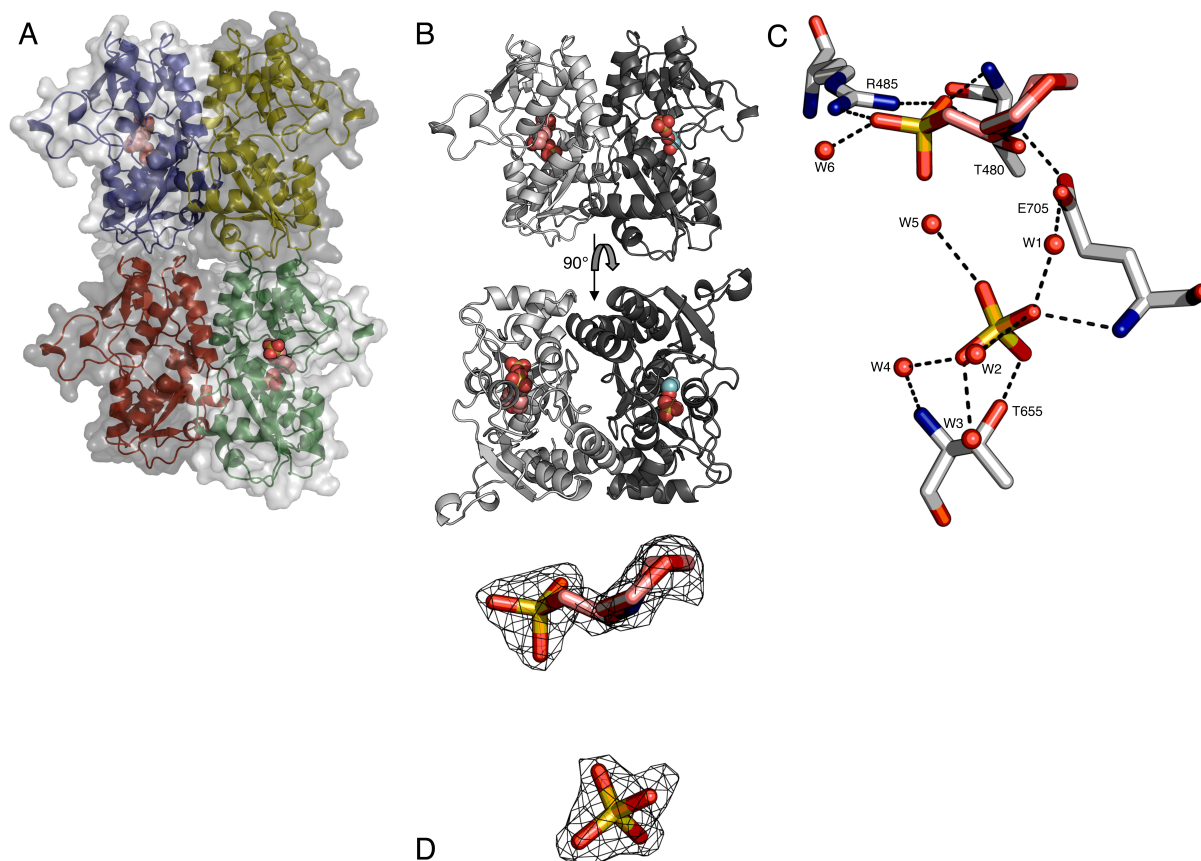


Figure 21: Dimers and ligand-binding site of the GluA2-LBD. (A) Translucent surface and cartoon representation of the non biological dimer of dimers structure of the GluA2-LBD with MES (salmon spheres) and sulfate ions (spheres) occupying two (protomer A and C) of the four LBDs (blue, yellow, green and red cartoons). Ethylene glycol and sulfate molecules (not shown) occupy the other two LBDs (protomer B and D). (B) One GluA2-LBD dimer (protomer A and B) consisting of two unequal protomers (light and dark gray cartoons, respectively) is shown in two different orientations (top perpendicular to and bottom along its dyad axis). Protomer A interacts with MES (salmon spheres) and a sulfate ion (spheres) and protomer B with ethylene glycol (cyan spheres) and a sulfate ion (spheres). (C) Interactions between MES (salmon sticks), a sulfate ion (sticks) and receptor residues (gray sticks). Trapped water molecules (red spheres) are shown and hydrogen bonds and ion pair interactions are indicated by black dashed lines. GluA2-LBD residues are numbered according to the mature protein without the signal peptide. (D) Omit $2F_o - F_c$ electron density map contoured at 1.0σ is shown as a gray mesh around MES (salmon sticks) and the sulfate ion (sticks).

Crystal packing produced a GluA2-LBD tetramer, as can be seen in **figure 21 A**. The tetramer is non-physiological when compared to the structure of the full-length

receptor, but consists of a pair of two physiological dimers⁶⁰. This crystal packing has already been observed for the GluA2-LBD⁵⁶. The LBDs of both dimers resemble the open conformation of the GluA2-LBD and one of the dimers is depicted in different orientations in **figure 21 B**. In each dimer, the binding cavity of one protomer is occupied by MES and a sulfate ion from the reservoir solution, whereas the other ligand-binding site is filled by a sulfate ion and an ethylene glycol molecule from the cryo protecting solution. Interactions of the MES molecule and the sulfate ion with the protein and associated water molecules are illustrated in **figure 21 C**. All the residues of the protein contacting either MES or the sulfate ion are part of the binding cavity of the natural ligand glutamate. The electron density of MES and the sulfate ion is shown in **figure 21 D**.

The sulfonate group of MES is in contact with a water molecule, is the counter ion of a highly conserved arginine (R485) and forms a hydrogen bond to the backbone NH of a threonine (T480). The protonated nitrogen atom of the morpholine ring forms a hydrogen bond to the γ -carboxyl group of a glutamate (E705) residue of the protein, which is additionally connected to the sulfate ion *via* a water-mediated hydrogen bond. Moreover, the backbone NH of this glutamate residue donates a proton to the sulfate ion. The sulfate ion forms hydrogen bonds to four more water molecules with one mediating an indirect contact to the backbone NH of a threonine (T655). When the ligand glutamate binds to the protein, the side chain of this threonine interacts with the γ -carboxyl group of glutamate⁵⁶. However, in this structure the side chain of the threonine forms a contact to the sulfate ion. Overall, the sulfate ion forms a cross-linked cluster of hydrogen bond contacts to water molecules as well as to the protein. In **figure 22** important key interactions of the GluA2-LBD with different ligands are pointed out. The structures have been aligned to the GluA2-LBD•MES structure and ligand–receptor contacts and orientations are compared (**Fig. 22 A – D**). The apo form of the GluA2-LBD is also considered (**Fig. 22 E**). Moreover, an alignment of the GluA2-LBD•MES structure and the GluK2-LBD•MES structure with interacting residues is shown (**Fig. 22 F**), but a statement comparing the structures of two different receptor subtypes with respect to the state would be highly speculative. However, as can be seen in the different alignments, the best match is achieved between the GluA2-LBD•MES structure and the apo structure. This similarity could indicate to consider the GluK2-LBD•MES structure as the first apo structure of

GluK2. Additionally, an alignment of the entire LBD in conjugation to the different ligands is shown (Fig. 22 G and H).

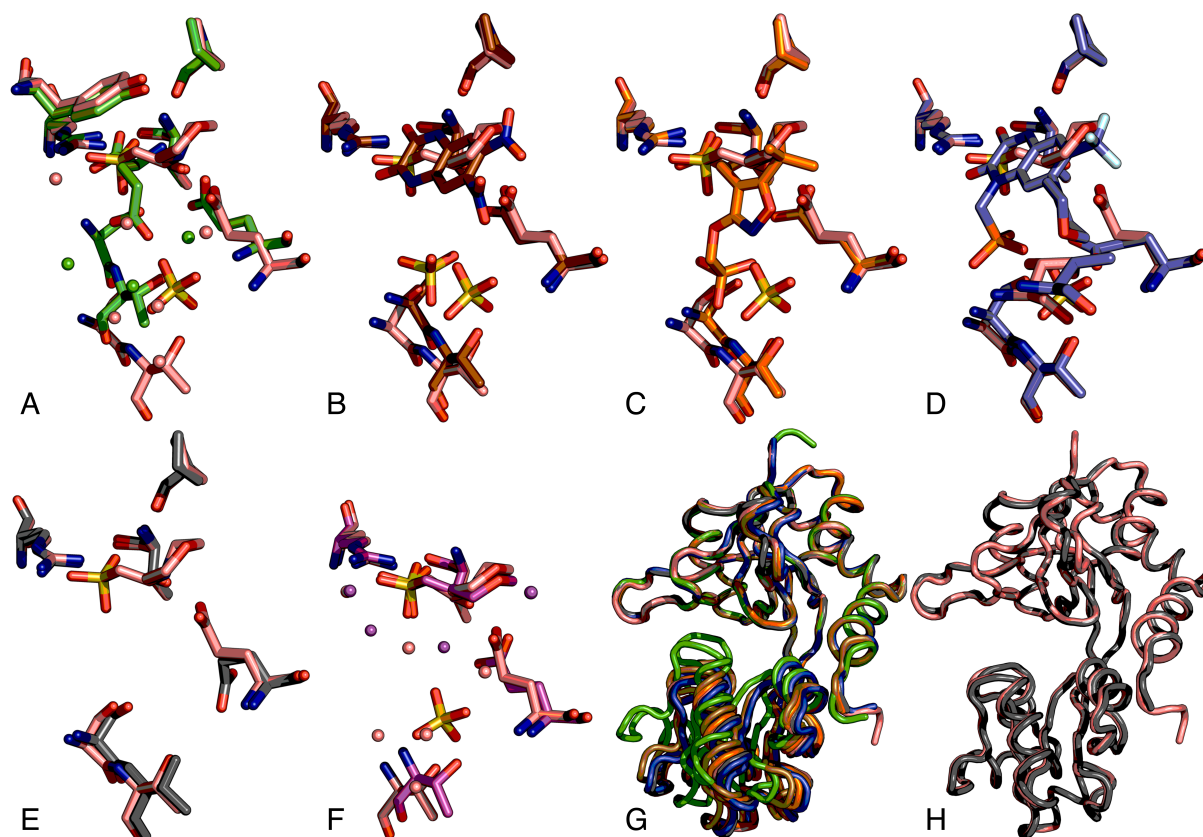


Figure 22: Superpositions of GluA2-LBD•MES with previously determined structures. (A – H) All superpositions have been made with D1 aligned and D2 free to move. (A – F) Illustration of superimposed binding-site residues of GluA2-LBD•MES (salmon sticks) with (A) GluA2-LBD•glutamate (green sticks, PDB entry 2UXA), (B) GluA2-LBD•DNQX (brown sticks, PDB entry 1FTL), (C) GluA2-LBD•ATPO (orange sticks, PDB entry 1N0T), (D) GluA2-LBD•ZK200775 (blue sticks, PDB entry 3KGC), (E) apo GluA2-LBD (dark gray sticks, PDB entry 1FTO) and (F) GluK2-LBD•MES (magenta sticks). In (A) and (F) water molecules are shown as spheres coloured according to the different residues. (G and H) Cartoon-tube representation of superimposed GluA2-LBDs with similar colours applying.

In all superpositions D1 has been aligned and D2 has been free to move. Therefore, D1 residues occupy similar positions, but D2 residues differ. The degree of rotation of D2 upon domain closure, which is in this case illustrated by the movement of D2 residues, is the greatest for the shown glutamate bound structure. While the full agonist glutamate induces a domain closure of 19° when compared to the apo structure, the antagonists DNQX, ATPO and ZK200775 stabilize the open conformation of the receptor^{59,60}. The demonstrated domain closure decreases from the GluA2-LBD•DNQX structure over the GluA2-LBD•ATPO structure to the GluA2-LBD•ZK200775 structure.

RESULTS AND DISCUSSION

With the LBD being in an open apo-conformation or being bound to antagonists, the formation of an interdomain contact between a glutamate (E402, PDB file: E13) and a threonine (T686, PDB file: T174) residue is prevented³⁰². Interdomain salt bridges and hydrogen bonds have an effect on a number of channel properties like deactivation rates and affinity, and these interdomain contacts underlie the differences between AMPA and kainate receptors in their rate of recovery from desensitization³⁰³. In the closed, glutamate bound structure this bridge is present, which is illustrated in **figure 23**. However, in the GluA2-LBD•MES structure this interdomain hydrogen bond is absent.

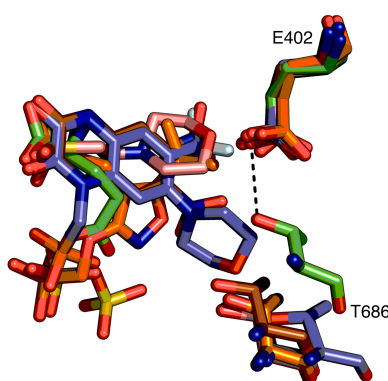
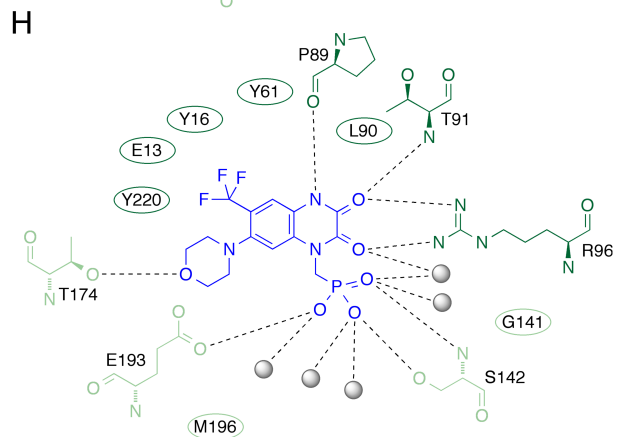
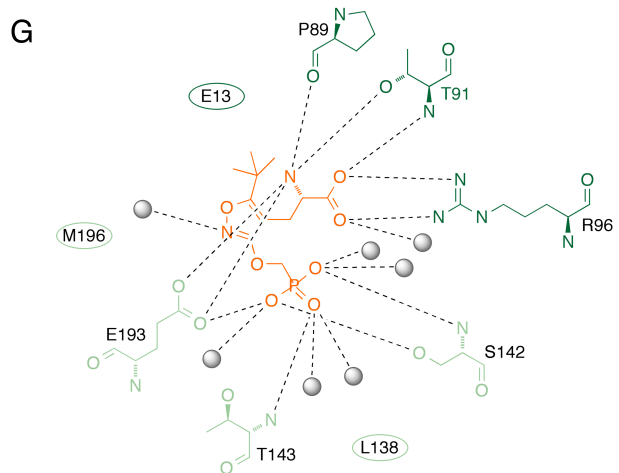
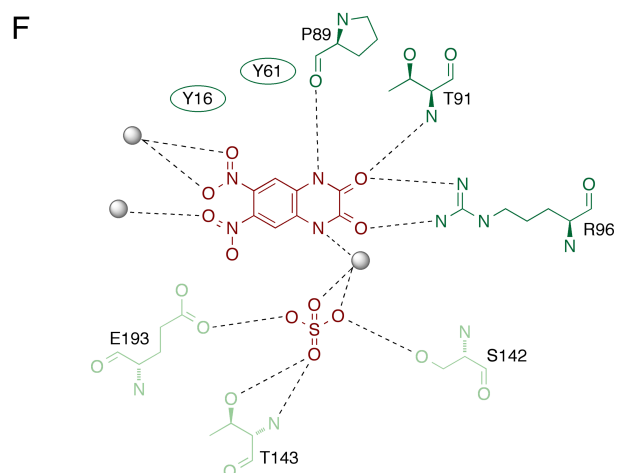
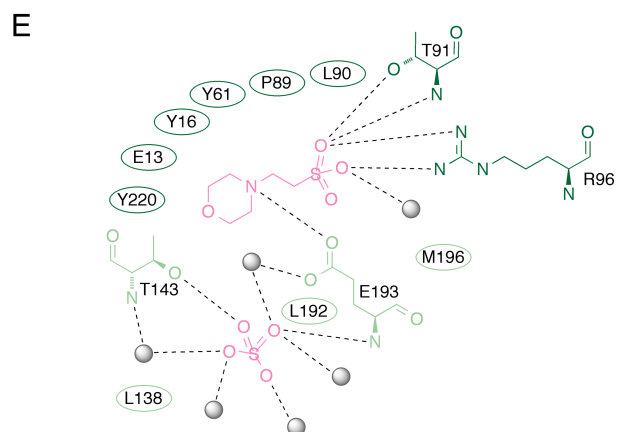
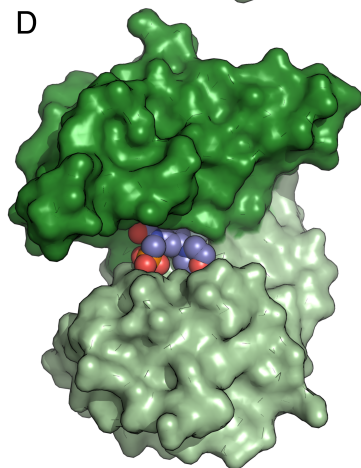
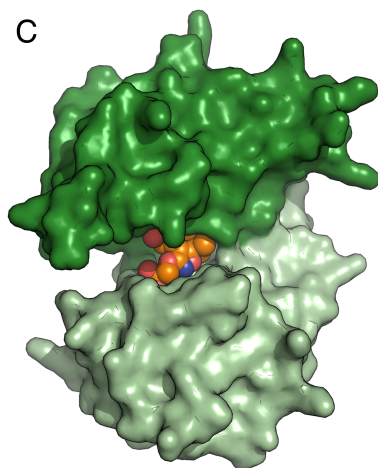
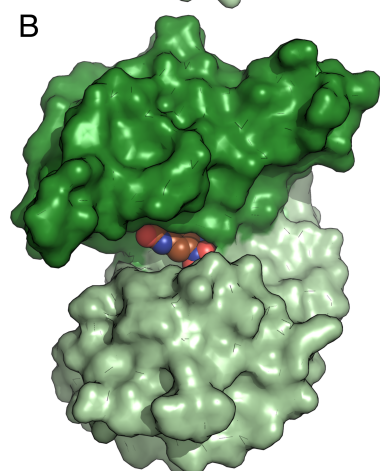
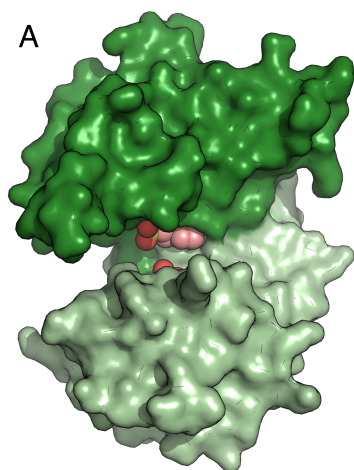


Figure 23: Interdomain contact. Superposition of GluA2-LBD•MES, GluA2-LBD•DNQX (PDB entry 1FTL), GluA2-LBD•ATPO (PDB entry 1N0T), GluA2-LBD•ZK200775 (PDB entry 3KGC), GluA2-LBD•apo (PDB entry 1FTO) and GluA2-LBD•glutamate (PDB entry 2UXA). D1 residues have been aligned and D2 has been free to move with similar colours applying as in figure 22. The hydrogen bond between Glu402 and Thr686 of the glutamate bound structure is shown as black dashed line.

In **figure 24** the positioning of MES and the selected three different antagonists within the GluA2-LBD is shown. All four cases represent the open conformation of the LBD, which is unambiguously pointed out by directly looking towards the ligand-binding cavity (**Fig. 24 A – D**). An observation of the ligand from this point of view is not possible in a closed, agonist bound state of the receptor (not shown, PDB entry 2UXA)³⁰⁴. Even partial agonist bound structures of the GluA2-LBD do not provide this intimate insight (not shown; PDB entries 3T96 and 3T9H)²⁹³.

Interactions between proteins and ligands are simplified and clearly laid out in the right part of the picture (**Fig. 24 E – H**). When comparing the protein–ligand interactions of the GluA2-LBD•MES structure (**Fig. 24 E**) with interactions of antagonist bound structures, some similarities draw the attention.

RESULTS AND DISCUSSION



RESULTS AND DISCUSSION

Figure 24: Premium positioning of MES in the GluA2-LBD and comparisons. (A – D) Surface representation of the GluA2-LBD (D1: dark green, D2: light green) with bound (A) MES (salmon spheres), (B) DNQX (brown spheres, PDB entry 1FTL), (C) ATPO (orange spheres, PDB entry 1N0T) and (D) ZK200775 (blue spheres, PDB entry 3KGC). (E – H) Overview of the molecular details. Receptor residues interacting with (E) MES and sulfate (salmon sticks), (F) DNQX (brown sticks), (G) ATPO (orange sticks) and (H) ZK200775 (blue sticks) *via* hydrogen bonds or salt bridges (black dashed lines) are shown as sticks, whereas residues mediating van der Waals contacts are depicted as ellipses. In general, protein residues are numbered according to the PDB file and are shown in shades of green according to their location on D1 or D2. Water molecules are shown as gray spheres. For simplicity, all residues have been flattened onto the plane of the page.

The structure with bound DNQX shows a sulfate ion interacting with residues of the protein contributing to the ligand-binding cavity (**Fig. 24 F**). The phosphonate group of ATPO is located at a similar position and is involved in an extensive hydrogen-bonding network with protein residues and water molecules (**Fig. 24 G**). This leads to the assumption that this site in GluA2 is favorable for being occupied by a large and negatively charged group. The antagonist ZK200775 can be considered as a hybrid of DNQX and ATPO, but the phosphonate group of ZK200775 is positioned at a slightly different site (**Fig. 24 H**). While the phosphonate of ATPO and the sulfate ion of the DNQX structure both form contacts to a serine (S142), a threonine (T143) and a glutamate (E193) residue of the protein, the phosphonate group of ZK200775 only interacts with the serine and glutamate residue. The sulfate ion of the GluA2-LBD•MES structure is stabilized by two out of three of these residues, namely the threonine and the glutamate residue of the protein. The spatial location of this sulfate ion differs from the position of the sulfate in the DNQX structure and from the position of the phosphonates of ATPO and ZK200775 as well. However, these different positions are antagonised and balanced by different degrees of clamshell closure.

With respect to the marked similarities, the MES molecule can, in combination with the sulfate ion, be considered as a lead structure for the design of a new class of GluA2 antagonists. For example, MES and the sulfate ion could be connected *via* a phenyl moiety. This is demonstrated and described more in detail in chapter 10. Finally, it should be mentioned that MES interestingly not only interacts with iGluRs, but also occupies the extracellular region of an mGluR, though in a different mode of action³⁰⁵.

Chapter 16: Synthesis of BAG

BAG (**3**) has been synthesized in good overall yields, when compared to similar literature^{5,258,259,296,306-308}. The overview and the experimental part is described in chapter 9 and 13.3, respectively, and spectra are shown in chapter 22.2. Ribosome display experiments with the molecule are currently under investigation in the group of Prof. A. Plückthun. If the group in Zurich will succeed in evolving a DARPin that binds specifically to this enantiomer, a novel protein scaffold recognizing and binding azobenzenes would have been created. Possible applications are in the field of life science research as well as in the biopharmaceutical industry and medical sciences.

Chapter 17: Synthesis, electrophysiological characterization and proposed binding mode of MOBIPHOS

After designing MOBIPHOS (**4**), the molecule and its derivative MOBIPHOSen (**38**) have been prepared in a good overall yield referring to related literature³⁰⁹⁻³¹². The design and the synthetic overview are given in chapter 10, the synthetic proceeding is described in chapter 13.5 and spectra are shown in chapter 22.4. A crystal structure of the bisphosphonate (**40**), which is depicted in **figure 25**, has been observed. Crystallographic data thereof are detailed in chapter 21.2.

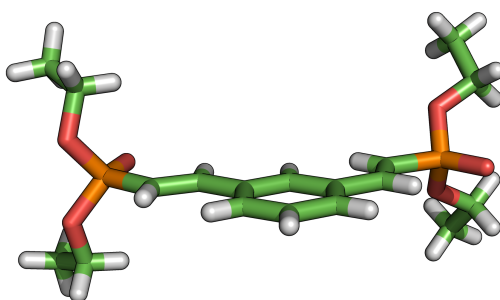


Figure 25: Crystal structure of bisphosphonate (**40**).

Electrophysiology experiments with HEK-293T cells expressing GluA2 have been performed by Dr. Martin Sumser and results thereof are shown in **figure 26**. As can be seen, MOBIPHOS (**4**) acts as a GluA2 antagonist (**Fig. 26 A**).

24 hours after transiently transfecting HEK293T cells with the non-desensitizing mutant GluA2 L504Y construct, cells have been voltage-clamped at -50 mV. Without MOBIPHOS (**4**) currents are triggered by application of a short pressure ejection

RESULTS AND DISCUSSION

pulse of glutamate (100 ms; 100 μ M) from a glass pipette located in proximity to the patched cell. After wash-in of an extracellular solution containing 2 mM (\pm)MOBIPHOS (**4**), the same application of glutamate is completely blocked. Glutamate-evoked currents are fully restored when MOBIPHOS (**4**) is washed out again.

With 2 mM (\pm)MOBIPHOSen (**38**) present in the extracellular solution, outward currents have been observed when glutamate has been applied (data not shown). However, without MOBIPHOSen (**38**) normal inward currents have occurred upon application of glutamate. Measurements have been repeated with MOBIPHOS (**4**) and led to the same results with outward currents appearing at this day of measurement. These contradictory results cannot be further explained without additional experiments that need to be performed in the future.

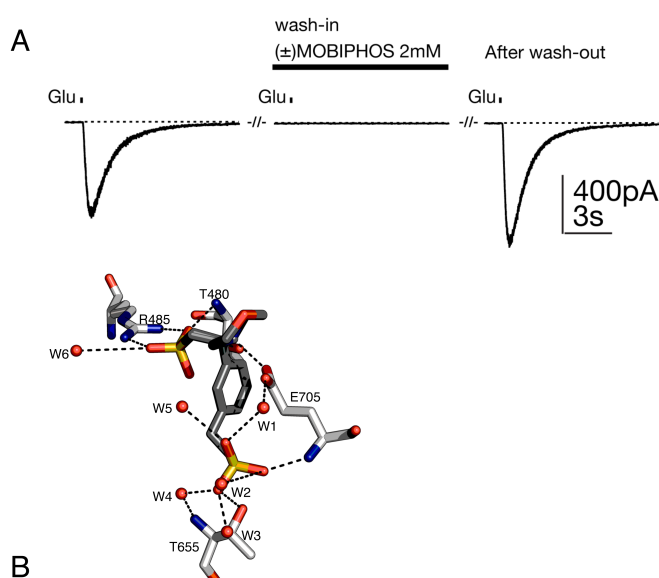


Figure 26: Electrophysiology results and proposed MOBIPHOS–receptor interactions in the binding pocket. (A) Voltage-clamp recordings in HEK cells. Glutamate applications are indicated by a short bar and the presence of MOBIPHOS (**4**) is shown as a long bar. (B) Proposed interactions between MOBIPHOS (**4**, dark gray sticks) and receptor residues (light gray sticks). Trapped water molecules (red spheres), hydrogen bonds and ion pair interactions (black dashed lines) are shown. GluA2 residues are numbered according to the mature protein without the signal peptide.

A proposed, modeled binding mode of MOBIPHOS (**4**) is shown in real space (**Fig. 26 B**). The MES part of the molecule would interact with an arginine (R485) and the backbone NH of a threonine (T480) residue of the protein *via* its substituted phosphonate group. This moiety would also form a hydrogen bond to a water molecule. The protonated nitrogen of the morpholine ring would donate a proton to

the γ -carboxyl group of a glutamate residue (E705) of the protein, which would be additionally bridged to the second phosphonate *via* a water molecule. Moreover, the backbone NH of this glutamate would contact the second phosphonate, which would be additionally stabilized by the side chain of a threonine (T655). Furthermore, the phosphonate would be connected to the backbone NH of this threonine in an indirect, water mediated fashion and would bind three more water molecules.

Although there is no X-ray structure of GluA2-LBD•MOBIPHOS, yet, a possible mechanism of binding to and acting on the receptor might be as follows. First, MOBIPHOS (**4**) might compete against the contact sites of the ligand glutamate on D1 within the open conformation of the binding pocket. Second, the phosphonate might occupy the position of the sulfate ion in the GluA2-LBD•MES structure. The phosphonate might interact with the same residues of D2 when compared to the γ -carboxyl group of the ligand glutamate, but would better fit into this position within the apo-like conformation of the protein. Third, the stiff phenyl ring might sterically inhibit clamshell closure *via* a foot in the closing door mechanism. Moreover, the open pocket might be stabilized by additional water molecules forming a hydrogen bonding network as already observed with the phosphonate group of ATPO and the sulfate ion of the GluA2-LBD•MES structure.

Chapter 18: Synthesis of ABA

ABA (**5**) has been synthesized following a literature procedure, but experiments towards a molecular motor in the group of Prof. T. Hugel are currently stalled at an early stage due to another part of the research involved³¹³. The synthetic overview is detailed in chapter 11, experiments are explained in chapter 13.6 and spectra are shown in chapter 22.5.

Chapter 19: Synthesis of *ortho*-substituted azobenzenes

The compounds have been prepared with good yields compared to literature, synthetic schemes are shown in chapter 9, the accomplishment is described in chapter 13.3 and 13.4 and spectra are shown in chapter 22.2 and 22.3¹⁸⁵. At the time of writing, optical activity measurements with 2,2',6,6'-tetramethyl-QAQ (**6**) and further experiments towards 2,2',6,6'-tetrachloro-MAG (**7**) have just been performed in the groups of Prof. E. Riedle and Prof. A. Woolley, respectively.

Part VI: CONCLUSION

CONCLUSION

The GluK2- and GluA2-LBDs have been overexpressed and purified and the synthesis of 4-Gluazo (**2**) has been achieved and even optimised. The affinity of 4-Gluazo (**2**) to different iGluRs has been determined by ITC and by the newly developed technique of label-free MST. Moreover, crystallization conditions have been developed to co-crystallize azobenzene ligands and proteins.

With the structure of the GluK2-LBD bound to 4-Gluazo (**2**), deeper mechanistic insights of the mode of action of a photoswitch on a receptor protein could be gained. Other experiments concerning the mechanism are currently under investigation by means of quantum-mechanical calculations and molecular dynamic simulations.

By illustrating the molecular details, the structure will help to design new molecules with higher affinity or selectivity. One can be sure, that with time, hard work and the already available methods and data more answers can be given to several important questions concerning the specificity of 4-Gluazo (**2**) to the different channel isotypes. 4-Gluazo (**2**) is already known to be a *trans*-agonist of kainate receptors, which is further confirmed by this structure. With affinity measurements the activity on AMPA receptors has been proved and newer data show 4-Gluazo (**2**) to act as a *cis*-agonist on NMDA receptors. Moreover, these data allow for the exact selection of attachment sites of PTLs. Also, the possibility to introduce further substituents on the phenyl rings in order to change the absorption behaviour of the photoswitch can be inspected. A red shifted version of 4-Gluazo (**2**) could for example have an impact on the ultimate, long-term goal of vision restoration.

BAG (**3**), the target molecule for DARPins during the ribosome display selection cycle has been synthesized. If the research concerning the development of a designed ankyrin repeat azobenzene binding protein will be crowned with success, completely new dimensions of applications regarding azobenzenes in biology will be accomplishable.

DARPins surpass antibodies in biophysical properties and can bridge the gap between chemistry and biology. Applications with fusion proteins and chemical conjugates would be possible. By fusing the azobenzene binding scaffold to other proteins of interest, they could thereby in turn be controlled with light. For example applications as intracellular protein binders or enzyme inhibitors could be possible,

CONCLUSION

with DARPins being an attractive, more stable and highly specific alternative to intrabodies³¹⁴.

Synthetic, switchable enzymes through domain fusion have already been reported³¹⁵. The technique to modulate enzyme function would be a key regulatory feature and the control of enzymes by a light signal would enable a wide array of sensing applications and therapeutics and would provide a powerful tool for the basic study of biology. DARPins have already been used as viral surface protein adapters, as tumor targeting molecules and could serve as diagnostic toolbox in general³¹⁶⁻³¹⁹. They could also serve as recognition molecules on protein chips for light-controllable proteomics studies in connection with target discovery and functional identification.

With the tetrameric structure of the GluA2-LBD harboring MES and a sulfate ion, a new binding mode has been identified and a novel class of GluA2 antagonists has been developed. MOBIPHOS (**4**) and MOBIPHOSen (**38**) have been prepared and electrophysiological experiments proved the antagonistic effect on GluA2.

When the mode of action of the molecules is further confirmed by additional crystal structures and thereby understood and described by a single molecular mechanism, high affinity drugs may possibly be designed and synthesized. Moreover, a photoswitchable version of this antagonist might be possible.

Although glutamate receptor antagonists have proven to be an effective research tool in receptor pharmacology, compounds modulating iGluR function have not yielded major successes as therapeutic agents, yet. An important characteristic of the effectiveness of substances in inhibiting nerve conduction depends in part on its solubility. To be taken up by the extracellular medium and to be conveyed to its binding position, the molecule has to be soluble in water. The antagonist DNQX and analogues thereof are highly insoluble in water, which led to their abandonment in clinical trials⁵⁹. In contrast MOBIPHOS (**4**) and MOBIPHOSen (**38**) are highly soluble in water, but the affinity to the receptor is expected to be not very high. However, upon structure-guided improvements this series may be of clinical interest. With the development of more potent compounds, many promising and exciting opportunities are tantalizingly close.

CONCLUSION

ABA (**5**) has been prepared, but experiments towards the creation of a molecular motor are currently stalling. With a molecular motor moving on a track in a light-driven fashion, specific operations or tasks at the molecular level could be performed in the future in the field of nanoscience. The molecular motor could possibly act as a transport device or it could perform other mechanical functions when incorporated into bigger structures. With artificial molecular motors a real nanomachinery built up of individual basis modules could be imaginable.

The key characteristic of 2,2',6,6'-tetramethyl-QAQ (**6**) is the stability of the chiral structure in the *Z* isomer and the synthesis of the molecule has been performed. Next, the molecular chirality needs to be detected, and the enantiomeric enrichment with circular polarized light needs to be induced. Further experiments, like circular dichroism could be used to investigate the photochemical isomerization and additionally the two enantiomers could possibly be separated by chiral HPLC. This molecule could for example be used as a chiral sensor.

The selective expression of LiGluRs in retinal ganglion cells could restore light sensitivity to the blind rd1 mouse retina and to the TKO mouse retina⁸. In order to perform further experiments to achieve the goal of vision restoration, the applied compounds need to be red-shifted. Therefore, treated mice could respond to more natural stimuli. MAG with its conventional azobenzene core is activated in the long-wave UV to blue range. However, most UV light cannot even reach the retina, but is filtered out by the cornea. A building block of the red-shifted 2,2',6,6'-tetrachloro-MAG (**7**) has been prepared and when the synthesis is completed, the molecule can be tested on rd1 mice. By using the adeno-associated viral vector gene therapy, chemically engineered LiGluRs can be expressed selectively in retinal ganglion cells, which consequently can be targeted with 2,2',6,6'-tetrachloro-MAG (**7**). The next step would be the synthesis of red-shifted PCLs for iGluRs. With PCLs there is no need to introduce genes and wild type endogeneous receptors can be targeted. A possibility would be a red-shifted 4-Gluazo (**2**) compound to target iGluRs, present in retinal ganglion cells³²⁰.

Part VII: APPENDIX

Chapter 20: Abbreviations

3-D	three-dimensional	DNA	deoxyribonucleic acid
ABA	azobenzene	DNase	deoxyribonuclease
	bis(iodoacetamide)	DNQX	6,7-dinitroquinoxaline- 2,3-dione
ABP	azobenzene-binding protein	dt	double triplet
AcOH	acetic acid	DTT	dithiothreitol
AMPA	α -amino-3-hydroxy-5- methyl-4- isoxazolepropionic acid	EC ₅₀	half-maximal effective concentration
A/NTD	amino- or N-terminal domain	<i>E. coli</i>	<i>Escherichia coli</i>
APS	ammonium persulfate	EDCI	1-ethyl-3-(3- dimethylaminopropyl) carbodiimide
ATPO	2-amino-3-[5- <i>tert</i> -butyl- 3-(phosphonomethoxy)- 4-isoxazolyl] propionic acid	EDTA	Ethylenediamine tetraacetic acid
ATR	attenuated total reflection	EI	electron ionization
BAG	biotin azobenzene glutamate	ER	endoplasmic reticulum
br	broad	ESI	electrospray ionization
BSA	bovine serum albumin	Et ₂ O	diethylether
Ca ²⁺	calcium ion	EtOAc	ethyl acetate
CaCl ₂	calcium chloride	FeSO ₄	ferrous sulphate
calc	calculated	GABA	γ -aminobutyric acid
CAM	cerium ammonium molybdate	GluA	glutamate receptor AMPA
CCDC	cambridge crystallographic data centre	GluK	glutamate receptor kainate
CDCl ₃	deuterated chloroform	<i>GRIA</i>	glutamate receptor, ionotropic, AMPA
Ce(SO ₄) ₂	cerium sulphate	<i>GRIK</i>	glutamate receptor, ionotropic, kainate
CH ₂ Cl ₂	dichloromethane	h	hour
CNS	central nervous system	H	proton
conc.	concentrated	HCl	hydrochloric acid
CsF	caesium fluoride	HEPES	4-(2-hydroxyethyl)-1- piperazineethanesulfonic acid
CTD	C-terminal domain	HOAc	acetic acid
CV	column volume	HOBt	1-hydroxybenzotriazole
D1	domain1	HPLC	high performance liquid chromatography
D2	domain2	(HR-)MS	(high resolution)-mass spectrometry
d	doublet	H ₂ SO ₄	sulphuric acid
DARPin	designed ankyrin repeat protein	HWE	Horner-Wadsworth- Emmons
dd	double doublet	Hz	hertz
DIPEA	diisopropylethylamine	i.e.	<i>id est</i>
DMF	dimethylformamide		

APPENDIX

iGluR	ionotropic glutamate receptor	MOBIPHOS	morpholino bisphosphonate
IPTG	isopropyl- β - <i>D</i> -thiogalactopyranoside	MOBIPHOS en	unsaturated morpholino bisphosphonate
IR	infrared	mRNA	messenger ribonucleic acid
ITC	isothermal titration calorimetry	MST	microscale thermophoresis
IUPHAR	international union of basic and clinical pharmacology	MW	molecular weight
<i>J</i>	coupling constant	MWCO	molecular weight cut off
K ⁺	potassium ion	<i>m/z</i>	mass to charge ratio
K ₂ CO ₃	potassium carbonate	n	n-orbital
KcsA	potassium channel from <i>S. lividans</i>	NaCl	sodium chloride
K _D	equilibrium dissociation constant	Na	sodium
KF	potassium fluoride	Na ⁺	sodium ion
kJ	kilojoule	NH ₄ Cl	ammonium chloride
KMnO ₄	potassium permanganate	NaHCO ₃	sodium hydrogen carbonate
KOH	potassium hydroxide	NaOAc	sodium acetate
LB	lysogeny broth	NaOH	sodium hydroxide
LBD	ligand-binding domain	Na ₂ S	sodium sulphide
LC-MS	liquid chromatography – mass spectrometry	Na ₂ SO ₄	sodium sulphate
LGIC	ligand-gated ion channel	NBQX	2,3-dihydroxy-6-nitro-7-sulfamoyl-benzo[f]quinoxaline
LiCl	lithium chloride	<i>n</i> -BuLi	<i>n</i> -butyllithium
LiGluR	light-gated ionotropic glutamate receptor	NEB	new england biolabs
LiHMDS	lithium hexamethyldisilazide	Ni-NTA	nickel-nitrilotriacetic acid
LMU	Ludwig-Maximilians-Universität	NMDA	<i>N</i> -methyl- <i>D</i> -aspartate
LiOH	lithium hydroxide	NMR	nuclear magnetic resonance
Li ₂ SO ₄	lithium sulfate	OD ₆₀₀	optical density at 600 nm
m	NMR: multiplet, IR: medium	ORF	open reading frame
MAG	maleimide – azobenzene – glutamate	π , π^*	π -, π^* -orbital
MeCN	acetonitrile	p.a.	pro analysi
MeOH	methanol	PCL	photochromic ligand
MES	2-(<i>N</i> -morpholino) ethane sulfonic acid	PCR	polymerase chain reaction
MgCl ₂	magnesium chloride	PDB	protein data bank
mGluR	metabotropic glutamate receptor	Pd/C	palladium on carbon
min	minute	PEG	polyethylene glycol
		PFP-TFA	pentafluorophenyl trifluoroacetate
		Φ	quantum yield
		pH	potentia hydrogenii
		ppm	parts per million
		Pt/C	platinum on carbon

APPENDIX

PTL	photoswitched tethered ligand	w ZnCl ₂	weak zinc chloride
P2X	purinergic receptor 2X		
q	quartet		
QAQ	quaternary-ammonium – azobenzene – quaternary-ammonium		
quint	quintet		
RBS	ribosome binding site		
R _f	retarding factor		
RNase	ribonuclease		
RP	reverse phase		
rpm	revolutions per minute		
RT-PCR	reverse transcriptase-polymerase chain reaction		
s	NMR: singlet , IR: strong		
scFv	single-chain Fv		
SDS	sodium dodecyl sulfate		
SDS-PAGE	sodium dodecyl sulfate polyacrylamide gel electrophoresis		
sec	second		
SELEX	systematic evolution of ligands by exponential enrichment		
SOC	super optimal broth with catabolite repression		
t	triplet		
TE	Tris EDTA		
TEA	triethylamine		
TEMED	tetramethylethylen-diamine		
TFA	trifluoroacetic acid		
THF	tetrahydrofurane		
TKO	triple knockout		
TLC	thin layer chromatography		
TMD	transmembrane domain		
TMS	tetramethylsilane		
TMSI	trimethylsilyl iodide		
Tris	tris(hydroxymethyl)-aminomethane		
tRNA	transfer ribonucleic acid		
TUM	technische Universität München		
UoT	University of Toronto		
UV	ultraviolet		
vs	very strong		

Chapter 21: Crystallographic data

21.1 GluK2-LBD and GluA2-LBD

	GluK2-LBD	GluA2-LBD
<i>Data collection</i>		
Space group	P6 ₁ 22	P2 ₁ 2 ₁ 2 ₁
Unit cell parameters [Å]; [°]	a = b = 102.61, c = 282.51; $\alpha = \beta = 90, \gamma = 120$	a = 61.99, b = 92.02, c = 196.51; $\alpha = \beta = \gamma = 90$
Wavelength [Å]	0.9184	0.9184
Resolution [Å]	20.0 – 2.0 (2.1 – 2.0)	20.0 – 1.8 (1.9 – 1.8)
Completeness [%]	99.8 (100.0)	99.9 (100.0)
Unique reflections	60248 (8042)	104825 (15487)
Multiplicity	10.6 (10.5)	8.1 (8.2)
Mean I/ σ (I)	27.5 (3.9)	15.2 (3.9)
R _{meas.} [%]	7.4 (63.6)	11.2 (55.6)
Wilson B-factor [Å ²]	34.3	21.1
<i>Refinement</i>		
Resolution [Å]	19.92 – 2.00 (2.05 – 2.00)	19.93 – 1.80 (1.85 – 1.80)
Reflections (working)	57203 (4115)	99587 (7227)
Reflections (test)	3042 (217)	5237 (354)
R _{cryst} [%]	17.3 (21.9)	17.4 (21.2)
R _{free} [%]	20.4 (27.2)	22.1 (26.1)
Number of atoms	4122 / 39 / 6 / 478	8109 / 44 / 60 / 1104
Proteins / ligands / ions / waters		

Table 11: Crystallographic data of the GluK2- and GluA2-LBD.

Values in parentheses refer to the highest resolution shell.

Coordinates and structure factors of the GluK2- and GluA2-LBD have been deposited in the Protein Data Bank with the accession codes 4H8I and 4H8J, respectively.

21.2 Propargyl pyroglutamate (11) and bisphosphonate (40)

	Propargyl pyroglutamate (11)	Bisphosphonate (40)
Space group	P2 ₁ 2 ₁ 2 ₁	Cmc2 ₁
Unit cell parameters [Å]; [°]	a = 8.91, b = 10.61, c = 16.88; $\alpha = \beta = \gamma = 90$	a = 12.70, b = 17.07, c = 9.99; $\alpha = \beta = \gamma = 90$
V [Å ³]	1596.3(5)	2166.7(3)
Z	4	4
$\rho_{\text{calc.}}$ [g · cm ⁻³]	1.229	1.233
μ [mm ⁻¹]	0.092	0.229
Reflections measured	8656	5889
R _{int}	0.0479	0.0304
Mean $\sigma(I)/I$	0.0488	0.0296
θ range	4.28 – 26.37	4.42 – 26.37
Observed reflections	2727	2112
Flack parameter	-0.8(17)	0.04(13)
Reflections in refinement	3237	2266
parameters	204	142
restraints	0	3
R(F _{obs})	0.0563	0.0409
R _w (F ²)	0.1494	0.1100
S	1.067	1.046
ρ_{max} [e · Å ⁻³]	0.315	0.370
ρ_{min} [e · Å ⁻³]	-0.248	-0.325

Table 12: Crystallographic data of propargyl pyroglutamate (11) and bisphosphonate (40).

Propargyl pyroglutamate:

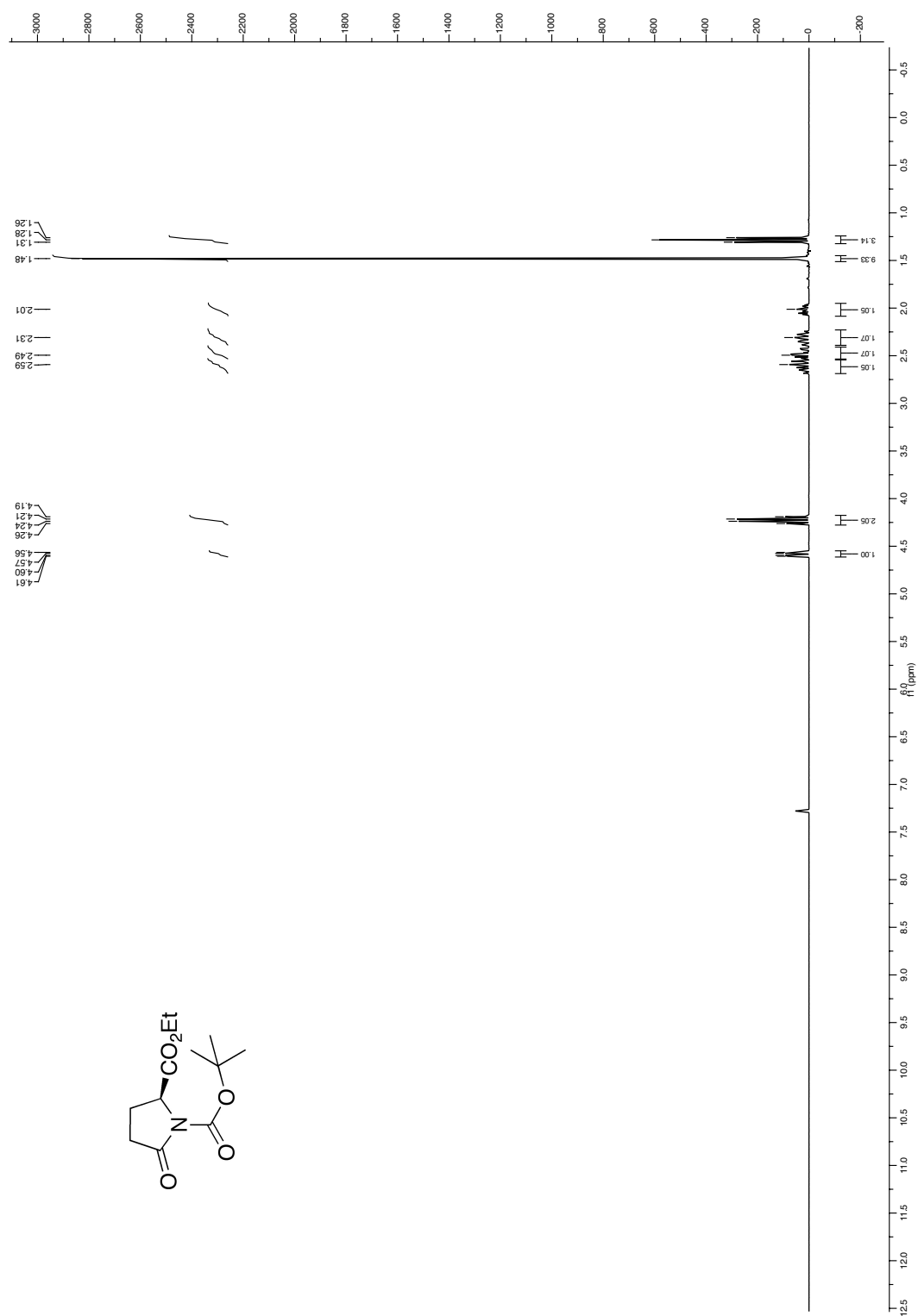
The flack parameter is meaningless. The absolute structure has been deduced from the synthesis. The disorder in an ethyl group has been handled by using the split model, with a sof ratio of 0.76/0.24.

Bisphosphonate:

The disorder of an ethyl group has been handled by using the split model, with a sof ratio of 0.46/0.54, split atoms have been refined isotropically.

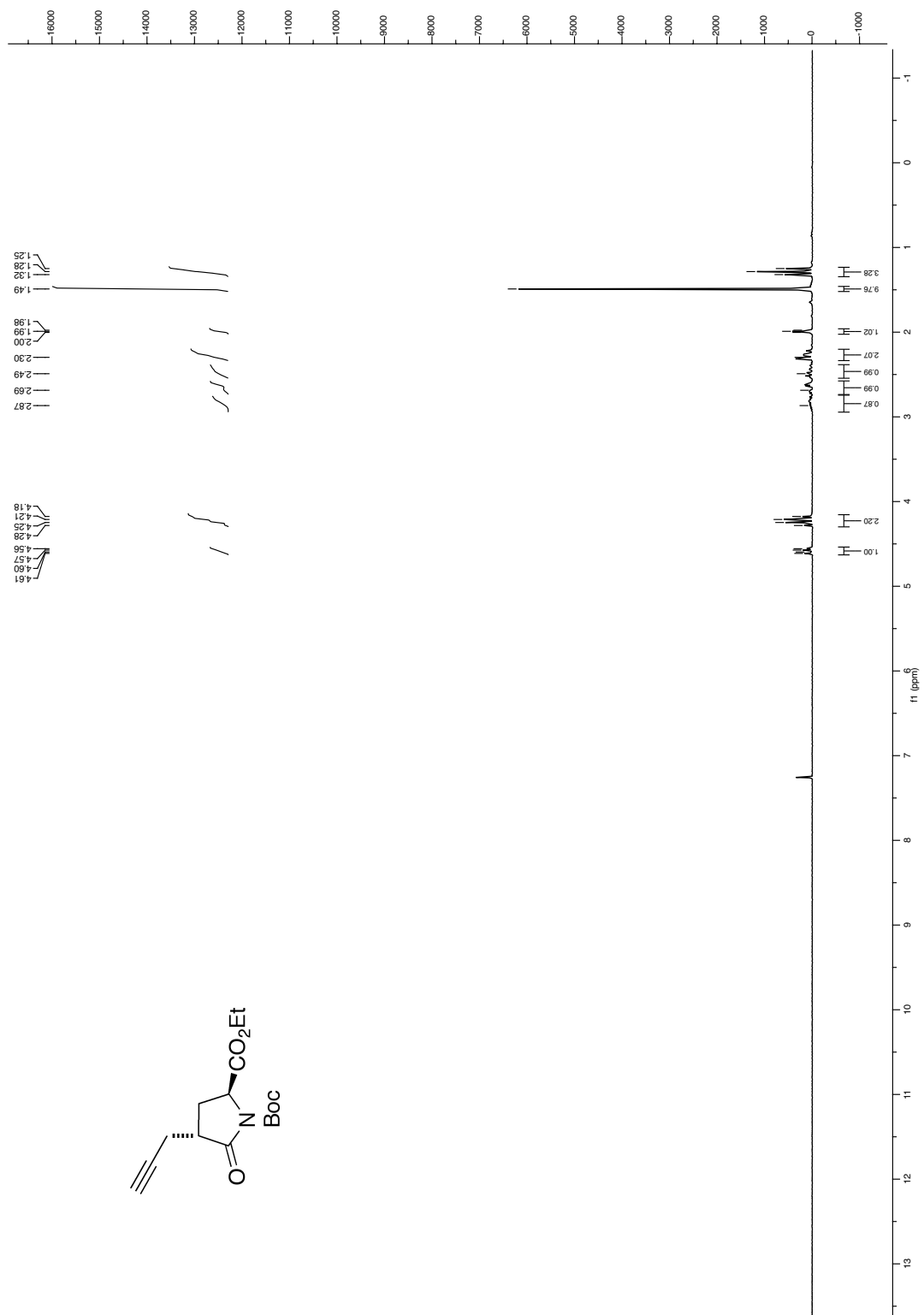
Chapter 22: NMR Spectra

22.1 Spectra of 4-Gluazo and intermediates

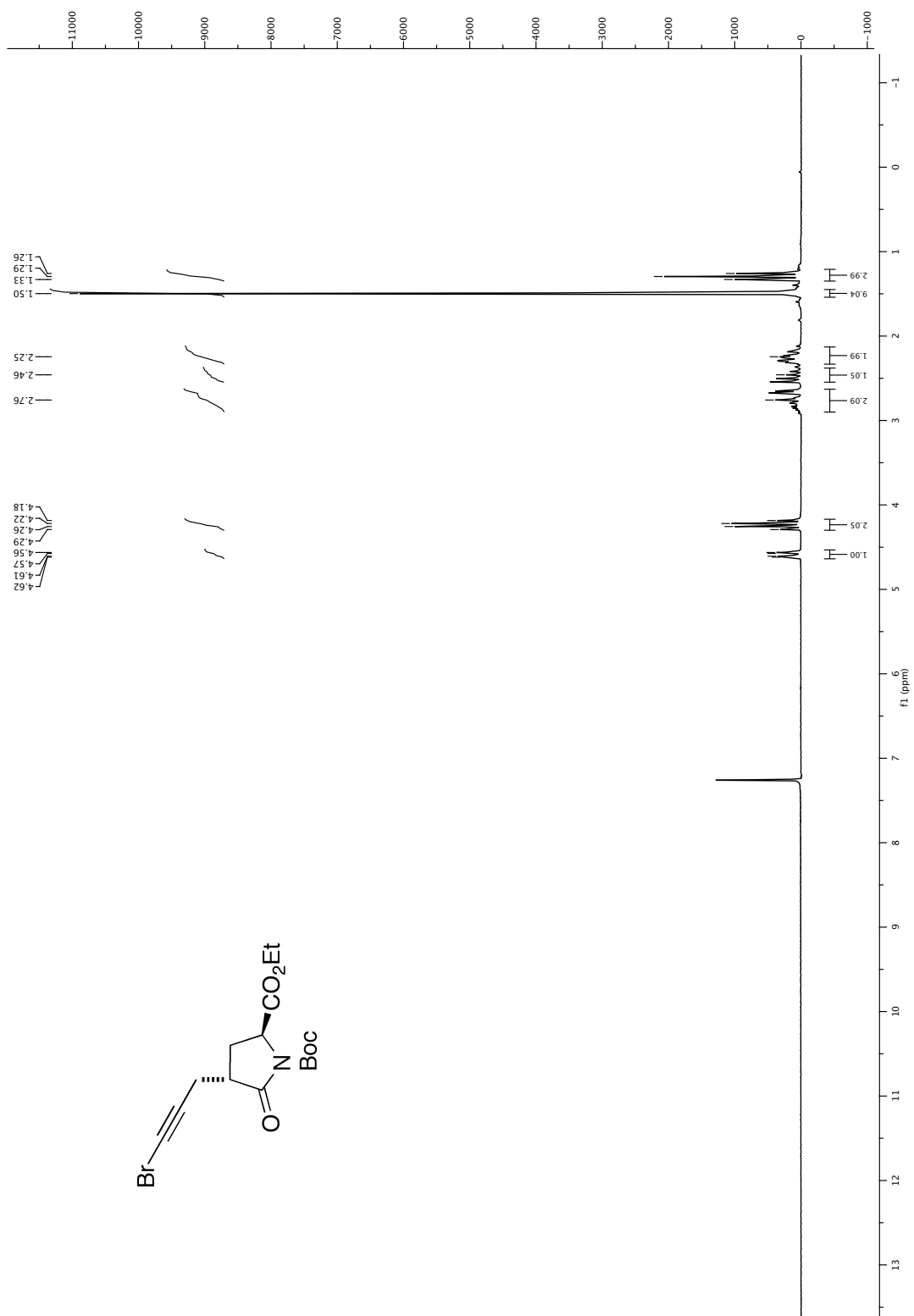
22.1.1 *N*-Boc-L-pyrroglutamic acid ethyl ester (10)

APPENDIX

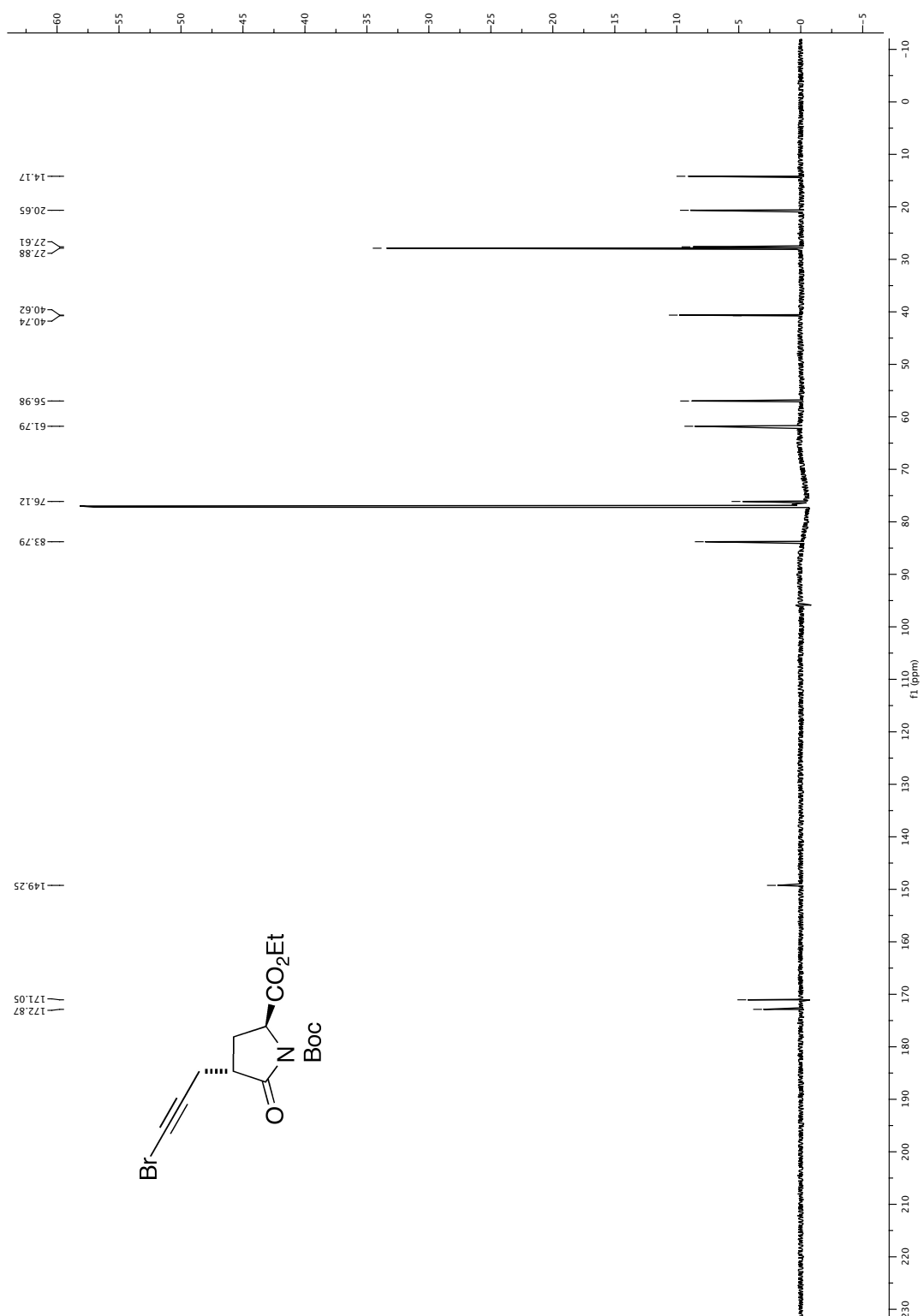
22.1.2 Propargyl pyroglutamate (11)



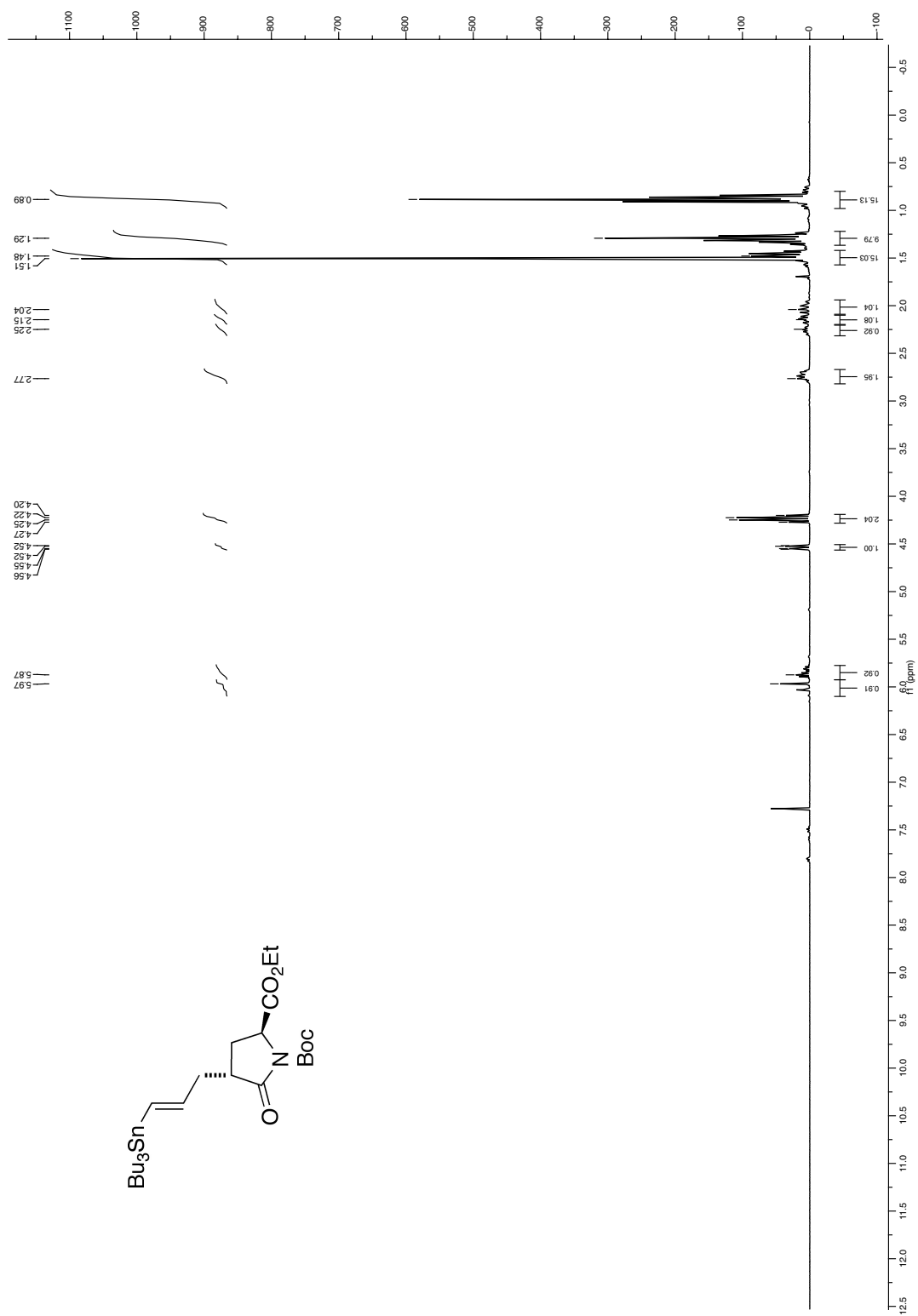
22.1.3 Bromoalkyne (12)



APPENDIX

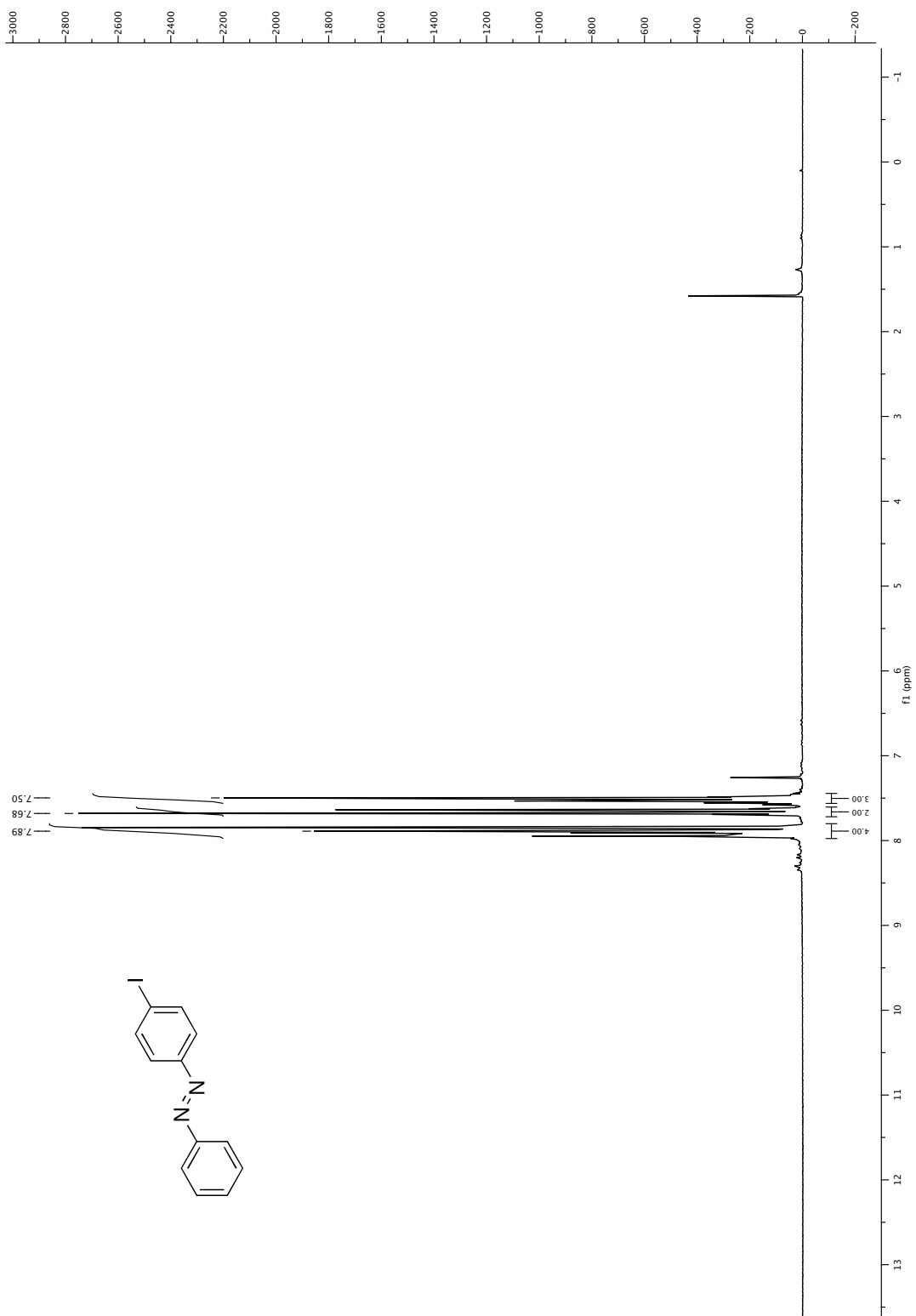


22.1.4 Vinyl stannane (13)

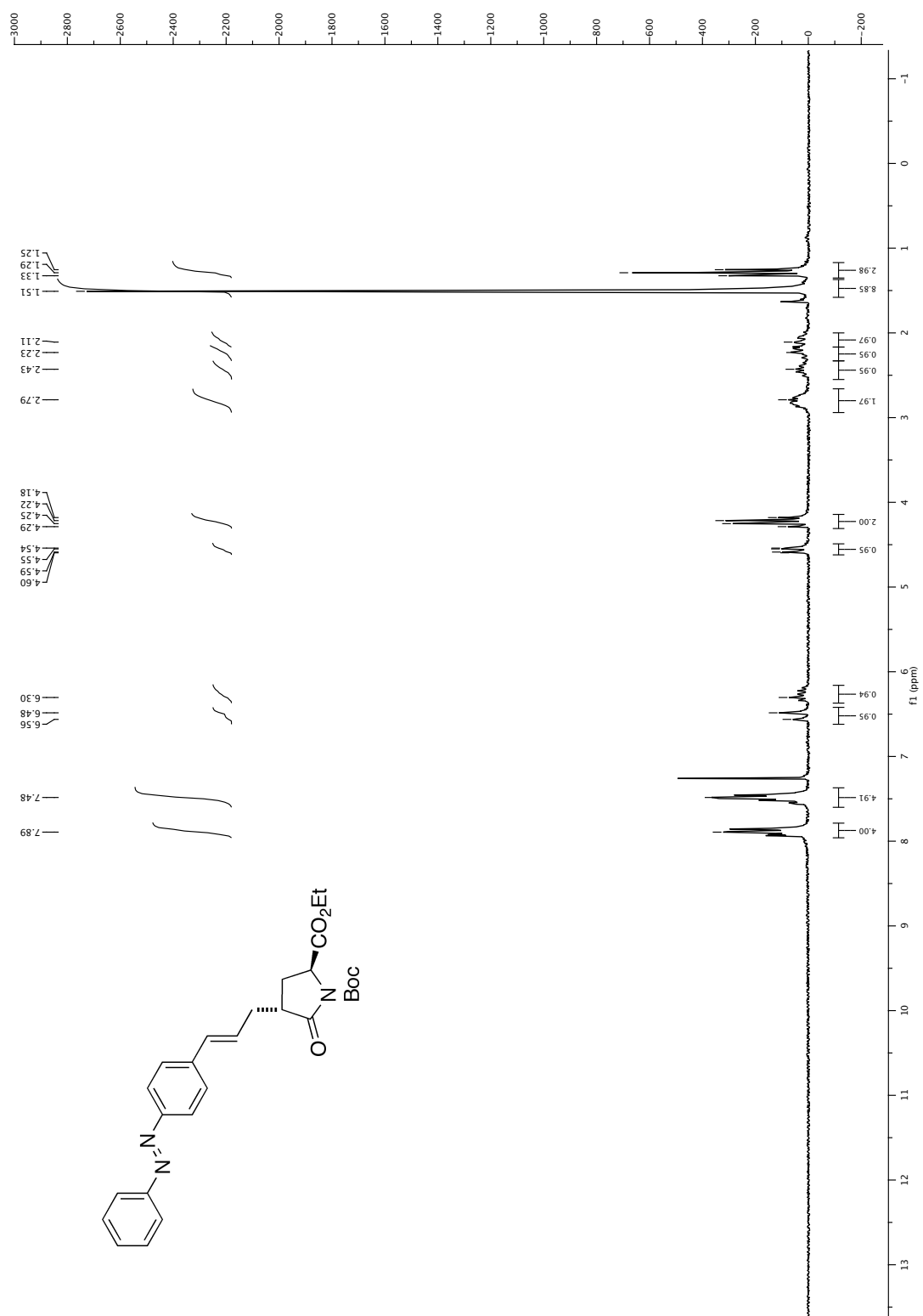


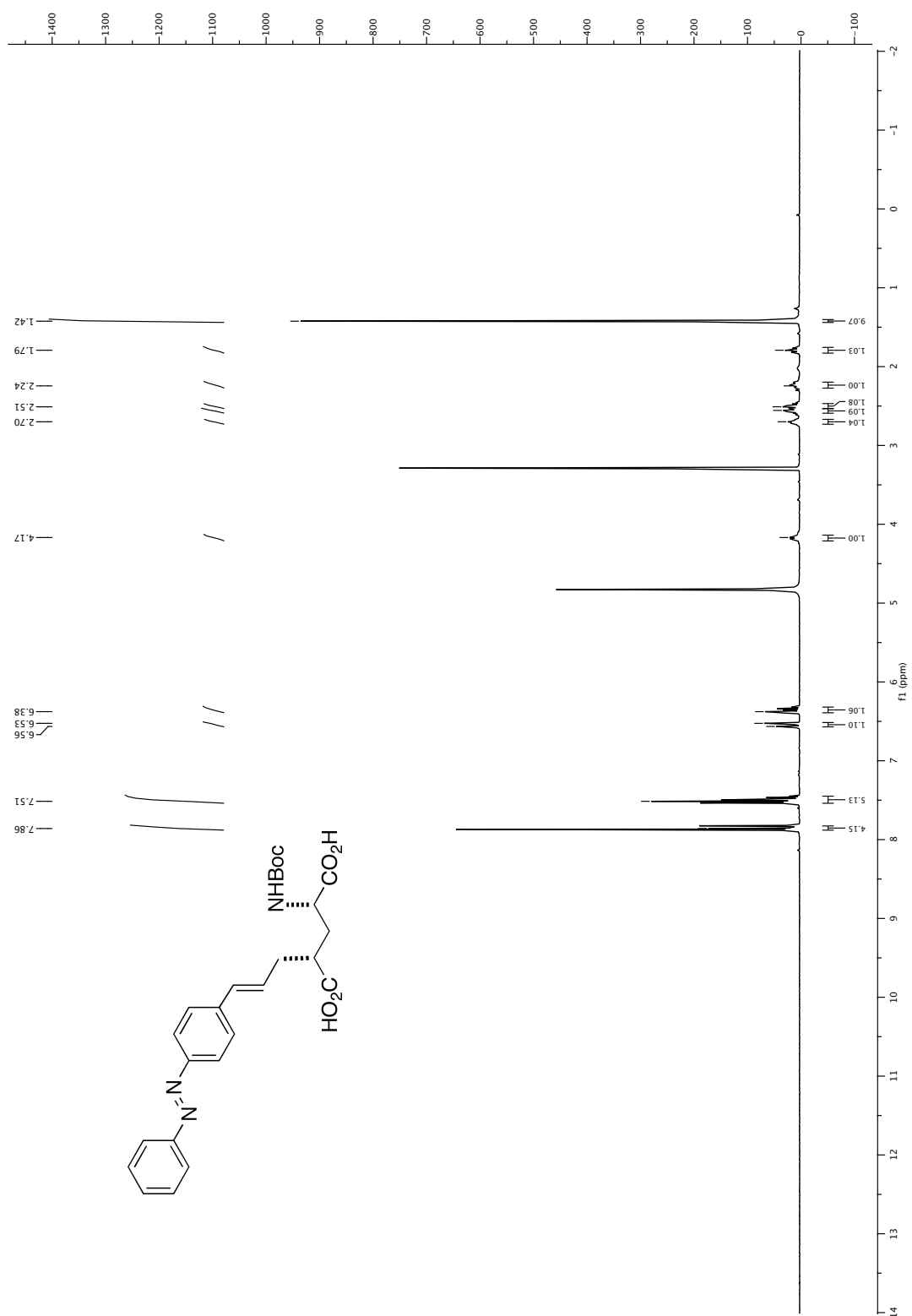
APPENDIX

22.1.5 Iodoazobenzene (14)



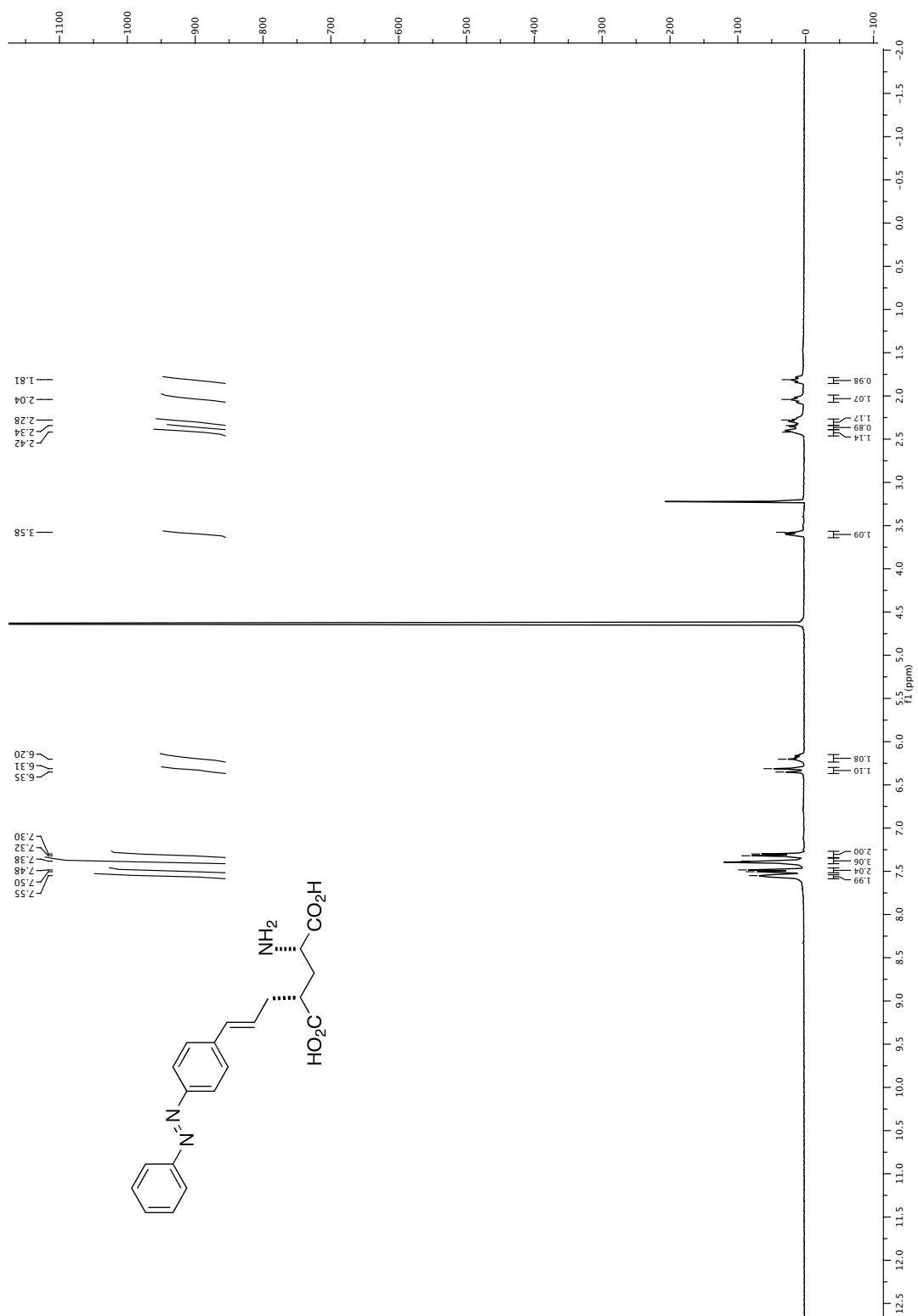
22.1.6 Azobenzene pyroglutamate (17)



22.1.7 *N*-Boc azobenzene glutamic acid (18)

APPENDIX

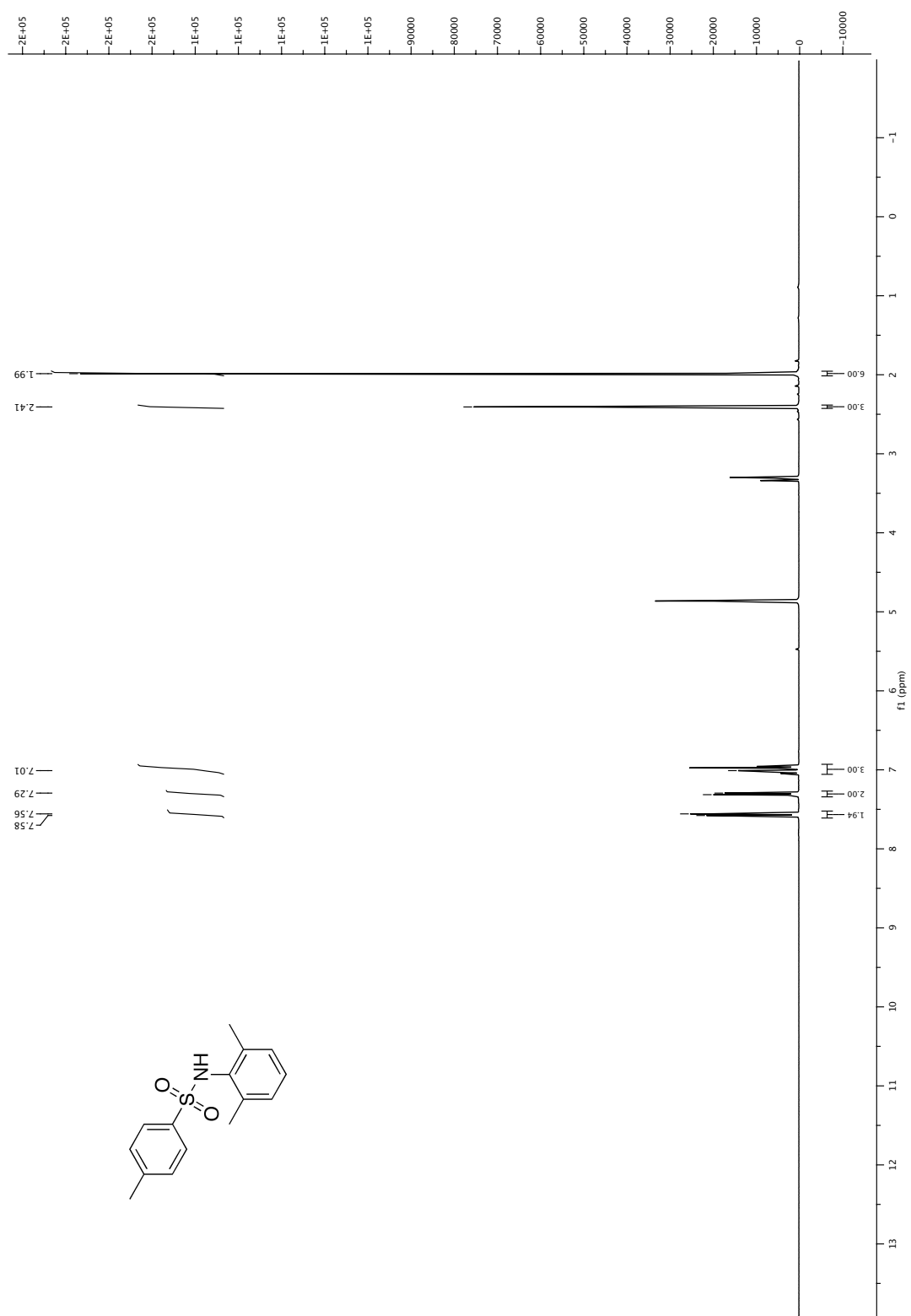
22.1.8 4-Gluazo (2)



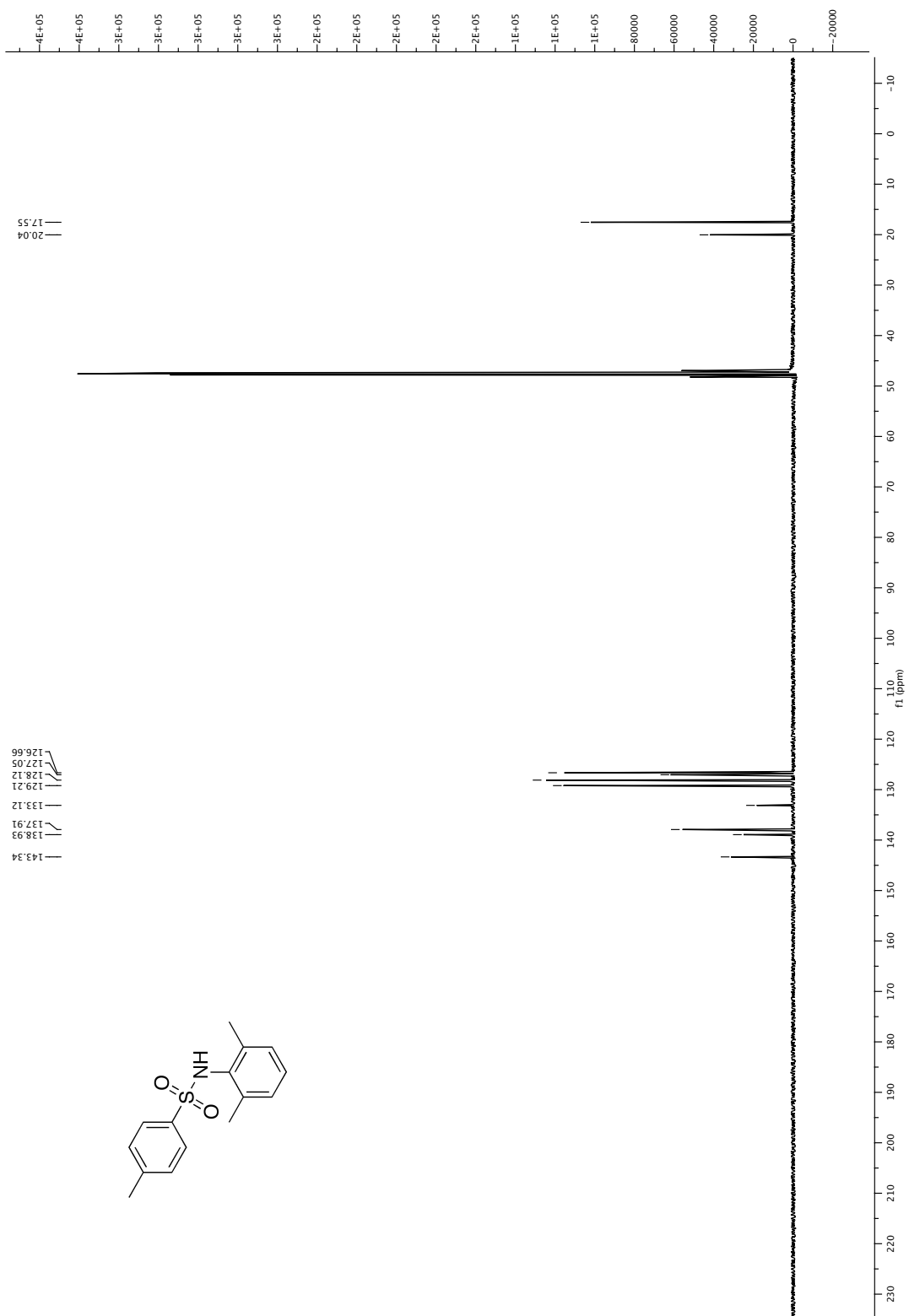
APPENDIX

22.2 Spectra of BAG and intermediates

22.2.1 *N*-tosyl-2,6-dimethylaniline (26)

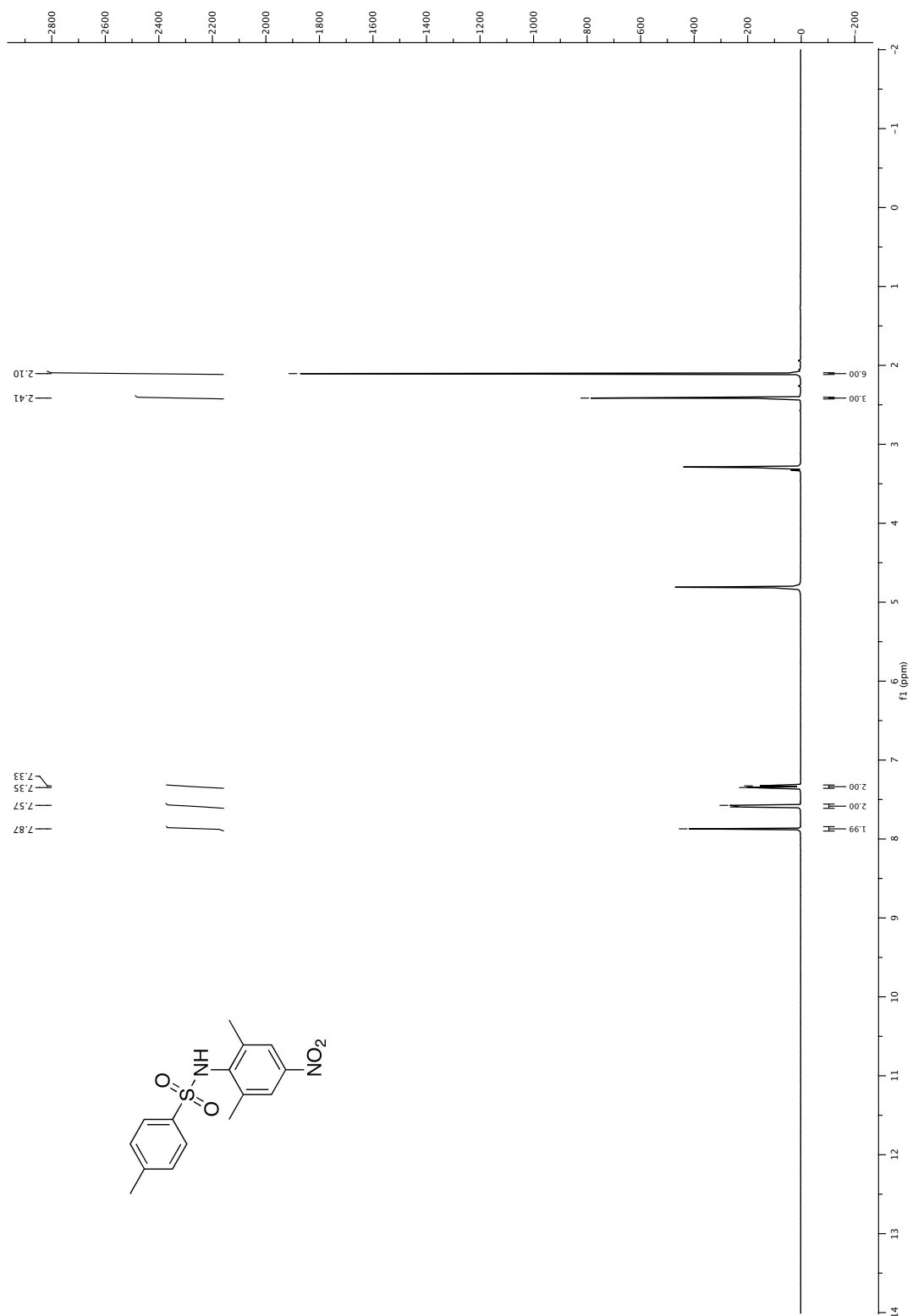


APPENDIX

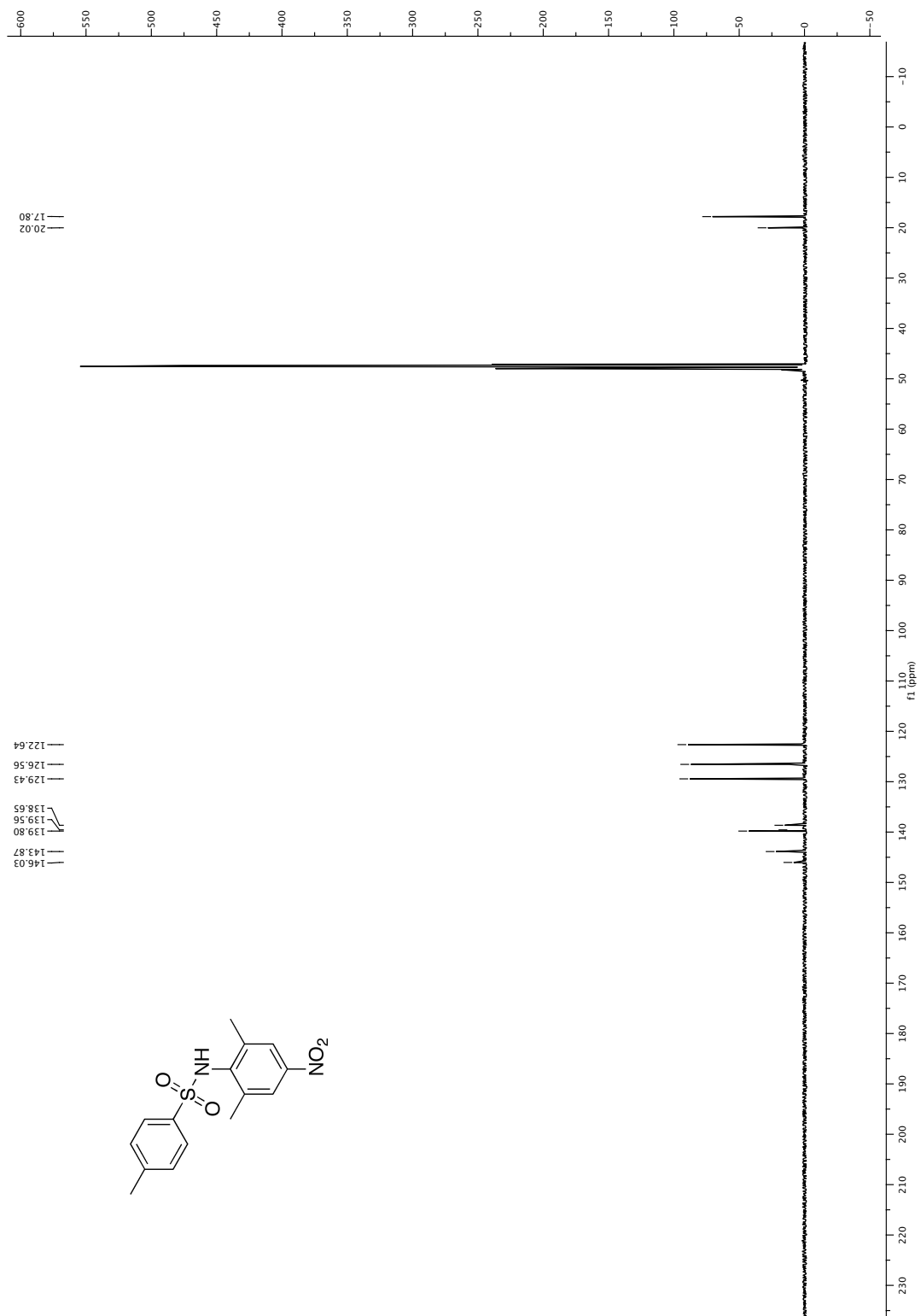


APPENDIX

22.2.2 *N*-tosyl-2,6-dimethyl-4-nitroaniline (27)

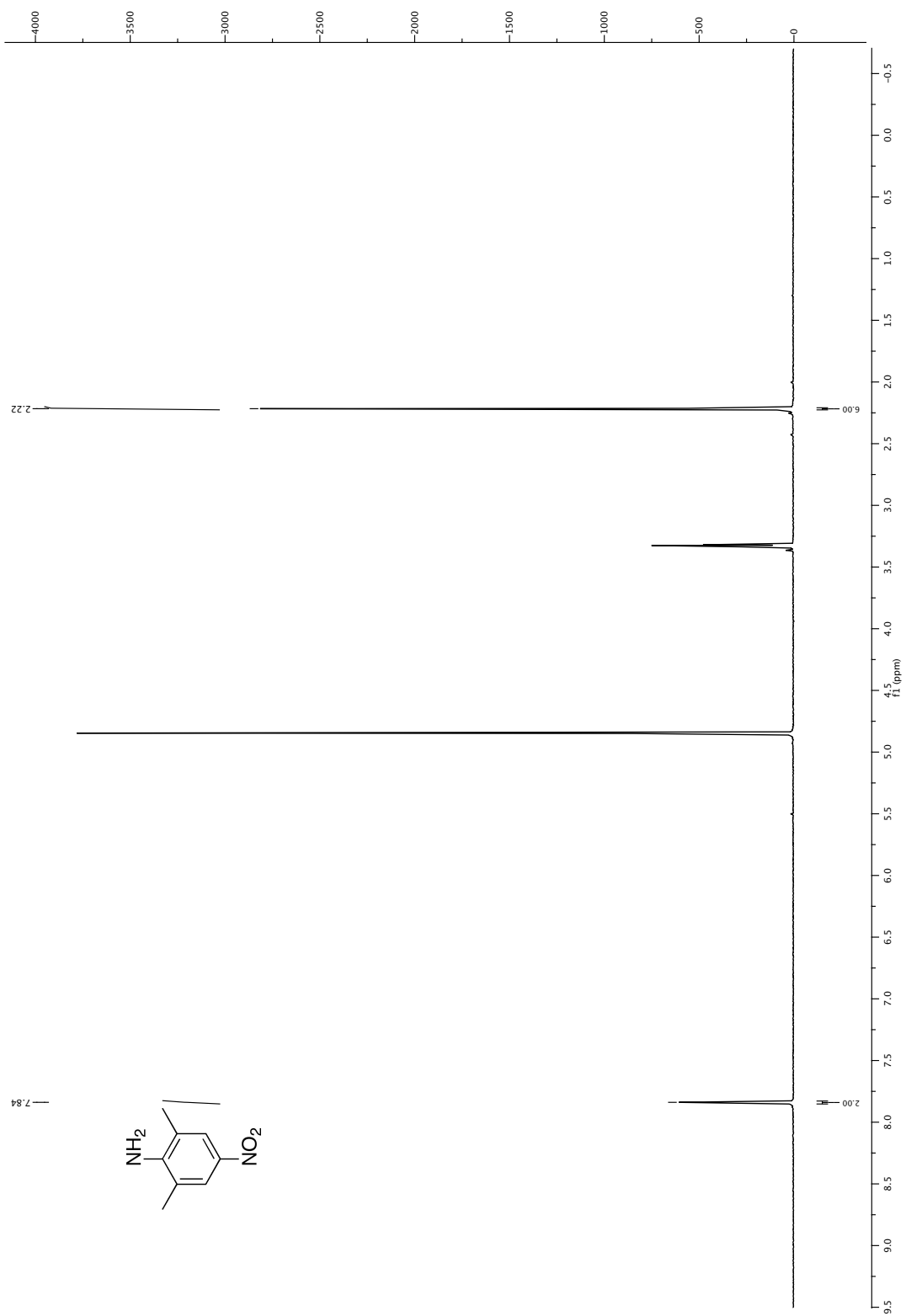


APPENDIX

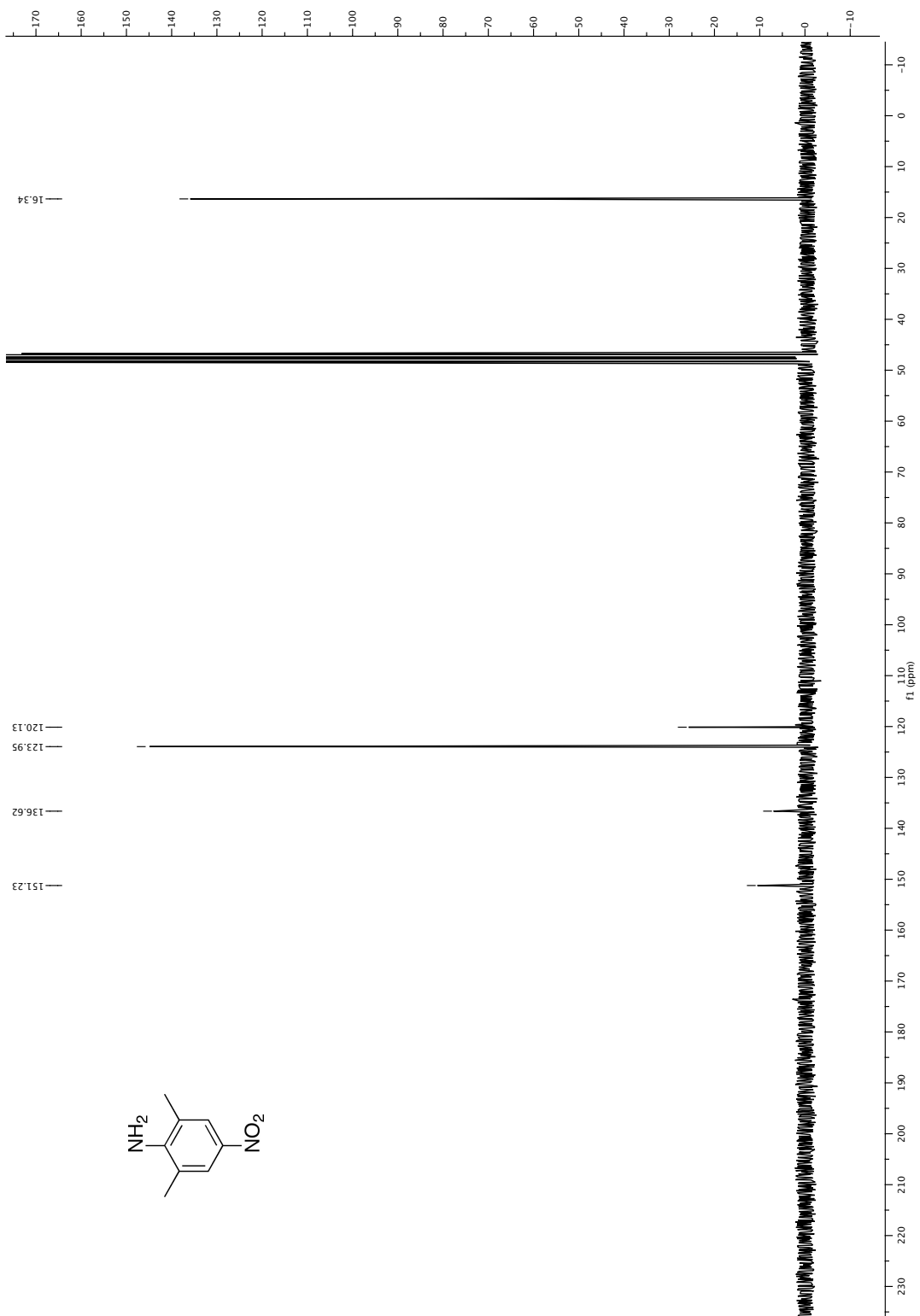


APPENDIX

22.2.3 2,6-dimethyl-4-nitroaniline (24)

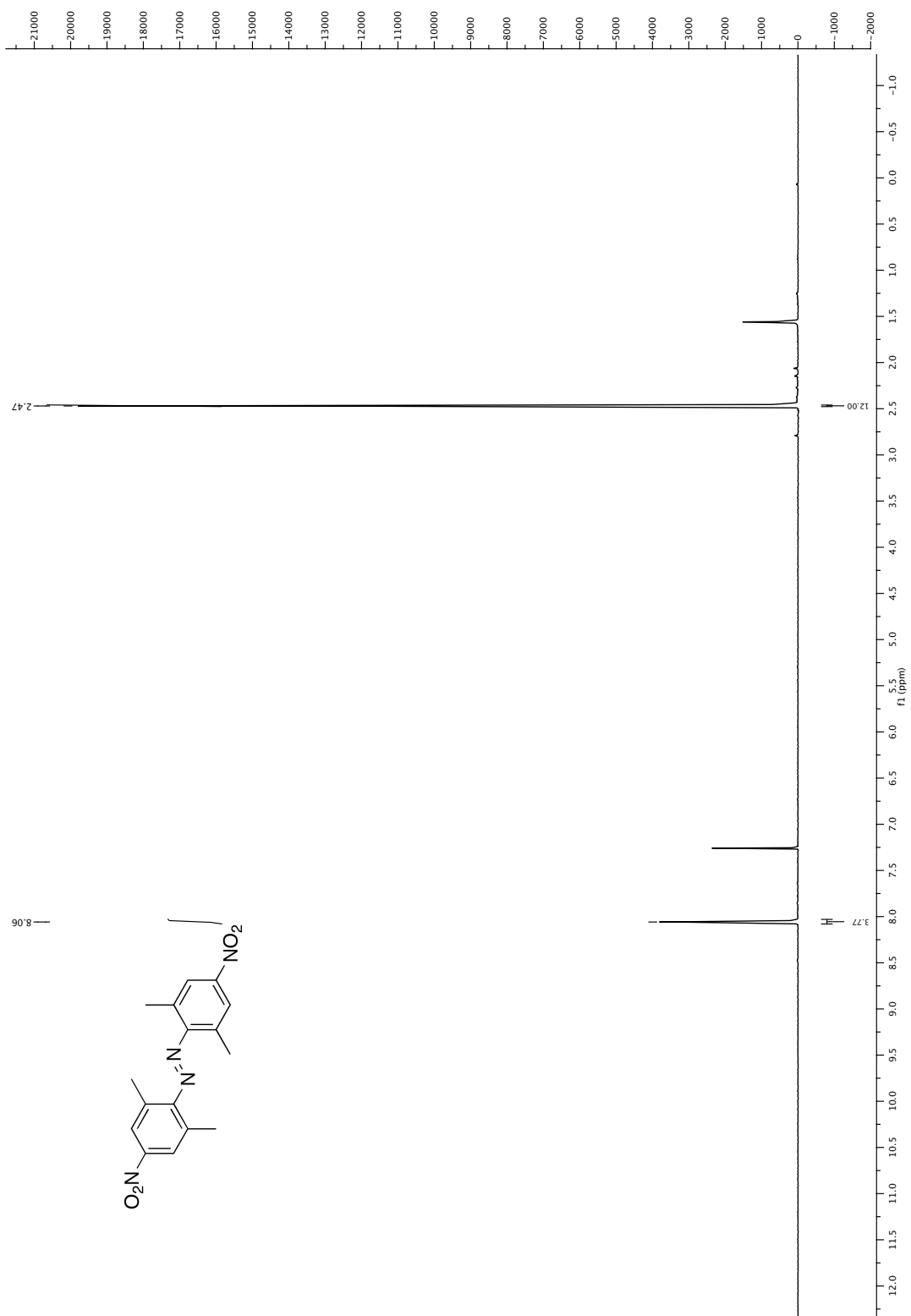


APPENDIX

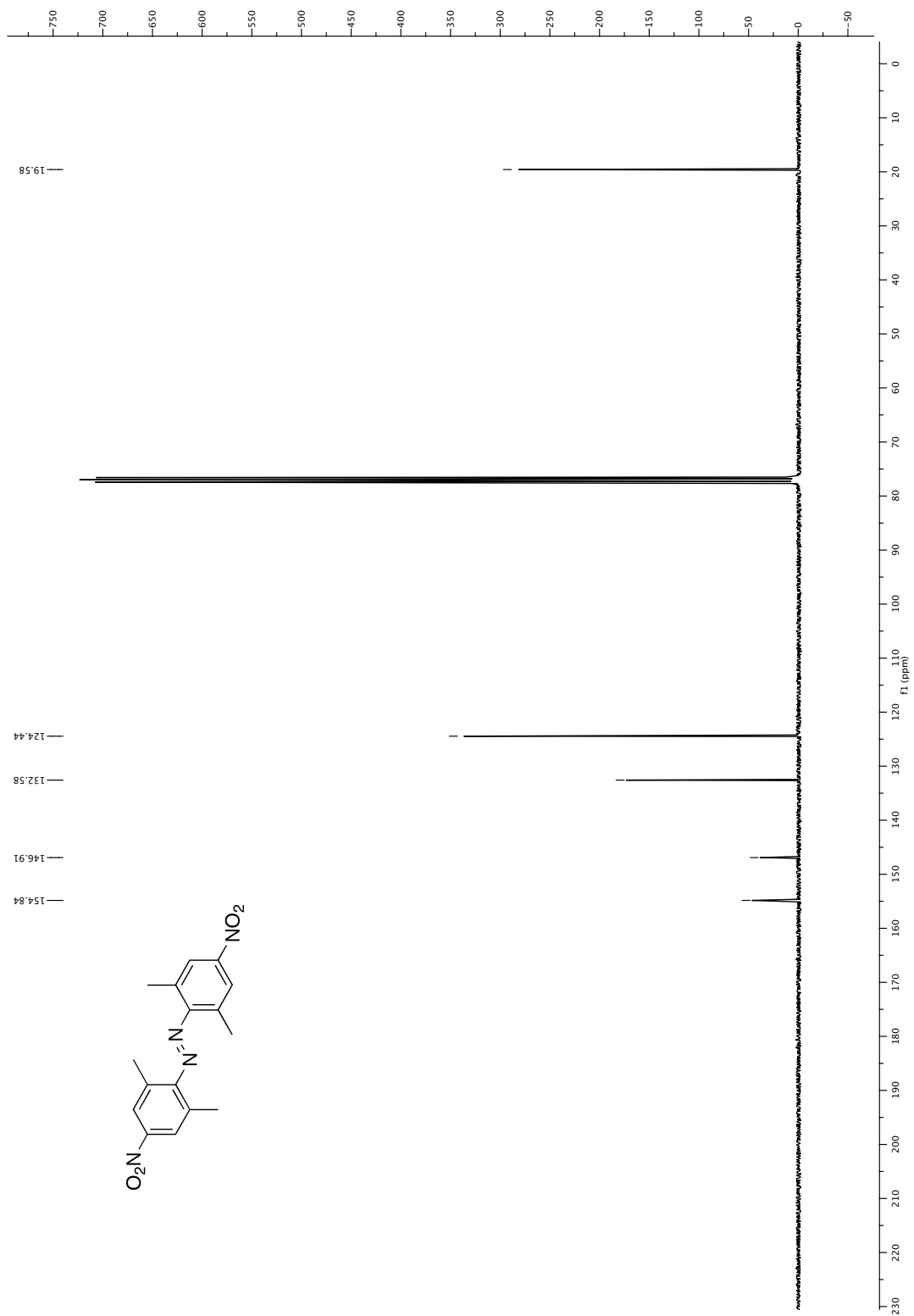


APPENDIX

22.2.4 Nitroazobenzene (28)



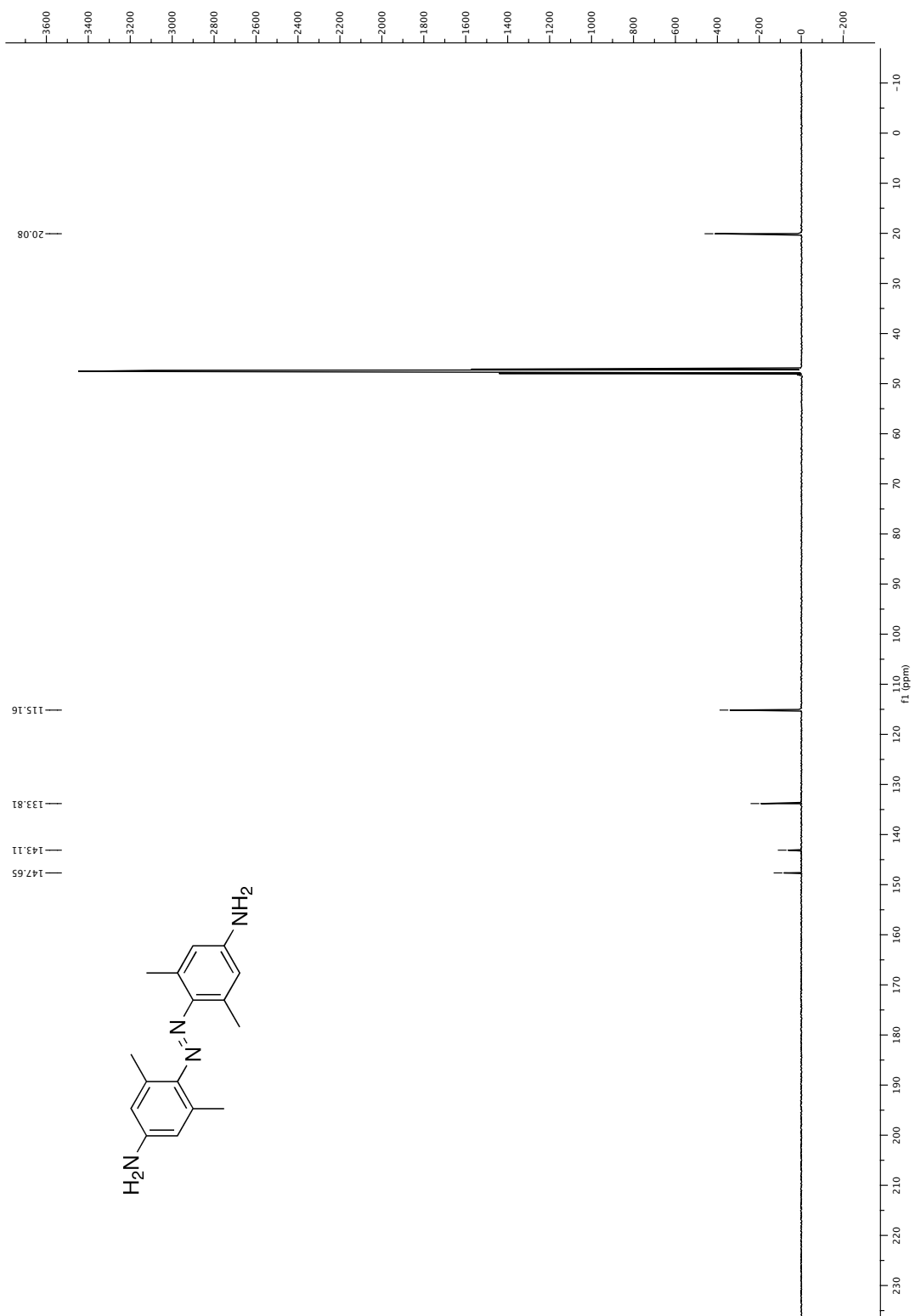
APPENDIX

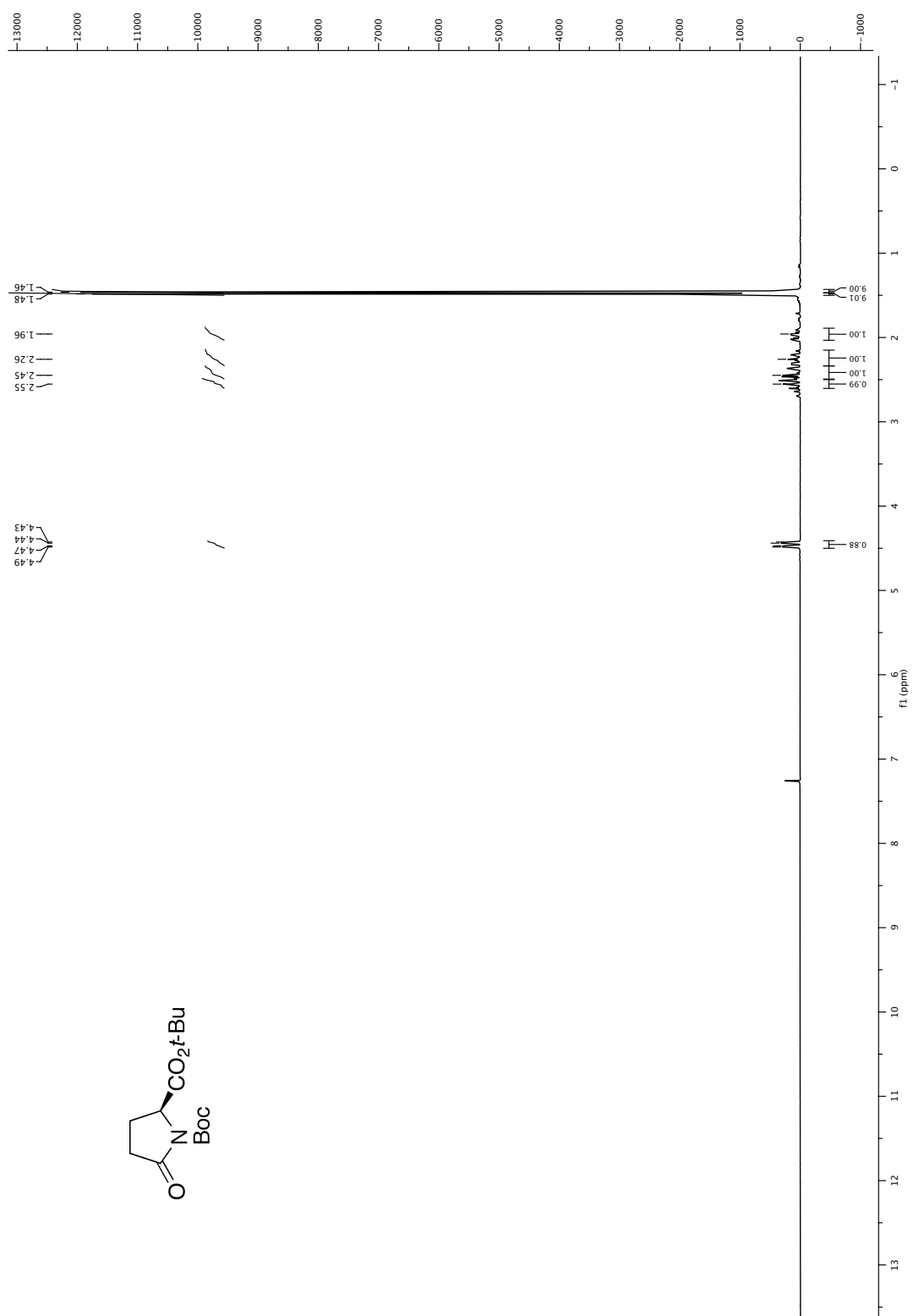


22.2.5 Aminoazobenzene (29)

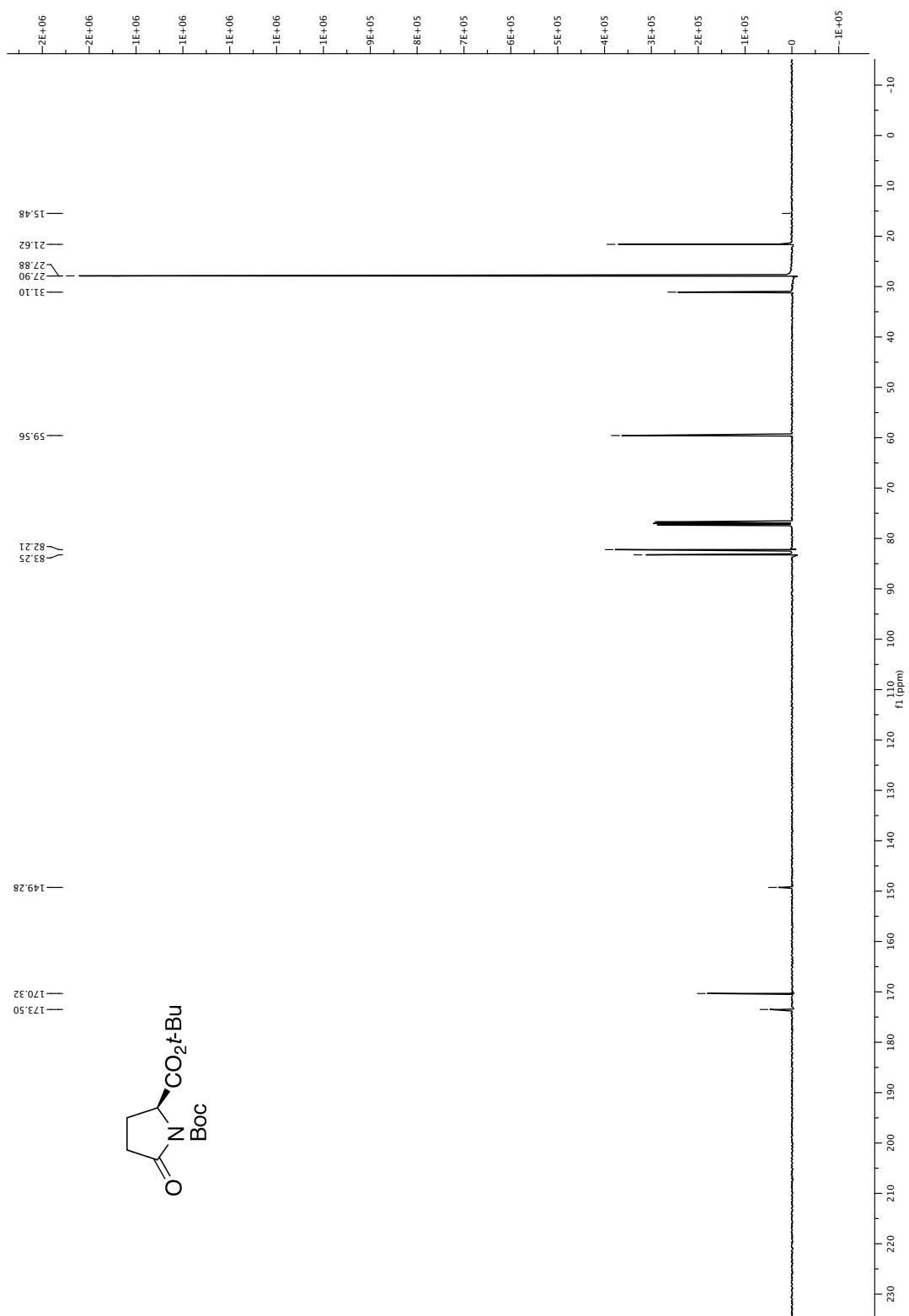


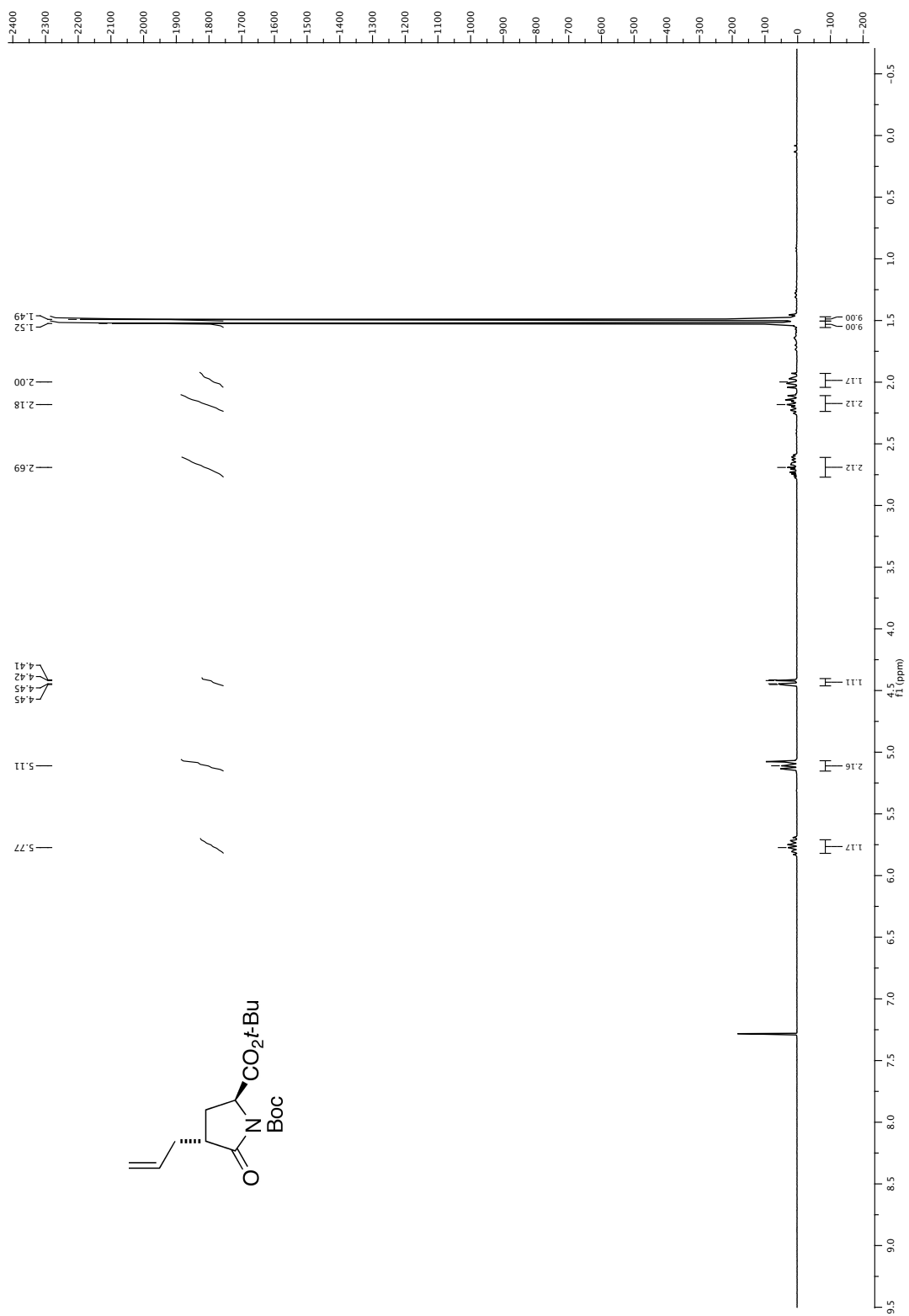
APPENDIX



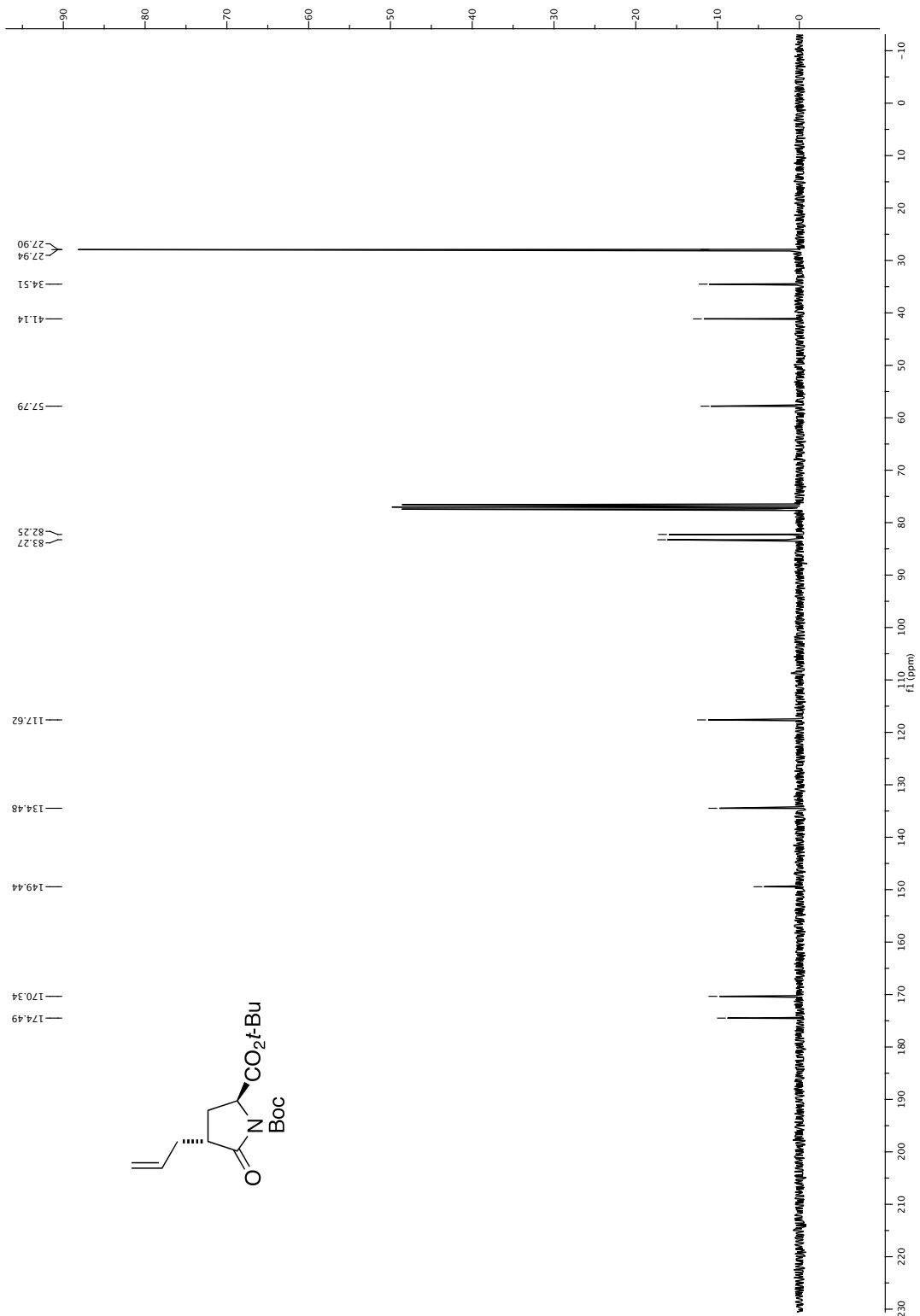
22.2.6 *N*-Boc-L-pyrroglutamic acid *tert*-butyl ester (20)

APPENDIX



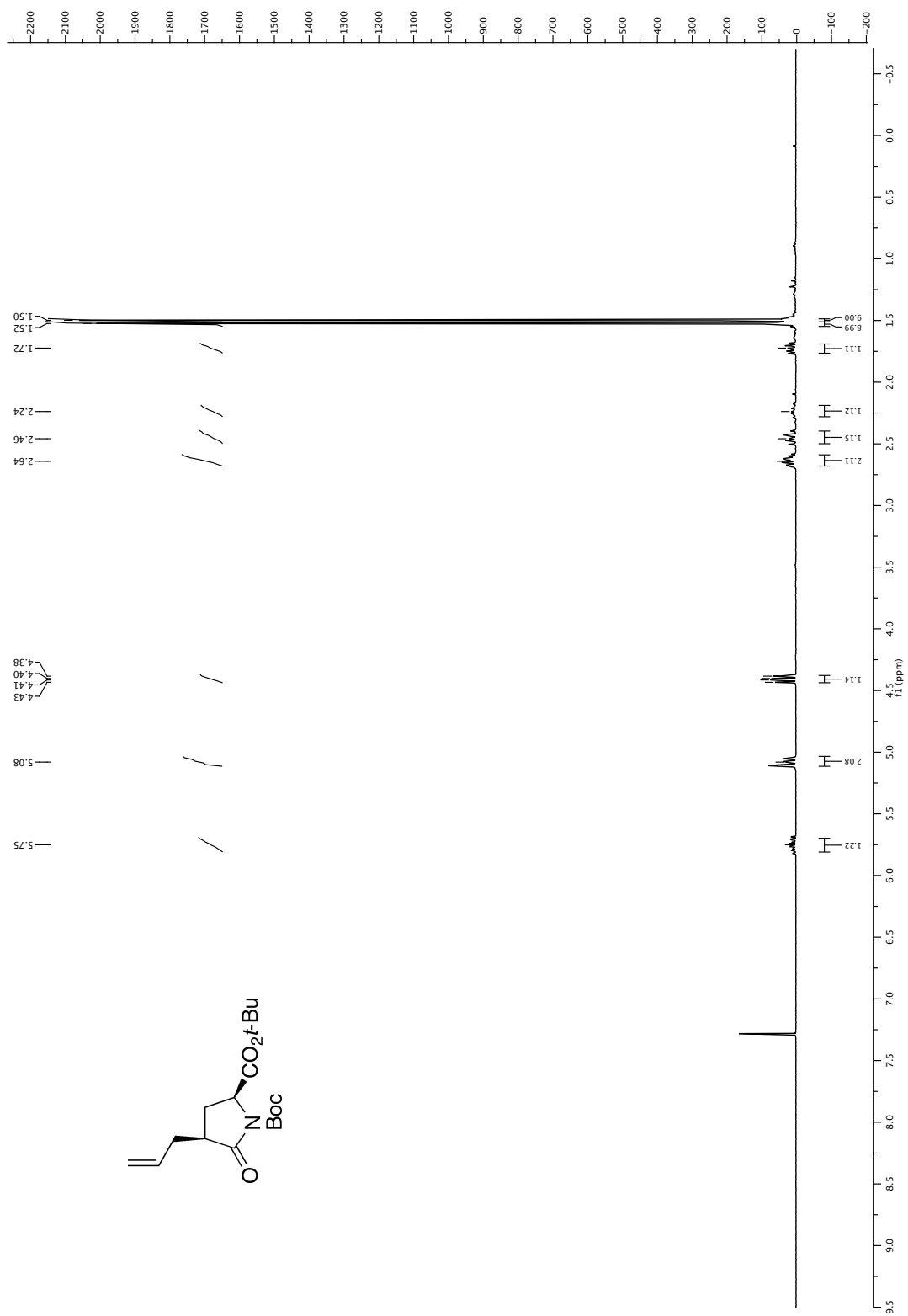
22.2.7 Allylpyroglutamate (21-*trans*)

APPENDIX

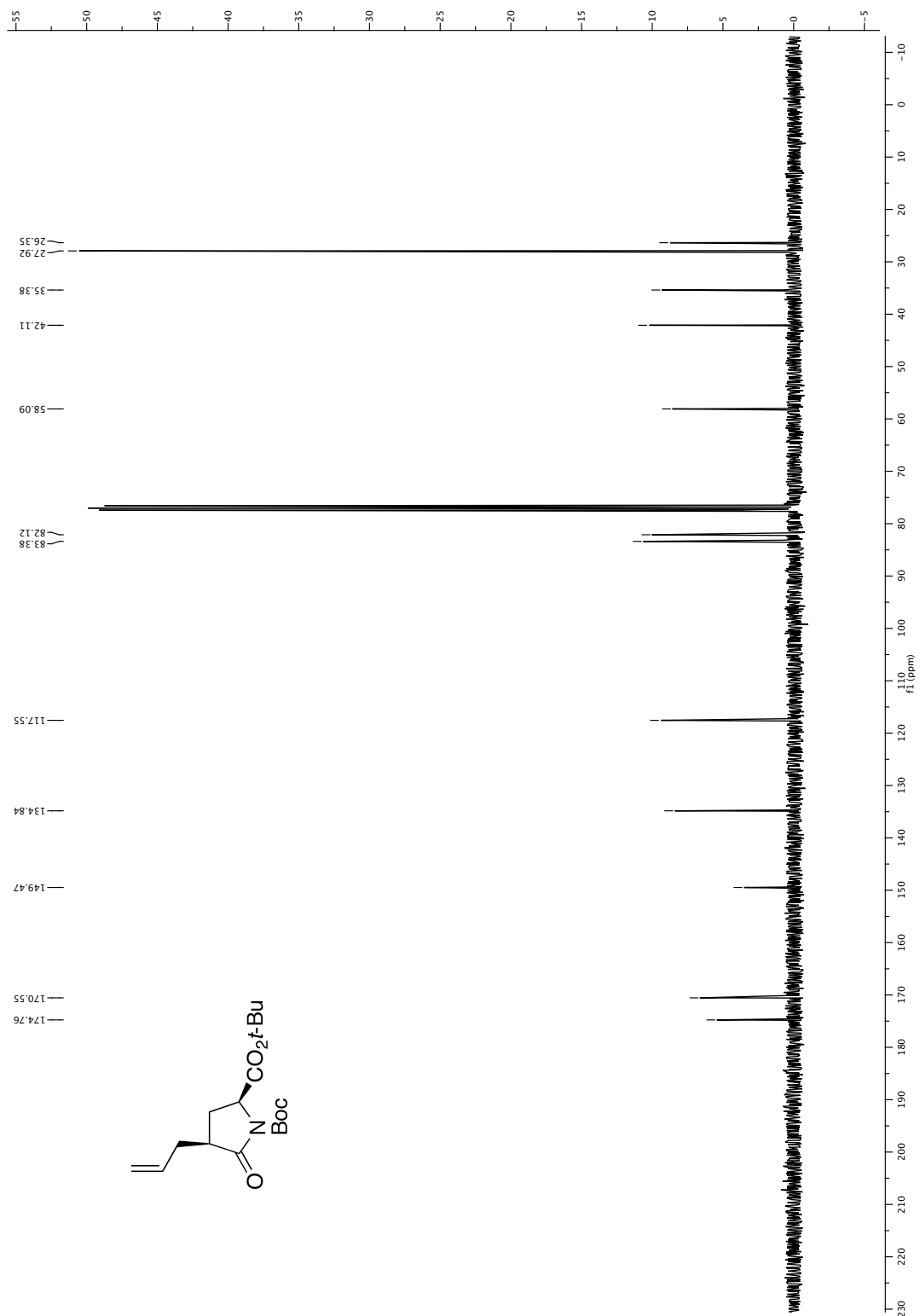


APPENDIX

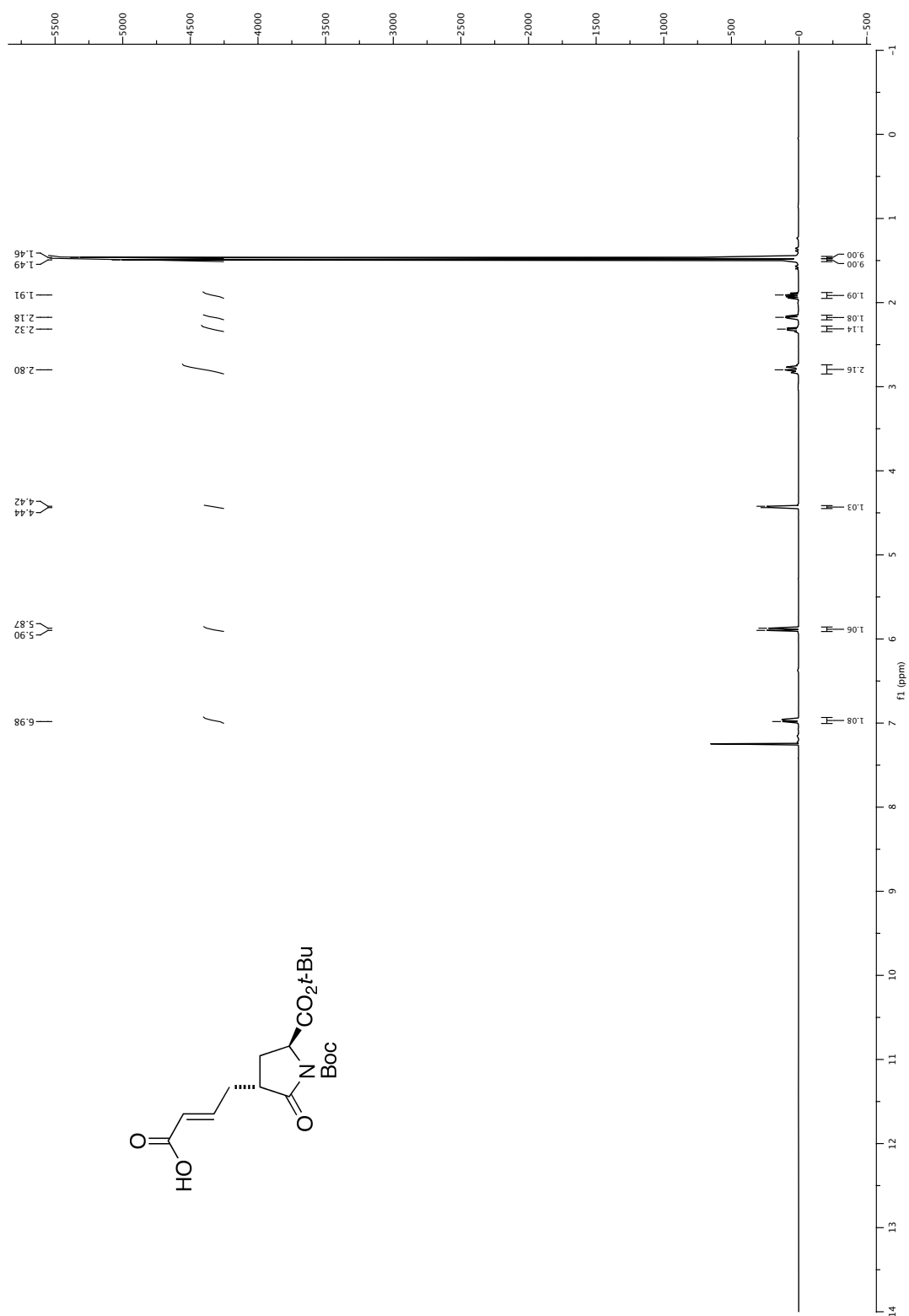
22.2.8 *Cis*-allylpyroglutamate (21-*cis*)



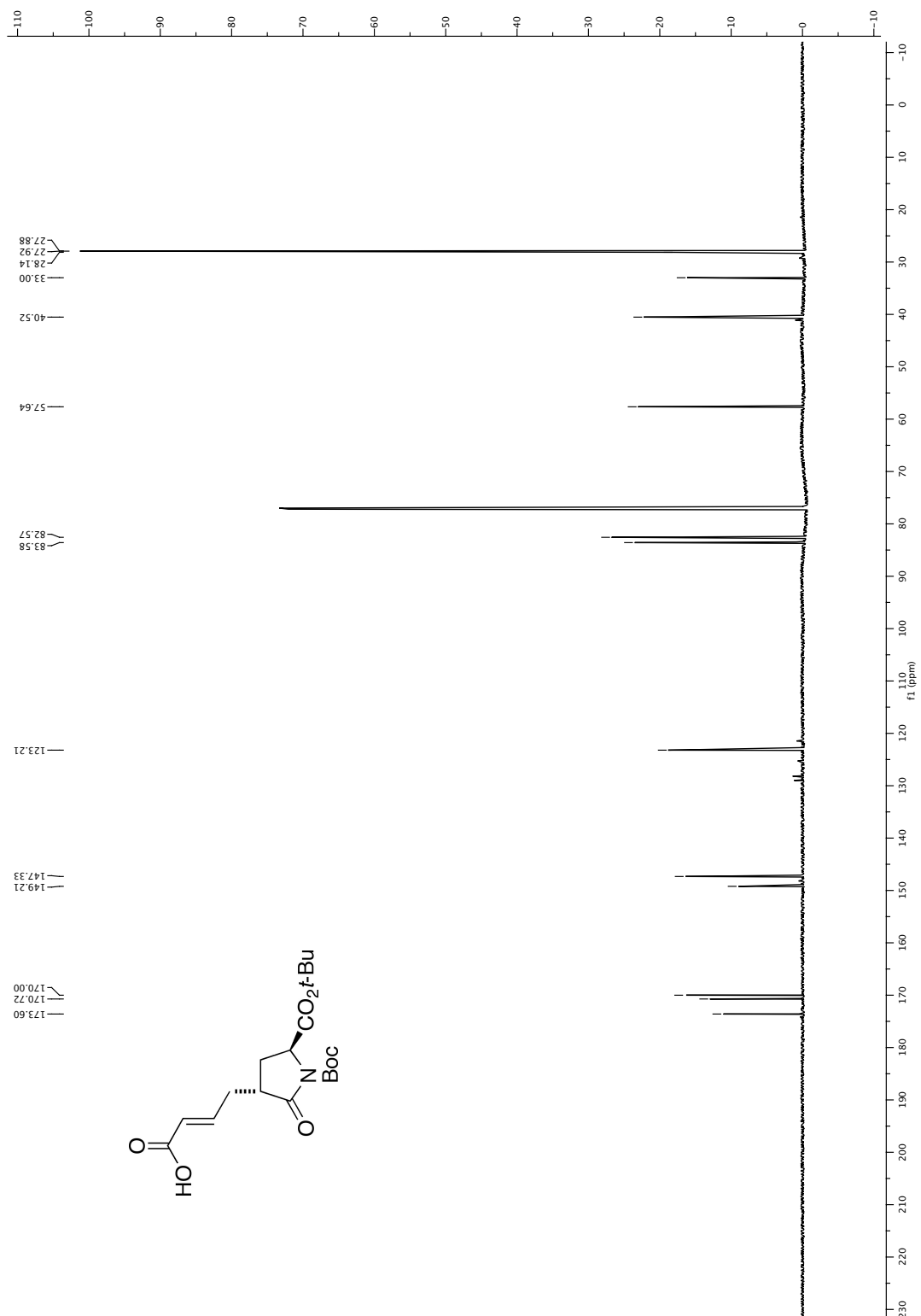
APPENDIX



22.2.9 Acrylic acid pyroglutamate (22)

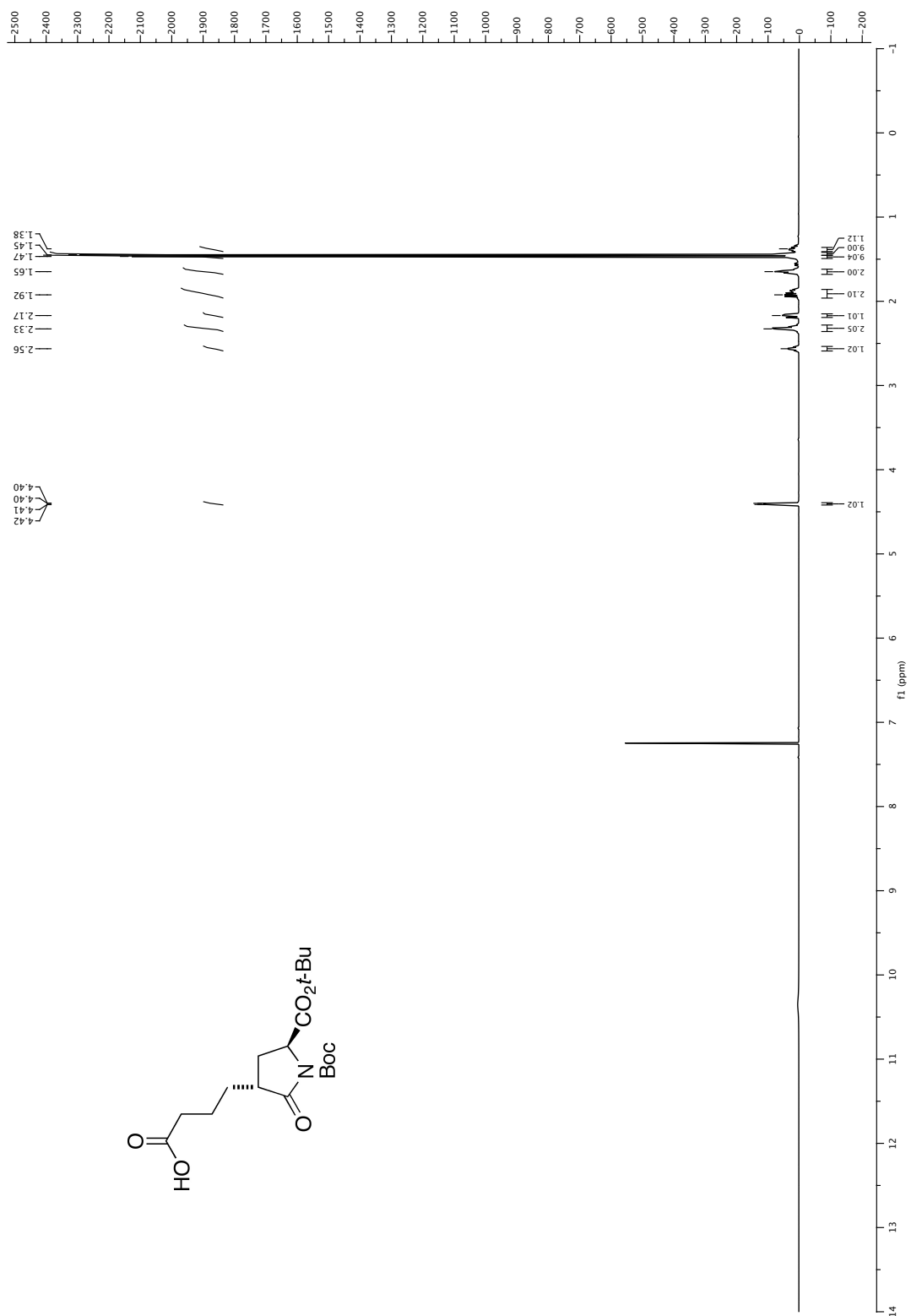


APPENDIX

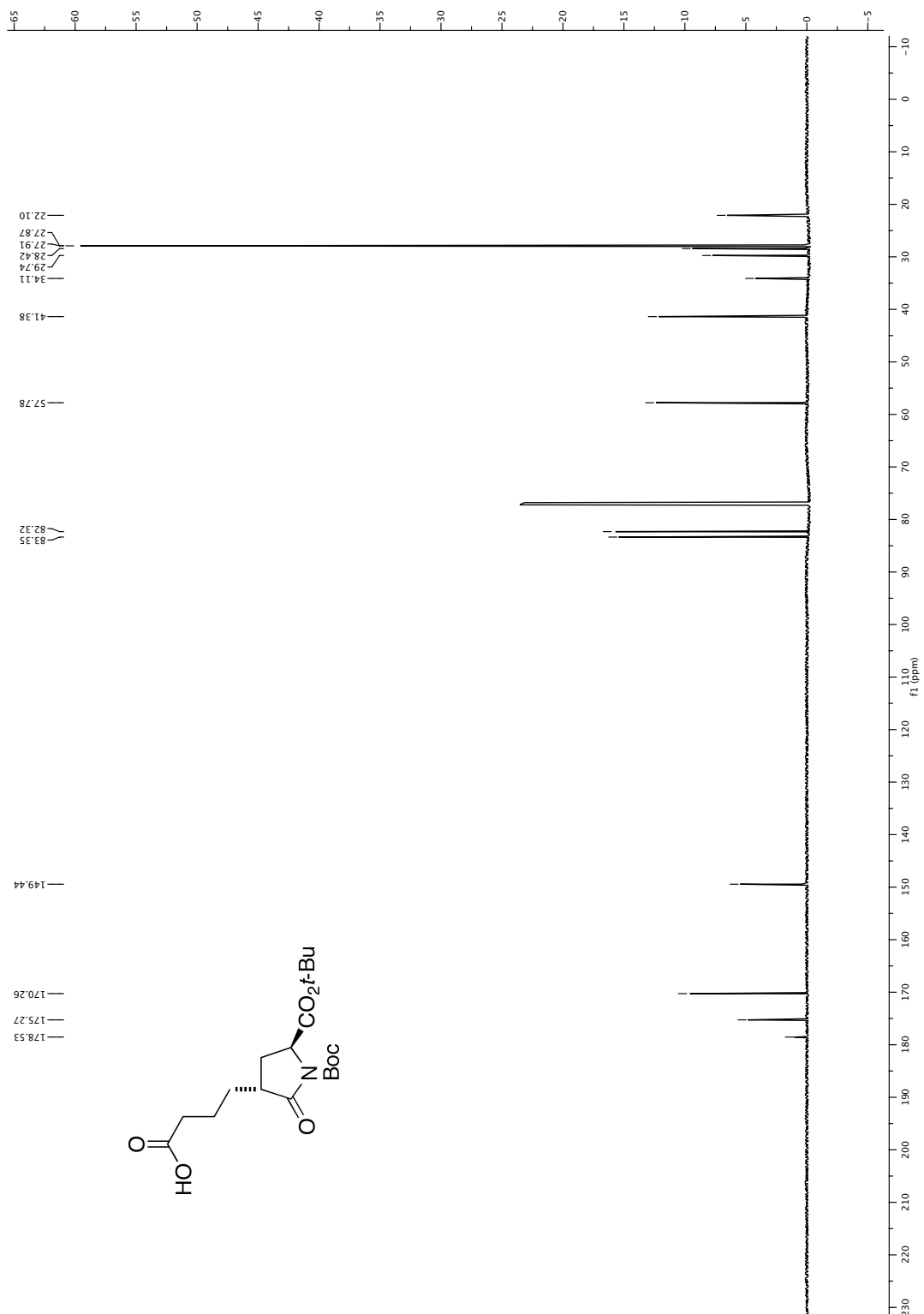


APPENDIX

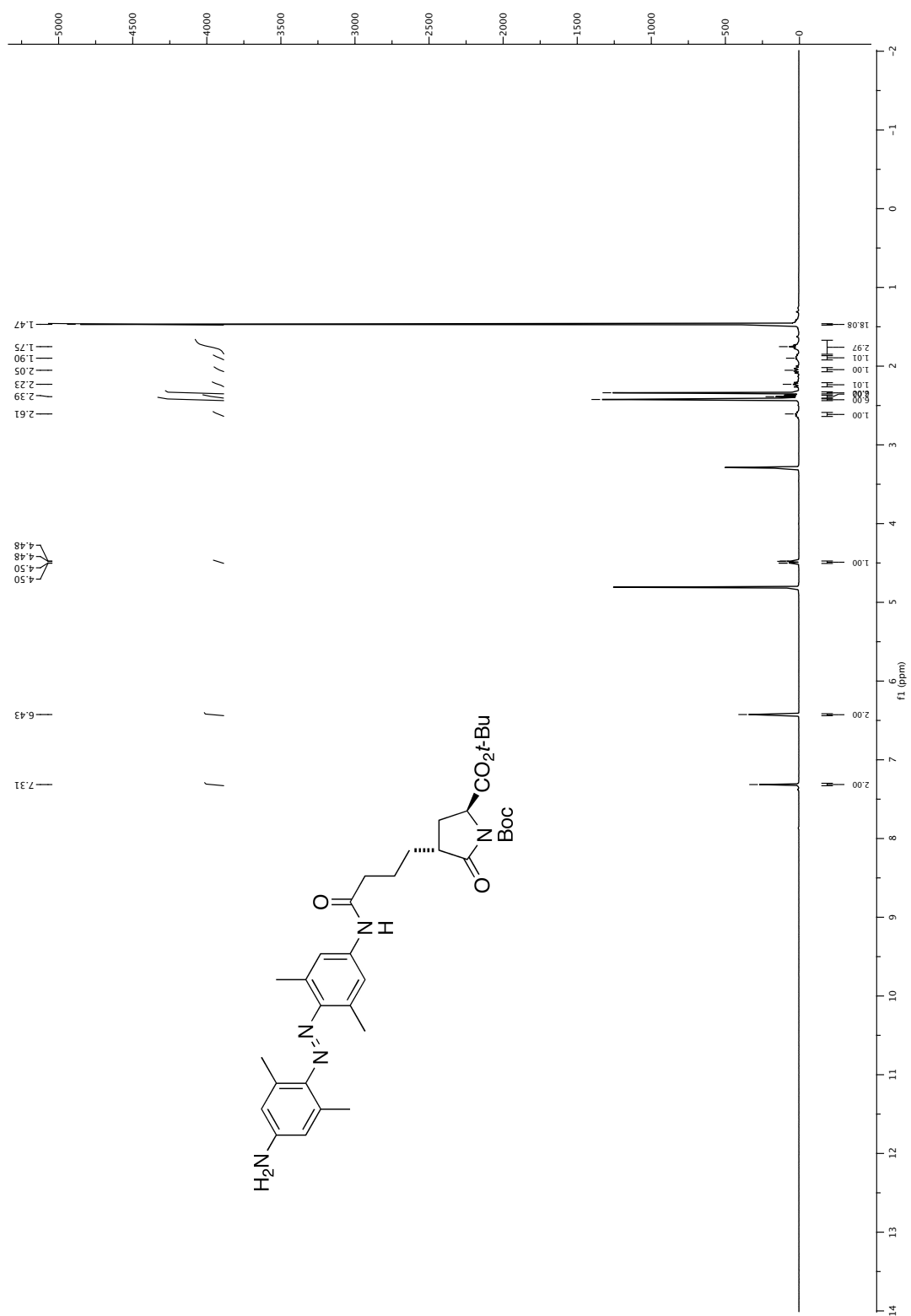
22.2.10 Carboxylic acid pyroglutamate (23)



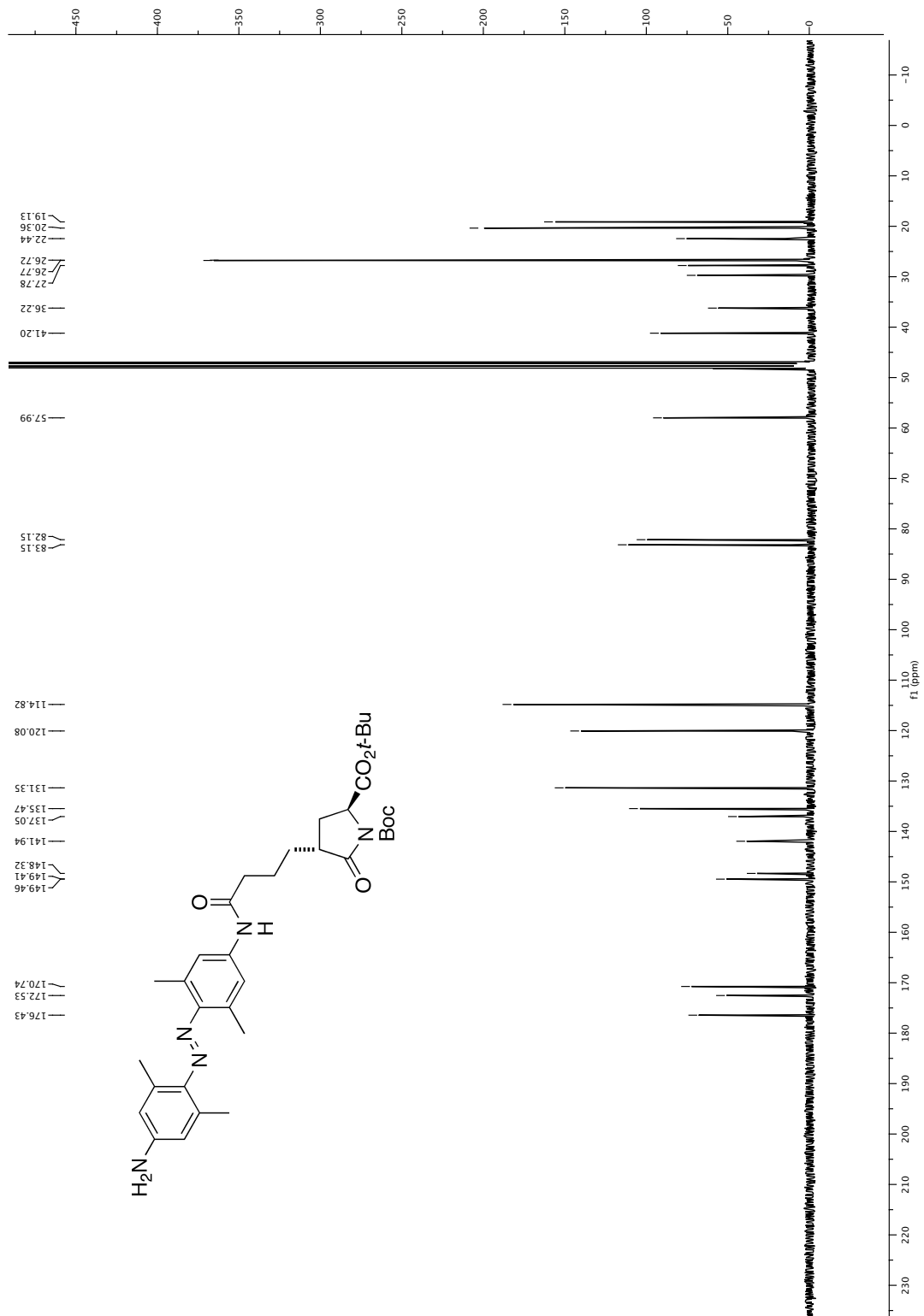
APPENDIX

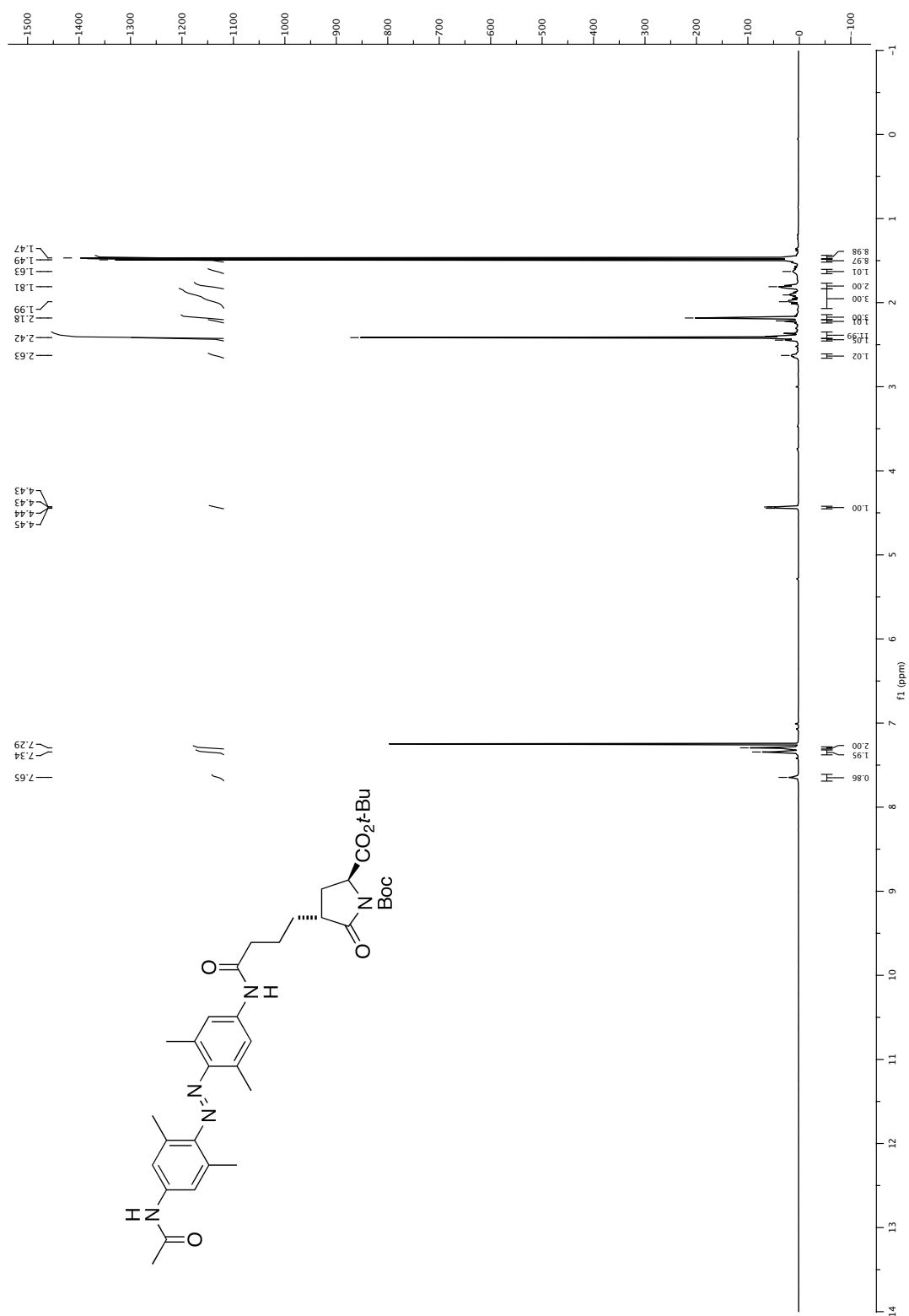


22.2.11 Aminoazobenzene pyroglutamate (30)

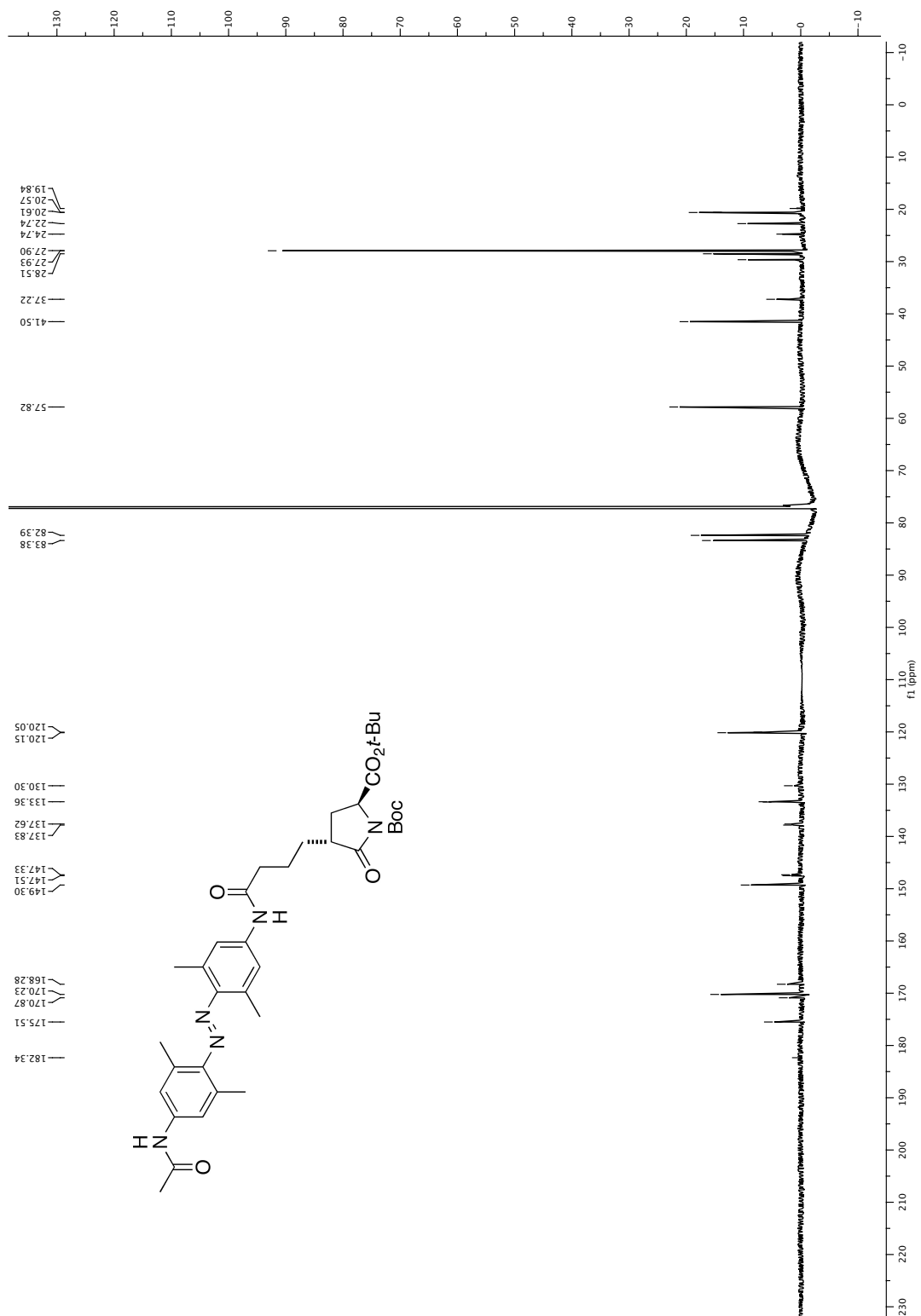


APPENDIX

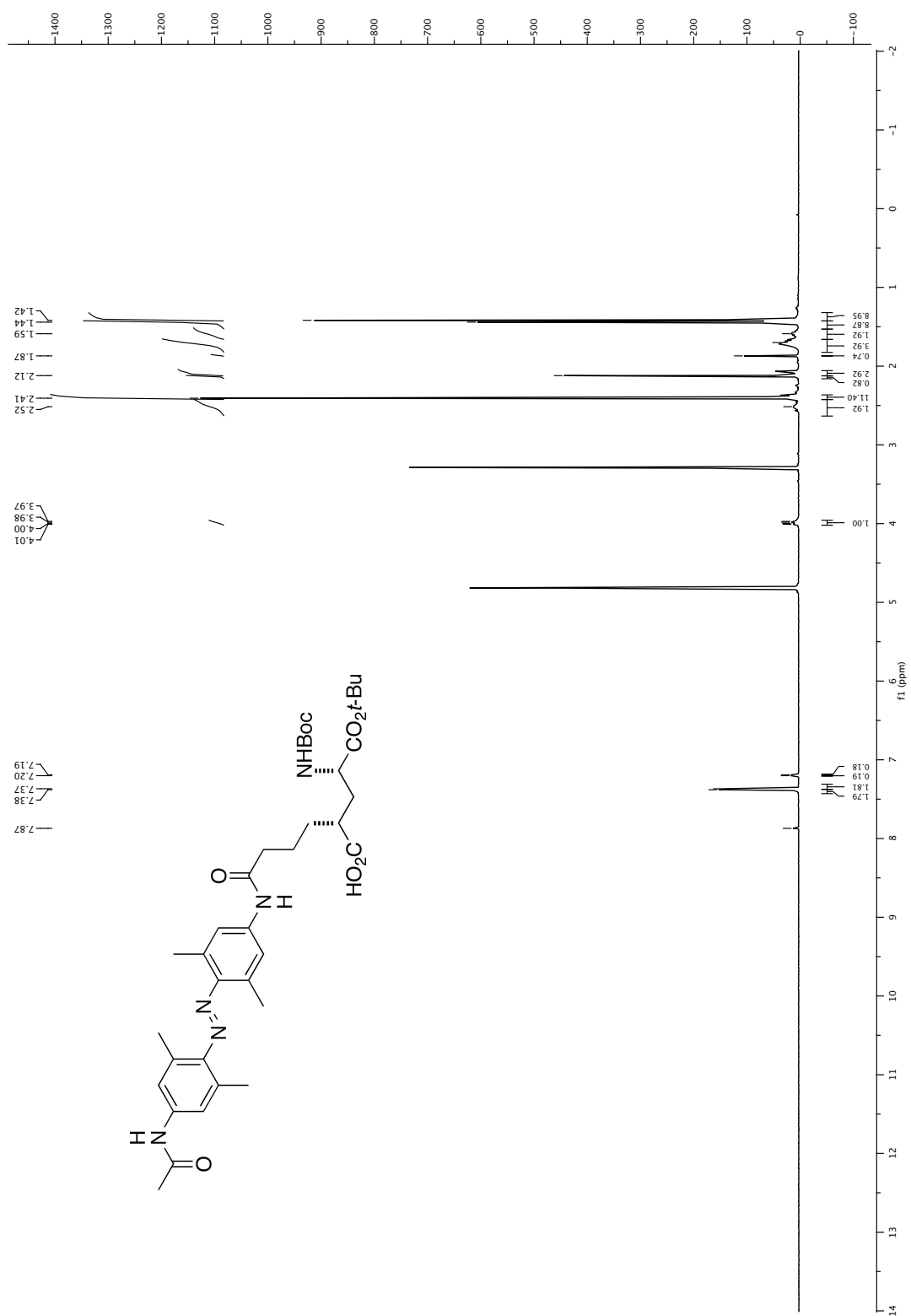


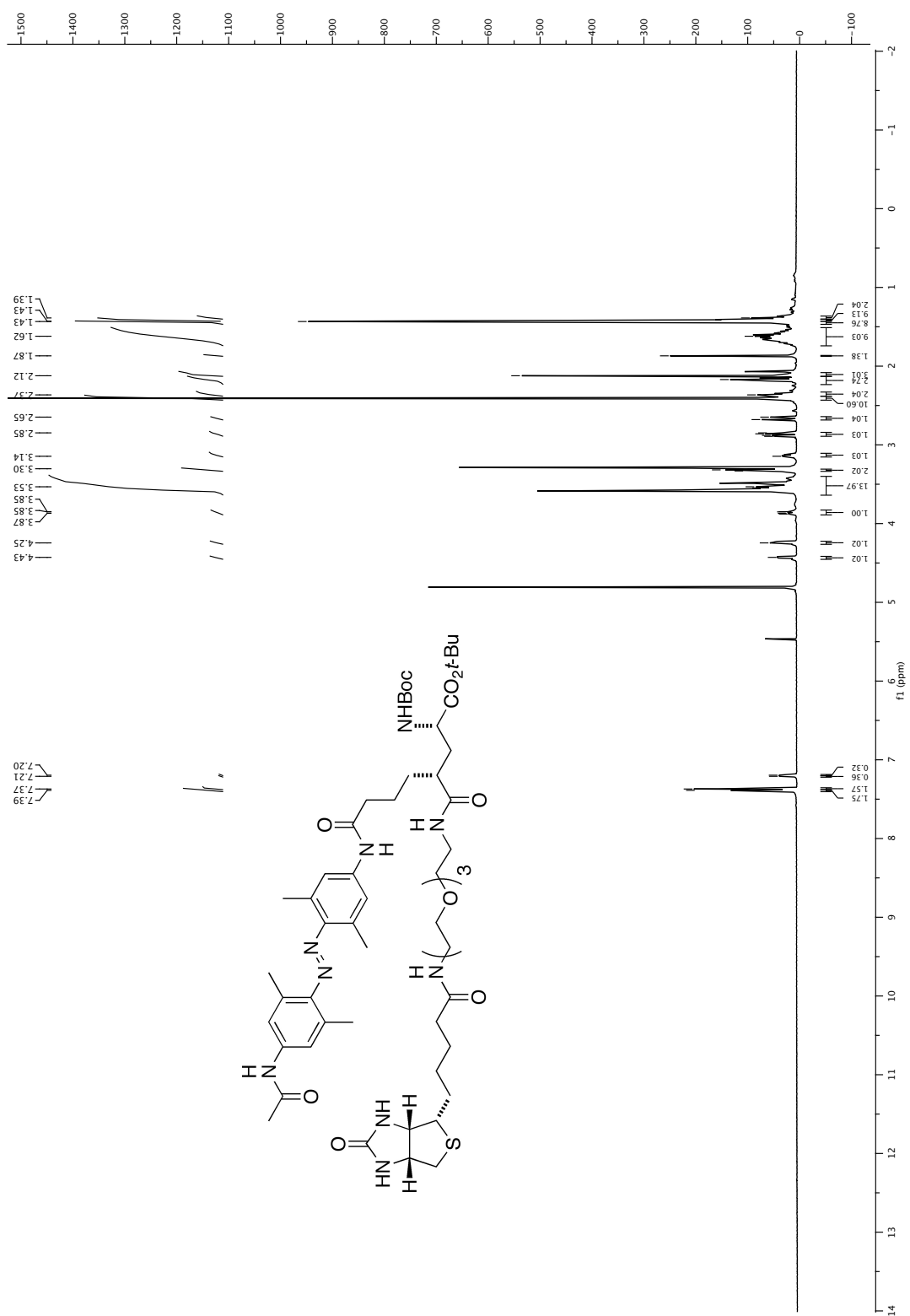
22.2.12 *N*-acyl-aminoazobenzene pyroglutamate (31)

APPENDIX

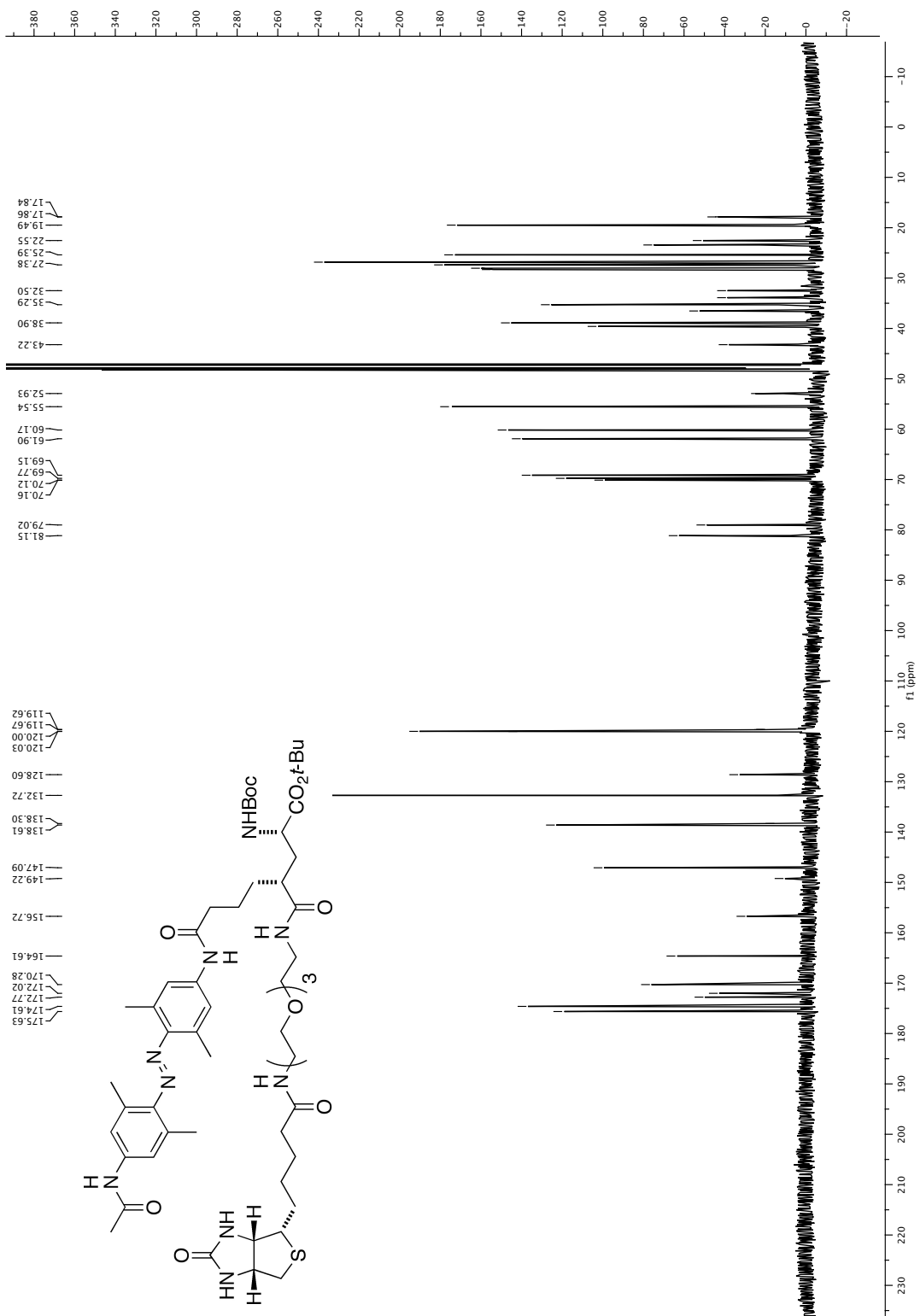


22.2.13 Azobenzene glutamic acid ester (32)



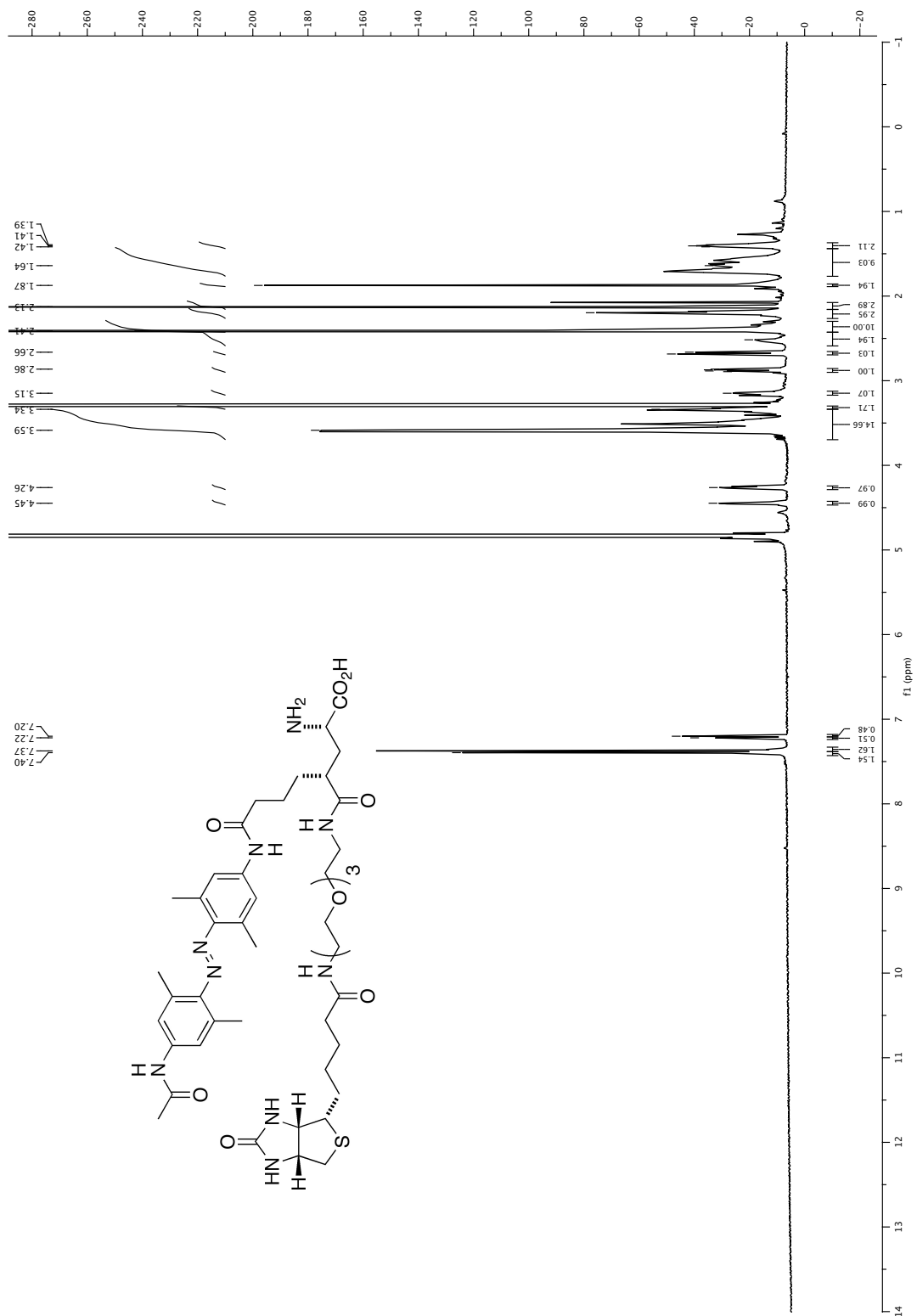
22.2.14 Biotin azobenzene glutamic acid ester γ -amide (34)

APPENDIX

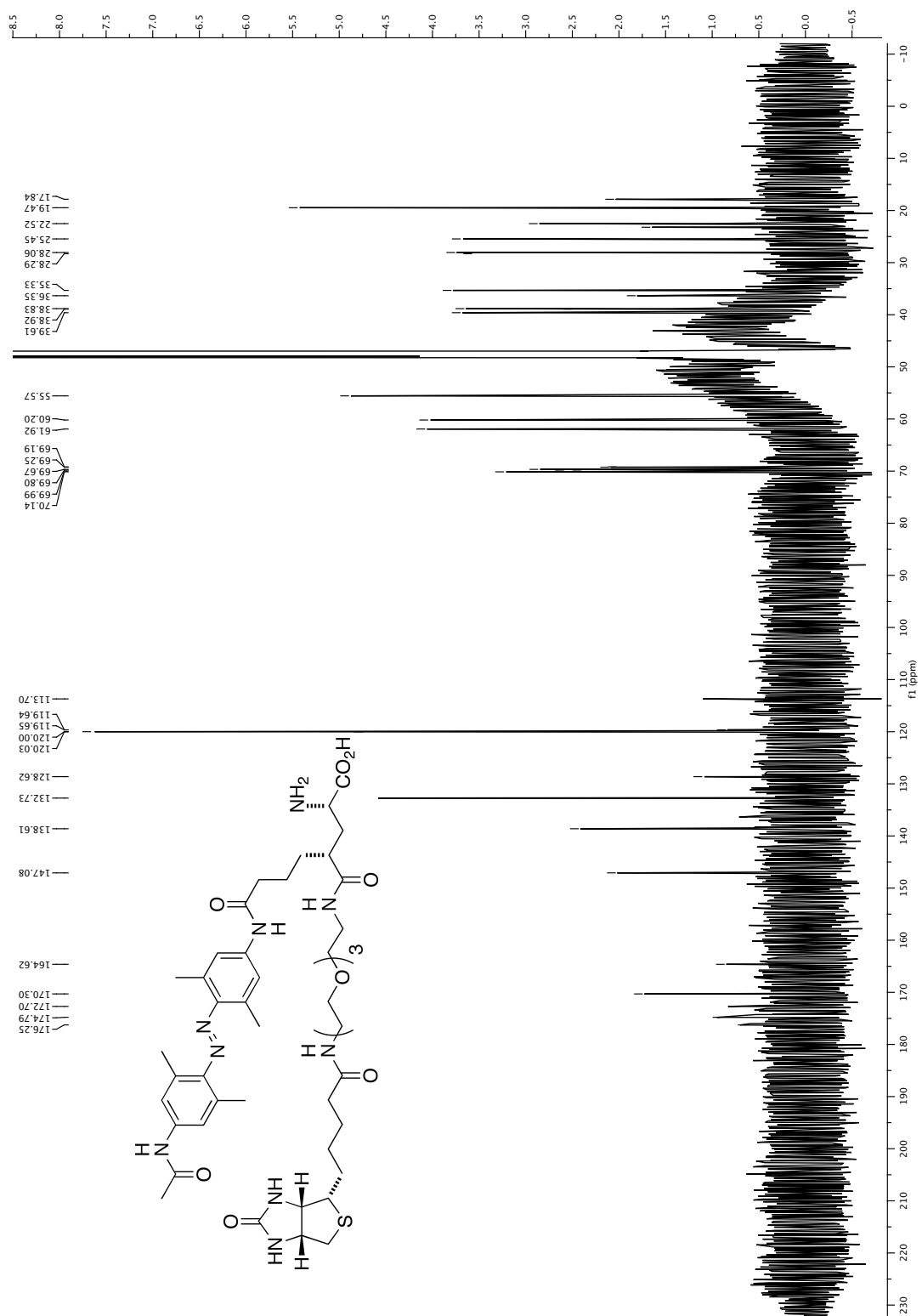


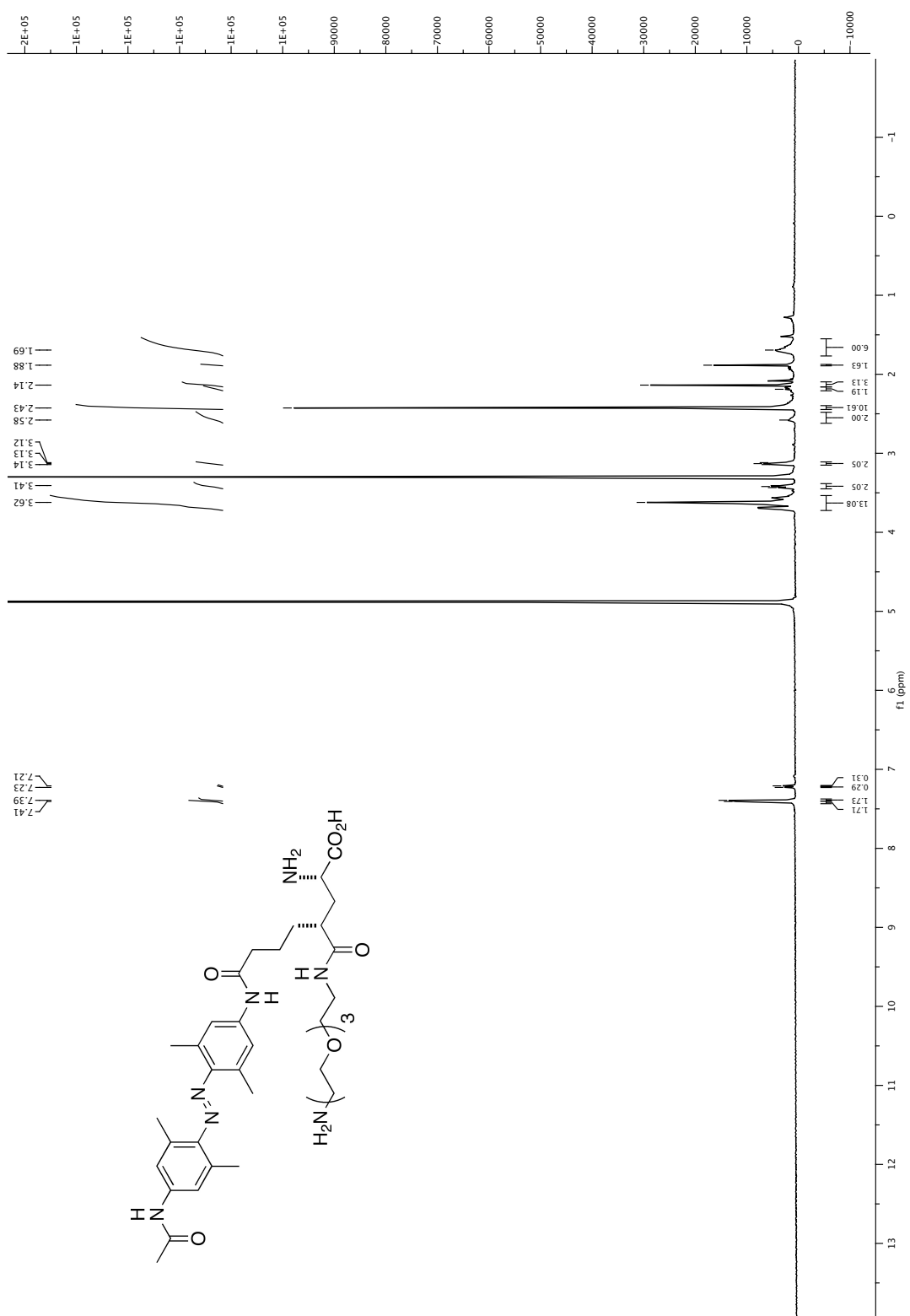
APPENDIX

22.2.15 BAG (3)



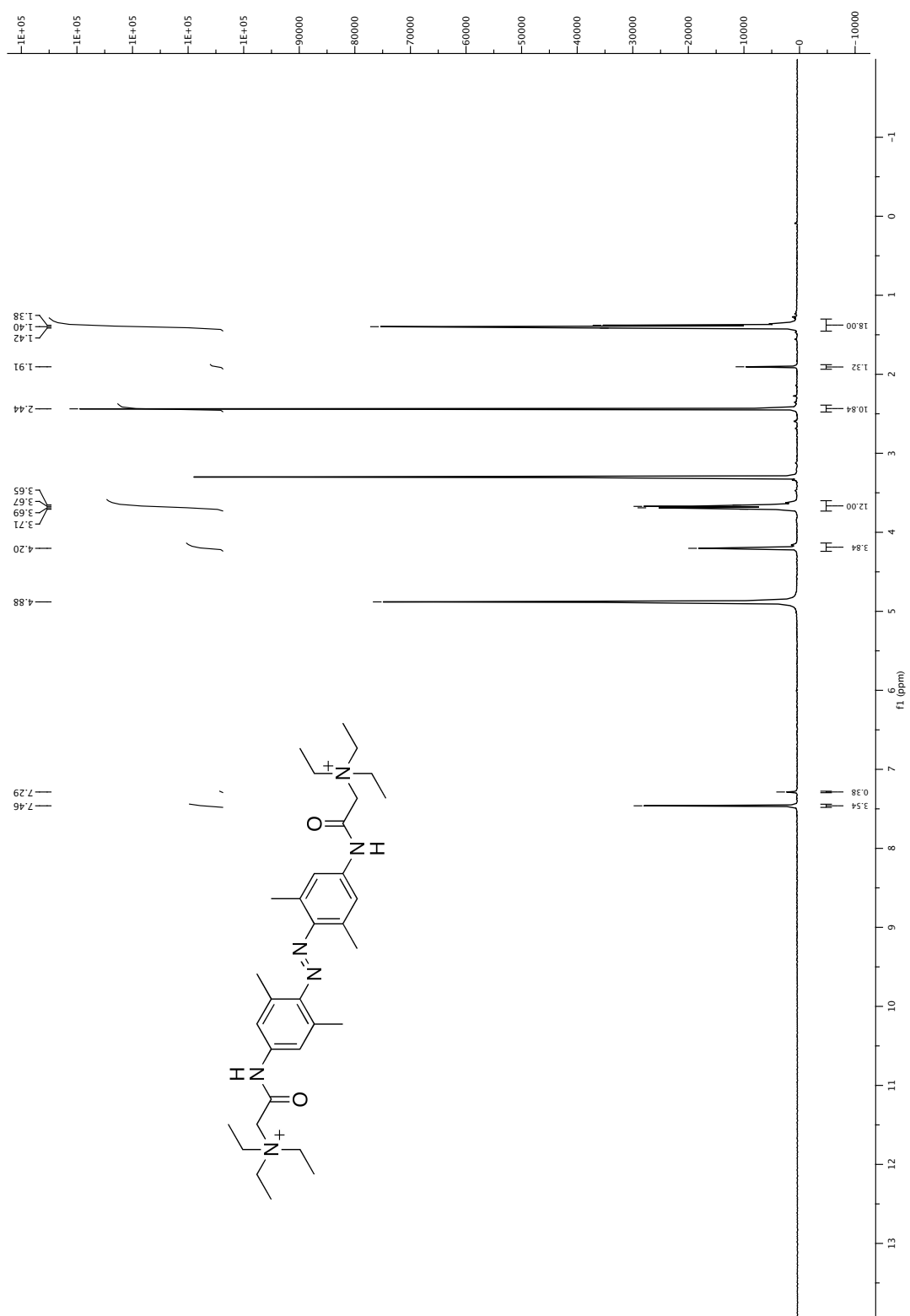
APPENDIX



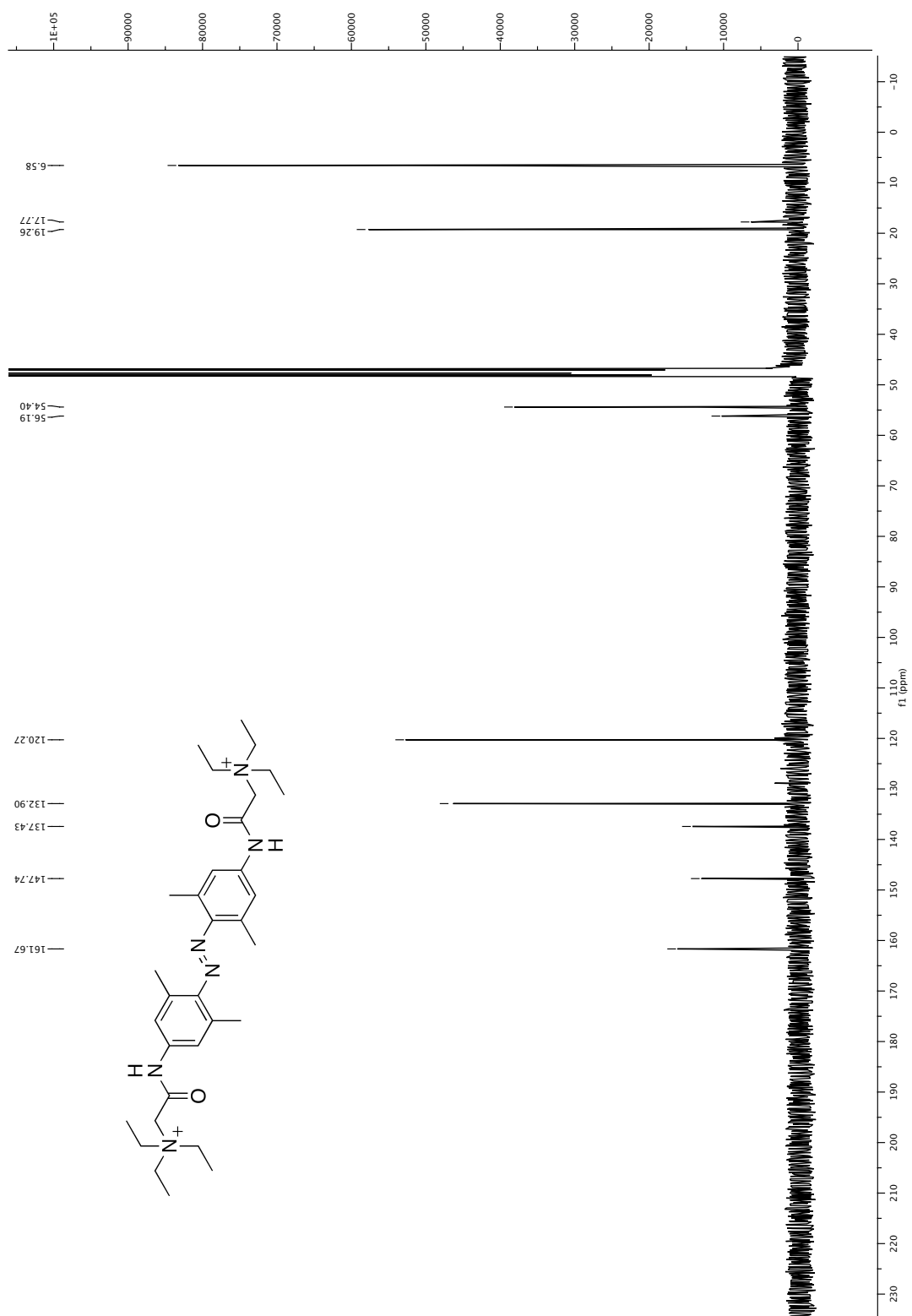
22.2.16 Azobenzene glutamic acid γ -amide (35)

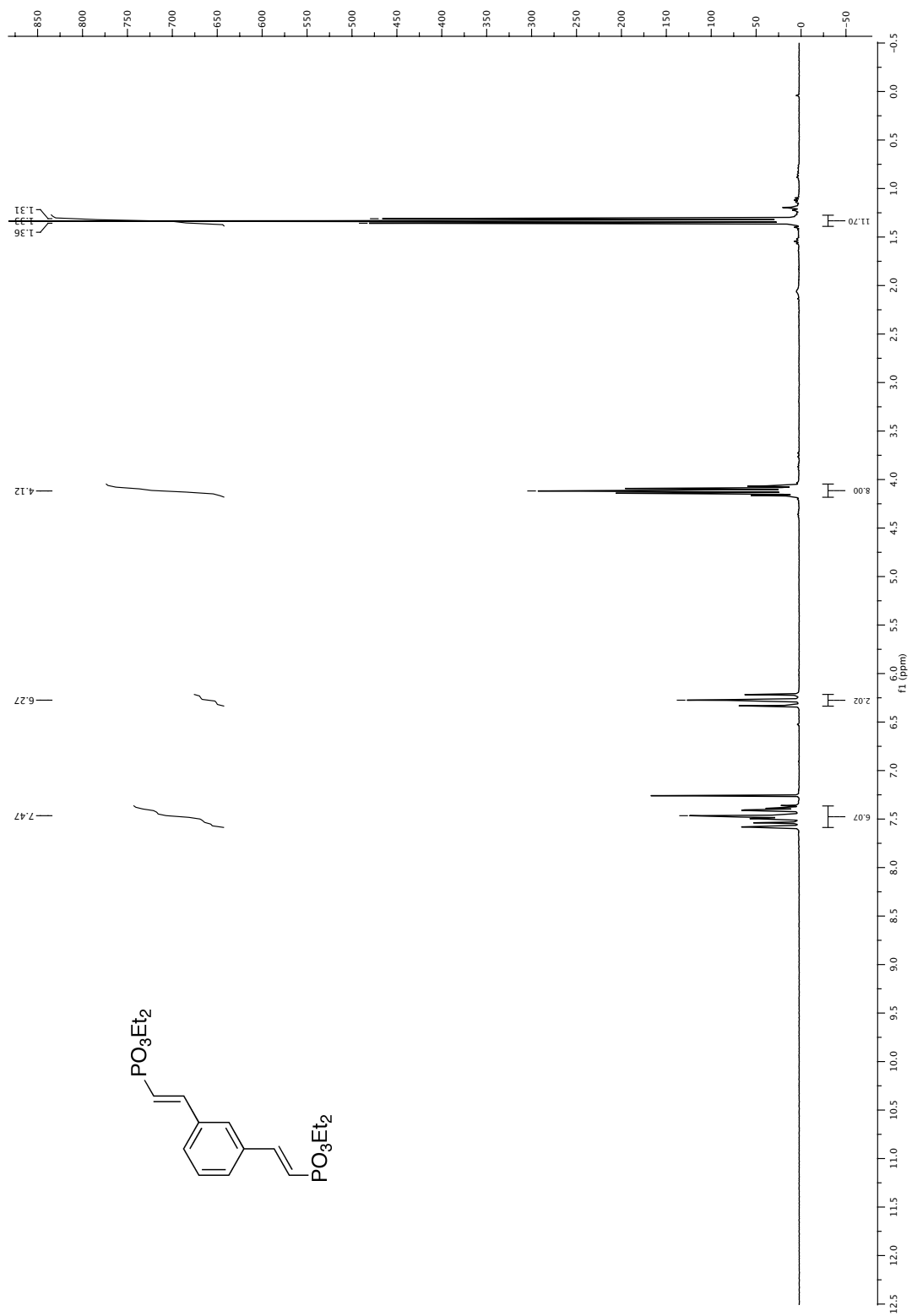
APPENDIX

22.3 Spectra of 2,2',6,6'-tetramethyl-QAQ (6)

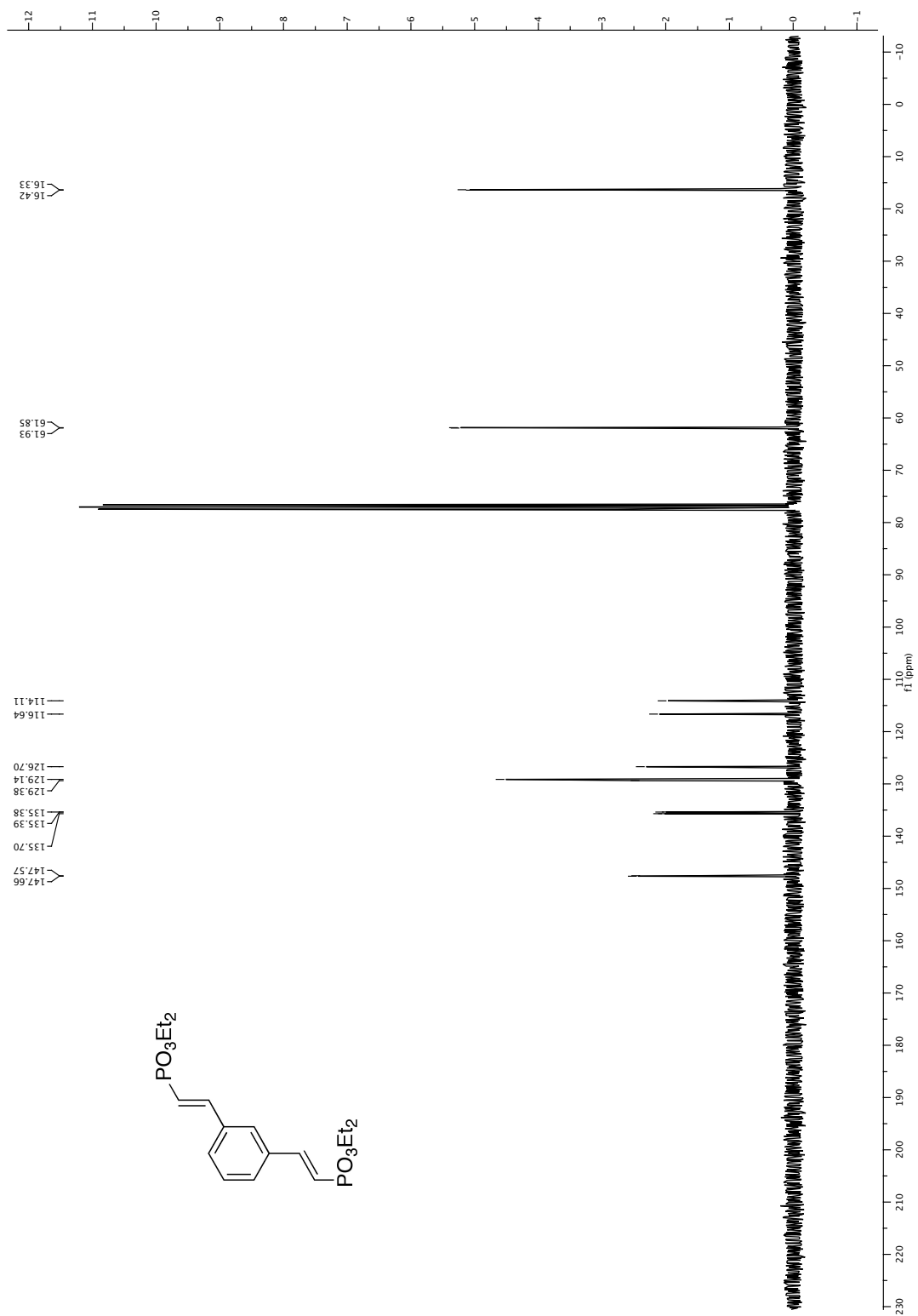


APPENDIX

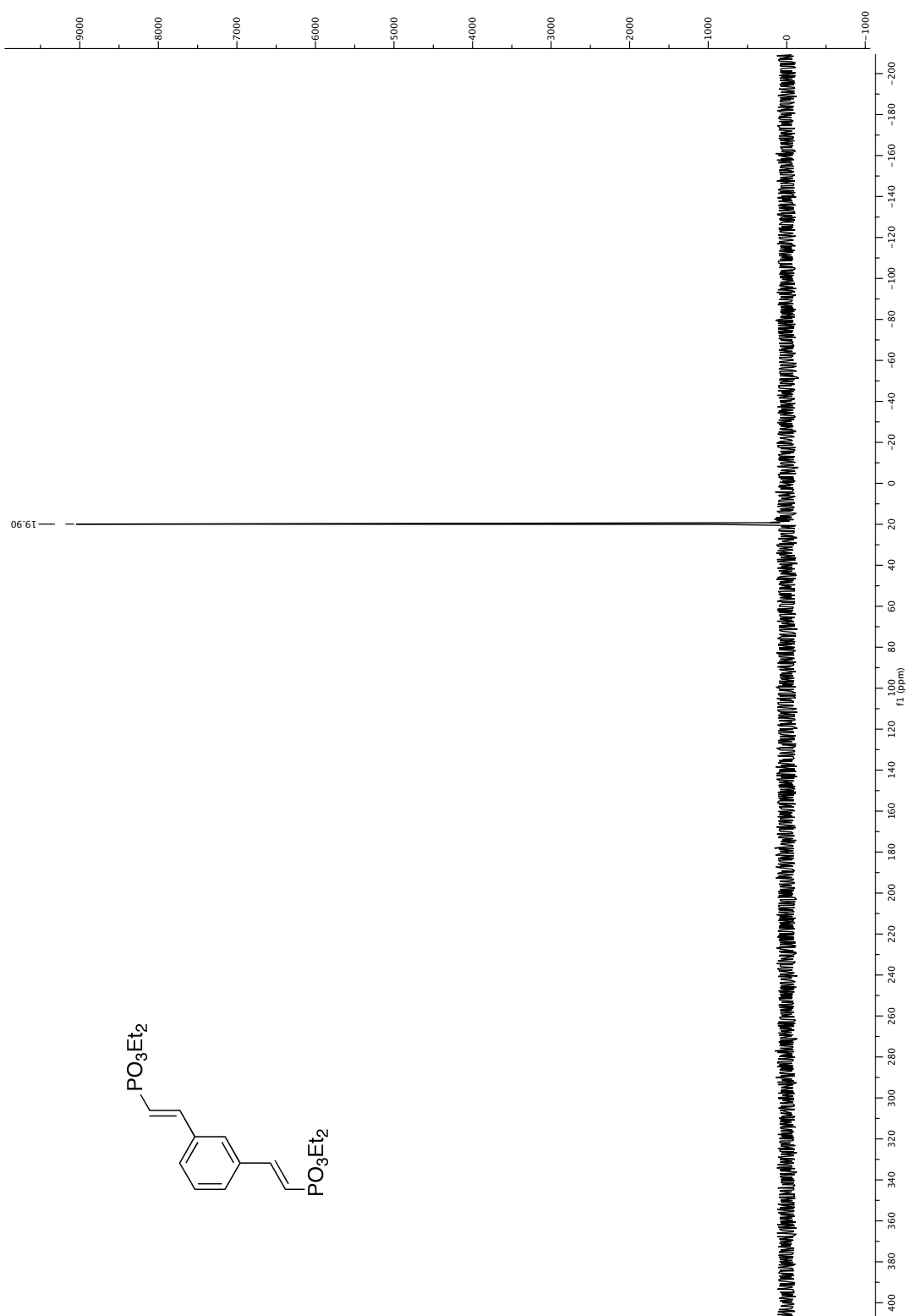


22.4 Spectra of MOBIPHOS, MOBIPHOSen and intermediates**22.4.1 Bisphosphonate (40)**

APPENDIX

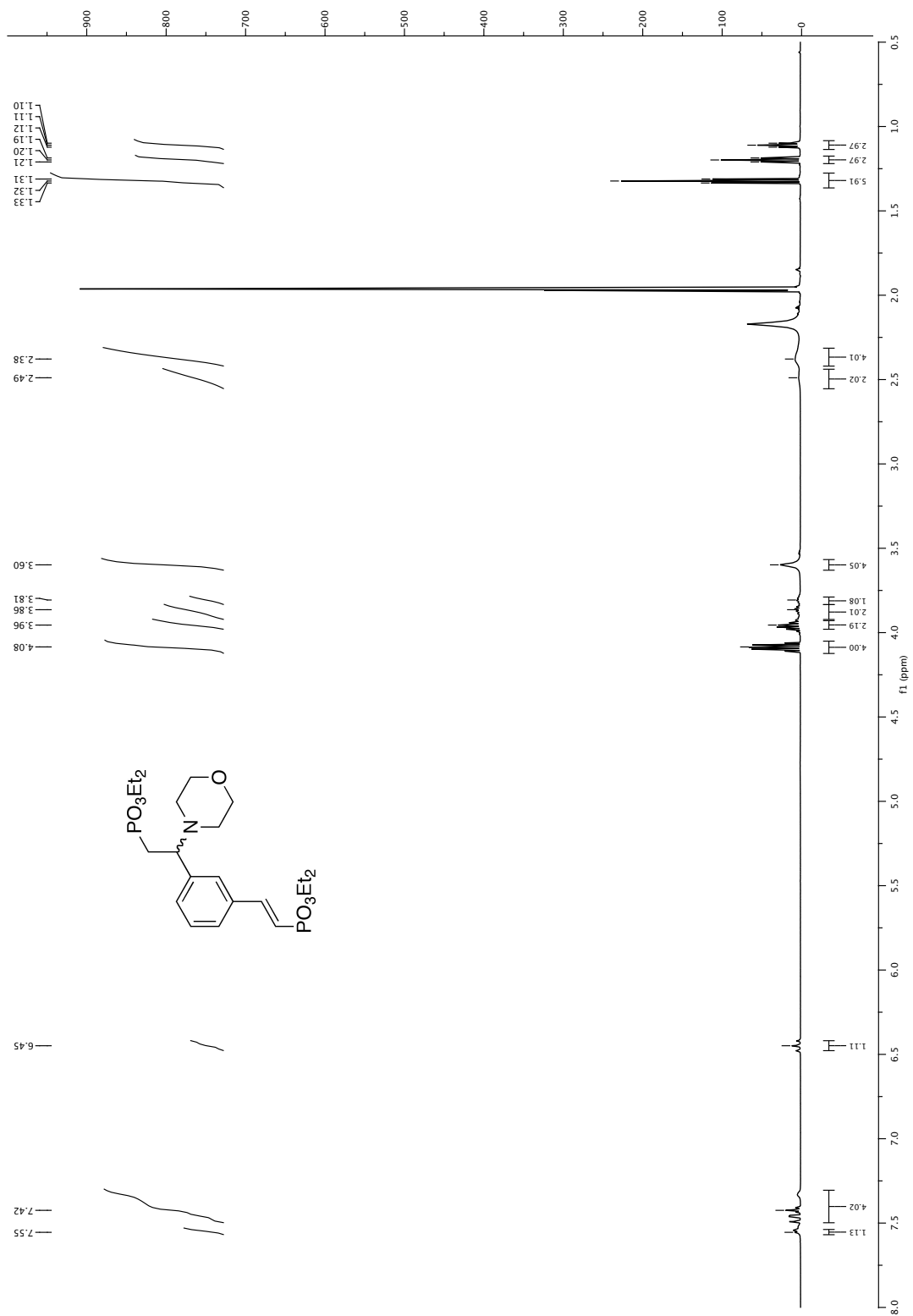


APPENDIX

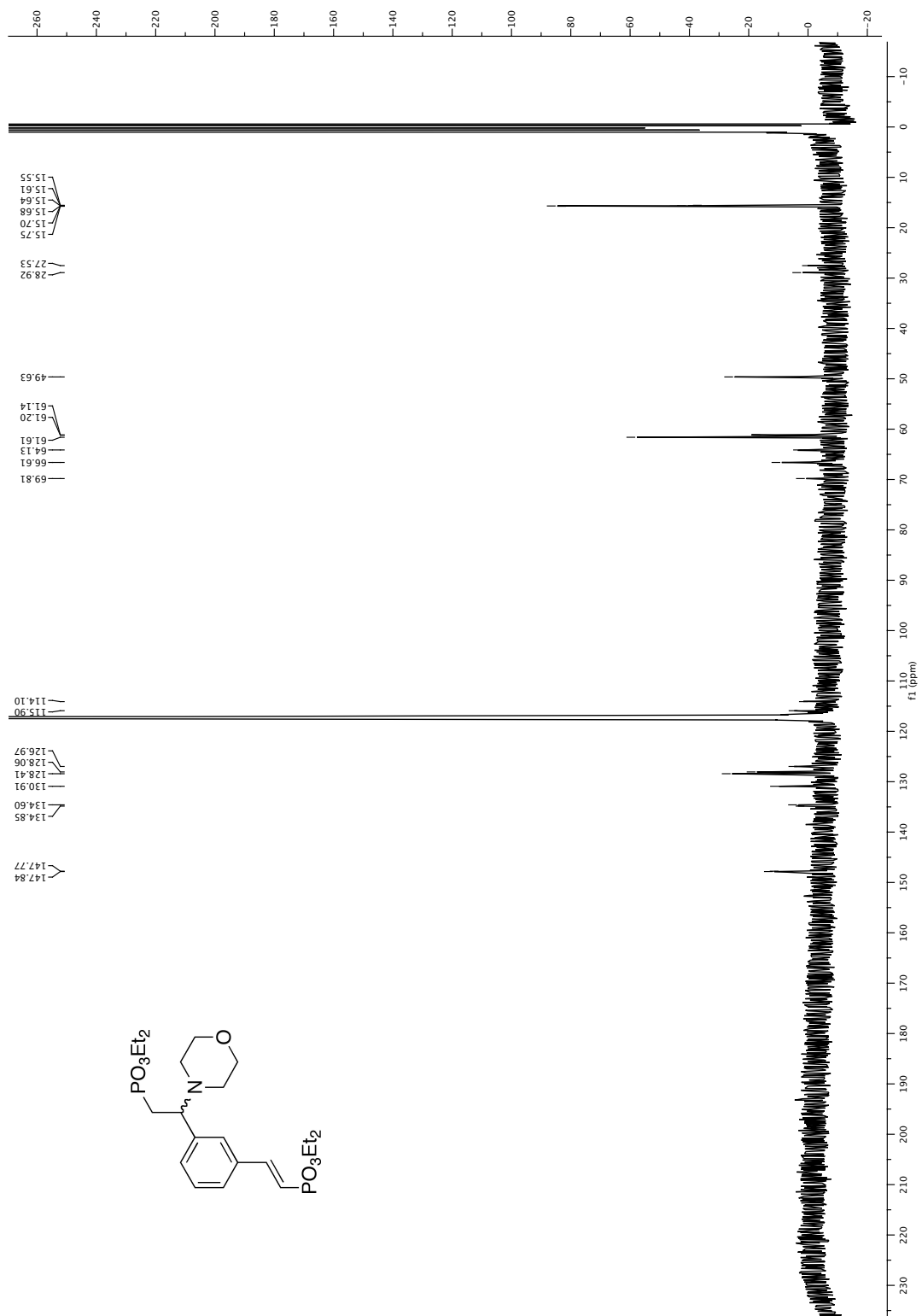


APPENDIX

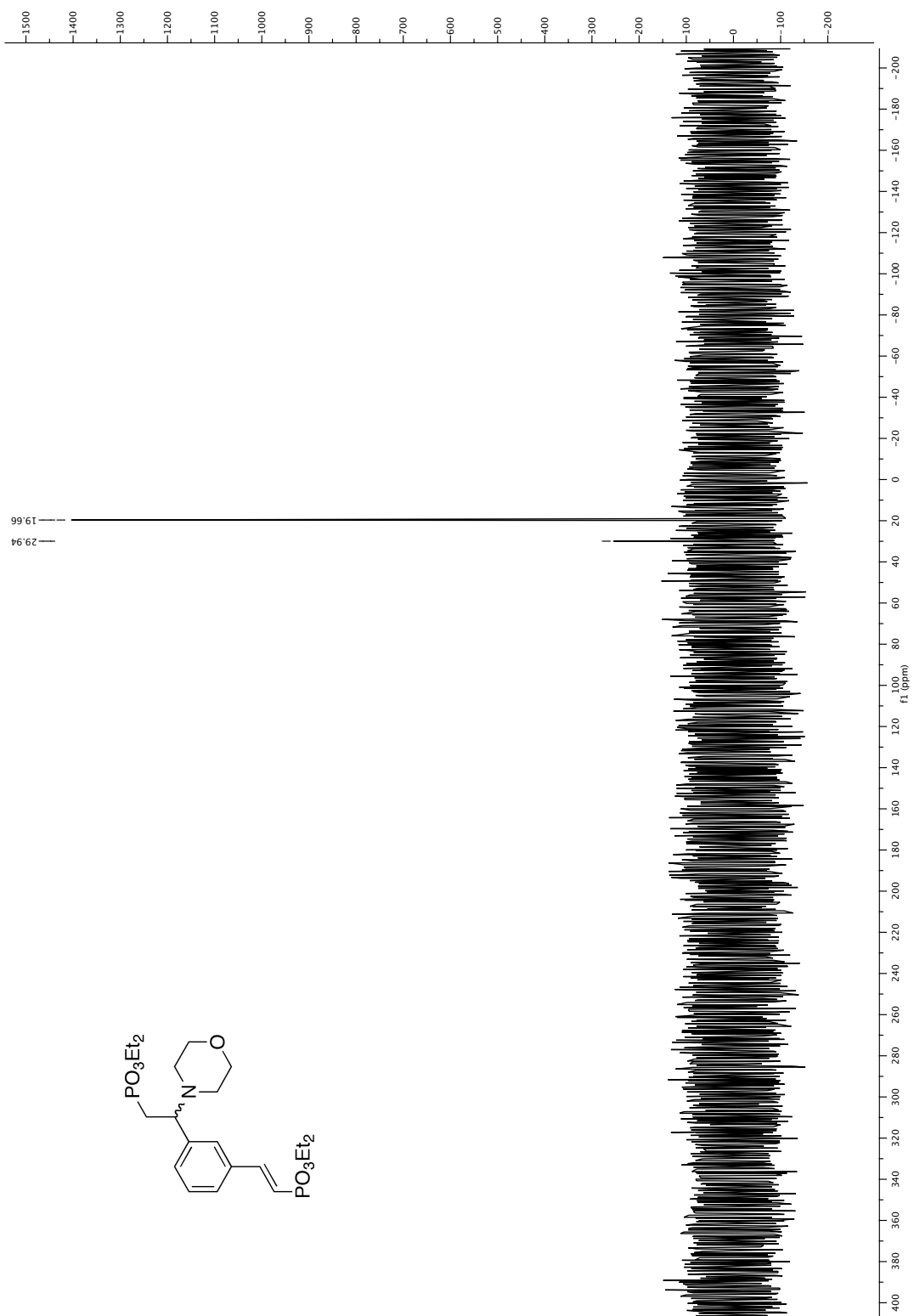
22.4.2 Morpholino bisphosphonate (41)



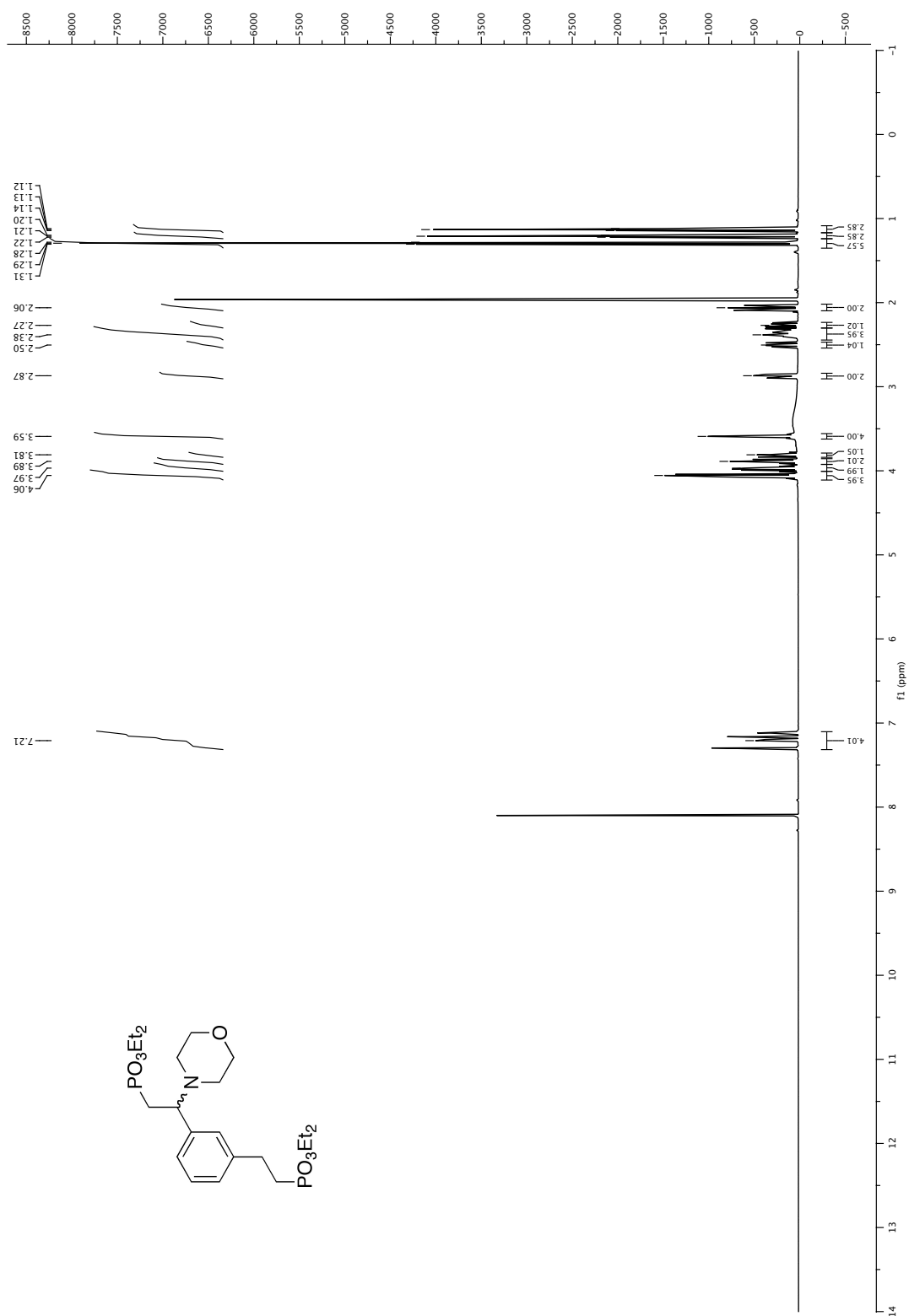
APPENDIX



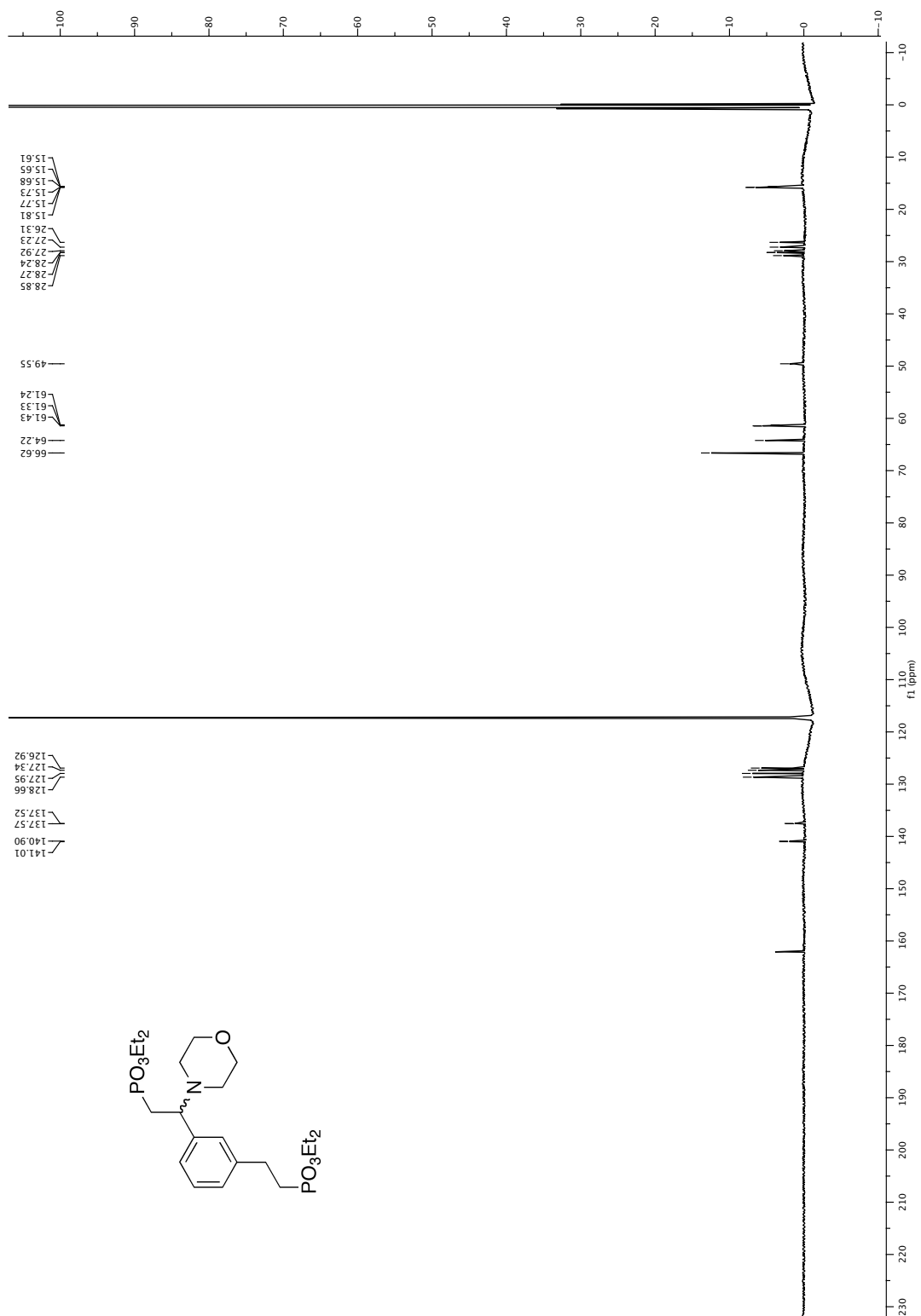
APPENDIX



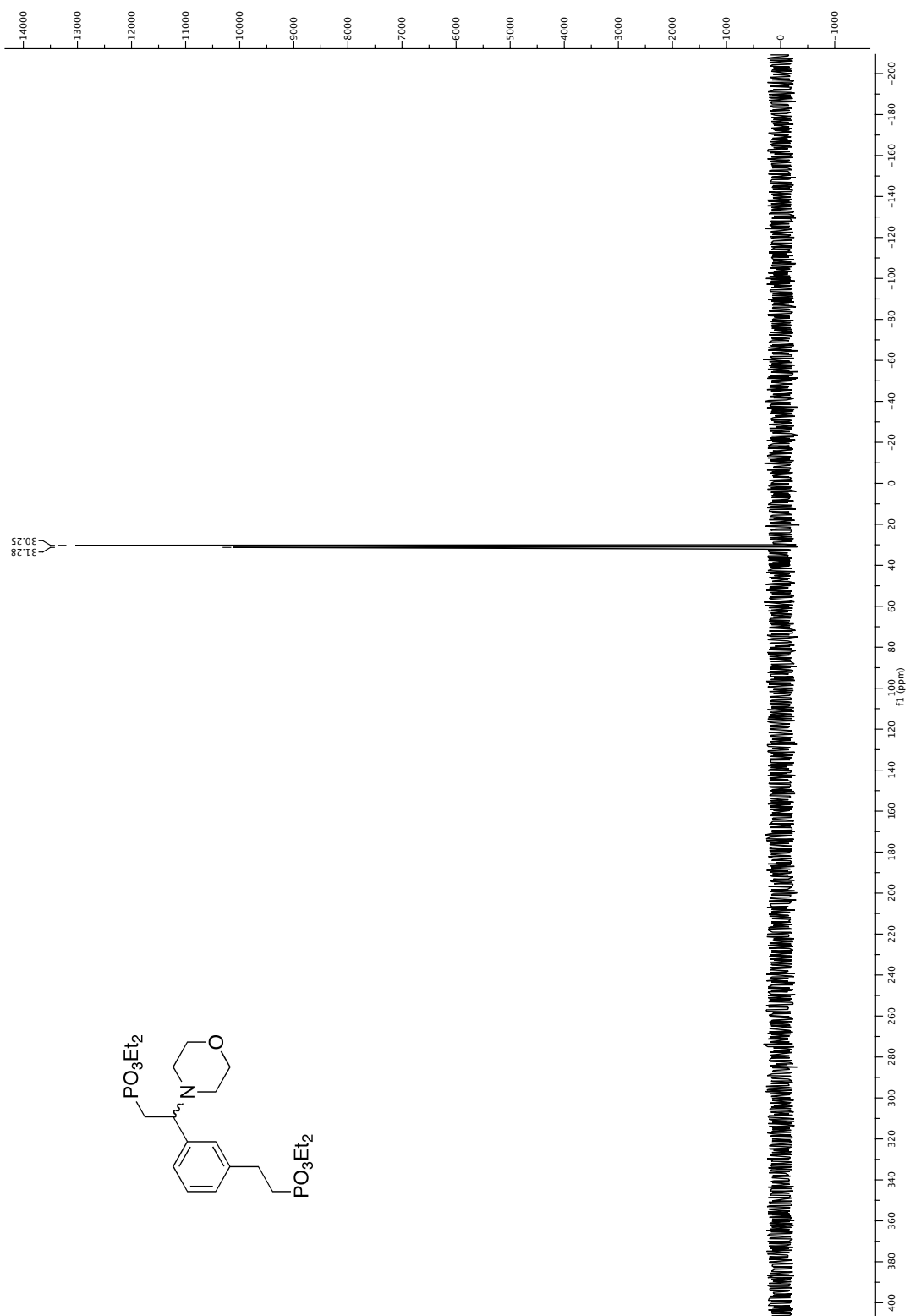
22.4.3 Morpholino dihydrobisphosphonate (42)



APPENDIX

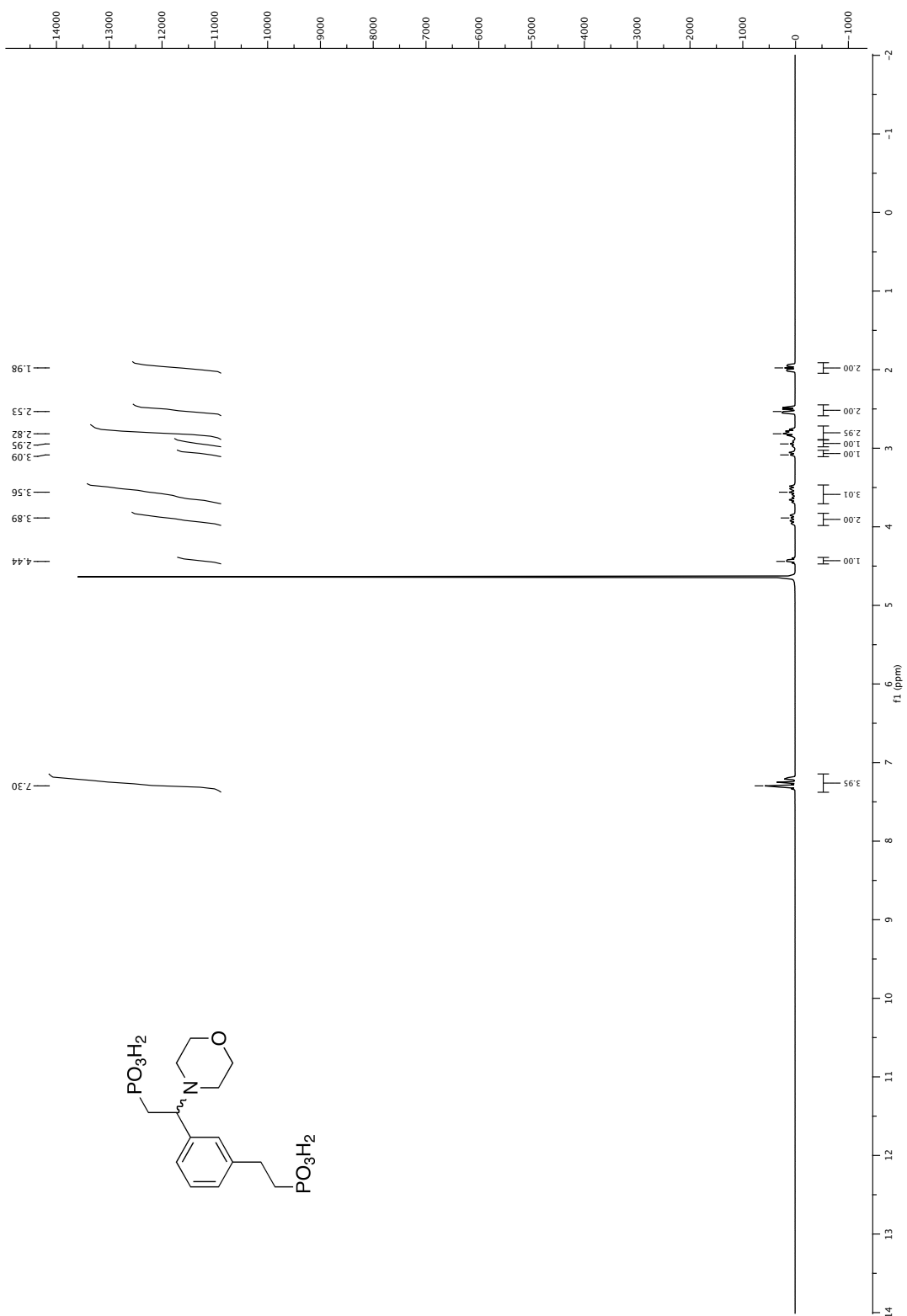


APPENDIX

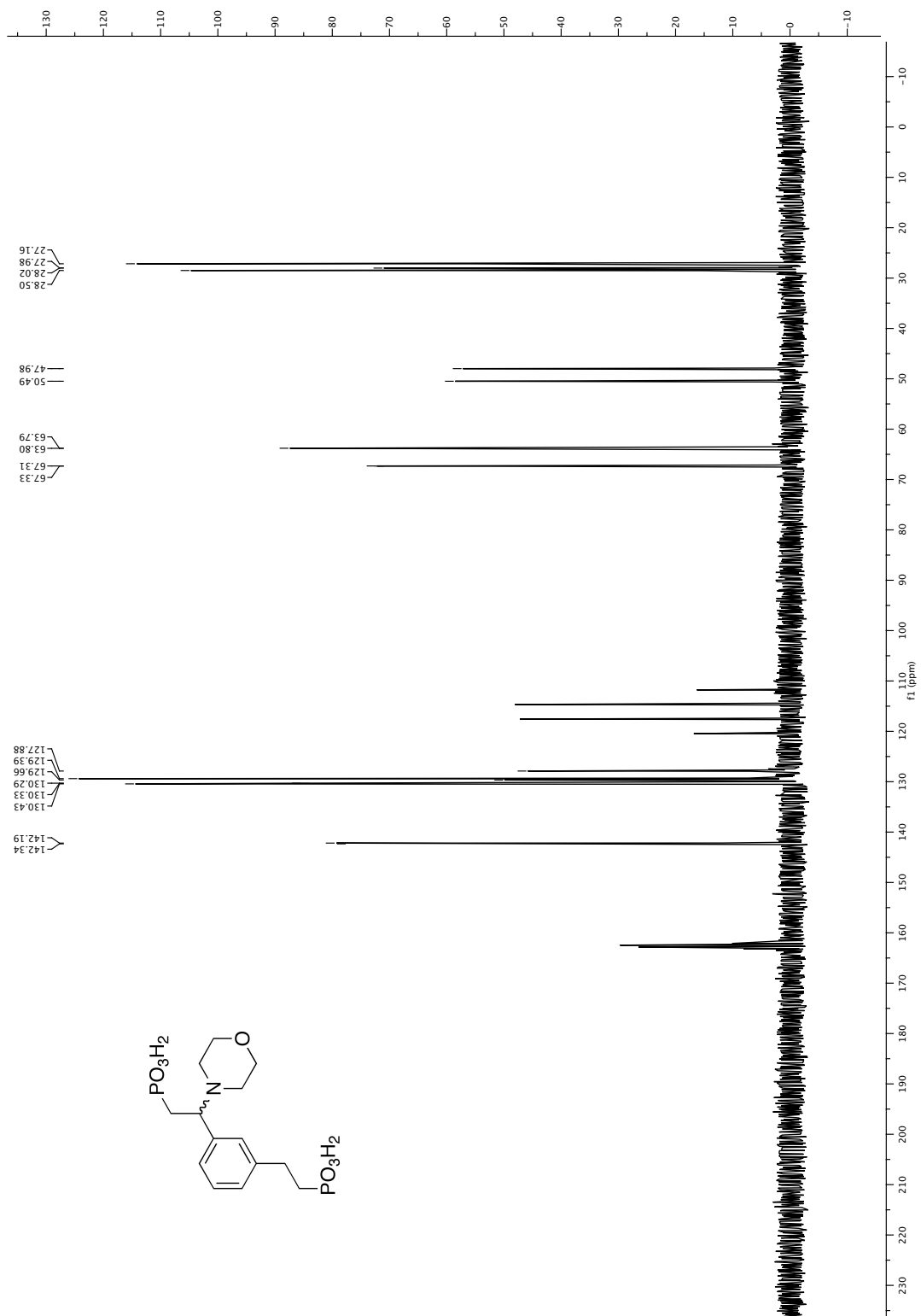


APPENDIX

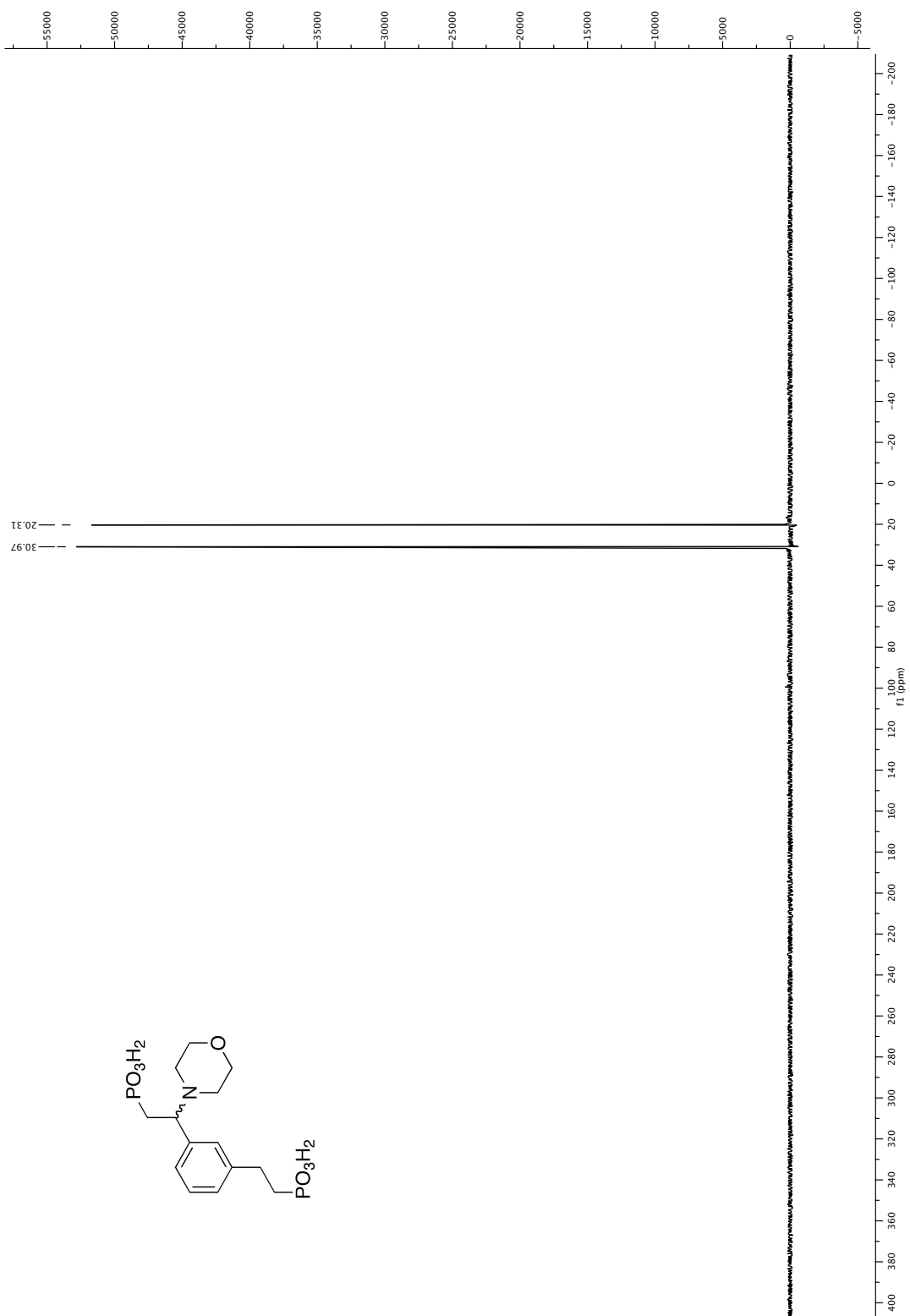
22.4.4 MOBIPHOS (4)



APPENDIX

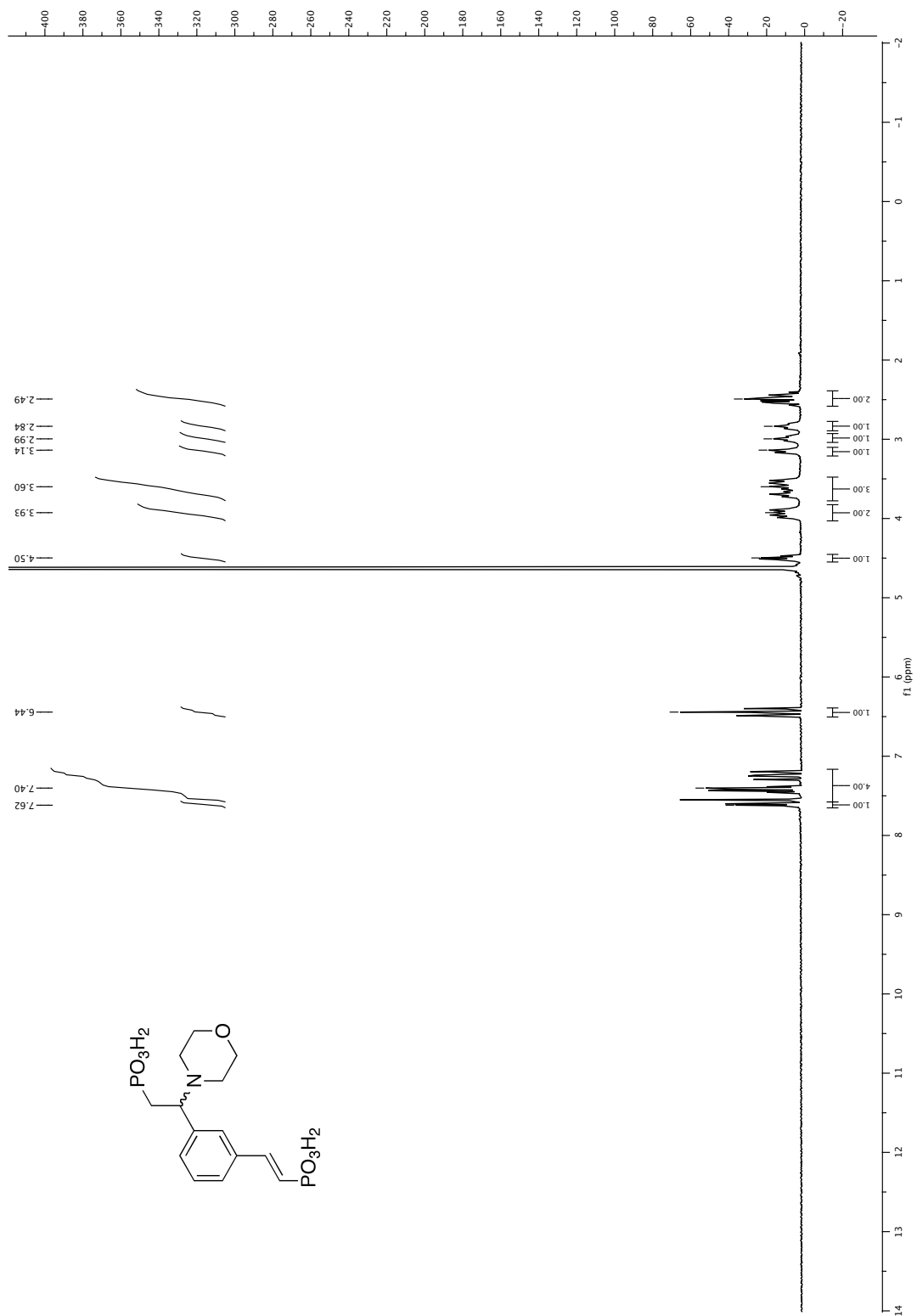


APPENDIX

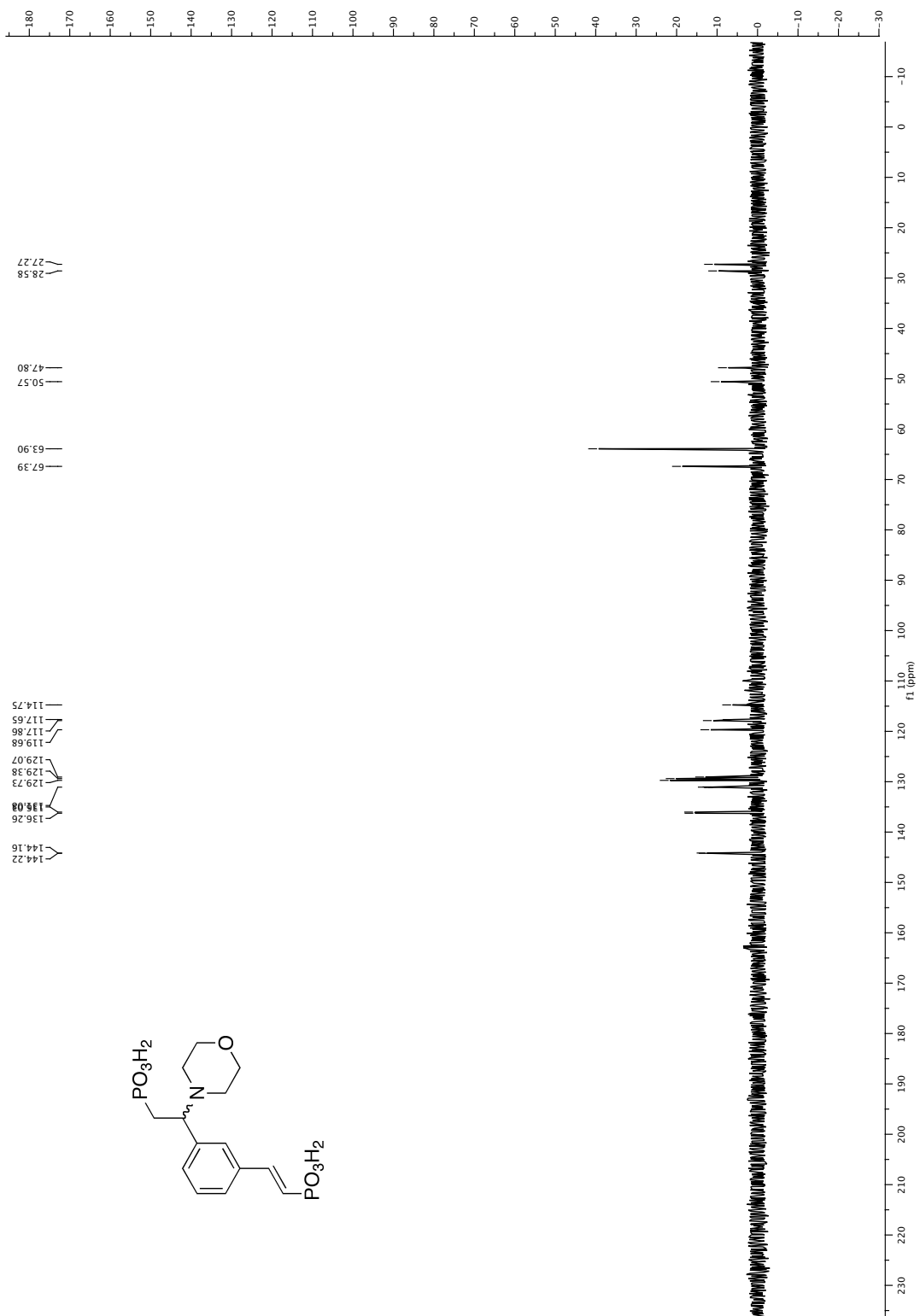


APPENDIX

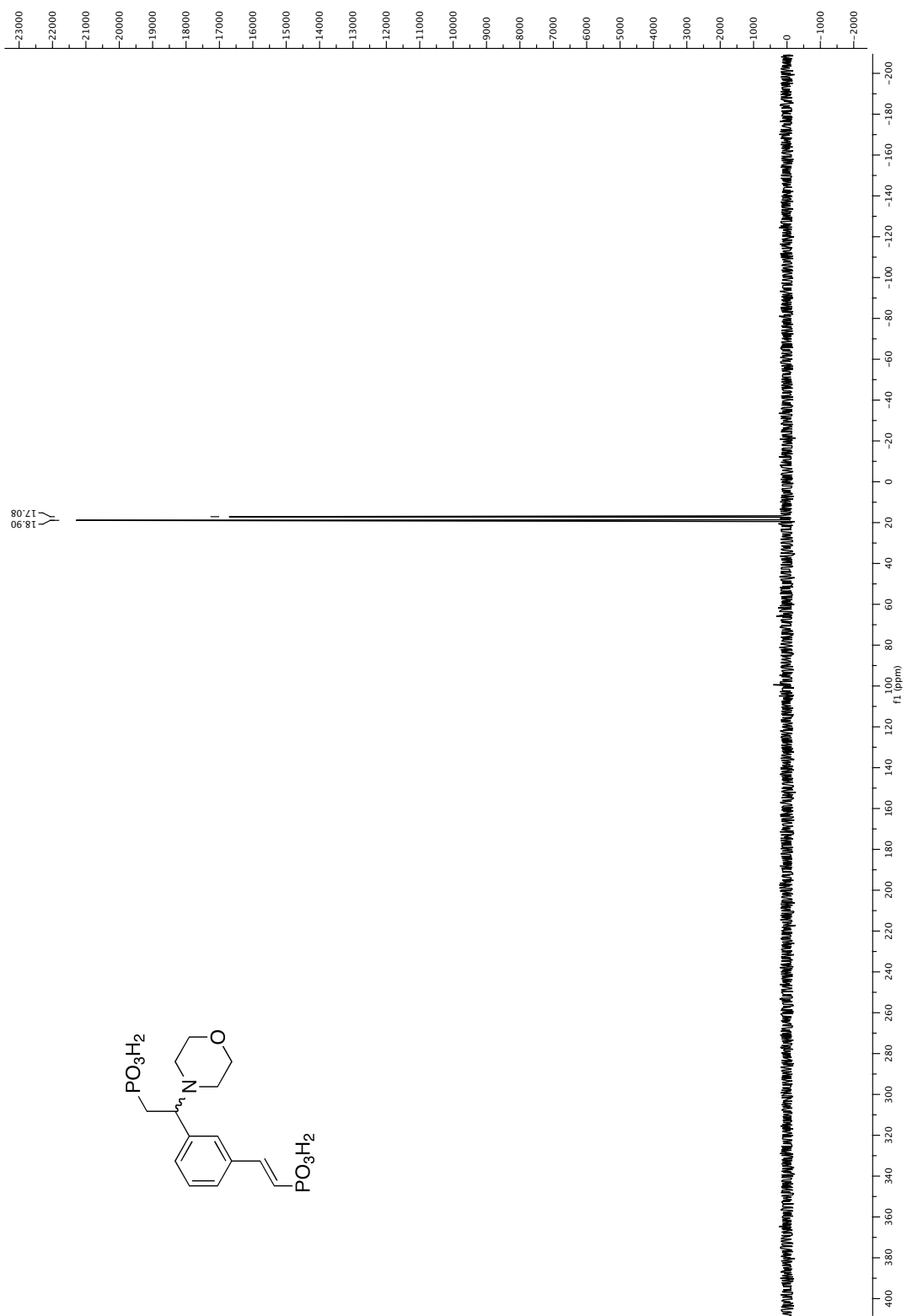
22.4.5 MOBIPHOSen (38)



APPENDIX

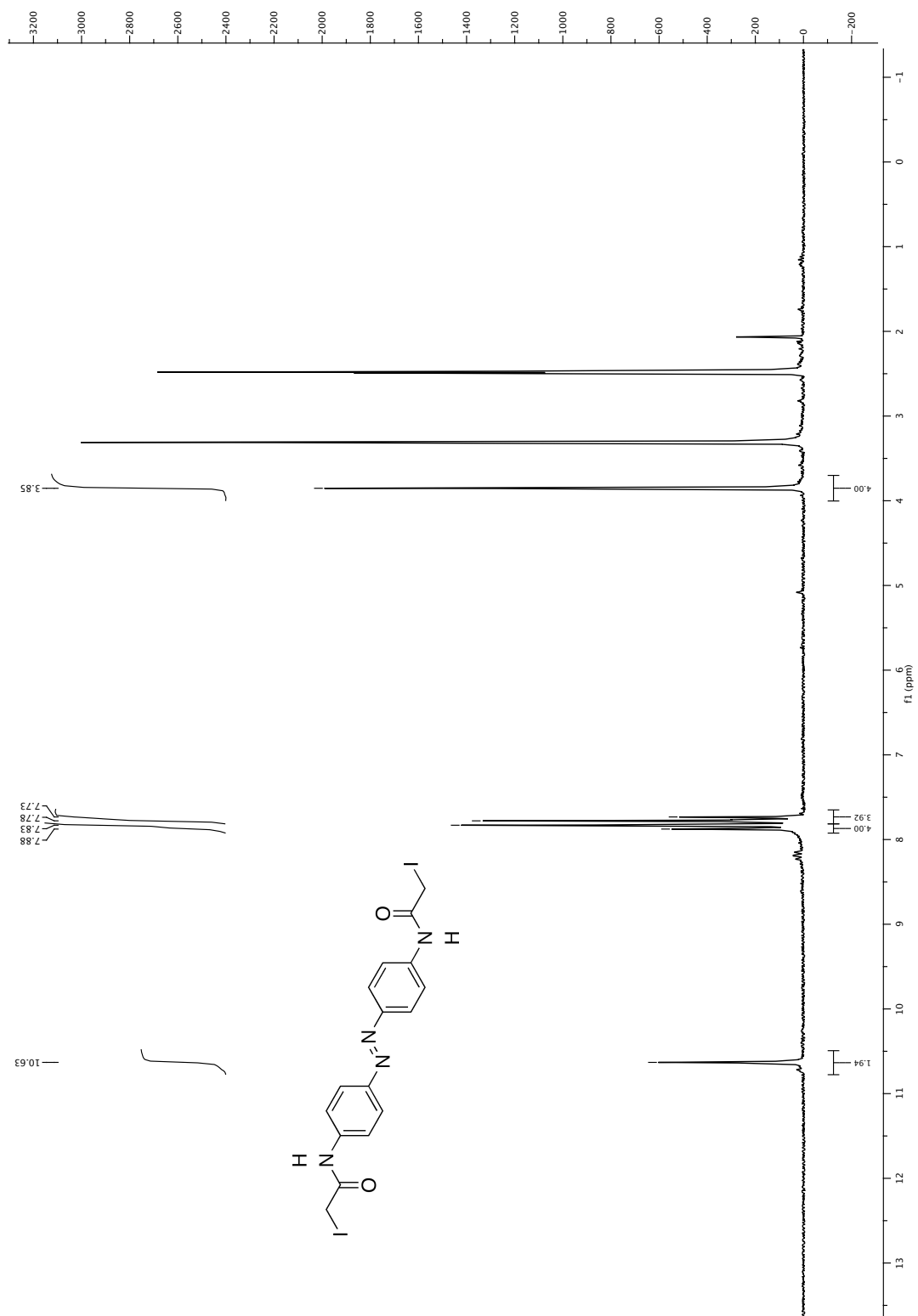


APPENDIX

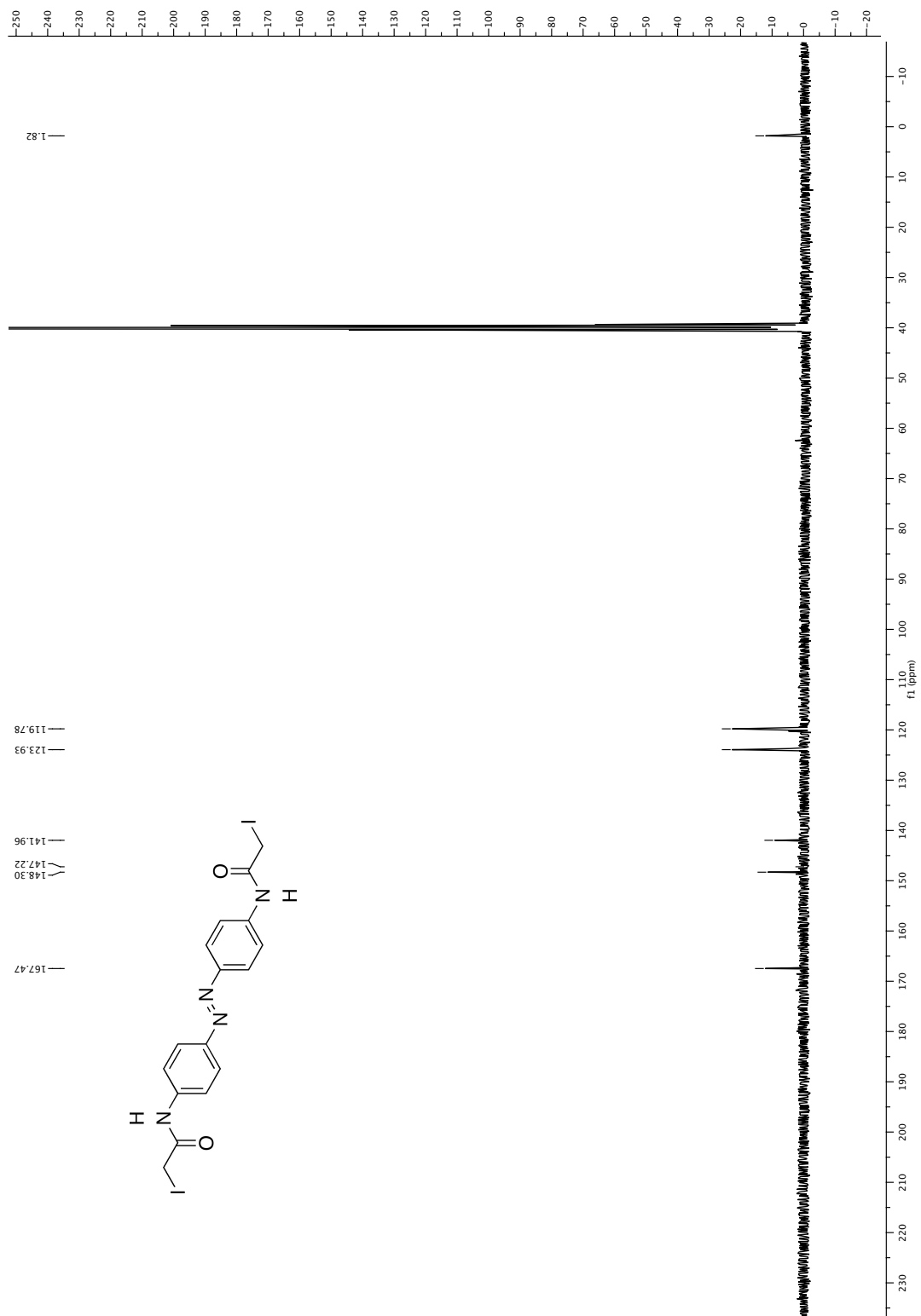


APPENDIX

22.5 Spectra of ABA (5)



APPENDIX



Chapter 23: Protein primary structures

23.1 GluK2-LBD amino acid sequence

```

at TTT Gtt taa CTT TAA GAA GGA GAT ATA CAT ATG CAC CAT Cat cat CAT CAT CAT CAC AGC AGC GGC CTG GTG CCC CGG GGC AGC AAT CGT TCT TTG AT < 100
M H H H H H H H H S S S G L V P R G S N R S L I
ta AAA Caa att GAA ATT CTT CCT CTA TAT GTA TAC GTG GTA Gta gta GTA GTA GTG TCG TCG CCG GAC CAC GGG GCC CCG TCG TTA GCA AGA AAC TA
10 20 30 40 50 60 70 80 90

T GTT ACC ACC ATT TTG GAA GAA CCG TAT GTT CTG TTT AAG AAG TCT GAC AAA CCA CTC TAT TGG AAT GAT CGA TTT GAA GGC TAC TGT ATT GAT CTC CTA < 200
V T T I L E E P Y V L F K S D K P L Y G N D R F E G C I D L L
A CAA TGG TGG TAA AAC CTT CTT GGC ATA CAA GAC AAA TTC TTC AGA CTG TTT GGT GAG ATA CCC TTA CTA GCT AAA CTT CCG ATG ACA TAA CTA GAG GAT
110 120 130 140 150 160 170 180 190

CGA GAG TTA TCT ACA ATC CTT GGC TTT ACA TAT GAG ATT AGG CTT GTG GAG GAT GGG AAA TAT GGA GCC CAG GAT GAT GTG AAC GGA CAA TGG AAT GGA A < 300
R E L S T I L G F T Y E I R L V E D G K Y G A Q D D V N G M
GCT CTC AAT AGA TGT TAG GAA CCG AAA TGT ATA CTC TAA TCC GAA CAC CTC CTA CCC TTT ATA CCT CGG GTC CTA CTA CAC TTG CCT GTT ACC TTA CCT T
210 220 230 240 250 260 270 280 290

TG GTT CGT GAA CTA ATC GAT CAT AAA GCT GAC CTT GCA GTT GCT CCA CTG GCT ATA ACC TAT GTT CGT GAG AAG GTC ATC GAC TTT TCA AAG CCG TTT AT < 400
V R E L I D H K A D L A V A P L A I T Y V R E K V I D F S K P F M
AC CAA GCA CTT GAT TAG CTA GTA TTT CGA CTG GAA CGT CAA CGA GGT GAC CGA TAT TGG ATA CAA GCA CTC TTC CAG TAG CTG AAA AGT TTC GGC AAA TA
310 320 330 340 350 360 370 380 390

G ACA CTT GGA ATA AGT ATT TTG TAC CGC AAG GGT ACC CCC ATT GAC TCT GCT GAC GAT TTA GCT AAG CAA ACC AAG ATA GAG TAT GGA GCA GTG GAG GAC < 500
T L G I S I L Y R K G T P I D S A D D L A K Q T K I E Y G A V E D
C TGT GAA CCT TAT TCA TAA AAC ATG GCG TTC CCA TGG GGT TAA CTG AGA CGA CTG CTA AAT CGA TTC GTT TGG TTC TAT CTC ATA CCT CGT CAC CTC CTG
410 420 430 440 450 460 470 480 490

GGC GCA ACC ATG ACG TTT TTT AAG AAA TCA AAA ATT TCA ACG TAT GAT AAA ATG TGG GCG TTT ATG AGC AGC AGG AGA CAG TCT GTG CTT GTC AAA AGC A < 600
G A T M T F F K K S K I S T Y D K M W A F M S S R R Q S V L V K S N
CCG CGT TGG TAC TGC AAA AAA TTC TTT AGT TTT TAA AGT TGC ATA CTA TTT TAC ACC CGC AAA TAC TCG TCG TCC TCT GTC AGA CAC GAA CAG TTT TCG T
510 520 530 540 550 560 570 580 590

AT GAG GAA GGG ATC CAA CGA GTC CTC ACC TCG GAT TAT GCT TTC TTA ATG GAG TCA ACA ACC ATC GAG TTT GTT ACA CAG CGG AAC TGT AAC CTC ACG CA < 700
E E G I Q R V L T S D Y A F L M E S T T I E F V T Q R N C N L T Q
TA CTC CTT CCG TAG GTT GCT CAG GAG TGG 630 640 650 660 670 680 690

G ATT GGC GGC CTT ATA GAC TCC AAA GGC TAT GGC GTT GGC ACT CCT ATG GGC TCT CCA TAT CGA GAC AAA ATC ACC ATA GCA ATT CTT CAG CTG CAG GAG < 800
I G G L I D S K G Y G V G T P M G S P Y R D K I T I A I L Q L Q E
C TAA CCG CCG GAA TAT CTG AGG TTT CCG ATA CCG CAA CCG TGA GGA TAC CCG AGA GGT ATA GCT CTG TTT TAG TGG TAT CGT TAA GAA GTC GAC GTC CTC
710 720 730 740 750 760 770 780 790

Gaa ggc AAG CTG CAC ATG ATG AAG gag aAA TGG TGG CGG ggc AAT GGC TGC Cca gag TGa CTC GAG CAC CAC CAC CAC CAC TgA gtc CgG cTG CTA A < 900
E G K L H M M K E K W W R G N G C P E
Ctt ccg TTC GAC TTG TAC TTC ctc tTT ACC ACC GCC ccg TTA CCG ACG GGT ctc Act GAG CTC GTG GTG GTG GTG GTG Act caq Gcc gAC GAT T
810 820 830 840 850 860 870 880 890

```

The N-terminal octa histidine tag, the thrombin cleavage site and the GT dipeptide are framed red, whereas the beginning and ending of S1 and S2 are framed blue.

APPENDIX

23.2 GluA2-LBD amino acid sequence

```

CTT TAn GAn GGa GaT aTa CAT ATG CAC CAT CAT cnn cAT CAT CAT CAC AGC AGC GGC CTg qtG CCG CGC GGC AGC GCC ATG GGC TCA GGA AAT GAC ACT A < 100
GAA ATn CTh CcT CtA tAt GTA TAC GTG CTA GTA gnn gTA GTA GTA GTG TCG TCG CCG GAC caC GGC GCG CCG TCG CGG TAC CCG AGT CCT TTA CTG TGA T
10 20 30 40 50 60 70 80 90

GT CGC GGT GCA AAC AAA ACT gtG GTG GTC ACC ACA ATA TTG GAA TCT CCA TAT GTT ATG ATG AAG AAA AAT CAT GAA ATG CTT GAA GGG AAT GAG CGT TA < 200
R G A N K T V V V T T L E S P Y M K N H E M L E G D K Y G A R Y
CA GCG CCA CGT TTG TTT TGA caC CAC CAG TGG TGT TAT AAC CTT AGA GGT ATA CAA TAC TAC TTC TTT TTA GTA CTT TAC GAA CTT CCC TTA CTC GCA AT
110 120 130 140 150 160 170 180 190

C GAG GGC TAC TGT GTT GAC TTA GCT GCA GAA ATT GCC AAA CAC TGT GGG TTC AAG TAC AAG CTG ACT ATT GTT GGG GAT GGC AAG TAT GGG GCC AGG GAT < 300
E G Y C N K I W N G M V T T I A K H C G F Y M M K L T I V G D K Y G A R Y
G CTC CCG ATG ACA CAA CTG AAT CGA CGT CTT TAA CCG TTT GTG ACA CCC AAG TTC ATG TTC GAC TGA TAA CAA CCC CTA CCG TTC ATA CCC CGG TCC CTA
210 220 230 240 250 260 270 280 290

GCC GAC ACC AAA ATT TGG AAT GGT ATG GTT GGA GAG CTT GTC TAC GGG AAA GCT GAC ATT GCA ATT GCT CCA TTA ACT ATC ACT CTC CTG AGA GAA GAG G < 400
A D T F S K P F M S L G I S I M I R K I G T P I E S A E D L S K Q T E
CGG CTG TGG TTT TAA ACC TTA CCA TAC CAA CCT CTC GAA CAG ATG CCC TTT CGA CTG TAA CGT TAA CGA GGT AAT TGA TAG TGA GAG CAC TCT CTT CTC C
310 320 330 340 350 360 370 380 390

TG ATT GAC TTC TCC AAG CCC TTC ATG AGT CTT GGA ATC TCT ATC ATG ATC AAG AAG GGT ACC CCC ATC GAA AGT GCT GAG GAT CTG TCT AAG CAA ACA GA < 500
I D F S K P F M S L G I S I M I R K I G T P I E S A E D L S K Q T E
AC TAA CTG AAG AGG TTC GGG AAG TAC TCA GAA CCT TAG AGA TAG TAC TAG TTC TCC CCA TGG GGG TAG CTT TCA CGA CTC CTA GAC AGA TTC GTT TGT CT
410 420 430 440 450 460 470 480 490

A ATT GCT TAT GGA ACA TTA GAC TCT GGC TCC ACT AAA GAG TTT TTC AGG AGA TCT AAA ATC GCA GTG TTT GAT AAA ATG TGG ACT TAT ATG AGG AGT GCA < 600
I A Y G T L D S G S T K E F R S K I A V F D K M W T Y M R S A
T TAA CGA ATA CCT TGT AAT CTG AGA CCG AGG TGA TTT CTC AAA AAG TCC TCT AGA TTT TAG CGT CAC AAA CTA TTT TAC ACC TGA ATA TAC TCC TCA CGT
510 520 530 540 550 560 570 580 590

GAG CCC TCT GTG TTT GTG AGG ACT ACC GCA GAA GGA GTA GCC AGA GTC CGG AAA TCC AAA GGA AAG TAT GCC TAC TTG CTG GAG TCC ACA ATG AAC GAG T < 700
E P S V F V R T T A E G V A R V R K S K G K Y A Y L L E S T M N E Y
CTC GGG AGA CAC AAA CAC TCC TGA TGG CGT CTT CCT CAT CGG TCT CAG GCC TTT AGG TTT CCT TCC ATA CCG ATG AAC GAC CTC AGG TGT TAC TTG CTC A
610 620 630 640 650 660 670 680 690

AC ATC GAG CAG AGG AAG CCT TGT GAC ACC ATG AAA GTG GGA GGA AAC TTG GAT TCC AAA GGC TAC GGC ATC GCC ACA CCT AAA GGA TCC TCA TTA GGA AA < 800
I E Q R K P C D T M K V G G N L D S K G Y G I A T P K G S S L G N
TG TAG CTC GTC TCC TTC GGA ACA CTG TGG TAC TTT CAC CCT TTG AAC CTA AGG TTT CCG ATG CCG TAG CGG TGT GGA TTT CCT AGG AGT AAT CCT TT
710 720 730 740 750 760 770 780 790

T GCG GTT AAC CTC GCA GTA CTA AAA CTG AAT GAA CAA GGC CTG TTG GAC AAA TTG AAA AAC AAA TGG TGG TAC GAC AAA GGA qaG TGC GGC AGC GGC TGA < 900
A V N L A V L K L N E Q G L L D K L K N K W W Y D K G E C G S
A CGC CAA TTG GAG CGT CAT GAT TTT GAC TTA CTT GTT CCG GAC AAC CTG TTT AAC TTT TTG TTT ACC ACC ATG CTG TTT Cct ctC ACg CCG TCG CCG ACT
810 820 830 840 850 860 870 880 890

```

The N-terminal octa histidine tag, the thrombin cleavage site and the GT dipeptide are framed red, whereas the beginning and ending of S1 and S2 are framed green.

Part VIII: REFERENCES

REFERENCES

- 1 Curtis, D. R., Phillis, J. W. & Watkins, J. C. Chemical excitation of spinal neurones. *Nature* **183**, 611-612 (1959).
- 2 Kawai, N., Yamagishi, S., Saito, M. & Furuya, K. Blockade of synaptic transmission in the squid giant synapse by a spider toxin (JSTX). *Brain research* **278**, 346-349 (1983).
- 3 Watkins, J. C. & Evans, R. H. Excitatory amino acid transmitters. *Annual review of pharmacology and toxicology* **21**, 165-204 (1981).
- 4 Wroblewski, J. T. & Danysz, W. Modulation of glutamate receptors: molecular mechanisms and functional implications. *Annual review of pharmacology and toxicology* **29**, 441-474 (1989).
- 5 Volgraf, M. *et al.* Allosteric control of an ionotropic glutamate receptor with an optical switch. *Nature chemical biology* **2**, 47-52 (2006).
- 6 Volgraf, M. *et al.* Reversibly caged glutamate: a photochromic agonist of ionotropic glutamate receptors. *Journal of the American Chemical Society* **129**, 260-261 (2007).
- 7 Seidel, S. A. *et al.* Label-free microscale thermophoresis discriminates sites and affinity of protein-ligand binding. *Angewandte Chemie (International ed. in English)* **51**, 10656-10659 (2012).
- 8 Caporale, N. *et al.* LiGluR restores visual responses in rodent models of inherited blindness. *Molecular therapy : the journal of the American Society of Gene Therapy* **19**, 1212-1219 (2011).
- 9 Park, H. S. *et al.* Design and evolution of new catalytic activity with an existing protein scaffold. *Science (New York, N.Y.)* **311**, 535-538 (2006).
- 10 Binz, H. K., Stumpp, M. T., Forrer, P., Amstutz, P. & Pluckthun, A. Designing repeat proteins: well-expressed, soluble and stable proteins from combinatorial libraries of consensus ankyrin repeat proteins. *Journal of molecular biology* **332**, 489-503 (2003).
- 11 Krosgaard-Larsen, P. & Hansen, J. J. *Excitatory amino acid receptors*. 1st edn, (Ellis Horwood Limited, 1992).
- 12 Hugel, T. *et al.* Single-molecule optomechanical cycle. *Science (New York, N.Y.)* **296**, 1103-1106 (2002).
- 13 Banghart, M. R. *Light-gated potassium channels for photocontrol of neuronal firing*, University of California, (2008).
- 14 Beharry, A. A., Sadovski, O. & Woolley, G. A. Azobenzene photoswitching without ultraviolet light. *Journal of the American Chemical Society* **133**, 19684-19687 (2011).
- 15 Gereau, R. W. & Swanson, G. T. *The glutamate receptors*. (Humana Press, 2008).
- 16 Mayer, M. L. Emerging models of glutamate receptor ion channel structure and function. *Structure (London, England : 1993)* **19**, 1370-1380 (2011).
- 17 Hucho, F. *Neurochemistry*. (VCH, 1986).
- 18 Nicholls, J. G., Martin, A. R. & Wallace, B. G. *Vom Neuron zum Gehirn* (Gustav Fischer Verlag, 1995).
- 19 Bradford, H. F. *Chemical neurobiology: an introduction to neurochemistry*. (W. H. Freeman and Company, 1986).
- 20 Rothstein, J. D. Neurobiology. Bundling up excitement. *Nature* **407**, 141, 143 (2000).
- 21 Cowan, W. M., Sudhof, T. C. & Stevens, C. F. *Synapses*. (The Johns Hopkins Univ. Press, 2001).

REFERENCES

- 22 Hayashi, T. Effects of sodium glutamate on the nervous system. *Keio J. Med.* **3**, 183-192 (1954).
- 23 Collingridge, G. L., Olsen, R. W., Peters, J. & Spedding, M. A nomenclature for ligand-gated ion channels. *Neuropharmacology* **56**, 2-5 (2009).
- 24 Dingledine, R., Borges, K., Bowie, D. & Traynelis, S. F. The glutamate receptor ion channels. *Pharmacological reviews* **51**, 7-61 (1999).
- 25 Jane, D. E., Lodge, D. & Collingridge, G. L. Kainate receptors: pharmacology, function and therapeutic potential. *Neuropharmacology* **56**, 90-113 (2009).
- 26 Lipton, S. A. Paradigm shift in neuroprotection by NMDA receptor blockade: memantine and beyond. *Nature reviews. Drug discovery* **5**, 160-170 (2006).
- 27 Alt, A., Nisenbaum, E. S., Bleakman, D. & Witkin, J. M. A role for AMPA receptors in mood disorders. *Biochemical pharmacology* **71**, 1273-1288 (2006).
- 28 Sugiyama, H., Ito, I. & Watanabe, M. Glutamate receptor subtypes may be classified into two major categories: a study on *Xenopus* oocytes injected with rat brain mRNA. *Neuron* **3**, 129-132 (1989).
- 29 Krogsgaard-Larsen, P., Honore, T., Hansen, J. J., Curtis, D. R. & Lodge, D. New class of glutamate agonist structurally related to ibotenic acid. *Nature* **284**, 64-66 (1980).
- 30 McLennan, H. & Lodge, D. The antagonism of amino acid-induced excitation of spinal neurones in the cat. *Brain research* **169**, 83-90 (1979).
- 31 Hansen, K. B., Yuan, H. & Traynelis, S. F. Structural aspects of AMPA receptor activation, desensitization and deactivation. *Current opinion in neurobiology* **17**, 281-288 (2007).
- 32 Paoletti, P. & Neyton, J. NMDA receptor subunits: function and pharmacology. *Current opinion in pharmacology* **7**, 39-47 (2007).
- 33 Mayer, M. L., Westbrook, G. L. & Guthrie, P. B. Voltage-dependent block by Mg²⁺ of NMDA responses in spinal cord neurones. *Nature* **309**, 261-263 (1984).
- 34 Johnson, J. W. & Ascher, P. Glycine potentiates the NMDA response in cultured mouse brain neurons. *Nature* **325**, 529-531 (1987).
- 35 Chen, G. Q., Cui, C., Mayer, M. L. & Gouaux, E. Functional characterization of a potassium-selective prokaryotic glutamate receptor. *Nature* **402**, 817-821 (1999).
- 36 Mano, I. & Teichberg, V.I. A tetrameric subunit stoichiometry for a glutamate receptor-channel complex. *Neuroreport* **9**, 327-331 (1998).
- 37 Rosenmund, C., Stern-Bach, Y. & Stevens, C. F. The tetrameric structure of a glutamate receptor channel. *Science (New York, N.Y.)* **280**, 1596-1599 (1998).
- 38 Hollmann, M. & Heinemann, S. Cloned glutamate receptors. *Annual review of neuroscience* **17**, 31-108 (1994).
- 39 Bleakman, D. & Lodge, D. Neuropharmacology of AMPA and kainate receptors. *Neuropharmacology* **37**, 1187-1204 (1998).
- 40 Hollmann, M., O'Shea-Greenfield, A., Rogers, S. W. & Heinemann, S. Cloning by functional expression of a member of the glutamate receptor family. *Nature* **342**, 643-648 (1989).
- 41 Bettler, B. *et al.* Cloning of a novel glutamate receptor subunit, GluR5: expression in the nervous system during development. *Neuron* **5**, 583-595 (1990).

REFERENCES

- 42 Egebjerg, J., Bettler, B., Hermans-Borgmeyer, I. & Heinemann, S. Cloning of a cDNA for a glutamate receptor subunit activated by kainate but not AMPA. *Nature* **351**, 745-748 (1991).
- 43 Werner, P., Voigt, M., Keinänen, K., Wisden, W. & Seeburg, P. H. Cloning of a putative high-affinity kainate receptor expressed predominantly in hippocampal CA3 cells. *Nature* **351**, 742-744 (1991).
- 44 Borges, K. & Dingledine, R. AMPA receptors: molecular and functional diversity. *Progress in brain research* **116**, 153-170 (1998).
- 45 Kohler, M., Kornau, H. C. & Seeburg, P. H. The organization of the gene for the functionally dominant alpha-amino-3-hydroxy-5-methylisoxazole-4-propionic acid receptor subunit GluR-B. *The Journal of biological chemistry* **269**, 17367-17370 (1994).
- 46 Burnashev, N. Calcium permeability of glutamate-gated channels in the central nervous system. *Current opinion in neurobiology* **6**, 311-317 (1996).
- 47 Paas, Y., Eisenstein, M., Medevielle, F., Teichberg, V. I. & Devillers-Thiery, A. Identification of the amino acid subsets accounting for the ligand binding specificity of a glutamate receptor. *Neuron* **17**, 979-990 (1996).
- 48 Paas, Y. The macro- and microarchitectures of the ligand-binding domain of glutamate receptors. *Trends in neurosciences* **21**, 117-125 (1998).
- 49 Mayer, M. L. Glutamate receptors at atomic resolution. *Nature* **440**, 456-462 (2006).
- 50 Leuschner, W. D. & Hoch, W. Subtype-specific assembly of alpha-amino-3-hydroxy-5-methyl-4-isoxazole propionic acid receptor subunits is mediated by their n-terminal domains. *The Journal of biological chemistry* **274**, 16907-16916 (1999).
- 51 Ayalon, G., Segev, E., Elgavish, S. & Stern-Bach, Y. Two regions in the N-terminal domain of ionotropic glutamate receptor 3 form the subunit oligomerization interfaces that control subtype-specific receptor assembly. *The Journal of biological chemistry* **280**, 15053-15060 (2005).
- 52 Stern-Bach, Y. *et al.* Agonist selectivity of glutamate receptors is specified by two domains structurally related to bacterial amino acid-binding proteins. *Neuron* **13**, 1345-1357 (1994).
- 53 Kuusinen, A., Arvola, M. & Keinänen, K. Molecular dissection of the agonist binding site of an AMPA receptor. *The EMBO journal* **14**, 6327-6332 (1995).
- 54 Chen, G. Q., Sun, Y., Jin, R. & Gouaux, E. Probing the ligand binding domain of the GluR2 receptor by proteolysis and deletion mutagenesis defines domain boundaries and yields a crystallizable construct. *Protein science : a publication of the Protein Society* **7**, 2623-2630 (1998).
- 55 Chen, G. Q. & Gouaux, E. Overexpression of a glutamate receptor (GluR2) ligand binding domain in Escherichia coli: application of a novel protein folding screen. *Proceedings of the National Academy of Sciences of the United States of America* **94**, 13431-13436 (1997).
- 56 Armstrong, N. & Gouaux, E. Mechanisms for activation and antagonism of an AMPA-sensitive glutamate receptor: crystal structures of the GluR2 ligand binding core. *Neuron* **28**, 165-181 (2000).
- 57 Lunn, M. L. *et al.* Three-dimensional structure of the ligand-binding core of GluR2 in complex with the agonist (S)-ATPA: implications for receptor subunit selectivity. *Journal of medicinal chemistry* **46**, 872-875 (2003).

REFERENCES

- 58 Jin, R., Banke, T. G., Mayer, M. L., Traynelis, S. F. & Gouaux, E. Structural basis for partial agonist action at ionotropic glutamate receptors. *Nature neuroscience* **6**, 803-810 (2003).
- 59 Hogner, A. *et al.* Competitive antagonism of AMPA receptors by ligands of different classes: crystal structure of ATPO bound to the GluR2 ligand-binding core, in comparison with DNQX. *Journal of medicinal chemistry* **46**, 214-221 (2003).
- 60 Sobolevsky, A. I., Rosconi, M. P. & Gouaux, E. X-ray structure, symmetry and mechanism of an AMPA-subtype glutamate receptor. *Nature* **462**, 745-756 (2009).
- 61 Mayer, M. L. Crystal structures of the GluR5 and GluR6 ligand binding cores: molecular mechanisms underlying kainate receptor selectivity. *Neuron* **45**, 539-552 (2005).
- 62 Mayer, M. L., Ghosal, A., Dolman, N. P. & Jane, D. E. Crystal structures of the kainate receptor GluR5 ligand binding core dimer with novel GluR5-selective antagonists. *The Journal of neuroscience : the official journal of the Society for Neuroscience* **26**, 2852-2861 (2006).
- 63 Nanao, M. H., Green, T., Stern-Bach, Y., Heinemann, S. F. & Choe, S. Structure of the kainate receptor subunit GluR6 agonist-binding domain complexed with domoic acid. *Proceedings of the National Academy of Sciences of the United States of America* **102**, 1708-1713 (2005).
- 64 Kohda, K., Wang, Y. & Yuzaki, M. Mutation of a glutamate receptor motif reveals its role in gating and delta2 receptor channel properties. *Nature neuroscience* **3**, 315-322 (2000).
- 65 Klein, R. M. & Howe, J. R. Effects of the lurcher mutation on GluR1 desensitization and activation kinetics. *The Journal of neuroscience : the official journal of the Society for Neuroscience* **24**, 4941-4951 (2004).
- 66 Wollmuth, L. P. & Sobolevsky, A. I. Structure and gating of the glutamate receptor ion channel. *Trends in neurosciences* **27**, 321-328 (2004).
- 67 Hollmann, M., Maron, C. & Heinemann, S. N-glycosylation site tagging suggests a three transmembrane domain topology for the glutamate receptor GluR1. *Neuron* **13**, 1331-1343 (1994).
- 68 Doyle, D. A. *et al.* The structure of the potassium channel: molecular basis of K⁺ conduction and selectivity. *Science (New York, N.Y.)* **280**, 69-77 (1998).
- 69 Kuner, T., Beck, C., Sakmann, B. & Seeburg, P. H. Channel-lining residues of the AMPA receptor M2 segment: structural environment of the Q/R site and identification of the selectivity filter. *The Journal of neuroscience : the official journal of the Society for Neuroscience* **21**, 4162-4172 (2001).
- 70 Soderling, T. R. & Derkach, V. A. Postsynaptic protein phosphorylation and LTP. *Trends in neurosciences* **23**, 75-80 (2000).
- 71 Tavalin, S. J. *et al.* Regulation of GluR1 by the A-kinase anchoring protein 79 (AKAP79) signaling complex shares properties with long-term depression. *The Journal of neuroscience : the official journal of the Society for Neuroscience* **22**, 3044-3051 (2002).
- 72 Lu, W. *et al.* Subunit composition of synaptic AMPA receptors revealed by a single-cell genetic approach. *Neuron* **62**, 254-268 (2009).
- 73 Mulle, C. *et al.* Subunit composition of kainate receptors in hippocampal interneurons. *Neuron* **28**, 475-484 (2000).

REFERENCES

- 74 Christensen, J. K., Paternain, A. V., Selak, S., Ahring, P. K. & Lerma, J. A. A mosaic of functional kainate receptors in hippocampal interneurons. *The Journal of neuroscience : the official journal of the Society for Neuroscience* **24**, 8986-8993 (2004).
- 75 Boulter, J. *et al.* Molecular cloning and functional expression of glutamate receptor subunit genes. *Science (New York, N.Y.)* **249**, 1033-1037 (1990).
- 76 Keinanen, K. *et al.* A family of AMPA-selective glutamate receptors. *Science (New York, N.Y.)* **249**, 556-560 (1990).
- 77 Sommer, B. *et al.* A glutamate receptor channel with high affinity for domoate and kainate. *The EMBO journal* **11**, 1651-1656 (1992).
- 78 Safflering, M. *et al.* First images of a glutamate receptor ion channel: oligomeric state and molecular dimensions of GluRB homomers. *Biochemistry* **40**, 13948-13953 (2001).
- 79 Tichelaar, W., Safflering, M., Keinanen, K., Stark, H. & Madden, D. R. The Three-dimensional Structure of an Ionotropic Glutamate Receptor Reveals a Dimer-of-dimers Assembly. *Journal of molecular biology* **344**, 435-442 (2004).
- 80 Nakagawa, T., Cheng, Y., Ramm, E., Sheng, M. & Walz, T. Structure and different conformational states of native AMPA receptor complexes. *Nature* **433**, 545-549 (2005).
- 81 Sun, Y. *et al.* Mechanism of glutamate receptor desensitization. *Nature* **417**, 245-253 (2002).
- 82 Jin, R. *et al.* Crystal structure and association behaviour of the GluR2 amino-terminal domain. *The EMBO journal* **28**, 1812-1823 (2009).
- 83 Kumar, J., Schuck, P., Jin, R. & Mayer, M. L. The N-terminal domain of GluR6-subtype glutamate receptor ion channels. *Nature structural & molecular biology* **16**, 631-638 (2009).
- 84 Weston, M. C., Schuck, P., Ghosal, A., Rosenmund, C. & Mayer, M. L. Conformational restriction blocks glutamate receptor desensitization. *Nature structural & molecular biology* **13**, 1120-1127 (2006).
- 85 Hogner, A. *et al.* Structural basis for AMPA receptor activation and ligand selectivity: crystal structures of five agonist complexes with the GluR2 ligand-binding core. *Journal of molecular biology* **322**, 93-109 (2002).
- 86 Pentikainen, O. T., Settimo, L., Keinanen, K. & Johnson, M. S. Selective agonist binding of (S)-2-amino-3-(3-hydroxy-5-methyl-4-isoxazolyl)propionic acid (AMPA) and 2S-(2alpha,3beta,4beta)-2-carboxy-4-(1-methylethenyl)-3-pyrrolidineacetic acid (kainate) receptors: a molecular modeling study. *Biochemical pharmacology* **66**, 2413-2425 (2003).
- 87 Nielsen, M. M., Liljefors, T., Krogsgaard-Larsen, P. & Egebjerg, J. The selective activation of the glutamate receptor GluR5 by ATPA is controlled by serine 741. *Molecular pharmacology* **63**, 19-25 (2003).
- 88 Swanson, G. T., Gereau, R. W. th, Green, T. & Heinemann, S. F. Identification of amino acid residues that control functional behavior in GluR5 and GluR6 kainate receptors. *Neuron* **19**, 913-926 (1997).
- 89 Siewertsen, R. *et al.* Highly efficient reversible Z-E photoisomerization of a bridged azobenzene with visible light through resolved S(1)(n pi*) absorption bands. *Journal of the American Chemical Society* **131**, 15594-15595 (2009).
- 90 Popescu, G. & Auerbach, A. The NMDA receptor gating machine: lessons from single channels. *The Neuroscientist : a review journal bringing neurobiology, neurology and psychiatry* **10**, 192-198 (2004).

REFERENCES

- 91 Gouaux, E. Structure and function of AMPA receptors. *The Journal of physiology* **554**, 249-253 (2004).
- 92 Madden, D. R., Armstrong, N., Svergun, D., Perez, J. & Vachette, P. Solution X-ray scattering evidence for agonist- and antagonist-induced modulation of cleft closure in a glutamate receptor ligand-binding domain. *The Journal of biological chemistry* **280**, 23637-23642 (2005).
- 93 Du, M., Reid, S. A. & Jayaraman, V. Conformational changes in the ligand-binding domain of a functional ionotropic glutamate receptor. *The Journal of biological chemistry* **280**, 8633-8636 (2005).
- 94 Abele, R., Keinanen, K. & Madden, D. R. Agonist-induced isomerization in a glutamate receptor ligand-binding domain. A kinetic and mutagenetic analysis. *The Journal of biological chemistry* **275**, 21355-21363 (2000).
- 95 Cheng, Q., Du, M., Ramanoudjame, G. & Jayaraman, V. Evolution of glutamate interactions during binding to a glutamate receptor. *Nature chemical biology* **1**, 329-332 (2005).
- 96 Horning, M. S. & Mayer, M. L. Regulation of AMPA receptor gating by ligand binding core dimers. *Neuron* **41**, 379-388 (2004).
- 97 Jones, K. S., VanDongen, H. M. & VanDongen, A. M. The NMDA receptor M3 segment is a conserved transduction element coupling ligand binding to channel opening. *The Journal of neuroscience : the official journal of the Society for Neuroscience* **22**, 2044-2053 (2002).
- 98 Zuo, J. *et al.* Neurodegeneration in Lurcher mice caused by mutation in delta2 glutamate receptor gene. *Nature* **388**, 769-773 (1997).
- 99 Kuner, T., Seeburg, P. H. & Guy, H. R. A common architecture for K⁺ channels and ionotropic glutamate receptors? *Trends in neurosciences* **26**, 27-32 (2003).
- 100 Long, S. B., Campbell, E. B. & Mackinnon, R. Crystal structure of a mammalian voltage-dependent Shaker family K⁺ channel. *Science (New York, N.Y.)* **309**, 897-903 (2005).
- 101 Tang, C. M., Shi, Q. Y., Katchman, A. & Lynch, G. Modulation of the time course of fast EPSCs and glutamate channel kinetics by aniracetam. *Science (New York, N.Y.)* **254**, 288-290 (1991).
- 102 Frandsen, A. & Schousboe, A. AMPA receptor-mediated neurotoxicity: role of Ca²⁺ and desensitization. *Neurochemical research* **28**, 1495-1499 (2003).
- 103 Stern-Bach, Y., Russo, S., Neuman, M. & Rosenmund, C. A point mutation in the glutamate binding site blocks desensitization of AMPA receptors. *Neuron* **21**, 907-918 (1998).
- 104 Mosbacher, J. *et al.* A molecular determinant for submillisecond desensitization in glutamate receptors. *Science (New York, N.Y.)* **266**, 1059-1062 (1994).
- 105 Jin, R. *et al.* Mechanism of positive allosteric modulators acting on AMPA receptors. *The Journal of neuroscience : the official journal of the Society for Neuroscience* **25**, 9027-9036 (2005).
- 106 Zhao, Y. & Ikeda, T. *Smart light-responsive materials – azobenzene-containing polymers and liquid crystals*. (Wiley, 2009).
- 107 Bandara, H. M. & Burdette, S. C. Photoisomerization in different classes of azobenzene. *Chemical Society reviews* **41**, 1809-1825 (2012).
- 108 Mitscherlich, E. Ueber das Stickstoffbenzid. *Ann. Pharm.* **12**, 311-314 (1834).

REFERENCES

- 109 Noble, A. III. Zur Geschichte des Azobenzols und des Benzidins. *Annalen der Chemie und Pharmacie* **98**, 253-256 (1856).
- 110 Hartley, G. S. The cis-form of azobenzene. *Nature* **140**, 281-281 (1937).
- 111 Brown, C. J. A refinement of the crystal structure of azobenzene. *Acta Crystallogr.* **21**, 146-152 (1966).
- 112 Mita, Itaru, Horie, Kazuyuki & Hirao, Katsuhiko. Photochemistry in polymer solids. 9. Photoisomerization of azobenzene in a polycarbonate film. *Macromolecules* **22**, 558-563 (1989).
- 113 Mostad, A. & Rømming, C. A Refinement of the Crystal Structure of cis-Azobenzene. *Acta Chem. Scand.* **25**, 3561-3568 (1971).
- 114 Rau, Hermann. Spectroscopic Properties of Organic Azo Compounds. *Angewandte Chemie International Edition in English* **12**, 224-235 (1973).
- 115 Monti, Sandra, Orlandi, Giorgio & Palmieri, Paolo. Features of the photochemically active state surfaces of azobenzene. *Chemical Physics* **71**, 87-99 (1982).
- 116 Brown, Ellis V. & Granneman, G. Richard. Cis-trans isomerism in the pyridyl analogs of azobenzene. Kinetic and molecular orbital analysis. *Journal of the American Chemical Society* **97**, 621-627 (1975).
- 117 Lamarre, L. & Sung, C. S. P. Studies of physical aging and molecular motion by azochromophoric labels attached to the main chains of amorphous polymers. *Macromolecules* **16**, 1729-1736 (1983).
- 118 Han, M., Ishikawa, D., Honda, T., Ito, E. & Hara, M. Light-driven molecular switches in azobenzene self-assembled monolayers: effect of molecular structure on reversible photoisomerization and stable cis state. *Chemical communications (Cambridge, England)* **46**, 3598-3600 (2010).
- 119 Nishimura, Norio *et al.* Thermal *Cis*-to-*Trans* Isomerization of Substituted Azobenzenes II. Substituent and Solvent Effects. *Bulletin of the Chemical Society of Japan* **49**, 1381-1387 (1976).
- 120 Rau, H. Radiationless deactivation of azo compounds and light fastness of azo dyes. *Berichte der Bunsen-Gesellschaft* **72**, 408-414 (1968).
- 121 Cusati, Teresa, Granucci, Giovanni, Persico, Maurizio & Spighi, Gloria. Oscillator strength and polarization of the forbidden $n \rightarrow \pi^*$ band of trans-azobenzene: A computational study. *The Journal of Chemical Physics* **128**, 194312 (2008).
- 122 Horspool, W. & Lenci, F. . *Handbook of organic photochemistry and photobiology*. 2nd edn, (CRC press, 2004).
- 123 Forber, Christine L., Kelusky, Eric C., Bunce, Nigel J. & Zerner, Michael C. Electronic spectra of cis- and trans-azobenzenes: consequences of ortho substitution. *Journal of the American Chemical Society* **107**, 5884-5890 (1985).
- 124 Hamm, P., Ohline, S. M. & Zinth, W. Vibrational cooling after ultrafast photoisomerization of azobenzene measured by femtosecond infrared spectroscopy. *The Journal of Chemical Physics* **106**, 519-529 (1997).
- 125 Lednev, I. K. *et al.* Femtosecond time-resolved UV-visible absorption spectroscopy of trans-azobenzene: dependence on excitation wavelength. *Chemical Physics Letters* **290**, 68-74 (1998).
- 126 Rabek, J. F. *Photochemistry and photophysics*. (CRC Press, 1990).
- 127 Hallas, Geoffrey, Marsden, Richard, Hepworth, John D. & Mason, Donald. The effects of cyclic terminal groups in 4-aminoazobenzene and related azo dyes.

REFERENCES

- Part 3. Electronic absorption spectra of some monoazo dyes derived from N-phenylmorpholine, N-(phenyl)thiomorpholine, N-(phenyl)thiomorpholine 1,1-dioxide, and N-acetyl-N[prime or minute]-phenylpiperazine. *Journal of the Chemical Society, Perkin Transactions 2* **0**, 123-126 (1986).
- 128 Dokic, J. *et al.* Quantum chemical investigation of thermal cis-to-trans isomerization of azobenzene derivatives: substituent effects, solvent effects, and comparison to experimental data. *The journal of physical chemistry. A* **113**, 6763-6773 (2009).
- 129 Zollinger, H. *Colour Chemistry, Synthesis, Properties, and Applications of Organic Dyes and Pigments.* (VCH, 1987).
- 130 Venkataraman, K. *The chemistry of synthetic dyes.* (Academic Press, 1956).
- 131 Magee, John L., Shand, William & Eyring, Henry. Non-adiabatic Reactions. Rotation about the Double Bond*. *Journal of the American Chemical Society* **63**, 677-688 (1941).
- 132 Curtin, David Y., Grubbs, Edward J. & McCarty, C. Gordon. Uncatalyzed syn-anti Isomerization of Imines, Oxime Ethers, and Haloimines¹. *Journal of the American Chemical Society* **88**, 2775-2786 (1966).
- 133 Xie, S., Natansohn, A. & Rochon, P. Recent developments in aromatic azo polymers research. *Chemistry of Materials* **5**, 403-411 (1993).
- 134 Gegiou, Dina, Muszkat, K. A. & Fischer, Ernst. Temperature dependence of photoisomerization. V. Effect of substituents on the photoisomerization of stilbenes and azobenzenes. *Journal of the American Chemical Society* **90**, 3907-3918 (1968).
- 135 Altomare, Angelina, Ciardelli, Francesco, Tirelli, Nicola & Solaro, Roberto. 4-Vinylazobenzene: Polymerizability and Photochromic Properties of Its Polymers. *Macromolecules* **30**, 1298-1303 (1997).
- 136 Angeli, Celestino, Cimiraglia, Renzo & Hofmann, Hans-Jörg. On the competition between the inversion and rotation mechanisms in the cis-trans thermal isomerization of diazene. *Chemical Physics Letters* **259**, 276-282 (1996).
- 137 Jursic, Branko S. Ab initio and density functional theory study of the diazene isomerization. *Chemical Physics Letters* **261**, 13-17 (1996).
- 138 Ikeda, T. & Tsutsumi, O. Optical switching and image storage by means of azobenzene liquid-crystal films. *Science (New York, N.Y.)* **268**, 1873-1875 (1995).
- 139 Uznanski, P., Kryszewski, M. & Thulstrup, E. W. Linear dichroism and trans-cis photoisomerization studies of azobenzene molecules in oriented polyethylene matrix. *Eur. Polym. J.* **27**, 41-43 (1991).
- 140 Hampson, G. C. & Robertson, J. Monteath. 78. Bond lengths and resonance in the cis-azobenzene molecule. *Journal of the Chemical Society (Resumed)* **0**, 409-413 (1941).
- 141 de Lange, J. J., Robertson, J. Monteath & Woodward, I. X-Ray Crystal Analysis of Trans-Azobenzene. *Proceedings of the Royal Society of London. Series A. Mathematical and Physical Sciences* **171**, 398-410 (1939).
- 142 Beharry, A. A. & Woolley, G. A. Azobenzene photoswitches for biomolecules. *Chemical Society reviews* **40**, 4422-4437 (2011).
- 143 Puntoriero, F., Ceroni, P., Balzani, V., Bergamini, G. & Vogtle, F. Photoswitchable dendritic hosts: a dendrimer with peripheral azobenzene groups. *Journal of the American Chemical Society* **129**, 10714-10719 (2007).

REFERENCES

- 144 Ferri, V. *et al.* Light-powered electrical switch based on cargo-lifting azobenzene monolayers. *Angewandte Chemie (International ed. in English)* **47**, 3407-3409 (2008).
- 145 Muraoka, T., Kinbara, K. & Aida, T. Mechanical twisting of a guest by a photoresponsive host. *Nature* **440**, 512-515 (2006).
- 146 Banghart, M., Borges, K., Isacoff, E., Trauner, D. & Kramer, R. H. Light-activated ion channels for remote control of neuronal firing. *Nature neuroscience* **7**, 1381-1386 (2004).
- 147 Feher, G., Allen, J. P., Okamura, M. Y. & Rees, D. C. STRUCTURE AND FUNCTION OF BACTERIAL PHOTOSYNTHETIC REACTION CENTERS. *Nature* **339**, 111-116 (1989).
- 148 Stryer, L. Cyclic GMP cascade of vision. *Annual review of neuroscience* **9**, 87-119 (1986).
- 149 Wald, G. The molecular basis of visual excitation. *Nature* **219**, 800-807 (1968).
- 150 Balasubramanian, D., Subramani, S. & Kumar, C. Modification of a model membrane structure by embedded photochrome. *Nature* **254**, 252-254 (1975).
- 151 Lester, H. A., Krouse, M. E., Nass, M. M., Wassermann, N. H. & Erlanger, B. F. Light-activated drug confirms a mechanism of ion channel blockade. *Nature* **280**, 509-510 (1979).
- 152 Holland, Nolan B. *et al.* Single Molecule Force Spectroscopy of Azobenzene Polymers: Switching Elasticity of Single Photochromic Macromolecules. *Macromolecules* **36**, 2015-2023 (2003).
- 153 Naito, Takuya, Horie, Kazuyuki & Mita, Itaru. Photochemistry in polymer solids. 11. The effects of the size of reaction groups and the mode of photoisomerization on photochromic reactions in polycarbonate film. *Macromolecules* **24**, 2907-2911 (1991).
- 154 Paik, Chong Sook & Morawetz, Herbert. Photochemical and Thermal Isomerization of Azoaromatic Residues in the Side Chains and the Backbone of Polymers in Bulk. *Macromolecules* **5**, 171-177 (1972).
- 155 Willner, Itamar & Rubin, Shai. Control of the Structure and Functions of Biomaterials by Light. *Angewandte Chemie International Edition in English* **35**, 367-385 (1996).
- 156 Sporlein, S. *et al.* Ultrafast spectroscopy reveals subnanosecond peptide conformational dynamics and validates molecular dynamics simulation. *Proceedings of the National Academy of Sciences of the United States of America* **99**, 7998-8002 (2002).
- 157 Ihalainen, J. A. *et al.* Folding and unfolding of a photoswitchable peptide from picoseconds to microseconds. *Proceedings of the National Academy of Sciences of the United States of America* **104**, 5383-5388 (2007).
- 158 Kusebauch, U. *et al.* Photocontrolled folding and unfolding of a collagen triple helix. *Angewandte Chemie (International ed. in English)* **45**, 7015-7018 (2006).
- 159 Renner, C., Kusebauch, U., Löweneck, M., Milbradt, A. G. & Moroder, L. Azobenzene as photoresponsive conformational switch in cyclic peptides*. *The Journal of Peptide Research* **65**, 4-14 (2005).
- 160 Woolley, G. A. Photocontrolling peptide alpha helices. *Accounts of chemical research* **38**, 486-493 (2005).

REFERENCES

- 161 Fissi, Adriano, Pieroni, Osvaldo & Ciardelli, Francesco. Photoresponsive polymers: Azobenzene-containing poly(L-lysine). *Biopolymers* **26**, 1993-2007 (1987).
- 162 Guerrero, L., Smart, O. S., Woolley, G. A. & Allemann, R. K. Photocontrol of DNA binding specificity of a miniature engrailed homeodomain. *Journal of the American Chemical Society* **127**, 15624-15629 (2005).
- 163 Willner, Itamar & Rubin, Shai. Reversible photoregulation of the activities of proteins. *Reactive Polymers* **21**, 177-186 (1993).
- 164 Inada, Taeko, Terabayashi, Takashi, Yamaguchi, Yoshiki, Kato, Koichi & Kikuchi, Koichi. Modulation of the catalytic mechanism of hen egg white lysozyme (HEWL) by photochromism of azobenzene. *Journal of Photochemistry and Photobiology A: Chemistry* **175**, 100-107 (2005).
- 165 Komori, K., Yatagai, K. & Tatsuma, T. Activity regulation of tyrosinase by using photoisomerizable inhibitors. *Journal of biotechnology* **108**, 11-16 (2004).
- 166 Nakayama, K., Endo, M. & Majima, T. Photochemical regulation of the activity of an endonuclease BamHI using an azobenzene moiety incorporated site-selectively into the dimer interface. *Chemical communications (Cambridge, England)*, 2386-2387 (2004).
- 167 Wang, L. & Schultz, P. G. Expanding the genetic code. *Angewandte Chemie (International ed. in English)* **44**, 34-66 (2004).
- 168 Bose, M., Groff, D., Xie, J., Brustad, E. & Schultz, P. G. The incorporation of a photoisomerizable amino acid into proteins in *E. coli*. *Journal of the American Chemical Society* **128**, 388-389 (2006).
- 169 Bredenbeck, Jens *et al.* Transient 2D-IR Spectroscopy: Snapshots of the Nonequilibrium Ensemble during the Picosecond Conformational Transition of a Small Peptide. *The Journal of Physical Chemistry B* **107**, 8654-8660 (2003).
- 170 Schrader, T. E. *et al.* Light-triggered beta-hairpin folding and unfolding. *Proceedings of the National Academy of Sciences of the United States of America* **104**, 15729-15734 (2007).
- 171 Singh, Anil K., Das, Joydip & Majumdar, Nirmalya. Novel Bacteriorhodopsin Analogues Based on Azo Chromophores. *Journal of the American Chemical Society* **118**, 6185-6191 (1996).
- 172 Shishido, H., Yamada, M. D., Kondo, K. & Maruta, S. Photocontrol of calmodulin interaction with target peptides using azobenzene derivative. *Journal of biochemistry* **146**, 581-590 (2009).
- 173 Nomura, A. & Okamoto, A. Photoresponsive tandem zinc finger peptide. *Chemical communications (Cambridge, England)*, 1906-1908 (2009).
- 174 Zhang, F. *et al.* Structure-based approach to the photocontrol of protein folding. *Journal of the American Chemical Society* **131**, 2283-2289 (2009).
- 175 Schierling, B. *et al.* Controlling the enzymatic activity of a restriction enzyme by light. *Proceedings of the National Academy of Sciences of the United States of America* **107**, 1361-1366 (2010).
- 176 Umeki, N. *et al.* Incorporation of an azobenzene derivative into the energy transducing site of skeletal muscle myosin results in photo-induced conformational changes. *Journal of biochemistry* **136**, 839-846 (2004).
- 177 Ellis-Davies, G. C. Caged compounds: photorelease technology for control of cellular chemistry and physiology. *Nature methods* **4**, 619-628 (2007).

REFERENCES

- 178 Kaufman, H., Vratsanos, S. M. & Erlanger, B. F. Photoregulation of an enzymic process by means of a light-sensitive ligand. *Science (New York, N.Y.)* **162**, 1487-1489 (1968).
- 179 Krouse, M. E., Lester, H. A., Wassermann, N. H. & Erlanger, B. F. Rates and equilibria for a photoisomerizable antagonist at the acetylcholine receptor of *Electrophorus electroplaques*. *The Journal of general physiology* **86**, 235-256 (1985).
- 180 Bartels, E., Wassermann, N. H. & Erlanger, B. F. Photochromic activators of the acetylcholine receptor. *Proceedings of the National Academy of Sciences of the United States of America* **68**, 1820-1823 (1971).
- 181 Stankovic, C. J., Heinemann, S. H. & Schreiber, S. L. Photo-modulated ion channels based on covalently linked gramicidins. *Biochimica et biophysica acta* **1061**, 163-170 (1991).
- 182 Sukhanov, S. V., Ivanov, B. B., Orekhov, S. Y., Barsukov, L. I. & Arseniev, A. S. MOLECULAR DESIGN OF PHOTO-MODULATED ION CHANNELS BASED ON GRAMICIDIN-A AND THEIR ELECTROCHEMICAL PROPERTIES. *Biologicheskie Membrany* **10**, 535-543 (1993).
- 183 Lien, Linda, Jaikaran, Dominic C. J., Zhang, Zhihua & Woolley, G. Andrew. Photomodulated Blocking of Gramicidin Ion Channels. *Journal of the American Chemical Society* **118**, 12222-12223 (1996).
- 184 Banghart, M. R., Volgraf, M. & Trauner, D. Engineering light-gated ion channels. *Biochemistry* **45**, 15129-15141 (2006).
- 185 Fortin, D. L. *et al.* Photochemical control of endogenous ion channels and cellular excitability. *Nature methods* **5**, 331-338 (2008).
- 186 Banghart, M. R. *et al.* Photochromic blockers of voltage-gated potassium channels. *Angewandte Chemie (International ed. in English)* **48**, 9097-9101 (2009).
- 187 Gorostiza, P. *et al.* Mechanisms of photoswitch conjugation and light activation of an ionotropic glutamate receptor. *Proceedings of the National Academy of Sciences of the United States of America* **104**, 10865-10870 (2007).
- 188 Abrams, Z. R., Warriar, A., Trauner, D. & Zhang, X. A Signal Processing Analysis of Purkinje Cells in vitro. *Frontiers in neural circuits* **4**, 13 (2010).
- 189 Szobota, S. *et al.* Remote control of neuronal activity with a light-gated glutamate receptor. *Neuron* **54**, 535-545 (2007).
- 190 Gorostiza, P. & Isacoff, E. Y. Optical switches for remote and noninvasive control of cell signaling. *Science (New York, N.Y.)* **322**, 395-399 (2008).
- 191 Harvey, J. H. & Trauner, D. Regulating enzymatic activity with a photoswitchable affinity label. *Chembiochem : a European journal of chemical biology* **9**, 191-193 (2008).
- 192 Tochitsky, I. *et al.* Optochemical control of genetically engineered neuronal nicotinic acetylcholine receptors. *Nature chemistry* **4**, 105-111 (2012).
- 193 Stein, M. *et al.* Azo-propofols: photochromic potentiators of GABA(A) receptors. *Angewandte Chemie (International ed. in English)* **51**, 10500-10504 (2012).
- 194 Wyart, C. *et al.* Optogenetic dissection of a behavioural module in the vertebrate spinal cord. *Nature* **461**, 407-410 (2009).
- 195 Levine, W. G. Metabolism of azo dyes: implication for detoxication and activation. *Drug metabolism reviews* **23**, 253-309 (1991).

REFERENCES

- 196 Brown, Mark A. & De Vito, Stephen C. Predicting azo dye toxicity. *Critical Reviews in Environmental Science and Technology* **23**, 249-324 (1993).
- 197 Boulegue, C., Loweneck, M., Renner, C. & Moroder, L. Redox potential of azobenzene as an amino acid residue in peptides. *Chembiochem : a European journal of chemical biology* **8**, 591-594 (2007).
- 198 Sadvovskii, O., Beharry, A. A., Zhang, F. & Woolley, G. A. Spectral tuning of azobenzene photoswitches for biological applications. *Angewandte Chemie (International ed. in English)* **48**, 1484-1486 (2009).
- 199 Zhang, F., Timm, K. A., Arndt, K. M. & Woolley, G. A. Photocontrol of coiled-coil proteins in living cells. *Angewandte Chemie (International ed. in English)* **49**, 3943-3946 (2010).
- 200 Beharry, A. A., Wong, L., Tropepe, V. & Woolley, G. A. Fluorescence imaging of azobenzene photoswitching in vivo. *Angewandte Chemie (International ed. in English)* **50**, 1325-1327 (2011).
- 201 Pluckthun, A. Ribosome display: a perspective. *Methods in molecular biology (Clifton, N.J.)* **805**, 3-28 (2012).
- 202 Jackel, C., Kast, P. & Hilvert, D. Protein design by directed evolution. *Annual review of biophysics* **37**, 153-173 (2008).
- 203 Tuerk, C. & Gold, L. Systematic evolution of ligands by exponential enrichment: RNA ligands to bacteriophage T4 DNA polymerase. *Science (New York, N.Y.)* **249**, 505-510 (1990).
- 204 Kraus, J. P. & Rosenberg, L. E. Purification of low-abundance messenger RNAs from rat liver by polysome immunoadsorption. *Proceedings of the National Academy of Sciences of the United States of America* **79**, 4015-4019 (1982).
- 205 Mattheakis, L. C., Bhatt, R. R. & Dower, W. J. An in vitro polysome display system for identifying ligands from very large peptide libraries. *Proceedings of the National Academy of Sciences of the United States of America* **91**, 9022-9026 (1994).
- 206 Hanes, J. & Pluckthun, A. In vitro selection and evolution of functional proteins by using ribosome display. *Proceedings of the National Academy of Sciences of the United States of America* **94**, 4937-4942 (1997).
- 207 Amstutz, P., Forrer, P., Zahnd, C. & Pluckthun, A. In vitro display technologies: novel developments and applications. *Current opinion in biotechnology* **12**, 400-405 (2001).
- 208 Zahnd, C., Amstutz, P. & Pluckthun, A. Ribosome display: selecting and evolving proteins in vitro that specifically bind to a target. *Nature methods* **4**, 269-279 (2007).
- 209 Malkin, L. I. & Rich, A. Partial resistance of nascent polypeptide chains to proteolytic digestion due to ribosomal shielding. *Journal of molecular biology* **26**, 329-346 (1967).
- 210 Smith, W. P., Tai, P. C. & Davis, B. D. Interaction of secreted nascent chains with surrounding membrane in *Bacillus subtilis*. *Proceedings of the National Academy of Sciences of the United States of America* **75**, 5922-5925 (1978).
- 211 Schaffitzel, C., Hanes, J., Jermutus, L. & Pluckthun, A. Ribosome display: an in vitro method for selection and evolution of antibodies from libraries. *Journal of immunological methods* **231**, 119-135 (1999).

REFERENCES

- 212 Kramer, G., Ramachandiran, V. & Hardesty, B. Cotranslational folding--omnia mea mecum porto? *The international journal of biochemistry & cell biology* **33**, 541-553 (2001).
- 213 Agrawal, R. K. & Frank, J. Structural studies of the translational apparatus. *Current opinion in structural biology* **9**, 215-221 (1999).
- 214 Pluckthun, A., Schaffitzel, C., Hanes, J. & Jermutus, L. In vitro selection and evolution of proteins. *Advances in protein chemistry* **55**, 367-403 (2000).
- 215 Hermes, J. D., Blacklow, S. C. & Knowles, J. R. Searching sequence space by definably random mutagenesis: improving the catalytic potency of an enzyme. *Proceedings of the National Academy of Sciences of the United States of America* **87**, 696-700 (1990).
- 216 Zacco, M., Williams, D. M., Brown, D. M. & Gherardi, E. An approach to random mutagenesis of DNA using mixtures of triphosphate derivatives of nucleoside analogues. *Journal of molecular biology* **255**, 589-603 (1996).
- 217 Cline, J., Braman, J. C. & Hogrefe, H. H. PCR fidelity of pfu DNA polymerase and other thermostable DNA polymerases. *Nucleic acids research* **24**, 3546-3551 (1996).
- 218 Lancet, D., Sadovsky, E. & Seidemann, E. Probability model for molecular recognition in biological receptor repertoires: significance to the olfactory system. *Proceedings of the National Academy of Sciences of the United States of America* **90**, 3715-3719 (1993).
- 219 Irving, R. A., Kortt, A. A. & Hudson, P. J. Affinity maturation of recombinant antibodies using *E. coli* mutator cells. *Immunotechnology : an international journal of immunological engineering* **2**, 127-143 (1996).
- 220 Horst, J. P., Wu, T. H. & Marinus, M. G. *Escherichia coli* mutator genes. *Trends in microbiology* **7**, 29-36 (1999).
- 221 Smith, G. P. Filamentous fusion phage: novel expression vectors that display cloned antigens on the virion surface. *Science (New York, N.Y.)* **228**, 1315-1317 (1985).
- 222 Gurevich, V. V., Pokrovskaya, I. D., Obukhova, T. A. & Zozulya, S. A. Preparative in vitro mRNA synthesis using SP6 and T7 RNA polymerases. *Analytical biochemistry* **195**, 207-213 (1991).
- 223 Glockshuber, R., Schmidt, T. & Pluckthun, A. The disulfide bonds in antibody variable domains: effects on stability, folding in vitro, and functional expression in *Escherichia coli*. *Biochemistry* **31**, 1270-1279 (1992).
- 224 He, M. *et al.* Selection of a human anti-progesterone antibody fragment from a transgenic mouse library by ARM ribosome display. *Journal of immunological methods* **231**, 105-117 (1999).
- 225 Hanes, J., Jermutus, L., Weber-Bornhauser, S., Bosshard, H. R. & Pluckthun, A. Ribosome display efficiently selects and evolves high-affinity antibodies in vitro from immune libraries. *Proceedings of the National Academy of Sciences of the United States of America* **95**, 14130-14135 (1998).
- 226 Amstutz, P. *et al.* In vitro selection for catalytic activity with ribosome display. *Journal of the American Chemical Society* **124**, 9396-9403 (2002).
- 227 Jermutus, L., Honegger, A., Schwesinger, F., Hanes, J. & Pluckthun, A. Tailoring in vitro evolution for protein affinity or stability. *Proceedings of the National Academy of Sciences of the United States of America* **98**, 75-80 (2001).

REFERENCES

- 228 Matsuura, T. & Pluckthun, A. Selection based on the folding properties of proteins with ribosome display. *FEBS letters* **539**, 24-28 (2003).
- 229 Groves, M. *et al.* Affinity maturation of phage display antibody populations using ribosome display. *Journal of immunological methods* **313**, 129-139 (2006).
- 230 Pelletier, J. N., Arndt, K. M., Pluckthun, A. & Michnick, S. W. An in vivo library-versus-library selection of optimized protein-protein interactions. *Nature biotechnology* **17**, 683-690 (1999).
- 231 Andrade, M. A., Perez-Iratxeta, C. & Ponting, C. P. Protein repeats: structures, functions, and evolution. *Journal of structural biology* **134**, 117-131 (2001).
- 232 Bork, P. Hundreds of ankyrin-like repeats in functionally diverse proteins: mobile modules that cross phyla horizontally? *Proteins* **17**, 363-374 (1993).
- 233 Grove, T. Z., Cortajarena, A. L. & Regan, L. Ligand binding by repeat proteins: natural and designed. *Current opinion in structural biology* **18**, 507-515 (2008).
- 234 Zahnd, C. *et al.* A designed ankyrin repeat protein evolved to picomolar affinity to Her2. *Journal of molecular biology* **369**, 1015-1028 (2007).
- 235 Gorina, S. & Pavletich, N. P. Structure of the p53 tumor suppressor bound to the ankyrin and SH3 domains of 53BP2. *Science (New York, N.Y.)* **274**, 1001-1005 (1996).
- 236 Sedgwick, S. G. & Smerdon, S. J. The ankyrin repeat: a diversity of interactions on a common structural framework. *Trends in biochemical sciences* **24**, 311-316 (1999).
- 237 Malek, S., Huxford, T. & Ghosh, G. Ikappa Balpha functions through direct contacts with the nuclear localization signals and the DNA binding sequences of NF-kappaB. *The Journal of biological chemistry* **273**, 25427-25435 (1998).
- 238 Milovnik, P., Ferrari, D., Sarkar, C. A. & Pluckthun, A. Selection and characterization of DARPins specific for the neurotensin receptor 1. *Protein engineering, design & selection : PEDS* **22**, 357-366 (2009).
- 239 Amstutz, P. *et al.* Intracellular kinase inhibitors selected from combinatorial libraries of designed ankyrin repeat proteins. *The Journal of biological chemistry* **280**, 24715-24722 (2005).
- 240 Forrer, P., Stump, M. T., Binz, H. K. & Pluckthun, A. A novel strategy to design binding molecules harnessing the modular nature of repeat proteins. *FEBS letters* **539**, 2-6 (2003).
- 241 Bandejas, T. M. *et al.* Structure of wild-type Plk-1 kinase domain in complex with a selective DARPIn. *Acta crystallographica. Section D, Biological crystallography* **64**, 339-353 (2008).
- 242 Binz, H. K. *et al.* High-affinity binders selected from designed ankyrin repeat protein libraries. *Nature biotechnology* **22**, 575-582 (2004).
- 243 Wetzel, S. K., Settanni, G., Kenig, M., Binz, H. K. & Pluckthun, A. Folding and unfolding mechanism of highly stable full-consensus ankyrin repeat proteins. *Journal of molecular biology* **376**, 241-257 (2008).
- 244 Lodge, D. & Danysz, W. *Ionotropic glutamate receptors as therapeutic targets.* (FP Graham Publishing Co., 2002).
- 245 Sheardown, M. J., Nielsen, E. O., Hansen, A. J., Jacobsen, P. & Honore, T. 2,3-Dihydroxy-6-nitro-7-sulfamoyl-benzo(F)quinoxaline: a neuroprotectant for cerebral ischemia. *Science (New York, N.Y.)* **247**, 571-574 (1990).
- 246 Nordholm, L., Sheardown, M. & Honore, T. *The NBQX story in excitatory amino acids: clinical results with antagonists.* (Academic Press, 1997).

REFERENCES

- 247 Turski, L. *et al.* ZK200775: a phosphonate quinoxalinedione AMPA antagonist for neuroprotection in stroke and trauma. *Proceedings of the National Academy of Sciences of the United States of America* **95**, 10960-10965 (1998).
- 248 Tang, X. & Dmochowski, I. J. Regulating gene expression with light-activated oligonucleotides. *Molecular bioSystems* **3**, 100-110 (2007).
- 249 Liu, M., Asanuma, H. & Komiyama, M. Azobenzene-tethered T7 promoter for efficient photoregulation of transcription. *Journal of the American Chemical Society* **128**, 1009-1015 (2006).
- 250 Green, S. J., Bath, J. & Turberfield, A. J. Coordinated chemomechanical cycles: a mechanism for autonomous molecular motion. *Physical review letters* **101**, 238101 (2008).
- 251 Rothmund, P. W. Folding DNA to create nanoscale shapes and patterns. *Nature* **440**, 297-302 (2006).
- 252 Sanderson, K. Bioengineering: What to make with DNA origami. *Nature* **464**, 158-159 (2010).
- 253 Wang, H. & Oster, G. Ratchets, power strokes, and molecular motors. *Appl Phys A* **75**, 315-323 (2002).
- 254 Hugel, T. & Lumme, C. Bio-inspired novel design principles for artificial molecular motors. *Current opinion in biotechnology* **21**, 683-689 (2010).
- 255 Fehrentz, T. *et al.* Exploring the pharmacology and action spectra of photochromic open-channel blockers. *Chembiochem : a European journal of chemical biology* **13**, 1746-1749 (2012).
- 256 Agranat, I., Caner, H. & Caldwell, J. Putting chirality to work: the strategy of chiral switches. *Nature reviews. Drug discovery* **1**, 753-768 (2002).
- 257 Zahn, S. & Canary, J. W. Electron-induced inversion of helical chirality in copper complexes of N,N-dialkylmethionines. *Science (New York, N.Y.)* **288**, 1404-1407 (2000).
- 258 Kolasa, Teodozyj & Miller, Marvin J. 1-Hydroxy-3-amino-2-piperidone (.delta.-N-hydroxycycloornithine) derivatives: key intermediates for the synthesis of hydroxamate-based siderophores. *The Journal of Organic Chemistry* **55**, 1711-1721 (1990).
- 259 Cockroft, S. L. *et al.* Substituent effects on aromatic stacking interactions. *Organic & biomolecular chemistry* **5**, 1062-1080 (2007).
- 260 Leavitt, S. & Freire, E. Direct measurement of protein binding energetics by isothermal titration calorimetry. *Current opinion in structural biology* **11**, 560-566 (2001).
- 261 Hammett, L. P., Walden, G. H. & Edmonds, S. M. New indicators for oxidimetry - Some phenanthroline and diphenylamine derivatives. *Journal of the American Chemical Society* **56**, 1092-1094 (1934).
- 262 Sambrook, J. & Russell, D. W. *Molecular Cloning*. (CSHL Press, 2001).
- 263 Vandie, I. M., Bergmans, H. E. N. & Hoekstra, W. P. M. TRANSFORMATION IN ESCHERICHIA-COLI - STUDIES ON THE ROLE OF THE HEAT-SHOCK IN INDUCTION OF COMPETENCE. *Journal of General Microbiology* **129**, 663-670 (1983).
- 264 Studier, F. W., Rosenberg, A. H., Dunn, J. J. & Dubendorff, J. W. USE OF T7 RNA-POLYMERASE TO DIRECT EXPRESSION OF CLONED GENES. *Methods in enzymology* **185**, 60-89 (1990).

REFERENCES

- 265 Benov, L. & Al-Ibraheem, J. Disrupting Escherichia coli: A comparison of methods. *Journal of Biochemistry and Molecular Biology* **35**, 428-431 (2002).
- 266 Laemmli, U. K. Cleavage of structural proteins during the assembly of the head of bacteriophage T4. *Nature* **227**, 680-685 (1970).
- 267 Neuhoff, V., Stamm, R. & Eibl, H. CLEAR BACKGROUND AND HIGHLY SENSITIVE PROTEIN STAINING WITH COOMASSIE BLUE DYES IN POLYACRYLAMIDE GELS - A SYSTEMATIC ANALYSIS. *Electrophoresis* **6**, 427-448 (1985).
- 268 Hochuli, E., Bannwarth, W., Dobeli, H., Gentz, R. & Stuber, D. Genetic Approach to Facilitate Purification of Recombinant Proteins with a Novel Metal Chelate Adsorbent. *Nat Biotech* **6**, 1321-1325 (1988).
- 269 Porath, J. & Flodin, P. Gel filtration: a method for desalting and group separation. *Nature* **183**, 1657-1659 (1959).
- 270 Peterson, E. A. & Sober, H. A. CHROMATOGRAPHY OF PROTEINS .1. CELLULOSE ION-EXCHANGE ADSORBENTS. *Journal of the American Chemical Society* **78**, 751-755 (1956).
- 271 Gearing, David P. *et al.* Production of Leukemia Inhibitory Factor in Escherichia coli by a Novel Procedure and Its Use in Maintaining Embryonic Stem Cells in Culture. *Nat Biotech* **7**, 1157-1161 (1989).
- 272 Lottspeich, F. & Engels, J. W. *Bioanalytik*. (Springer Spektrum, 2006).
- 273 Wienken, C. J., Baaske, P., Rothbauer, U., Braun, D. & Duhr, S. Protein-binding assays in biological liquids using microscale thermophoresis. *Nature communications* **1**, 100 (2010).
- 274 Duhr, S. & Braun, D. Why molecules move along a temperature gradient. *Proceedings of the National Academy of Sciences of the United States of America* **103**, 19678-19682 (2006).
- 275 Baaske, P., Wienken, C. J., Reineck, P., Duhr, S. & Braun, D. Optical thermophoresis for quantifying the buffer dependence of aptamer binding. *Angewandte Chemie (International ed. in English)* **49**, 2238-2241 (2010).
- 276 Lippok, S. *et al.* Direct detection of antibody concentration and affinity in human serum using microscale thermophoresis. *Analytical chemistry* **84**, 3523-3530 (2012).
- 277 Beyer, Stefan, Dittmer, Wendy U. & Simmel, Friedrich C. Design Variations for an Aptamer-Based DNA Nanodevice. *Journal of Biomedical Nanotechnology* **1**, 96-101 (2005).
- 278 Gale, R. *Crystallography made crystal clear*. (Academic Press, 2006).
- 279 McRee, D. *Practical protein crystallography*. (Academic Press, 1993).
- 280 Kabsch, W. XDS. *Acta crystallographica. Section D, Biological crystallography* **66**, 125-132 (2010).
- 281 McCoy, A. J. *et al.* Phaser crystallographic software. *Journal of applied crystallography* **40**, 658-674 (2007).
- 282 Chaudhry, C., Weston, M. C., Schuck, P., Rosenmund, C. & Mayer, M. L. Stability of ligand-binding domain dimer assembly controls kainate receptor desensitization. *The EMBO journal* **28**, 1518-1530 (2009).
- 283 Beich-Frandsen, M. *et al.* Structures of the ligand-binding core of iGluR2 in complex with the agonists (R)- and (S)-2-amino-3-(4-hydroxy-1,2,5-thiadiazol-3-yl)propionic acid explain their unusual equipotency. *Journal of medicinal chemistry* **51**, 1459-1463 (2008).

REFERENCES

- 284 Blow, D. *Outline of crystallography for biologists*. (Oxford University Press Inc., 2002).
- 285 Emsley, P., Lohkamp, B., Scott, W. G. & Cowtan, K. Features and development of Coot. *Acta crystallographica. Section D, Biological crystallography* **66**, 486-501 (2010).
- 286 Winn, M. D., Isupov, M. N. & Murshudov, G. N. Use of TLS parameters to model anisotropic displacements in macromolecular refinement. *Acta crystallographica. Section D, Biological crystallography* **57**, 122-133 (2001).
- 287 Schuttelkopf, A. W. & van Aalten, D. M. PRODRG: a tool for high-throughput crystallography of protein-ligand complexes. *Acta crystallographica. Section D, Biological crystallography* **60**, 1355-1363 (2004).
- 288 Davis, I. W. *et al.* MolProbity: all-atom contacts and structure validation for proteins and nucleic acids. *Nucleic acids research* **35**, W375-383 (2007).
- 289 Krissinel, E. & Henrick, K. Inference of macromolecular assemblies from crystalline state. *Journal of molecular biology* **372**, 774-797 (2007).
- 290 CCP4. The CCP4 suite: programs for protein crystallography. *Acta crystallographica. Section D, Biological crystallography* **50**, 760-763 (1994).
- 291 Krissinel, E. & Henrick, K. Secondary-structure matching (SSM), a new tool for fast protein structure alignment in three dimensions. *Acta crystallographica. Section D, Biological crystallography* **60**, 2256-2268 (2004).
- 292 DeLano, W. L. . The PyMOL Molecular Graphics System. *DeLano Scientific* (2002).
- 293 Ahmed, A. H., Wang, S., Chuang, H. H. & Oswald, R. E. Mechanism of AMPA receptor activation by partial agonists: disulfide trapping of closed lobe conformations. *The Journal of biological chemistry* **286**, 35257-35266 (2011).
- 294 Boden, Christopher D. J., Pattenden, Gerald & Ye, Tao. Palladium-catalysed hydrostannylations of 1-bromoalkynes. A practical synthesis of (E)-1-stannylalk-1-enes. *Journal of the Chemical Society, Perkin Transactions 1* **0**, 2417-2419 (1996).
- 295 Mee, S. P., Lee, V. & Baldwin, J. E. Stille coupling made easier-the synergic effect of copper(I) salts and the fluoride ion. *Angewandte Chemie (International ed. in English)* **43**, 1132-1136 (2004).
- 296 Charrier, J. D., Hadfield, D. S., Hitchcock, P. B. & Young, D. W. Synthesis of (2S,4S)- and (2S,4R)-5-fluoroleucine and (2S,4S)-[5,5-2H₂]-5-fluoroleucine. *Organic & biomolecular chemistry* **2**, 474-482 (2004).
- 297 Volgraf, M. *Photocontrol of Ionotropic Glutamate receptors and Total Synthesis of Exiguamine A and B*, University of California, (2008).
- 298 Kasper, C. *et al.* The structure of a mixed GluR2 ligand-binding core dimer in complex with (S)-glutamate and the antagonist (S)-NS1209. *Journal of molecular biology* **357**, 1184-1201 (2006).
- 299 Plested, A. J. & Mayer, M. L. Structure and mechanism of kainate receptor modulation by anions. *Neuron* **53**, 829-841 (2007).
- 300 Partin, K. M., Patneau, D. K., Winters, C. A., Mayer, M. L. & Buonanno, A. Selective modulation of desensitization at AMPA versus kainate receptors by cyclothiazide and concanavalin A. *Neuron* **11**, 1069-1082 (1993).
- 301 Wong, A. Y., Fay, A. M. & Bowie, D. External ions are coactivators of kainate receptors. *The Journal of neuroscience : the official journal of the Society for Neuroscience* **26**, 5750-5755 (2006).

REFERENCES

- 302 Pohlsgaard, J., Frydenvang, K., Madsen, U. & Kastrup, J. S. Lessons from more than 80 structures of the GluA2 ligand-binding domain in complex with agonists, antagonists and allosteric modulators. *Neuropharmacology* **60**, 135-150 (2011).
- 303 Weston, M. C., Gertler, C., Mayer, M. L. & Rosenmund, C. Interdomain interactions in AMPA and kainate receptors regulate affinity for glutamate. *The Journal of neuroscience : the official journal of the Society for Neuroscience* **26**, 7650-7658 (2006).
- 304 Greger, I. H., Akamine, P., Khatri, L. & Ziff, E. B. Developmentally regulated, combinatorial RNA processing modulates AMPA receptor biogenesis. *Neuron* **51**, 85-97 (2006).
- 305 Muto, T., Tsuchiya, D., Morikawa, K. & Jingami, H. Structures of the extracellular regions of the group II/III metabotropic glutamate receptors. *Proceedings of the National Academy of Sciences of the United States of America* **104**, 3759-3764 (2007).
- 306 Ashley, J. N., Barber, H. J., Ewins, A. J., Newbery, G. & Self, A. D. H. 20. A chemotherapeutic comparison of the trypanocidal action of some aromatic diamidines. *Journal of the Chemical Society (Resumed)* **0**, 103-116 (1942).
- 307 Barman, Dhiren C., Saikia, Pramod, Prajapati, Dipak & Sandhu, Jagir S. HETEROGENEOUS PERMANGANATE OXIDATIONS. A NOVEL METHOD FOR THE DEAMINATION USING SOLID SUPPORTED IRON-PERMANGANATE. *Synthetic Communications* **32**, 3407-3412 (2002).
- 308 McReynolds, K. D., Bhat, A., Conboy, J. C., Saavedra, S. S. & Gervay-Hague, J. Non-natural glycosphingolipids and structurally simpler analogues bind HIV-1 recombinant Gp120. *Bioorganic & medicinal chemistry* **10**, 625-637 (2002).
- 309 Foss, F. W., Jr. *et al.* Synthesis and biological evaluation of gamma-aminophosphonates as potent, subtype-selective sphingosine 1-phosphate receptor agonists and antagonists. *Bioorganic & medicinal chemistry* **15**, 663-677 (2007).
- 310 Bower, J. F., Szeto, P. & Gallagher, T. Cyclic sulfamidates as precursors to alkylidene pyrrolidines and piperidines. *Organic letters* **9**, 4909-4912 (2007).
- 311 Mandal, P. K. *et al.* Potent and selective phosphopeptide mimetic prodrugs targeted to the Src homology 2 (SH2) domain of signal transducer and activator of transcription 3. *Journal of medicinal chemistry* **54**, 3549-3563 (2011).
- 312 Rohbogner, Christoph J., Wunderlich, Stefan H., Clososki, Giuliano C. & Knochel, Paul. New Mixed Li/Mg and Li/Mg/Zn Amides for the Chemoselective Metallation of Arenes and Heteroarenes. *European Journal of Organic Chemistry* **2009**, 1781-1795 (2009).
- 313 Kumita, J. R., Smart, O. S. & Woolley, G. A. Photo-control of helix content in a short peptide. *Proceedings of the National Academy of Sciences of the United States of America* **97**, 3803-3808 (2000).
- 314 Cattaneo, A. & Biocca, S. The selection of intracellular antibodies. *Trends in biotechnology* **17**, 115-121 (1999).
- 315 Ostermeier, M. Designing switchable enzymes. *Current opinion in structural biology* **19**, 442-448 (2009).
- 316 Dreier, B. *et al.* Her2-specific multivalent adapters confer designed tropism to adenovirus for gene targeting. *Journal of molecular biology* **405**, 410-426 (2011).

REFERENCES

- 317 Zahnd, C. *et al.* Efficient tumor targeting with high-affinity designed ankyrin repeat proteins: effects of affinity and molecular size. *Cancer research* **70**, 1595-1605 (2010).
- 318 Theurillat, J. P. *et al.* Designed ankyrin repeat proteins: a novel tool for testing epidermal growth factor receptor 2 expression in breast cancer. *Modern pathology : an official journal of the United States and Canadian Academy of Pathology, Inc* **23**, 1289-1297 (2010).
- 319 Martin-Killias, P., Stefan, N., Rothschild, S., Pluckthun, A. & Zangemeister-Wittke, U. A novel fusion toxin derived from an EpCAM-specific designed ankyrin repeat protein has potent antitumor activity. *Clinical cancer research : an official journal of the American Association for Cancer Research* **17**, 100-110 (2011).
- 320 Matsui, K., Hosoi, N. & Tachibana, M. Excitatory synaptic transmission in the inner retina: paired recordings of bipolar cells and neurons of the ganglion cell layer. *The Journal of neuroscience : the official journal of the Society for Neuroscience* **18**, 4500-4510 (1998).

ALWIN RALF REITER

PERSÖNLICHE DATEN

Geburtsdatum: 08.09.1982
Geburtsort: Temeschburg
Staatsangehörigkeit: Deutsch

PROMOTION

05.2009 – 04.2013: Promotion an der LMU München

Titel: Proteins and Azobenzenes

Arbeitsgruppe: Prof. Dr. Dirk Trauner

STUDIUM

10.2003 – 07.2007: Bachelorstudium an der LMU München

Fächer: Anorganische Chemie, Biochemie, Organische Chemie, Physikalische Chemie

04.2007 – 07.2007: Bachelorarbeit

Titel: Synthesis of Sterically Hindered Tertiary Amines *via* Oxidative Coupling of Lithium Organo-amidocuprates: Applications in Photochemistry

Arbeitsgruppe: Prof. Dr. Paul Knochel

12.07.2007: Abschluss Bachelor of Science

10.2007 – 03.2009: Masterstudium an der LMU München

Hauptfächer: Organische Chemie und Physikalische Chemie

Nebenfach: Strukturbiologie

03.2007: Strukturbiologiepraktikum

Arbeitsgruppe: Prof. Dr. Patrick Cramer und Prof. Dr. Karl-Peter Hopfner

10.2007 – 12.2007: Forschungspraktikum an der Universität von Toronto

Arbeitsgruppe: Prof. Dr. Robert Batey

01.2008 – 04.2008: Forschungspraktikum in biophysikalischer Chemie

Arbeitsgruppe: Prof. Dr. Jens Michaelis

09.2008 – 02.2009: Masterarbeit

Titel: Towards the Crystal Structure of the Ligand-binding Domain of iGluR6 with an Optical Switch and Synthesis of Potassium Channel Blockers

Arbeitsgruppe: Prof. Dr. Dirk Trauner

17.03.2009: Abschluss Master of Science

ZIVILDIENTST

12.2002 – 09.2003: Bayerisches-Rotes-Kreuz Kreisverband Ingolstadt

SCHULAUUSBILDUNG

09.1993 – 06.2002: Christoph-Scheiner-Gymnasium Ingolstadt

28.06.2002: Abschluss Abitur